

Effect of silica nanoparticles on the morphology of polymer blends

Citation for published version (APA):

Li, W. (2011). *Effect of silica nanoparticles on the morphology of polymer blends*. [Phd Thesis 1 (Research TU/e / Graduation TU/e), Chemical Engineering and Chemistry]. Technische Universiteit Eindhoven.
<https://doi.org/10.6100/IR719366>

DOI:

[10.6100/IR719366](https://doi.org/10.6100/IR719366)

Document status and date:

Published: 01/01/2011

Document Version:

Publisher's PDF, also known as Version of Record (includes final page, issue and volume numbers)

Please check the document version of this publication:

- A submitted manuscript is the version of the article upon submission and before peer-review. There can be important differences between the submitted version and the official published version of record. People interested in the research are advised to contact the author for the final version of the publication, or visit the DOI to the publisher's website.
- The final author version and the galley proof are versions of the publication after peer review.
- The final published version features the final layout of the paper including the volume, issue and page numbers.

[Link to publication](#)

General rights

Copyright and moral rights for the publications made accessible in the public portal are retained by the authors and/or other copyright owners and it is a condition of accessing publications that users recognise and abide by the legal requirements associated with these rights.

- Users may download and print one copy of any publication from the public portal for the purpose of private study or research.
- You may not further distribute the material or use it for any profit-making activity or commercial gain
- You may freely distribute the URL identifying the publication in the public portal.

If the publication is distributed under the terms of Article 25fa of the Dutch Copyright Act, indicated by the "Taverne" license above, please follow below link for the End User Agreement:

www.tue.nl/taverne

Take down policy

If you believe that this document breaches copyright please contact us at:

openaccess@tue.nl

providing details and we will investigate your claim.

Effect of silica nanoparticles on the morphology of polymer blends

PROEFSCHRIFT

ter verkrijging van de graad van doctor aan de Technische Universiteit Eindhoven, op gezag van de rector magnificus, prof.dr.ir. C.J. van Duijn, voor een commissie aangewezen door het College voor Promoties in het openbaar te verdedigen op woensdag 23 november 2011 om 16.00 uur

door

Weizhen Li

geboren te Shanghai, China

Dit proefschrift is goedgekeurd door de promotor:

prof.dr. P.J. Lemstra

Copromotor:

dr.ir. J.G.P. Goossens

A catalogue record is available from the Eindhoven University of Technology Library.
ISBN: 978-90-386-2889-9

Copyright © 2011 by Weizhen Li

The work described in this thesis is performed at the Laboratory of Polymer Technology (SKT) within the Department of Chemical Engineering and Chemistry, Eindhoven University of Technology, The Netherlands. This work was funded by STW under project #07057.

Cover design by Julia Nazarenko

Printed by Ipskamp Drukkers

Table of contents

Summary.....	1
--------------	---

Chapter 1 Introduction

1.1 Polymer blends.....	6
1.1.1 The Phase behavior of binary polymer blends	6
1.1.2 The phase behavior of polymer blends with block copolymers.....	8
1.1.3 Relation between morphology and mechanical properties	9
1.2 Effect of particles on the phase behavior of polymer blends.....	10
1.2.1 Nanoparticles in the partially miscible polymer blends: effect on phase behavior and kinetics of phase separation.....	11
1.2.2 Nanoparticles in immiscible polymer blends	12
1.2.2.1 Selective localization of nanoparticles in polymer blends	12
1.2.2.2 Compatibilization effect of nanoparticles.....	14
1.2.2.3 Nanoparticles in block copolymer blends.....	15
1.2.3 Control of the dispersion of nanoparticles	17
1.3 Choice of systems and experimental approaches.....	18
1.4 Scope and outline of the thesis.....	18
1.5 References.....	19

Chapter 2 Effect of silica nanoparticles on the partially miscible polymer blend PMMA/SAN

2.1 Introduction.....	24
2.2 Experimental	27
2.2.1 Materials.....	27
2.2.2 Sample preparation.....	27
2.2.3 Characterization techniques	29
2.3 Results and discussion	30
2.3.1 Structure development of PMMA/SAN blends	30
2.3.2 The effect of silica nanoparticles on the structure development of PMMA/SAN blends	33
2.3.3 The effect of silica nanoparticles on the spinodal decomposition kinetics	36
2.3.3.1 Analysis of early stage of phase separation	39
2.3.3.2 Analysis of intermediate and late stages of phase separation.....	40
2.3.4 Phase behavior of silica-filled PMMA/SAN blends evaluated by rheology.....	44
2.4 Conclusions.....	48
2.5 References.....	49

Chapter 3 Morphology and Rheology of silica-filled PC/PMMA blends

3.1 Introduction.....	52
3.2 Experimental.....	54
3.2.1 Materials.....	54
3.2.2 Blend preparation.....	54
3.2.3 Characterization techniques.....	56
3.3 Results.....	57
3.3.1 The influence of the solvent-casting conditions on the miscibility of PC and PMMA.....	57
3.3.2 The influence of the compounding sequence on the morphology of hydrophilic silica-filled PC/PMMA systems.....	59
3.3.3 Rheology of hydrophilic silica-filled PC/PMMA blends.....	62
3.3.4 Stability of the morphology in relation to polymer-silica interaction.....	67
3.4 Discussion.....	68
3.5 Conclusions.....	71
3.6 References.....	72

Chapter 4 Morphology control of PS-PB-PMMA/PMMA blends by silica nanoparticles

4.1 Introduction.....	76
4.2 Experimental.....	78
4.2.1 Materials.....	78
4.2.2 Sample preparation.....	79
4.2.3 Characterization techniques.....	80
4.3 Results and discussion.....	81
4.3.1 The effect of silica nanoparticles on the morphology of the SBM triblock copolymer.....	82
4.3.2 The effect of silica nanoparticles on the morphology of solvent-cast PMMA/S ₂₀ B ₂₅ M ₅₅ blends.....	83
4.3.2.1 The morphology of PMMA/S ₂₀ B ₂₅ M ₅₅ blends and the effect of the molar mass distribution of the PMMA.....	83
4.3.2.2 The suppression effect of silica nanoparticles.....	86
4.3.2.3 The effect of the molar mass distribution of the homopolymer PMMA.....	89
4.3.3 Morphology development of triblock copolymer/monomer with addition of silica nanoparticles upon in-situ polymerization.....	92
4.3.4 Morphologies of PMMA/S ₂₀ B ₂₅ M ₅₅ nanocomposites: Melt-mixing.....	97
4.4 Conclusions.....	98
4.5 References.....	99

Chapter 5 Selective distribution of silica nanoparticles and the morphology control of PS-PB-PMMA/PS blends

5.1 Introduction.....	102
5.2 Experimental.....	103
5.2.1 Materials.....	103
5.2.2 Sample preparation.....	103
5.2.3 Characterization techniques	104
5.3 Results and discussion	106
5.3.1 The effect of silica nanoparticles on the morphology of the SBM triblock copolymer.....	106
5.3.2 The effect of silica nanoparticles on the morphology of solvent-cast PS/SBM blends	108
5.3.2.1 The selective distribution of MEK-ST silica nanoparticles in PS/S ₂₀ B ₂₅ M ₅₅	109
5.3.2.2 The suppression effect of the TOL-ST silica nanoparticles in PS/S ₅₂ B ₃₀ M ₁₈	111
5.3.3 Morphology development of triblock copolymer/monomer with addition of silica nanoparticles upon in-situ polymerization.....	112
5.3.4 Morphologies of PS/SBM nanocomposites: Melt mixing	117
5.3.4.1 Controlling the localization of silica nanoparticles by compounding	117
5.3.4.2 Suppression effect of the silica nanoparticles.....	118
5.3.5 Deformation mechanism	120
5.4 Conclusions.....	121
5.5 References.....	122

Chapter 6 Effect of silica nanoparticles on the morphology of PMMA-PBA-PCL triblock copolymer blends with a crystallizable block

6.1 Introduction.....	126
6.2 Experimental.....	129
6.2.1 Materials.....	129
6.2.2 Sample preparation.....	130
6.2.3 Characterization techniques	130
6.3 Results and discussion	131
6.3.1 Morphology of the pure triblock copolymer M ₅₄ B ₂₃ C ₁₀ and blends with PMMA..	131
6.3.2 The effect of silica nanoparticles on the morphology	132
6.3.3 Thermal behavior of the triblock copolymers and its blends with PMMA.....	133
6.3.3.1 Effect of silica nanoparticles on the glass transition temperatures of the different blocks	133
6.3.3.2 Effect of silica nanoparticles on the fractionated crystallization of the PCL block and the morphology of the triblock copolymer	135
6.4 Conclusions.....	140
6.5 References.....	141

Appendix 1 The effect of silica nanoparticles on the deformation behavior of PS/SBS blends

A.1 The effect of silica nanoparticles on the morphology of PS/SBS blends 144
A.2 The effect of silica nanoparticles on the deformation behavior of PS/SBS blends 146
A.3 References..... 148

Technology assessment 149

Samenvatting 151

Acknowledgements 155

Curriculum vitae 159

Effect of silica nanoparticles on the morphology of polymer blends

Summary

Polymeric materials are often a combination of different polymers and plasticizers, stabilizers, and (in)organic additives to tailor the properties. The type and fineness of the morphology is the key factor for the ultimate properties of polymer blends. Recently, the use of inorganic nanoparticles, such as carbon black, organoclay, carbon nanotubes, and silica, has come up to control the morphology of polymer blends.

The objective of the research described in the thesis is to investigate the effect of the silica nanoparticles on the morphology of polymer blends. Since polymer blends are classified into several categories based on their miscibility, the effect of silica nanoparticles is studied with different blend categories. The first category is called a fully miscible blend, in which the polymers are miscible over a wide range of temperatures and at all compositions due to specific interactions. The second category is called a partially miscible blend, for which miscibility is only observed in a specific temperature and/or concentration window. The third category is called an immiscible blend, in which the polymers are not miscible at any temperature or concentration. Since complete miscibility among polymer pairs is exceptional, this study is focused on partially miscible and immiscible blends.

For the category of partially miscible polymer blends, a blend consisting of poly(methyl methacrylate) (PMMA) and poly(styrene-*co*-acrylonitrile) (SAN) with a lower critical solution temperature (LCST) was used as the model system. The interaction between the surface of the particles and the polymer components was found to be the key factor to control the distribution of the silica nanoparticles, which can either be in one of the polymer phases or at the PMMA/SAN interface after phase separation. Hydrophilic silica nanoparticles preferentially migrate to the PMMA phase due to the strong interaction of the hydroxyl groups on the surface of silica with the carbonyl groups of the PMMA. The migration of the particles leads to a slow down of the coarsening rate and a lower phase separation temperature. Three explanations were considered for this effect: i) local increase of the

viscosity because of an increase of the silica concentration; ii) selective adsorption of low molar mass PMMA chains on the surface of the silica nanoparticles, thereby increasing the average molar mass of the bulk, which is consistent with the shift of the phase diagram; iii) reduction of the interfacial tension. The hydrophobic silica nanoparticles were localized at the PMMA/SAN interface, which might act as a solid barrier between the polymers which influences the interfacial mobility.

For the category of immiscible polymer blends, a blend consisting of PMMA and poly(carbonate) (PC) was used as the model system with two types of silica particles, i.e. hydrophilic and hydrophobic. For the hydrophilic silica, selective distribution of the nanoparticles in the PMMA phase was observed, which was independent of the compounding sequence. The stabilization of the finer morphology can be attributed to the local increase of the viscosity and a concomitant reduction of the mobility of the PMMA phase. For the hydrophobic silica, localization of the nanoparticles at the PC/PMMA interface is the thermodynamically preferred state, but the kinetics of coarsening can be influenced by the compounding sequence. The observed stabilization effect of the hydrophobic silica particles might be related to the presence of an immobilized layer of nanoparticles around the polymer droplets. This mechanism is very efficient to control the morphology.

For immiscible polymer blends containing block copolymers, macrophase separation between the homopolymer and di- or triblock copolymers occurs for systems with $N_{Ah} > N_{Ac}$ (the degree of the polymerization of polymer A in both the homopolymer, N_{Ah} , and the copolymer, N_{Ac}). The silica nanoparticles show a suppression effect on the extent of macrophase separation between the PMMA homopolymer and poly(styrene)-*b*-poly(butadiene)-*b*-poly(methyl methacrylate) (SBM) triblock copolymer, which is related to the strong hydrogen bonding interaction between the hydroxyl groups on the surface of silica nanoparticles with the carbonyl groups of the PMMA. By using different molar mass distributions of the PMMA homopolymer, the suppression effect of nanoparticles can be attributed to selective adsorption of the high molar mass PMMA on the surface of the silica particles, which may force the system into the 'wet-brush' regime. For blends of SBM with poly(styrene) (PS), silica nanoparticles with different surface characteristics were used. The location of the silica particles depends on the interaction between the silica surface and the polymer, which can also be influenced by the compounding procedure. Upon adding hydrophilic silica to the PS/SBM blend, the silica nanoparticles are found preferentially in the core (PMMA phase) of the core-shell structures without macrophase separation due to the strong hydrogen bonding interaction between the silica surface and PMMA. On the other

hand, hydrophobic silica nanoparticles suppress the extent of macrophase separation between the homopolymer and block copolymer blend based on a selective distribution within the PS phase. The suppression effect on the phase separation and the concomitant kinetics can be controlled by the preparation method, i.e. solvent-, melt processing or in-situ polymerization.

The toughness of brittle amorphous, glassy polymers can be improved by the addition of ABA or ABC block copolymers containing one rubbery block and one semi-crystalline block, which form micellar or cylindrical structures within the matrix. Upon cooling, additional internal stresses can build up during fractionated crystallization, i.e. homogeneous and heterogeneous nucleation, which induce pre-cavitation, as shown in a previous study on systems with a cylindrical morphology. After adding the silica nanoparticles, the morphology of the PMMA/poly(methyl methacrylate)-*b*-poly(butyl acrylate)-*b*-poly(ϵ -caprolactone) (MBC) blend shows a transition from spherical to spherical/cylindrical structure, which arises from the separation of the triblock copolymer MBC and the diblock copolymer BC, together with the localization of the silica particles in the spherical PCL domains, leading a fractionated crystallization of PCL.

In this thesis, it was shown that silica nanoparticles have a significant effect on the morphology of partially miscible, immiscible polymer blends and blends with block copolymers. The distribution of the nanoparticles is governed by the interaction between the polymers and the silica surface and can be at the interface or preferentially in one of the phases. The kinetics of (re)distribution can be influenced by the preparation method, i.e. solution processing, melt compounding and in-situ polymerization in the presence of nanoparticles.

Chapter 1

Introduction

Polymeric materials are rarely used in their pure state. Blending different polymers has been identified as the most versatile and economic method to satisfy the complex demands for performance, such as optical, adhesion, and fracture toughness.^{1,2}

Depending on the interactions between the polymers, the blends can be classified into three categories. The first category is a fully miscible blend, in which the polymers are miscible over a wide range of temperatures and at all compositions due to specific interactions. The second category is a partially miscible blend, in which miscibility is only observed in a specific temperature and/or concentration window. The third category is an immiscible blend, in which the polymers are not thermodynamically miscible (at a molecular scale) at any temperature or concentration. Considering that there are only a few examples of fully miscible polymer pairs, the majority of studies were focused on partially miscible and immiscible blends.³

Polymer blends consist of not only different polymers, but also can contain plasticizers, stabilizers, and organic/inorganic particles. Fillers, such as carbon black, organoclay, talc, calcium carbonate, and silica, are used as a way to improve the mechanical, thermal or barrier properties, processibility, and conductivity.^{4,5} In addition, the morphology of polymer blends which is a key factor in improving the product properties can be controlled by using inorganic nanoparticles, due to its large specific surface.⁶ A lot of research has thus focused on modifying the phase stability of polymer blends via nanoparticles.⁷ This chapter summarizes the current status on the morphology control of binary polymer blends and the influence of the nanofillers.

1.1 Polymer blends

1.1.1 The Phase behavior of binary polymer blends

Properties of polymer blends such as mechanical, rheological and barrier properties are strongly influenced by the type and fineness of the morphology. Thus, the control of the morphology of polymer blends has attracted lots of interest in the last decades.⁸

Polymer blends are most often in the immiscible category due to entropic reasons which disfavours the miscibility of polymer blends. These binary polymer blends can be divided into two major types: blends with a co-continuous phase structure and blends with a phase structure as droplets dispersed in matrix. The co-continuous phase structure can be defined as the coexistence phases of two continuous structures within the same volume while each component has its own internal network-like structure. Different continuities can be achieved by varying the blend compositions above the certain threshold values. Co-continuous polymer blends are ideal for a wide range of applications because of their special phase structures. The useful properties of co-continuous polymer blends include synergistic mechanical properties, controlled electrical conductivity, and selective permeability.^{9,10} Co-continuous structures can be characterized via microscopy with image analysis, electrical conductivity measurements, and rheological measurements.¹¹

During melt mixing of immiscible polymers, processes such as liquid drop stretching into threads, breakup of the threads into smaller droplets, and coalescence of the droplets into larger ones occur,¹² resulting in the droplets and matrix morphology. The balance of these competing processes determines the final particle sizes of the blends which result upon the properties of the blends. Furthermore, the droplet and matrix morphology and droplet sizes are related to parameters such as the viscosity ratio, blend composition, elasticity ratio, shear stress, and interfacial tension.⁸

For the droplet and matrix morphology, the major challenge is to achieve the ideal nanosized domains of the dispersed phase. The coarsening of the morphology occurs due to coalescence of the dispersed droplets, especially in the low shear rate regions. After processing, the improved properties of polymer blend materials may be compromised over long time scales because of a general tendency towards demixing. One of the classical methods to prevent coarsening between the phases (reduction in the interfacial tension) is the use of compatibilizers, such as a block copolymer or inorganic nanoparticles.^{6,8} This classical compatibilization strategy has been widely used to produce a variety of industrial polymer blends and will be discussed in details in Section 1.2.

Although most polymer pairs are immiscible, partially miscible polymer blends still attract an abundance of interest because of their special phase behavior. The phase separation in partially miscible polymer blends occurs either by increasing the temperature, which is identified as a lower critical solution temperature (LCST) behavior, or by decreasing the temperature, which is identified as an upper critical solution temperature (UCST) behavior. It is well known that the phase separation of LCST or UCST may occur via two different mechanisms: binodal decomposition, for which the system is thermodynamically metastable, and spinodal decomposition, for which the system is thermodynamically unstable. Due to the complex phase behavior, the final morphology of the partially miscible blends is generally controlled by phase separation kinetics.

In literature, a large number of comprehensive experimental and theoretical studies on spinodal decomposition have been reported based on either UCST or LCST behavior. Controlling the LCST/UCST phase boundary is of practical importance because the quench depth (distance in temperature into the two-phase region) is a determining factor governing the stability of these multiphase mixtures against macroscopic phase separation. There are a number of studies focusing on the addition of block copolymers or block copolymers formed in-situ in suppressing the spinodal decomposition. Park *et al.* studied the late-stage coarsening behavior of PS/PB blends in the presence of PS-*b*-PB block copolymers. The block copolymer retarded the coarsening rate and the extent of retardation increased with increasing amounts of block copolymer and upon increasing the molecular weight of the copolymer.¹³ The nature of the end groups of polymers is found to be another efficient factor which influences the phase diagram. Schacht *et al.* demonstrated that the incorporation of a fluorosilane group at the end of poly(styrene) (PS) chains shifted the phase diagram to higher temperature of the PS/poly(vinyl methyl ether) (PVME) resulting of the enhancement of the miscibility (LCST).¹⁴ Lee *et al.* showed that by varying the end group from methyl to amide attached to poly(dimethylsiloxane) (PDMS) the UCST of poly(isoprene) (PI)/PDMS decreases by 165 °C.¹⁵ Prusty *et al.* observed that the acid groups of poly(methyl methacrylate) (PMMA) can enhance the miscibility of PMMA/poly(styrene-*co*-acrylonitrile) (SAN), because of the additional interaction between acid groups and nitrile groups of SAN.¹⁶ It is also reported that a change of the phase diagram can be induced by nanofillers, which will be discussed in Section 1.2.

In this thesis, the phase behavior of the partially miscible and immiscible system is studied for two typical binary blends. For the immiscible blends, the structure development of

a mixture of homopolymer/block copolymer is also investigated because of the importance of the copolymer's microstructure.

1.1.2 The phase behavior of polymer blends with block copolymers

The phase behavior of block copolymers or their blends is the subject of extensive research over the last thirty years.¹⁷⁻²⁰ The unique properties of block copolymers arise from their ability to self-assemble into a variety of ordered structures with nanoscale periodicities via the process of microphase separation.^{19,20} In blends of a homopolymer with a block copolymer, there is an interplay between macrophase separation of the homopolymer/block copolymer and microphase separation of the block copolymer. The phase behavior of the blends is primarily governed by the length of the homopolymer chain compared to that of the copolymer. Depending on the degree of the polymerization of polymer A in both the homopolymer N_{Ah} and the copolymer N_{Ac} , Hashimoto and Winey identified three regimes as illustrated in Figure 1.1.²¹⁻²⁶

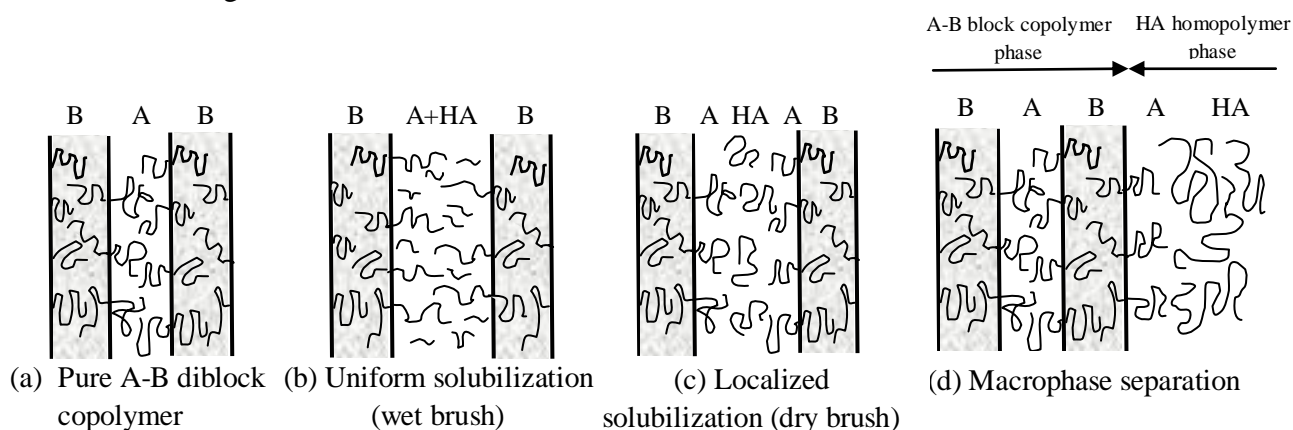


Figure 1.1: The phase behavior of block copolymers is governed by the length of the homopolymer chains (N_{Ah}) relative to the miscible block (N_{Ac}).

If $N_{Ah} < N_{Ac}$, the homopolymer A tends to be selectively solubilized in the A domains of the microphase-separated block copolymer and is thus weakly segregated towards the domain centre. This regime has been termed ‘wet brush’, as shown in Figure 1.1b, because the copolymer chains in the strong segregation limit can be considered to be polymeric brushes and in this case they are ‘wetted’ by the penetration of homopolymer chains. If $N_{Ah} \sim N_{Ac}$, the homopolymer is still selectively solubilized in the A-block microdomains. However, it does not significantly swell the A block chains and tends to be more localized in the middle of the A-block microdomains as shown in Figure 1.1c. The conformations of the B chains are not

significantly perturbed. This is the ‘dry brush’ regime. If $N_{Ah} > N_{Ac}$, macrophase separation occurs (Figure 1.1d) with the domains of microphase-separated block copolymer in the homopolymer matrix. Depending on the architecture of the block copolymer, microstructures of all sorts, such as spheres, cylinders, wormlike, vesicles, can be formed in the matrix with or without a long range order, which is determined by the block copolymer concentration and the polydispersity.

Considering that unique properties of polymer blends are directly attributed to the presence of structures with dimensions in the range of nanometer, nanostructured polymer blend systems have become increasingly important, especially in block copolymer blends with homopolymers.^{8,27} Nanostructured polymer blends refer to the systems that the scale of the dispersed polymer is below 100 nm. The effect of nanoscale morphology in a polymer blend will be further discussed.

1.1.3 Relation between morphology and mechanical properties

Since polymers are often used as construction materials, the mechanical performance under high loading is, therefore, a general requirement for successful application of their products. As a consequence, toughness (impact property) enhancement has been subject of many studies and great attention has been paid to reveal the fundamentals of different toughening mechanisms.^{8, 28}

It has been well known for many years that the fracture toughness of thermoplastics can be improved up to one order of magnitude by incorporation of a certain amount of elastomer (rubber toughening).²⁸ The impact modification by rubber toughening involves the incorporation of 3 to 20 vol% rubber in rigid polymeric materials such as glassy thermoplastics, semi-crystalline thermoplastics, and thermosets.⁸ An enhanced toughness can be achieved when delocalization of the strain occurs in the rubbery domains, arising from cavitation in the rubbery phase. This helps to weaken the rubber particle’s resistance to deformation, thereby initiating yielding of the matrix at reduced stress and allowing the particles to cold draw. Further stretching of the rubber fibrils within the cavitated particles results in an increased strain hardening.

The major disadvantage of the rubber modification of thermoplastics is the loss in stiffness.²⁸ To keep or improve the stiffness, optimization of rubber toughening should be carried out: low rubber content (less than 10 wt%), nanosized rubber particles, small interparticle distance and good adhesion between the rubbery particles and the matrix.⁸ The

size of the rubbery particles should thus be kept as small as possible in order to keep the volume fraction of rubber low (to preserve the modulus and yield stress) and for optical clarity. The critical interparticle distance should be that small that no craze initiation can occur. However, a drawback of a smaller dispersed rubber phase is their increased difficulty to cavitate.^{29,30} The ultimate toughness modifier thus is to use precavitated nanosized rubber particles.³¹⁻³³ Jansen *et al.* modified brittle PMMA with (aliphatic) epoxy and obtained an extremely small dispersed phase in the order of 30 nm.³⁴ The system was pre-deformed under a low deformation rate to achieve precavitation of the rubbery phase. The samples proved to be tough. Van Casteren and Kierkels^{32,33} introduced self-assembly of a tri- or diblock copolymer in brittle amorphous polymer PS/PMMA matrix in order to form a nanosized precavitated rubbery phases. The precavitated particles consist of a rubber shell and an easily cavitated (semi-crystalline) core-forming block that shrinks upon crystallization. The proposed morphology for optimal toughening, a nanosized core-shell structure which contains an easily cavitating core and a rubber shell, is schematically depicted in Figure 1.2. Meijer and co-workers validated a theoretical prediction for optimal toughening that a homogeneous distribution of easily cavitating rubber particles of approximately 30 nm would induce a transition from crazing to shear yielding (in case of glassy matrices).^{35,36}

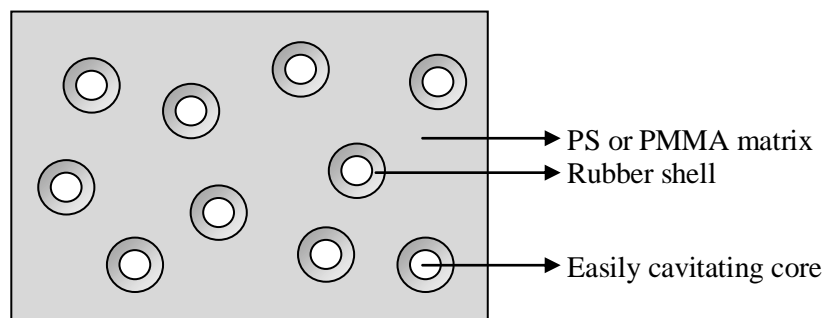


Figure 1.2: Proposed morphology for optimal toughening: precavitated nanosized core shell morphology.

In this thesis, the controlled nanostructure of polymeric matrices by the self-assembly of a linear ABC/ABA triblock copolymer was prepared and studied using different blending methods with the addition of silica nanoparticles.

1.2 Effect of particles on the phase behavior of polymer blends

Composite materials may consist of mixtures of several components, not only different polymers, but also plasticizers, stabilizers, and organic/inorganic particles. In recent years, it has been recognized that small fractions of nanometer-sized particles can impart performance

enhancements above what is achieved with conventional micrometer-sized particles.^{7, 37-41} This comes from the large specific surface area of nanoparticles, which can drastically change processibility,^{40,41} modulus,⁴² impact strength, physical aging,⁴³ and conductivity.⁴⁴ In addition, one significant advance of nanoparticles is found in the processing of polymer blends: they can be used as a compatibilizer to arrest domain coarsening or stabilize evolving morphologies. However, the effects of nanoparticles on the overall phase behavior and performance of the polymer blends need further study.

1.2.1 Nanoparticles in the partially miscible polymer blends: effect on phase behavior and kinetics of phase separation

Recently, it was shown that the addition of nanoparticles to partially miscible polymer blends leads to astonishing behavior, such as increasing or decreasing the temperatures of phase separation, modifying the shape of the phase diagram or changing the kinetics of phase separation.⁴⁵⁻⁵⁰

Depending on the interaction between nanoparticles and polymer blends, the phase boundary can be shifted either up or down.^{45,46} Lipatov and co-workers investigated, with the addition of silica nanoparticles, chlorinated poly(ethylene)/poly(ethylene-*co*-vinyl acetate) (EVA) blends and observed either an increase or decrease of the temperature of phase separation depending on the particles concentration.⁴⁷ One of the explanations is related to specific interactions and preferential adsorption on the filler by one of the components of the blend.⁴⁹ Another probable reason is the possible selective adsorption of low (or high) molar mass fractions to the nanofiller surface which modifies the local molar mass distribution.^{47,48}

In the case of phase separation kinetics, Composto and co-workers showed experimentally that the addition of silica nanoparticles slowed down the phase separation process in PMMA/SAN blends.^{49,50} This was explained by an increased viscosity of the PMMA-rich phase induced by the migration of nanoparticles to this phase. In the PS/PVME blend studied by Gharachorlou *et al.*, the fumed silica segregated in the PVME-rich phase during phase separation and acted as an obstacle to the coarsening of the morphology.⁵¹

Furthermore, Ginzburg and co-workers developed a model to show that the addition of nanoparticles can either promote or hinder demixing of two polymers, which depends on the particle radius R_p and the degree of polymerization N .⁵² Meanwhile, the shape and the location of the spinodal curve can be influenced by the size of nanoparticles R_p . If $R_p < R_g$ (the radius of gyration of the macromolecule), the addition of the nanoparticles stabilizes the

homogeneous region because they reduce the number of unfavorable polymer/polymer interaction and therefore decrease the enthalpy of the blend. If $R_p \gg R_g$, even very small amounts of nanoparticles can induce the particle-rich phase segregation from the blend.

1.2.2 Nanoparticles in immiscible polymer blends

From an industrial point of view, blends of immiscible polymer blends are of great interest.⁶ The major challenging difficulty of immiscible blends is to overcome the inherent immiscibility of polymers to allow for nanometer-sized domains of the dispersed phase. The use of nanofillers can have a large impact on the morphology of the immiscible polymer blends.

Adding solid particles in immiscible polymer blends is a traditional technique in rubber and thermoplastic processing. Originally, the purpose of adding particles in blends was obviously an applicative objective like obtaining high electrical conductivity or improving the mechanical properties.⁶ Since the typical size of classical particles (calcium carbonate, talc, silica) was of the same order of magnitude or greater than the size of the dispersed polymer phase, these particles were not found to interfere significantly with the blend morphology. The development of nanosized particles like carbon black were later extended to influence the compatibilization of a blend, which mainly aims to minimize the proportion of conductive additives needed to induce electrical conductivity.^{53,54} Recent investigations on the effects of nanoparticles in immiscible mixtures focus on using the particles to stabilize morphologies or arrest the domain coarsening. In addition, to control the blend morphology includes not only the shape and size of the dispersed polymer domains, but also the state of dispersion and the distribution of the particles.

1.2.2.1 Selective localization of nanoparticles in polymer blends

In the majority of blends, the nanoparticles distribute unequally between the polymer phases. This selective localization of nanoparticles in polymer blends is affected by parameters such as the interactions between nanoparticles and polymers, compounding procedures, and the viscosity ratio of polymers.

The physical interactions between the surface of the nanoparticles and the polymer components are key to control the localization of nanoparticles in polymer blends. The uneven particle distribution between different polymer phases depends on the balance of

interfacial energies and can be predicted by calculating the wetting parameter, ω_{12} (Equation 1.1), if kinetic effects do not interfere.⁶

$$\omega_{12} = \frac{\gamma_{S-2} - \gamma_{S-1}}{\gamma_{12}} \quad (1.1)$$

where γ_{S-i} is the interfacial tension between the nanoparticle and polymer i , γ_{12} is the interfacial tension between two polymers. If $\omega_{12} > 1$, the particles are only present in polymer 1, while $\omega_{12} < -1$, they are only found in polymer 2. If $-1 < \omega_{12} < 1$, the particles are concentrated at the interface between two polymers. The last case corresponds to $|\gamma_{S-2} - \gamma_{S-1}| < \gamma_{12}$ which is more likely to occur in polymer blends with a high degree of incompatibility or when the differences in the filler/polymer interactions are small.

Equation 1.1 has been successfully applied to different polymer blends, such as silica particles dispersed in poly(propylene) (PP)/PS and PP/EVA by Elias *et al.*,^{55,56} carbon black dispersed in poly(ethylene) (PE)/PP and PP/PMMA by Sumita *et al.*,^{57,58} and EVA/PLA filled with carbon black by Katada *et al.*⁵⁹ However, the calculation was performed at room temperature. The surface tension of polymers in molten state can be different from that in solid state. For that, Elias *et al.* corrected their data with help of the expression proposed by Guggenheim.⁶⁰

In addition to the physical interactions, the final equilibrium of the distribution of nanoparticles is influenced by the mixing process. The order of addition of the components is of importance and can have a strong effect on the kinetics because it has a direct influence on the medium with which the particles will be in contact during the course of its incorporation. The simplest procedure and the most reported in literature is to add the components simultaneously into a mixer in the molten state. The mixing of nanoparticles and polymers, evolution of morphology of the polymer blend together with the dispersion and migration of the nanoparticles inside the molten material occur concurrently. However, in this case, the nanoparticles may be incorporated in the polymer which has a lower melting temperature than the other, even though they do not have better affinity. An alternative is to incorporate the nanoparticles into the first polymer and then introducing the second polymer. In all cases, the nanoparticles may also have a chance to transfer from one phase to the other to reach its equilibrium distribution depending on affinity. The easiest way to highlight the existence of particle mobility inside a blend is to incorporate the solid particles in the polymer which has a lower affinity with the nanoparticles, and then to add the other polymer. Elias *et al.* studied the selection of silica nanoparticles in the PP/PS blend using different compounding

procedures. It was found that all the hydrophilic silica transferred from the PP phase with which it has lower affinity to the PS phase.⁵⁵ Chung *et al.* presented a systematic study of partitioning of silica nanoparticles into the PMMA-rich phase during phase separation of a PMMA/SAN blend.^{49,50} Pötschke *et al.* incorporated multiwall carbon nanotubes (MWNTs) into poly(carbonate) (PC)/SAN blends, and MWNTs preferred to be in the PC phase, independent of the blending procedures.⁶¹ A series of studies was carried out by Gubbels *et al.* and they introduced carbon black in PS/PE blend to obtain electrical conductivity. It was observed that if mixing was stopped at certain time when the solid particles were transferring from one phase to the other, the particles would remain at the interface upon cooling the blend.⁶²

The viscosity ratio of two polymers plays a dominant role on the localization of the nanoparticles in polymer blends. Feng *et al.* studied the effects of viscosity ratio based on PP/PMMA/carbon black blends, in which PMMA is the minority phase, and these three components were added at the same time in the mixer. PMMA with three different molar masses were used, while the molar mass of PP was constant. Based on the calculated ω_{12} , the carbon particles should be dispersed in the PMMA phase. However, the confinement of carbon black in the PMMA phase was only attained in the system where the viscosity ratio of PP and PMMA was close to 1.⁶³ Persson *et al.* hypothesized that the viscous ratio effects were weak and dominated only when the difference of interactions between polymer 1/filler and polymer 2/filler was small.⁶⁴

1.2.2.2 Compatibilization effect of nanoparticles

The compatibilization of immiscible polymer blends is most often achieved by adding block copolymers.⁸ The localization of the block copolymer at the interface decreases the interfacial energy which can lead to an improved dispersion and the interfacial adhesion between two immiscible polymers. An efficient compatibilization results in a reduction of the characteristic size of the polymer domains, their stabilization against processing or annealing, and thus good mechanical properties. In addition, a newly explored compatibilization method is to use inorganic nanoparticles due to their large specific surface area. The first reported nanoparticles utilized as a compatibilizer is carbon black dispersed in elastomers.⁶⁵ Studies have also been carried out using silica particles and layered silicates acting as compatibilizing agents in immiscible polymer blends.⁶ The most pronouncing compatibilizing effect can be achieved when the particles are present at the interface between two polymer phases.^{55, 66}

Numerous experimental works confirm the compatibilizing effect of nanoparticles on binary polymer blends, while several interpretations are proposed. Fenouillot *et al.* summarized several possibilities: i) a reduction of the interfacial energy induced by the nanoparticles, ii) the inhibition of coalescence by the presence of a solid barrier (the nanoparticles) around the minor polymer drops,⁶⁷ iii) the increase of the viscosity of the phases due to an uneven distribution of the fillers,⁶⁸ iv) the immobilization of the dispersed drops (or of the matrix) due to the formation of a physical network of nanoparticles when the concentration of solid is above a certain threshold value, and v) the steric hindrance caused by the strong interaction of polymer chains onto the solid particles.⁶

Distinguishes between these potential mechanisms are difficult due to the lack of models and experimental works with the objective to separate the related parameters (thermodynamic effects, kinetic effects, particle localization, and transfer of particles). Furthermore, the viscosity evolution of the phases, which is related to the local filler concentration and (time dependent) state of dispersion or exfoliation, is very complex.

The stability of the morphology is another important aspect in the development of new materials. Most of the time, the experiment consists in annealing the samples and observing the morphology after several hrs at high temperature. Gubbels *et al.* studied the PE/PS 45/55 co-continuous blends.⁵⁴ The morphology coarsening was found to be reduced when the amount of carbon black was above 2 wt%.

1.2.2.3 Nanoparticles in block copolymer blends

Considering that the microphase separation of the copolymer can direct the spatial distribution of nanoparticles and thereby develop functional hybrid materials, the organization of nanoparticles within self-assembled block copolymers has attracted substantial attention. Abundant efforts have devoted to use block copolymers as scaffolds to arrange nanoscopic elements spatially to tailor electrical, magnetic, or photonic properties of materials.⁶⁹ Meanwhile, nanoparticles can also interact with block copolymers, and thus alter both the orientation and morphology of the block copolymer microdomains.⁷⁰⁻⁷²

Theories and experiments imply that the spatial distribution of nanoparticles in the microphase-separated morphologies can be controlled by tailoring the nanoparticle ligands and varying the size of the nanoparticles R_p relative to the radius of gyration of the polymer R_g .^{73, 74} Polymer chains stretch around the solid nanoparticles, leading to a loss in conformational entropy, which increases with R_p . In the absence of specific interactions, the

larger nanoparticles are expelled from the bulk of the copolymers, whereas the smaller particles are still inside the bulk. The spatial distribution of nanoparticles and the global structure of the particle-filled systems are thus affected. Thompson *et al.* predicted that larger A-like particles, i.e., particles that are compatible with the A blocks of AB copolymers, are localized at the center of the A microdomains, whereas smaller particles are more uniformly dispersed within a specific microdomain.⁷³ Lee *et al.* used theory and computational modeling to show that, at a fixed diblock composition, interaction energies, and particle volume fractions, an increase in particle size was sufficient to transform a lamellar morphology into a cylindrical morphology.⁷²

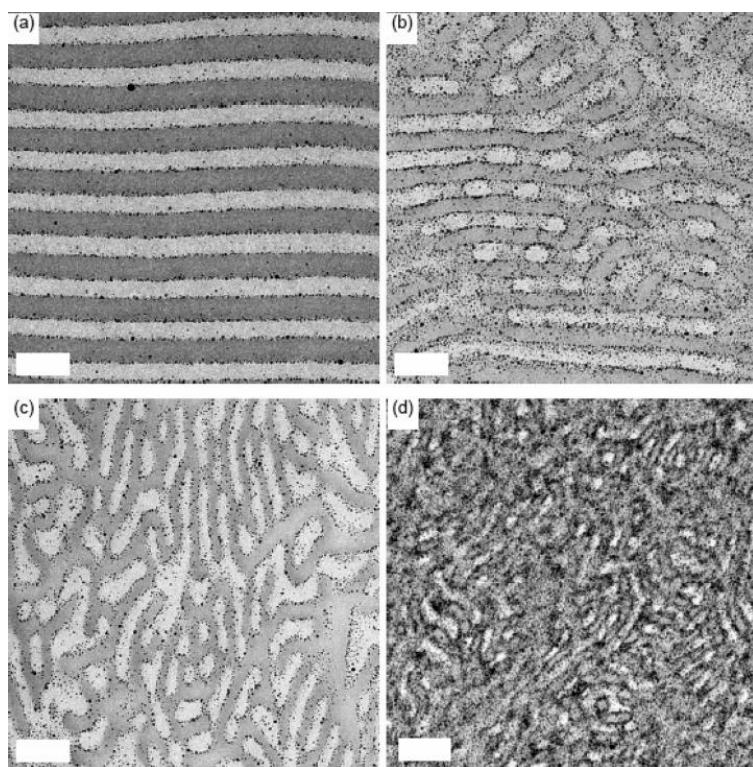


Figure 1.3: TEM images of PS-*b*-P2VP block copolymer containing PS-Au 0.92 nanoparticles at various nanoparticle volume fractions: (a) 0.04, (b) 0.07, (c) 0.09, and (d) 0.28. The scale bar is 100 nm. The gold nanoparticles (dark dots) segregated at the interfaces between the PS and P2VP domains.⁷⁵

By varying not only size but also the surface chemistry of the particles, the nanoparticles placements within a block copolymer matrix as well as the structures around the nanoparticles can be well tailored. Fredrickson and co-workers treated the surfaces of nanoparticles to promote strong binding to the A/B interfaces of AB diblock copolymer, which reduced interfacial energies.⁷⁵ The transition from lamellar to bicontinuous

morphology was observed with increasing the volume fractions of nanoparticles, see Figure 1.3. A similar phenomenon was detected by Kramer and co-workers. They used thiol-terminated polymers on gold nanoparticles to create ‘neutral’ or nonselective particles that localized at the interface between the PS and poly(2-vinylpyridine) (P2VP) microdomains.⁷⁶

In summary, nanoparticles can be patterned over large areas with nanoscale precision and selectivity in block copolymer and their related polymer blends. In this thesis, this organizational ability is verified via a block copolymer with a homopolymer (matrix).

1.2.3 Control of the dispersion of nanoparticles

One of the key limitations in the large-scale production and commercialization of nanocomposites is the absence of cost-effective methods for controlling the state of dispersion of the nanoparticles in polymeric matrices. Without proper dispersion and distribution of the fillers, the high surface area is sheltered, and the formation of the aggregates can limit properties. Processing techniques which are effective on the nanoscale yet are applicable to macroscopic processing, need to be established.

There are three general ways of dispersing nanoparticles in polymers.⁵ The first one is the direct mixing of the polymers and nanoparticles either as discrete phase or in solution. This method takes advantage of well-established polymer processing techniques. The drawback is that only a smaller amount of nanoparticles can be dispersed successfully. Furthermore, the viscosity might increase rapidly with the addition of nanoparticles, which in turn can limit the feasibility of this processing method. The limitations of the melt viscosity can be overcome via solution processing. The solution can then be cast into a film or be isolated from solution by solvent evaporation or precipitation. In this case, the intrinsic property of the solvent as well as the removal of solvent afterwards affects the state of dispersion of the nanoparticles strongly. The major disadvantage of the solution method is the removal of solvent.

The second method to disperse nanoparticles in polymer is in-situ polymerization in the presence of nanoparticles. Here, nanoscale particles are dispersed in the monomer or monomer solution, and the resulting mixture is polymerized by standard polymerization methods. The key to in-situ polymerization is an appropriate dispersion of the filler in the monomer.

The third is in-situ formation of nanoparticles in the polymer matrix. The typical method of in-situ formation of the nanoparticles is in-situ sol-gel reaction, which allows versatile accesses to chemically designed organic-inorganic hybrid materials.

In this thesis, the direct mixing and in-situ polymerization methods were used and compared.

1.3 Choice of systems and experimental approaches

Since the polymer blends are classified into different categories based on their miscibility, the effect of silica nanoparticles on the morphology of the blends could be different. Therefore, this silica nanoparticles study is separated into two parts, i.e. the effect on partially miscible polymer blends and the effect on immiscible polymer blends.

PMMA/SAN was chosen as a partially miscible blend with LCST behavior because of sufficient contrast between two polymers, which is suitable for small-angle light scattering (SALS) experiments, and a similar glass transition temperature between both polymers, meaning that the differences in mobility are marginal.

PC/PMMA was chosen as an immiscible blend, when it is prepared by melt-mixing, since it is one of the amorphous engineering thermoplastics with a wide variety of applications.

PMMA/poly(styrene)-*b*-poly(butadiene)-*b*-poly(methyl methacrylate) (SBM), PS/SBM, PMMA/poly(methyl methacrylate)-*b*-poly(butyl acrylate)-*b*-poly(ϵ -caprolactone) (MBC) were chosen as the immiscible polymer blends which contain block copolymers since unique properties could be brought from block copolymers due to their ability to self-assemble into a variety of nanoscale ordered structures via the process of microphase separation.

The silica nanoparticles were chosen since they are commercially available and can be purchased either in the form of powder or suspensions. The surface of the hydrophilic silica nanoparticles are covered with methyl and hydroxyl groups. The hydrophobic silica nanoparticles has a surface treated with methacrylsilane or dimethyldichlorosilane. There is no further surface modification in this thesis.

Both partially miscible polymer blends and immiscible polymer blends were blended with silica nanoparticles via different preparation methods, i.e. solvent casting, melt-mixing and in-situ polymerization.

1.4 Scope and outline of the thesis

The aim of this thesis is to control the morphology of the binary polymer blends via the addition of silica nanoparticles. The first part of this thesis is the silica effect in homopolymer blends which include partially miscible and immiscible blends. The second part is focused on the silica effect in immiscible polymer blends which contain block copolymers.

Chapter 2 describes the partially miscible PMMA/SAN polymer blend. Attention is paid to the effect of silica nanoparticles on phase separation kinetics and the phase diagram based on SALS experiments and a rheological study.

Chapter 3 focuses on the selective localization of silica nanoparticles in the binary polymer blend PC/PMMA, which is dependent on the interaction between the silica surface and polymer chains. The morphology of the blend is influenced by the silica nanoparticles and is investigated by TEM and rheological analysis.

In Chapter 4, the PMMA homopolymer was blended with SBM triblock copolymer and the effect of silica nanoparticles on its morphology is discussed. In this study, macrophase separation can be avoided and a co-continuous morphology can be stabilized by the silica nanoparticles.

Chapter 5 studies the different effects of silica nanoparticles, based on their selective localization, on the morphology of the polymer blend with block copolymers, containing PS and the triblock copolymer SBM.

Chapter 6 studied the blends of PMMA toughened by the triblock copolymer MBC with a crystallizable block. The influence of silica nanoparticles on the morphology and thermal behavior of the blend is discussed, which is related to the crystallizable block.

In this study, the effect of silica nanoparticles on the morphology of binary polymer blends is observed in both partially miscible and immiscible blends. Depending on the selective distribution of the nanoparticles, different effects can be found and particles can be used as a smart additive. Except controlling morphology of the polymer blends, the specific particles can also be applied into a multilayer blend to functionalize the variable properties of the final products.

1.5 References

- ¹ Utracki, L. A., *Polymer blends handbook*, Academic Publishers, Dordrecht, the Netherlands, **2002**.
- ² Paul, D. R., Newman, S., *Polymer blends*, Academic Press, New York, **1978**.
- ³ Utracki, L. A., *Commercial polymer blends*, Chapman & Hall, London, **1998**.
- ⁴ Paul, D. R., Robeson, L. M., *Polymer*, **2008**, 49, 3187-3204.
- ⁵ Ajayan, P. M., Schadler, L. S., Braun, P. V., *Nanocomposite science and technology*, Wiley-VCH, **2003**.
- ⁶ Fenouillot, F., Cassagnau, P., Majeste, J. C., *Polymer*, **2009**, 50, 1333-1350.
- ⁷ Balazs, A. C., Emrick, T., Russell, T. P., *Science*, **2006**, 314, 1107-1110.
- ⁸ Harrats, C., Thomas, S., Groeninckx, G., *Micro- and nanostructured multiphase polymer blend systems: Phase morphology and interfaces*, CRC Press, Taylor & Francis Group, **2006**.
- ⁹ Galloway, J. A., Koester, K. J., Paasch, B. J., Macosko, C. W., *Polymer*, **2004**, 45, 423-428.
- ¹⁰ Lyngaae-Jorgensen, J., Utracki, L. A., *Polymer*, **2003**, 44, 1661-1669.
- ¹¹ Pötschke, P., Paul, D. R., *J. Macromol. Sci. Part C: Polymer Reviews*, **2003**, C43, 87-141.
- ¹² Macosko, C. W., Guegan, Ph., Khandpur, K., Nakayama, A., Marechal, Ph., Inoue, T., *Macromolecules*,

- 1996, 29, 5590-5598.
- ¹³ Park, D. W., Roe, R. J., *Macromolecules*, **1991**, 24, 5324-5329.
- ¹⁴ Schacht, P. A., Koberstein, J. T., *Polymer*, **2002**, 43, 6527-6534.
- ¹⁵ Lee, M. H., Fleischer, C. A., Morales, A. N., Koberstein, J. T., Koningsveld, R., *Polymer*, **2001**, 42, 9163-9172.
- ¹⁶ Prusty, M., *De-black boxing of reactive blending: An experimental and computational approach*, Ph.D. Thesis, TU/e, Eindhoven, the Netherlands, **2006**, Chapter 5.
- ¹⁷ Bates, F. S., Fredrickson, G. H., *Ann. Rev. Phys. Chem.*, **1990**, 41, 525-557.
- ¹⁸ Muller, A. J., Balsamo, V., Arnal, M. L., *Adv. Polym. Sci.*, **2005**, 190, 1-63.
- ¹⁹ Abetz, V., Simon, P. F. W., *Adv. Polym. Sci.*, **2005**, 189, 125-212.
- ²⁰ Hamley, I. W., *The Physics of Block copolymers*, Oxford University Press, Oxford New York, **1998**.
- ²¹ Hashimoto, T., Koizumi, S., Hasegawa, H., Izumitani, T., Hyde, S. T., *Macromolecules*, **1992**, 25, 1433-1439.
- ²² Hashimoto, T., Yamasaki, K., Koizumi, S., Hasegawa, H., *Macromolecules*, **1993**, 26, 2895-2904.
- ²³ Koizumi, S., Hasegawa, H., Hashimoto, T., *Macromolecules*, **1994**, 27, 7893-7906.
- ²⁴ Winey, K. I., Thomas, E. L., Fetters, L. J., *Macromolecules*, **1991**, 24, 6182-6188.
- ²⁵ Winey, K. I., Thomas, E. L., *J. Chem. Phys.*, **1991**, 95, 9367-9375.
- ²⁶ Kinning, D. J., Thomas, E., Fetters, L. J., *J. Chem. Phys.*, **1989**, 90, 5806-5825.
- ²⁷ Sumpter, B. G., Noid, D. W., Barnes, M. D., *Polymer*, **2003**, 44, 4389-4403.
- ²⁸ Bucknall, C. B., *Toughened plastics*, Applied Science Publishers Ltd., London, **1977**.
- ²⁹ Bucknall, C. B., Karpodinis, A., Zhang, X. C., *J. Mat. Sci.*, **1994**, 29, 3377-3383.
- ³⁰ Dompas, D., Groeninckx, G., *Polymer*, **1994**, 35, 4743-4749.
- ³¹ Jansen, B. J. P., Rastogi, S., Meijer, H. E. H., Lemstra, P. J., *Macromolecules*, **1999**, 32, 6283-6289.
- ³² Van Casteren, I. A., *Control of microstructures to induce ductility in brittle amorphous polymers*, Ph.D. Thesis, TU/e, Eindhoven, the Netherlands, **2003**.
- ³³ Kierkels, J. T. A., *Tailoring the mechanical properties of amorphous polymers*, Ph.D. Thesis, TU/e, Eindhoven, the Netherlands, **2006**.
- ³⁴ Jansen, B. J. P., Rastogi, S., Meijer, H. E. H., Lemstra, P. J., *Macromolecules*, **2001**, 34, 3998-4006.
- ³⁵ Jansen, B. J. P., Rastogi, S., Meijer, H. E. H., Lemstra, P. J., *Macromolecules*, **2001**, 34, 4007-4018.
- ³⁶ Jansen, B. J. P., Rastogi, S., Meijer, H. E. H., Lemstra, P. J., *Macromolecules*, **1999**, 32, 6290-6297.
- ³⁷ Kim, B. J., Fredrickson, G. H., Hawker, C. J., Kramer, E. J., *Langmuir*, **2007**, 23, 7804-7809.
- ³⁸ Bansal, A., Yang, H., Li, C., Cho, K., Benicewicz, B. C., Kumar, S. K., Schadler, L. S., *Nat. Mater.*, **2005**, 4, 693-698.
- ³⁹ Rittigstein, P., Priestley, R. D., Broadbelt, L. J., Torkelson, J. M., *Nat. Mater.*, **2007**, 6, 278-282.
- ⁴⁰ Tuteja, A., Duxbury, P. M., Mackay, M. E., *Macromolecules*, **2007**, 40, 9427-9434.
- ⁴¹ Jain, S., Goossens, J. G. P., Peters, G. W. M., Van Duin, M., Lemstra, P. J., *Soft Matter*, **2008**, 4, 1848-1854.
- ⁴² Theunissen, E., Overbergh, N., Reynaers, H., Antoun, S., Jerome, R., Mortensen, K., *Polymer*, **2004**, 45, 1857-1865.
- ⁴³ Rittigstein, P., Torkelson, J. M., *J. Pol. Sci. Part B: Pol. Phys.*, **2006**, 44, 2935-2943.
- ⁴⁴ Liu, J., Tanaka, T., Sivula, K., Alivisatos, A. P., Frechet, J. M. J., *J. Am. Chem. Soc.*, **2004**, 126, 6550-6551.
- ⁴⁵ Lipatov, Y. S., *Prog. Polym. Sci.*, **2002**, 27, 1721-1801.
- ⁴⁶ Lipatov, Y. S., *J. Macromol. Sci. Part B: Phys.*, **2006**, 45, 871-888.
- ⁴⁷ Lipatov, Y. S., Nesterov, A. E., Ignatova, T. D., Nesterov, D. A., *Polymer*, **2002**, 43, 875-880.
- ⁴⁸ Huang, Y., Jiang, S., Li, G., Chen, D., *Acta Mater.*, **2005**, 53, 5117-5124.
- ⁴⁹ Chung, H.-J., Ohno, K., Fukuda, T., Composto, R. J., *Macromolecules*, **2007**, 40, 384-388.
- ⁵⁰ Chung, H.-J., Fukuda, T., Deshmukh, R. D., Composto, R. J., *Europhys. Lett.*, **2004**, 68, 219-225.
- ⁵¹ Gharachorlou, A., Goharpey, F., *Macromolecules*, **2008**, 41, 3276-3283.
- ⁵² Ginzburg, V. V., *Macromolecules*, **2005**, 38, 2362-2367.
- ⁵³ Huang, J. C., *Adv. Polym. Technol.*, **2002**, 21, 299-313.
- ⁵⁴ Gubbels, F., Blacher, S., Vanlathem, E., Jerome, R., Deltour, R., Brouers, F., Teyssié, Ph., *Macromolecules*, **1995**, 28, 1559-1566.
- ⁵⁵ Elias, L., Fenouillot, F., Majeste, J. C., Cassagnau, P., *Polymer*, **2007**, 48, 6029-6040.
- ⁵⁶ Elias, L., Fenouillot, F., Majeste, J. C., Alcouffe, P., Cassagnau, P., *Polymer*, **2008**, 49, 4378-4385.
- ⁵⁷ Sumita, M., Sakata, K., Asai, S., Miyasaka, K., Nakagawa, H., *Polym. Bull.*, **1991**, 25, 265-271.
- ⁵⁸ Asai, S., Kazuya, S., Sumita, M., Miyasaka, K., *Polym. J.*, **1992**, 24, 415-420.
- ⁵⁹ Katada, A., Buys, Y. R., Tominaga, Y., Asai, S., Sumita, M., *Colloid Polym. Sci.*, **2005**, 284, 134-141.
- ⁶⁰ Elias, L., Fenouillot, F., Majeste, J. C., Martin, G., Cassagnau, P., *J. Polym. Sci. Part B: Polym. Phys.*, **2008**, 46, 1976-1983.
- ⁶¹ Goldel, A., Kasaliwal, G., Pötschke, P., *Macromol. Rapid Commun.*, **2009**, 30, 423-429.
- ⁶² Gubbels, F., Jerome, R., Teyssié, Ph., Vanlathem, E., Deltour, R., Calderone, A., Parenté, V., Brédas, J. L.,

- Macromolecules*, **1994**, 27, 1972-1974.
- ⁶³ Feng, J., Chan, C-M., Li, J-X., *Polym. Eng. Sci.*, **2003**, 42, 1058-1063.
- ⁶⁴ Persson, A. L., Bertilsson, H., *Polymer*, **1998**, 23, 5633-5642.
- ⁶⁵ Callan, J. E., Hess, W. M., Scott, C. E., *Rubber Chem. Technol.*, **1971**, 44, 814-837.
- ⁶⁶ Clarke, J., Clarke, B., Freakley, P. K., Sutherland, I., *Plast. Rubber Compos.*, **2001**, 30, 39-44.
- ⁶⁷ Kelnar, I., Khunova, V., Kotek, J., Kapralkova, L., *Polymer*, **2007**, 48, 5332-5339.
- ⁶⁸ Liu, Y., Kontopoulou, M., *Polymer*, **2006**, 47, 7731-7739.
- ⁶⁹ Zhang, Q., Xu, T., Butterfield, D., Misner, M. J., Ryu, D. Y., Emrick, T., Russell, T. P., *Nano Letters*, **2005**, 5, 357-361.
- ⁷⁰ Lee, J. Y., Shou, Z., Balazs, A. C., *Phys. Rev. Lett.*, **2003**, 91, 136103.
- ⁷¹ Lin, Y., Böker, A., Sill, K., Xiang, H., Abetz, C., Wang, J., Emrick, T., Balazs, A., Russell, T. P., *Nature*, **2005**, 434, 55-59.
- ⁷² Lee, J. Y., Thompson, R. B., Jasnow, D., Balazs, A. C., *Macromolecules*, **2002**, 35, 4855-4858.
- ⁷³ Thompson, R., Ginzburg, V., Matsen, M., Balazs, A. C., *Science*, **2001**, 292, 2469-2472.
- ⁷⁴ Lee, J. Y., Thompson, R. B., Jasnow, D., Balazs, A. C., *Phys. Rev. Lett.*, **2002**, 89, 155503.
- ⁷⁵ Kim, B. J., Fredrickson, G. H., Hawker, C. J., Kramer, E. J., *Langmuir*, **2007**, 23, 7804-7809.
- ⁷⁶ Kim, B. J., Bang, J., Hawker, C. J., Kramer, E. J., *Macromolecules*, **2006**, 39, 4108-4114.

Chapter 2

Effect of silica nanoparticles on the partially miscible polymer blend PMMA/SAN

The influence of silica nanoparticles on the LCST phase behavior and phase separation kinetics of a blend consisting of poly(methyl methacrylate) (PMMA) and poly(styrene-co-acrylonitrile) (SAN), was studied via a high-throughput experimentation (HTE) approach, which combines a composition (ϕ) and a temperature (T) gradient. The evolution of the phase separation process was studied by optical microscopy (OM), small-angle light scattering (SALS), transmission electron microscopy (TEM), and rheology. Depending on the specific interaction between the silica surface and the polymers, the distribution of silica particles during phase separation can be controlled to be either in one of the polymer phases or at the PMMA/SAN interface. The hydrophilic silica nanoparticles preferentially migrated to the PMMA phase due to the strong interaction of the hydroxyl groups on the surface of silica with the carbonyl groups of the PMMA, leading to a slow down of the coarsening rate and a lower phase separation temperature. The hydrophobic silica nanoparticles were localized at the PMMA/SAN interface, the inhibition of coalescence corresponds to the presence of a solid barrier (the nanoparticles) between the polymers prevent the coarsening process. A distinction of the slow-down effect between the two types of silica nanoparticles is that the slow-down effect of the hydrophilic silica particles is prominent in all stages of the phase separation, while the hydrophobic silica particles are mainly effective in the intermediate and late stages. This could be related to the movement of the hydrophobic particles towards the interface, which occurs in the early stage of the phase separation, therefore, only active during the intermediate and late stages of the phase separation.

2.1 Introduction

Blending of polymers is a convenient route to develop new materials with specific properties. However, most polymer pairs are immiscible and have a coarse morphology. It has been shown in numerous studies that the mechanical properties of polymer blends are highly dependent on the morphology and in many cases it has been shown that a finer morphology gives the best properties. Furthermore, because of the high interfacial tension for immiscible polymer blends, the interface thickness is small and adhesion between the two phases is relatively poor, which results in poor mechanical properties. Different compatibilization strategies have been developed to reduce the interfacial tension and suppress the coalescence, either by adding premade block copolymers or by in-situ formed block and graft copolymers, which resulted in much finer morphologies.

Apart from fully immiscible polymer blends, which comprise most of the used polymer pairs, and a very small number of polymer blends which are fully miscible over the entire composition range, a significant number of blends are partially miscible. They have attracted a lot of interest, because the morphology of partially miscible blends can be controlled by the mechanism and the kinetics of phase separation.¹ It is well known that the miscibility of this type of blends is only observed in a specific temperature and/or concentration window and two main types can be distinguished. Systems with a lower critical solution temperature (LCST) behavior display phase separation on increasing the temperature, while systems with an upper critical solution temperature (UCST) behavior display phase separation on decreasing the temperature. In both cases, phase separation may occur via two different mechanisms: binodal decomposition, for which the system is thermodynamically metastable, and spinodal decomposition, for which the system is thermodynamically unstable.

A large number of studies have been reported on the spinodal decomposition behavior of binary polymer blends having either UCST or LCST behavior. UCST systems such as poly(butadiene) (PB)/poly(isoprene) (PI) were studied by Hashimoto and coworkers,² and they showed that three stages of spinodal decomposition can be distinguished, i.e. early, intermediate and late stages. Similar studies were reported on spinodal decomposition of polycarbonate (PC)/poly(styrene-*co*-acrylonitrile) (SAN), poly(vinyl methyl ether) (PVME)/poly(styrene) (PS) and poly(methyl methacrylate) (PMMA)/SAN, all having a LCST behavior. From all these blends, the combination of PMMA and SAN is most suitable for experimentation, because the refractive index difference between PMMA and SAN is large enough to have sufficient contrast for small-angle light scattering measurements, the primary technique to study phase separation

kinetics, and both polymers have a similar glass transition temperature, meaning that the differences in mobility are marginal.

Recently, there is a considerable interest in studying the influence of nanoparticles on the phase separation of immiscible and partially miscible polymer blends.³⁻⁷ This interest is related to the large specific surface of nanoparticles, which can drastically change the bulk behavior of polymers and polymer blends at relatively low volume fractions of the nanoparticles.⁸⁻¹¹ Some studies showed that nanoparticles can shift the phase boundary of systems with a LCST or UCST behavior either up or down.¹²⁻¹⁴ Furthermore, some researchers found the nanoparticles can slow down the phase separation process between two polymers.⁸⁻¹¹ Nesterov *et al.* observed that the LCST curve of a poly(vinyl acetate)/PMMA blend was shifted to higher temperatures, i.e. the miscibility window is enlarged in the presence of nanoparticles.¹⁵ Composto and co-workers showed experimentally that the addition of silica nanoparticles slowed down the phase separation process in PMMA/SAN blends.^{5,11} This was explained by an increase of the viscosity of the PMMA-rich phase due to migration of the nanoparticles to this phase. In line with this study, Bose *et al.* showed that for PMMA/poly[(α -methyl styrene)-*co*-acrylonitrile] (P α MSAN) blends the coalescence can be suppressed to a large extent by the addition of multiwall carbon nanotubes (MWNT) and selective migration to one of the phases.⁹ Ginzburg and co-workers^{16,17} developed a model to demonstrate that the addition of nanoparticles can either promote or hinder demixing of two polymers depending on the particle radius R_p and the degree of polymerization N .

The miscibility of polymer blends is typically studied by light scattering techniques to determine the coexistence curve by cloud points.¹⁸ However, cloud-point measurements and the determination of phase domain sizes are generally time consuming. Therefore, fine tuning of the miscibility gap of polymer blends by small variations in the chemical structure of the blend components or molar mass (distribution) is highly impracticable. Because of the expected time reduction, combinatorial methods for the evaluation of the phase evolution of polymer blends have recently received more attention.¹⁹⁻²⁴

A convenient approach to study the miscibility of polymer blends is based on the preparation of composition-temperature (ϕ -T) gradient films, where one single film can provide extensive information on the phase diagram and the phase-separated morphology of the mixture.^{19,21,23} The main limitations of the currently reported techniques lie in the achievable ϕ range, which is typically from ~ 15-65 wt%, the reproducibility of the ϕ gradients, due to manual sampling and deposition methods, and the restriction to use polymers that dissolve at room temperature, which makes the preparation of ϕ gradients of most semi-crystalline polymers impossible.

Here, we used a high-throughput experimentation (HTE) setup for the preparation of ϕ -T gradient film libraries developed in our group,²³ which can rapidly screen the phase behavior of polymer blends, similar to the work of Amis and co-workers.^{19,21} The picture and scheme of this setup are shown in Figure 2.1 and the procedure for the preparation of ϕ -T gradient film libraries was described in the paper of l’Abee *et al.* by using blends of PMMA and SAN.²³ To enhance mixing of the two component solutions, we now replaced the dispersion tip by a static mixer with an internal volume of 50 μL , as shown in Figure 2.1(b). The composition of the library films was quantitatively determined by using Fourier-transform infrared (FTIR) spectroscopy by comparing the ratio of the integrated intensity of the absorption band of the phenyl stretching vibration of SAN at 698 cm^{-1} to the integrated intensity of the absorption band of the carbonyl stretching vibration of PMMA at 1740 cm^{-1} to a calibration curve.^{23,25} The experimental reproducibility of the composition gradient film is excellent, since the sampling and deposition processes are fully automated. The setup enables the preparation of ϕ -T gradients over the whole composition range and a linear temperature gradient between 25 and 300 $^{\circ}\text{C}$.

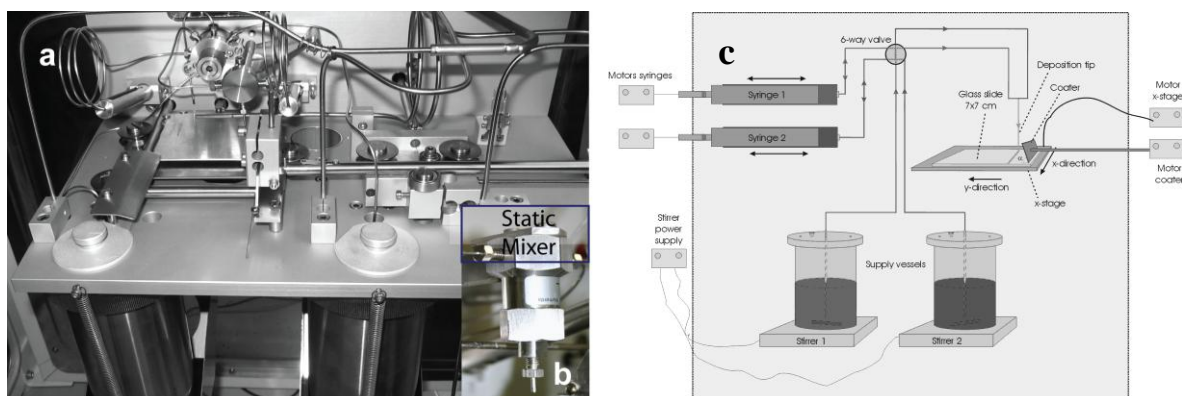


Figure 2.1: (a-b) Picture and (c) schematic representation of the HTE setup.

In this chapter, the HTE setup is used to study the effect of nanoparticles on the phase behavior and phase separation kinetics of partially miscible PMMA/SAN blends. In addition, the morphology development and different stages of phase separation at the composition of 70/30 PMMA/SAN were investigated by optical microscopy (OM), small-angle light scattering (SALS) and dynamic shear rheology.

2.2 Experimental

2.2.1 Materials

PMMA was provided by Arkema (France), with a number-averaged molar mass (M_n) of 42 kg/mol and a polydispersity index (PDI) of 2.1. Small amounts of ethyl acrylate (EA) are usually incorporated into PMMA to prevent unzipping of the polymer at elevated temperatures during processing. The PMMA used in this study contains 0.5 wt% EA. SAN with 28 wt% acrylonitrile (AN) was obtained from the Dow Chemical Company with a M_n and a PDI of 41 kg/mol and 2.2, respectively. Methyl ethyl ketone (MEK) was obtained from Sigma Aldrich and was used as received. Two types of silica nanoparticles were used. One is a pre-made hydrophilic colloidal silica nanoparticle with a diameter of 10-15 nm, dispersed in methyl ethyl ketone (MEK) with approx. 30 wt% silica, which was purchased from Nissan Chemical (USA) and a surface covered with methyl and hydroxyl groups^{11,26}. This hydrophilic silica nanoparticle will be referred to as MEK-ST in this thesis. The other silica particles are hydrophobic silica nanoparticles, Aerosil R7200, with a diameter of 12 nm, which were supplied by Evonik (Germany) and has a surface treated with methacrylsilane. This hydrophobic silica nanoparticle will be referred to as Si-R7200.

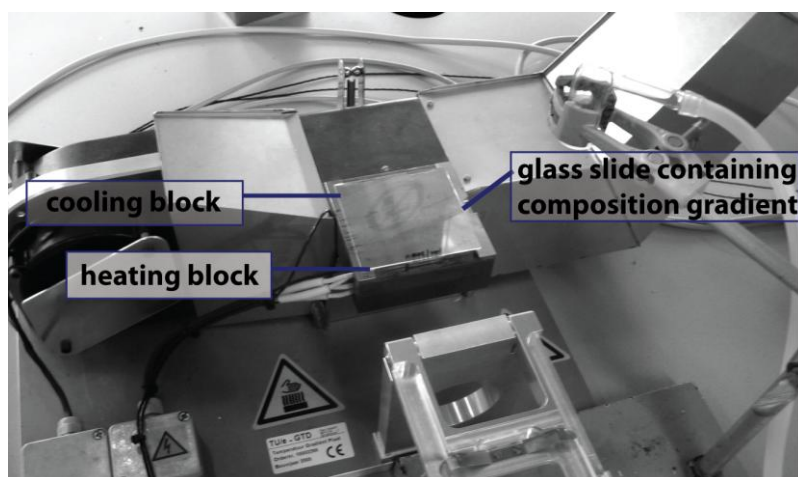


Figure 2.2: Picture of the temperature gradient heating stage.

2.2.2 Sample preparation

Solvent casting: HTE setup

The polymers and MEK-ST nanoparticles were dissolved separately in MEK and the two solutions were mixed and cast on a glass substrate with a size of 70 x 70 mm by the HTE setup, which is shown in Figure 2.1. For a detailed description of the film gradient preparation, see reference 23. The following settings for the HTE setup were used: a maximum syringe speed of

0.85 mm/s, a table speed of 5.5 mm/s and a coater speed of 10 mm/s. The distance and angle between the coater and the substrate were typically 200-600 μm and 75-85 $^\circ$, respectively. A dispersion delay time of 7 s was applied to compensate for the dead volume of the static micromixer. By using these settings, the whole film preparation takes less than 20 s and the thickness of the coating varied from 1.0 to 1.8 μm in the direction orthogonal to the ϕ -gradient.

A thin film with a ϕ -gradient was obtained after evaporating the solvent at room temperature for 24 hrs, followed by an additional drying step at 130 $^\circ\text{C}$ under reduced pressure with a low nitrogen flow for 24 hrs to ensure complete removal of the solvent. The PMMA/SAN ϕ -gradient films were treated on the T-gradient heating stage (Figure 2.2) with temperatures ranging from 200 to 290 $^\circ\text{C}$ for 10 min under a nitrogen flow and were subsequently quenched to room temperature.

Solvent casting: thick films for SALS

The thick films used for SALS measurement were prepared by solvent casting on a thin glass slide and a doctor blade was used to control the thickness of the film. The polymer concentration in the solution was approximately 25 wt%. The solvent-cast samples were put into a fume-hood at room temperature for 3 days followed by a drying step at 60, 100, 120 and 150 $^\circ\text{C}$ under reduced pressure with a low nitrogen flow for 5 more days to ensure complete solvent removal. The final thickness of the samples was between 20-30 μm .

Melt mixing

PMMA/SAN/MEK-ST or PMMA/SAN/Si-R7200 nanocomposites with different silica content were blended by using a twin-screw mini-extruder. The temperature was set at 185 $^\circ\text{C}$. The extruder was filled with 6 g of material. The screw speed was set at 35 rpm and the total mixing time was fixed at 10 min. All the experiments were performed under a nitrogen atmosphere in order to prevent oxidative degradation. Approx. 0.1 wt% processing stabilizer tris(2,4-ditert-butylphenyl)phosphate was added to the polymer powder before further processing. PMMA and SAN were dried under reduced pressure with a low nitrogen flow for 12 hrs at 120 $^\circ\text{C}$, before compounding. The silica nanoparticles were used without any further surface modification.

Compression molding

PMMA/SAN/silica nanocomposite sheets were prepared by using compression molding at 185 $^\circ\text{C}$ for 5 min at a pressure of 100 bars. Samples for rheological characterization (25 mm in diameter, 1 mm in thickness) and for parts of SALS measurement (100 μm in thickness) were prepared under these conditions. The films are still transparent after compression molding.

2.2.3 Characterization techniques

Optical microscopy (OM)

The morphologies of PMMA/SAN blends were analyzed with a Zeiss Axioplan 2 optical microscope equipped with an Axiocam digital camera. The phase contrast mode was used to obtain contrast between the phases. The images were recorded at a magnification of 32.

Transmission electron microscopy (TEM)

Morphological investigations were performed by using a Tecnai 20 transmission electron microscopy (TEM), operated at 200 kV. Ultrathin sections (50-70 nm) were obtained at room temperature by using a Leica Ultracut E microtome. Chemical staining of the sections was not required, since the electron density difference between two polymers is large enough and that of silica is much higher than that of polymers.

Thermogravimetric analysis (TGA)

A Q500 TGA (TA Instruments) was used for the quantitative determination of the silica content in the nanocomposites. Samples were heated under a pressed air atmosphere at 10 °C/min from 30 to 800 °C and held at 800 °C for 15 min. The residue was assumed to be only composed of silica.

Rheology

Dynamic shear measurements were performed on a stress-controlled AR-G2 rheometer (TA Instruments) by using a 25 mm parallel plate-plate geometry and disk-shaped specimens (25 mm in diameter; 1 mm in thickness). Frequency sweeps were performed in one sequence decreasing the frequency from 500 to 0.01 rad/s at a given temperature, with a constant strain of 1%, which was within the linear viscoelastic range. Dynamic temperature sweeps were carried out by measuring the storage and loss modulus at a fixed frequency (0.1 rad/s) and a uniform rate of heating (0.5 °C/min) from the homogeneous to the phase-separated region at a strain of 1%. All measurements were carried out under a N₂ atmosphere to prevent degradation or absorption of moisture.

Small-angle light scattering (SALS)

Small-angle light scattering (SALS) was used to follow the kinetics of phase separation. A 1 mW HeNe laser was used as incident light source and the light was guided through a pinhole collimator and the sample, of which the temperature was controlled by a Linkam THMS600 hotstage. The scattered light was projected on a semi-transparent poly(propylene) screen. The scattering patterns were captured with a 16 bit 512×512-CCD camera (Versarray: 512B Princeton CCD with a ST-133 controller), equipped with a Rodenstock Rodagon 50 mm f 1:2,8

lens with a variable focal distance. The CCD-camera was linked to a personal computer for data acquisition and analysis. The scattering angles were calibrated with a 100 lines/mm grid. The data acquisition time was typically 70 ms per image and was controlled by a home-made script running under V++ for Windows (version 4.0, Digital Optics Ltd). The scattering patterns were radially averaged using the V++ program.

Atomic force microscopy (AFM)

The AFM investigations were performed by using a Smena P47H microscope (NT-MDT Ltd, Moscow, Russia). The AFM was operated in semi-contact mode under an air atmosphere using a silicon cantilever (NSG 11 NT-MDT), which was coated with a gold layer for a higher laser beam reflectivity. The resonance frequencies applied were 115-190 kHz.

2.3 Results and Discussion

2.3.1 Structure development of PMMA/SAN blends

The phase behavior of PMMA/SAN blends as a model system was successfully mapped by the HTE setup. The phase diagram of PMMA/SAN blends obtained by the HTE setup shows the typically lower critical solution temperature (LCST)-phase behavior (Figure 2.3). After putting the composition gradient film on the temperature gradient for 10 min, the coexistence curve (i.e. the binodal curve) was obtained by visual inspection of the phase-separated film. It is well known that phase separation may occur via two different mechanisms: via spinodal decomposition if the system is thrust into the thermodynamically unstable region inside the dashed line in Figure 2.3 (representing the spinodal curve), or via binodal decomposition (also known as nucleation and growth) when the system is thrust into the thermodynamically metastable region between the dashes and solid lines in Figure 2.3.

In order to distinguish between the two phase separation mechanisms, six positions (a-f in Figure 2.3) were chosen and the morphology was studied by OM, of which the results are shown in Figure 2.4. The blend composition at positions a, b and c is very close to the critical composition of PMMA/SAN, which is around 70/30 for this system. Figures 2.4a-c show co-continuous morphologies indicative for spinodal decomposition at positions a-c and illustrate the effect of temperature on the phase separation kinetics, i.e. the characteristic length scale of the morphology increases with increasing temperature due to a larger quench depth and a higher mobility, similar to previous observations on this system.²⁷ Figures 2.4d-f show morphologies of spherical domains dispersed in a matrix reflecting the occurrence of binodal decomposition at positions d-f. At higher temperatures, the size of the spherical domains increases.

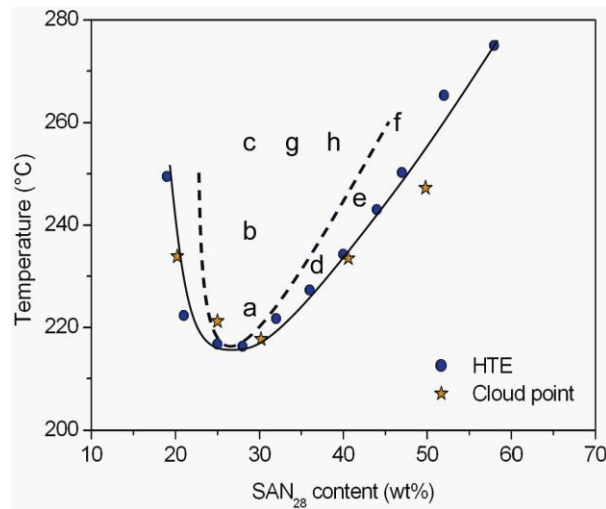


Figure 2.3: Phase diagram of PMMA/SAN obtained from ϕ - T gradient films as prepared with the HTE setup. The cloud points are reproduced.

The position of the border line between spinodal and binodal decomposition (indicated by the dashed line in Figure 2.3) can be calculated by the Flory-Huggins theory using spinodal conditions, but cannot be distinguished by these experiments, since a fixed time of 10 min is used for the phase separation process to take place on the temperature gradient setup. As mentioned, characteristic for the spinodal decomposition mechanism is that the phase separation process generally starts with concentration fluctuations around the initial concentration after a temperature jump into the spinodal region of the binary phase diagram. In the early stage, concentration fluctuations start to develop with different correlation lengths, which are related to the quench depth, but only the concentration fluctuations with a certain dominant correlation length continue to increase, while the concentration fluctuations with other correlation lengths damp out. In the intermediate stage, the concentration fluctuations with the dominant correlation length continue to grow, while also the correlation length increases: the structure coarsens. In the late stage, the correlation length still changes, but the concentration fluctuations have reached the equilibrium concentrations. If off-critical compositions are used, the initial stage of the spinodal decomposition is the same, but the intermediate and late stages become dominated by the interfacial tension and a change of the morphology from co-continuous to a matrix/dispersion morphology takes place. The final morphology is similar to that of blends demixed via binodal decomposition, as is apparent from Figures 2.4g and h, which show the matrix/dispersion morphology at positions g and h, which are at the same temperature as point c, but at varying compositions. Because of this breakdown behavior in spinodal decomposition under off-critical conditions, a distinction between the two different phase separation mechanisms cannot be made

with the HTE approach, even with changing the residence time of the sample on the temperature gradient heating stage. Small-angle light scattering (SALS) experiments can be used to determine the mechanism of phase separation. The details will be discussed in section 2.3.3.

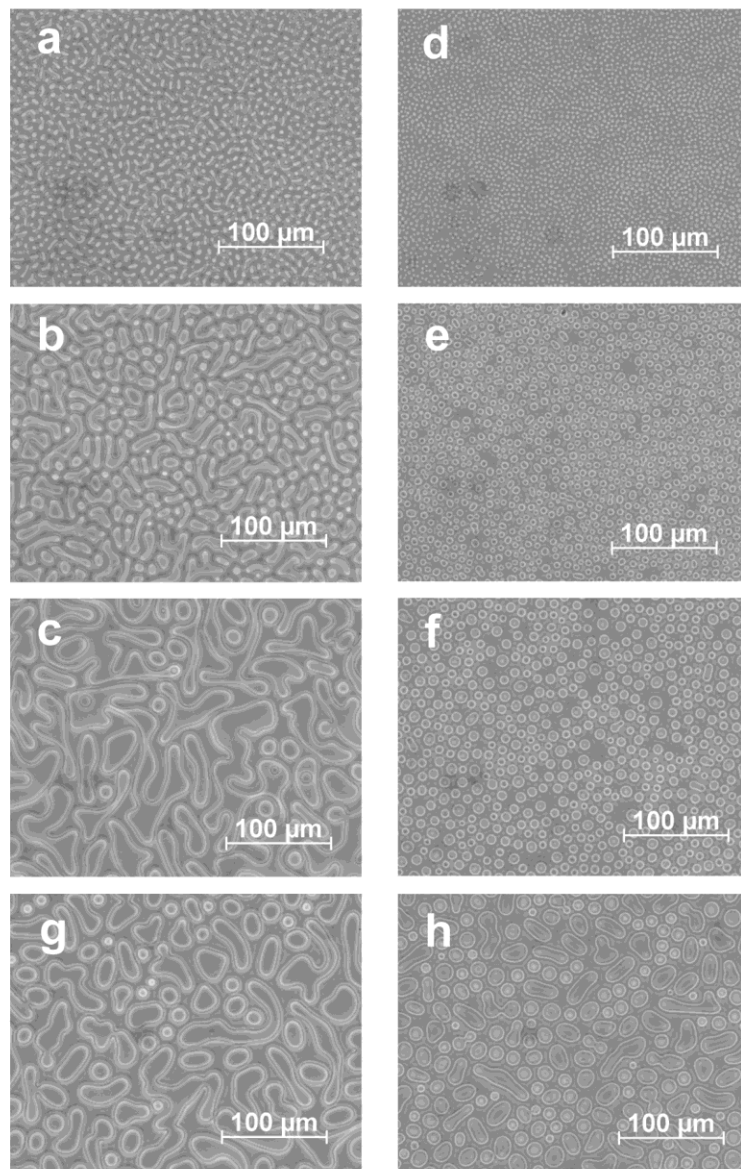


Figure 2.4: OM images of PMMA/SAN blends in the region of spinodal decomposition (a-c and g-h) and binodal decomposition (d-f).

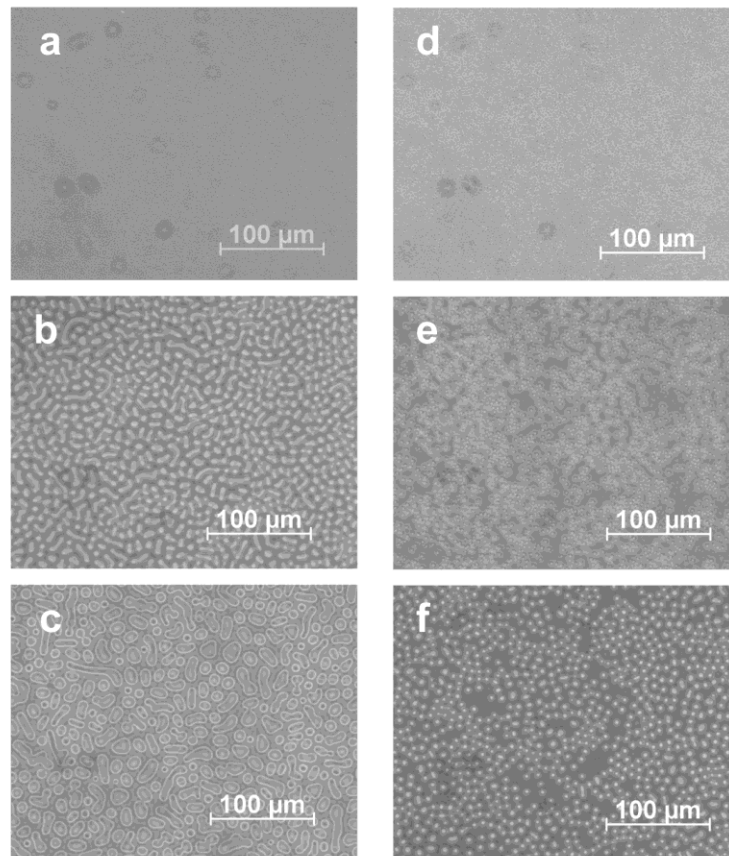


Figure 2.5: OM images of PMMA/SAN blends with 2 wt% MEK-ST silica in the region of spinodal decomposition (a-c) and binodal decomposition (d-f).

2.3.2 The effect of silica nanoparticles on the structure development of PMMA/SAN blends

To study the effect of hydrophilic MEK-ST silica nanoparticles on the structure development of the PMMA/SAN blends, both starting solutions were mixed with MEK-ST silica to a final weight percentage of 2 wt%. Using the same settings as for the blends without silica, films with the required composition gradient were prepared on the glass substrates with the HTE setup. The 2 wt% MEK-ST silica/PMMA/SAN blend gradient films were subsequently put on the temperature gradient heating stage for 10 min, similar to the silica-free PMMA/SAN blends. The morphologies of the composition gradient were investigated at the same positions a-f as indicated in Figure 2.3, of which the results are shown in Figure 2.5. The OM images clearly show a decrease of the domain size with the addition of the silica nanoparticles. On comparing Figures 2.4a-c with Figures 2.5a-c, it is evident that the addition of silica particles has a significant impact on the coarsening rate during spinodal decomposition, i.e. the characteristic length scale is strongly reduced at the same temperature. On comparing Figure 2.4c with Figure 2.5c at the

same temperature jump region, the average characteristic length of the domains decreases from 70 to 25 μm upon the addition of silica nanoparticles. Next to that, a disruption of the co-continuous morphology is observed. The slow-down of domain growth also occurs in the binodal decomposition region, as shown in Figures 2.5d-f.

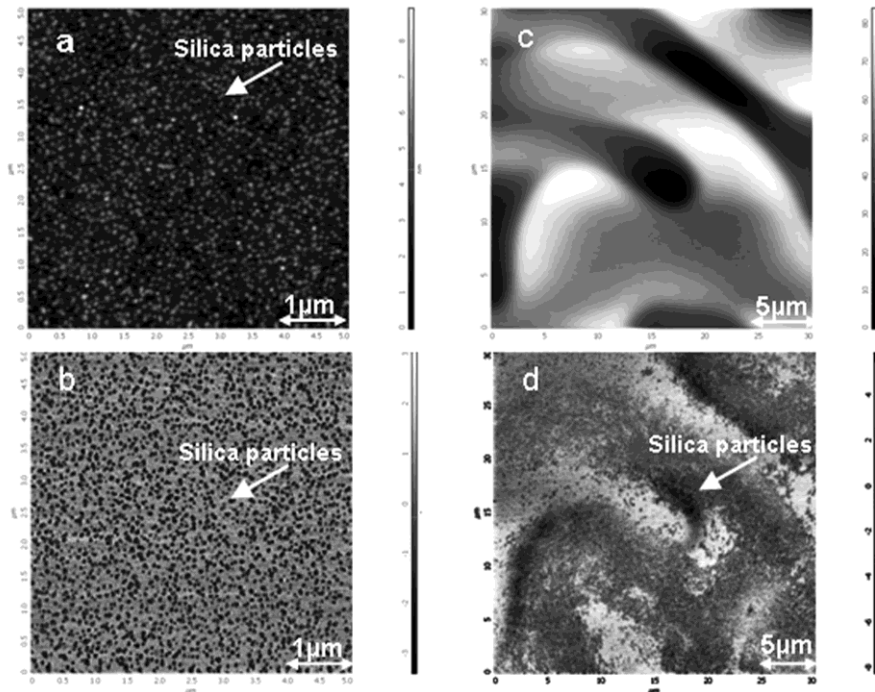


Figure 2.6: AFM height and phase angle images of a PMMA/SAN blend with 2 wt% MEK-ST silica prepared by HTE setup: (a,b) before and (c,d) after treatment on the temperature gradient heating stage. The measured point is located at position c in Figure 2.3. The dark regions in the phase angle images correspond to lower phase angles or higher stiffness and are the silica nanoparticles. Light regions correspond to the polymer domains.

In order to obtain a higher spatial resolution, AFM was chosen to study the dispersion of the silica nanoparticles and the resulting images are shown in Figure 2.6. Initially, i.e. before the temperature jump into the spinodal or binodal region, the silica nanoparticles are homogeneously dispersed in the matrix of the one-phase PMMA/SAN blend, as visualized by the AFM-height as well as the AFM-phase angle images in Figures 2.6a and b, respectively. After annealing on the temperature gradient heating stage, phase separation sets in and the coarsening of the structure occurs. The AFM-height image as depicted in Figure 2.6c clearly shows a co-continuous structure on the length scale of the scanned area, i.e. $30 \times 30 \mu\text{m}^2$. Because of the relatively large difference between the stiffness of the silica nanoparticles and that of PMMA and SAN, the silica nanoparticles can clearly be distinguished in the AFM-phase angle image (Figure 2.6d), where the dark and the light domains represent the silica particles and the polymers, respectively. It

seems that silica nanoparticles have a preference to be dispersed in one of the phases, which is consistent with the work of Composto *et al.*^{5,11} that silica particles migrate to the PMMA layers during phase separation, although the SAN used in that study contained 33 wt% AN, which leads to a lower critical temperature and a shift of the critical composition to 50 wt% PMMA instead of approximately 70 wt% for the current study. The observed phenomenon is the result of the strong hydrogen bonding interaction of MEK-ST silica nanoparticles with the carbonyl groups of the PMMA due to the existence of hydroxyl groups on the surface of hydrophilic silica. The slow-down effect of the silica particles on the rate of coarsening, as observed in the OM images, may be explained by the reduced mobility of PMMA due to the preferential attraction of the silica surface. The explanation will be discussed later.

The uneven distribution of nanoparticles is found in more polymer blends and it was shown that this depends on the interaction between the particles and the polymers.^{9,28,29} For the hydrophilic silica MEK-ST, selective migration to the PMMA phase is found in the used PMMA/SAN blend. When the surface of the nanoparticles is changed to more hydrophobic (Aerosil Si-R7200), the distribution of silica nanoparticles is changed and this has an impact on the phase separation kinetics. Since the hydrophobic silica is not stable in MEK, which was used as the common solvent for the non-filled systems, preparation of the blends was all done by melt-mixing at 185 °C, which is below the cloud point temperature. For this system, it proved that the order of mixing proved is essential for the final morphology, particularly the localization of the silica nanoparticles. The results presented in the next part are obtained by using the following procedure: The hydrophobic silica Si-R7200 powder or MEK-ST silica was pre-compounded with SAN, followed by blending the obtained material (SAN/silica) with the second polymer PMMA during a second extrusion step. The morphologies as visualized by TEM are shown in Figures 2.7 and show a homogeneous dispersion of silica in the binary polymer system before phase separation. After phase separation at 230 °C for 30 min, a co-continuous morphology is found due to the spinodal decomposition for the neat and the silica-filled PMMA/SAN 70/30 blends. For the blend with the hydrophobic silica (Aerosil Si-R7200), the nanoparticles are localized at the interface between the two polymers after phase separation (Figure 2.7e).

On comparing Figure 2.7c-e, the average characteristic length of the domains of the PMMA/SAN decreases upon the addition of MEK-ST silica nanoparticles, while the Aerosil Si-R7200 particles do not influence the coarsening of the blends.

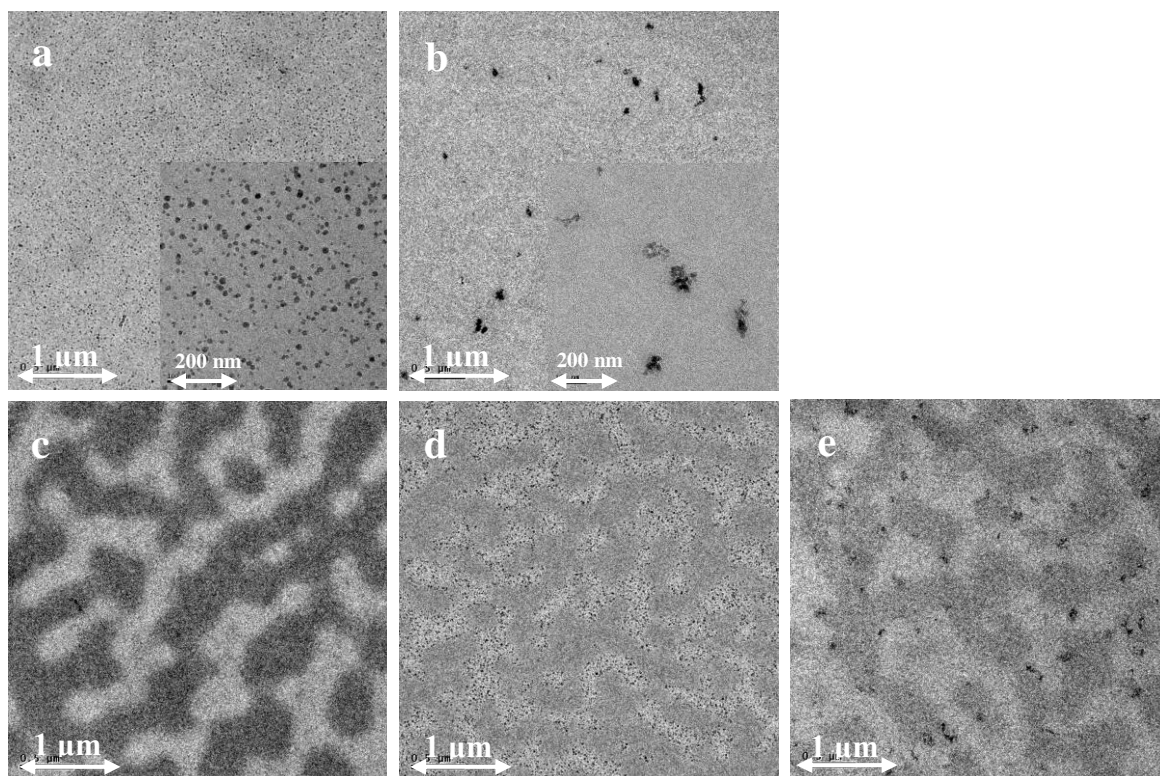


Figure 2.7: TEM images of PMMA/SAN 70/30 blend: (a-b) homogeneously dispersion of 5 wt% MEK-ST and 1.5 wt% Aerosil Si-R7200 in the blend before annealing, (c-e) neat, 5 wt% MEK-ST silica-filled and 1.5 wt% Aerosil Si-R7200 silica-filled blend after annealing at 230 °C for half hour. The bright phase corresponds to the PMMA domains, and the grey phase corresponds to SAN domains. The electron density of silica is much higher than that of polymer.

2.3.3 The effect of silica nanoparticles on the spinodal decomposition kinetics

Knowing the phase behavior and the critical composition from the phase diagram of PMMA/SAN system (Figure 2.3), the different stages of the spinodal decomposition were studied by several temperature jump experiments at the critical composition (70 wt% PMMA) with or without addition of MEK-ST silica particles. The samples were prepared by solvent casting and the final thickness of the films was between 20-30 μm .

The scattering patterns obtained at 240 °C collected after different time intervals are shown in Figure 2.8. The first image shows only the scattered light of the incident beam in the neat PMMA/SAN blend. The second image which was taken at 1000 sec shows a diffuse scattering ring at higher scattering angle, indicating that the phase separation process has started and that periodic structures develop, characteristic for the spinodal decomposition process. The intensity of the ring progressively increases, implying that the refractive index differences increase, i.e. the concentration fluctuations grow. After 1500 sec, the scattering angle of the ring decreases as a

function of time, indicating that the structure size grows, which is a typical feature of the intermediate stage. For the MEK-ST silica-filled PMMA/SAN blend, the scattering ring appears at approx. 1500 sec and the decrease of the scattering angle of the ring occurs around 2000 sec. The coarsening of the filled polymer blend progresses much slower than for the neat polymer blend.

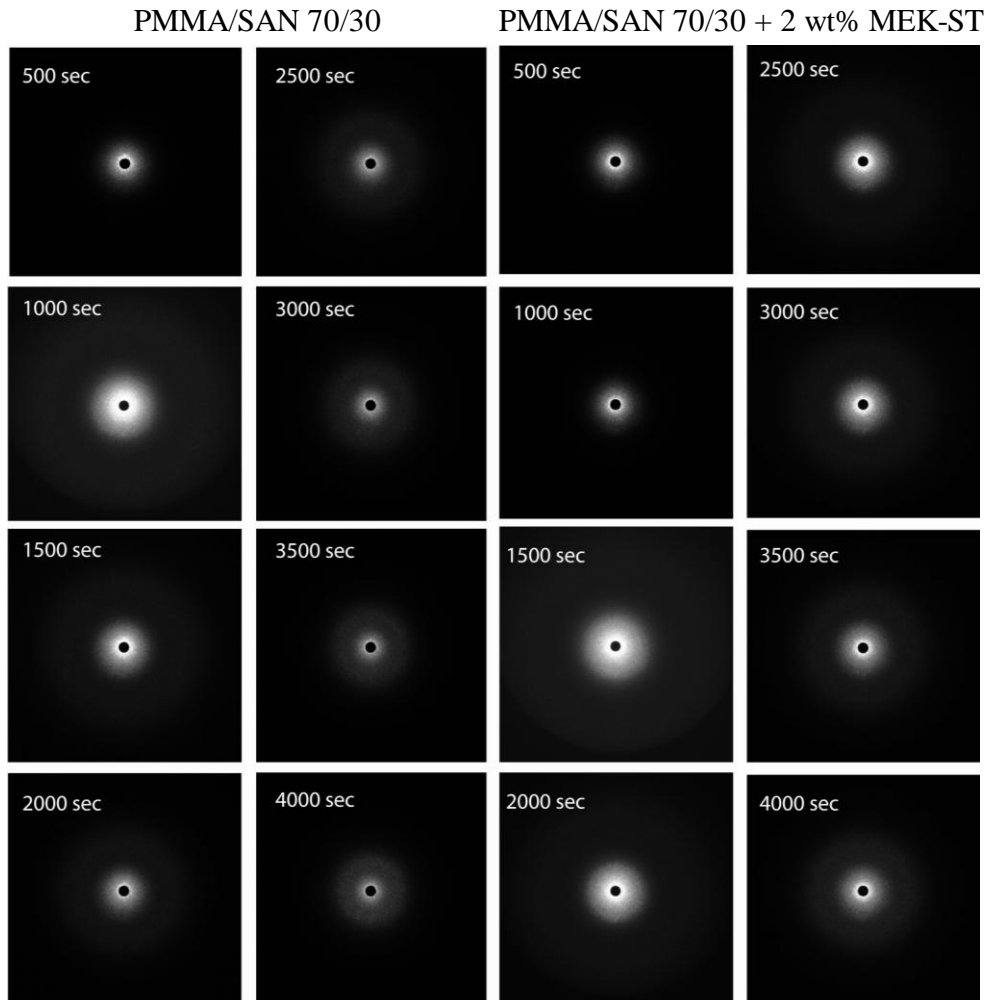


Figure 2.8: Time evolution of the 2D-scattering patterns of neat and 2 wt% MEK-ST silica-filled 70/30 PMMA/SAN collected at 240 °C.

The 2-D scattering images were integrated to obtain a better signal-to-noise ratio and presented as a curve of the scattered intensity as a function of the scattering vector q (defined as: $q = 4\pi/\lambda \sin \theta$, where 2θ is the scattering angle and λ is the wavelength of the incident light, 632.8 nm), see Figure 2.9. When the scattered intensity I is plotted against q for the time intervals of the initial and late stage of the phase separation, a clear difference can be observed in Figures 2.9a and b for the temperature jump to 240 °C. In the early stage (Figure 2.9a), the peak

at q_{max} is only growing in intensity but the peak position remains constant. However, in the subsequent intermediate and late stages (Figure 2.9b), not only the intensity increases but also the peak position of q_{max} starts to shift to lower q -values, indicating that the structure grows.

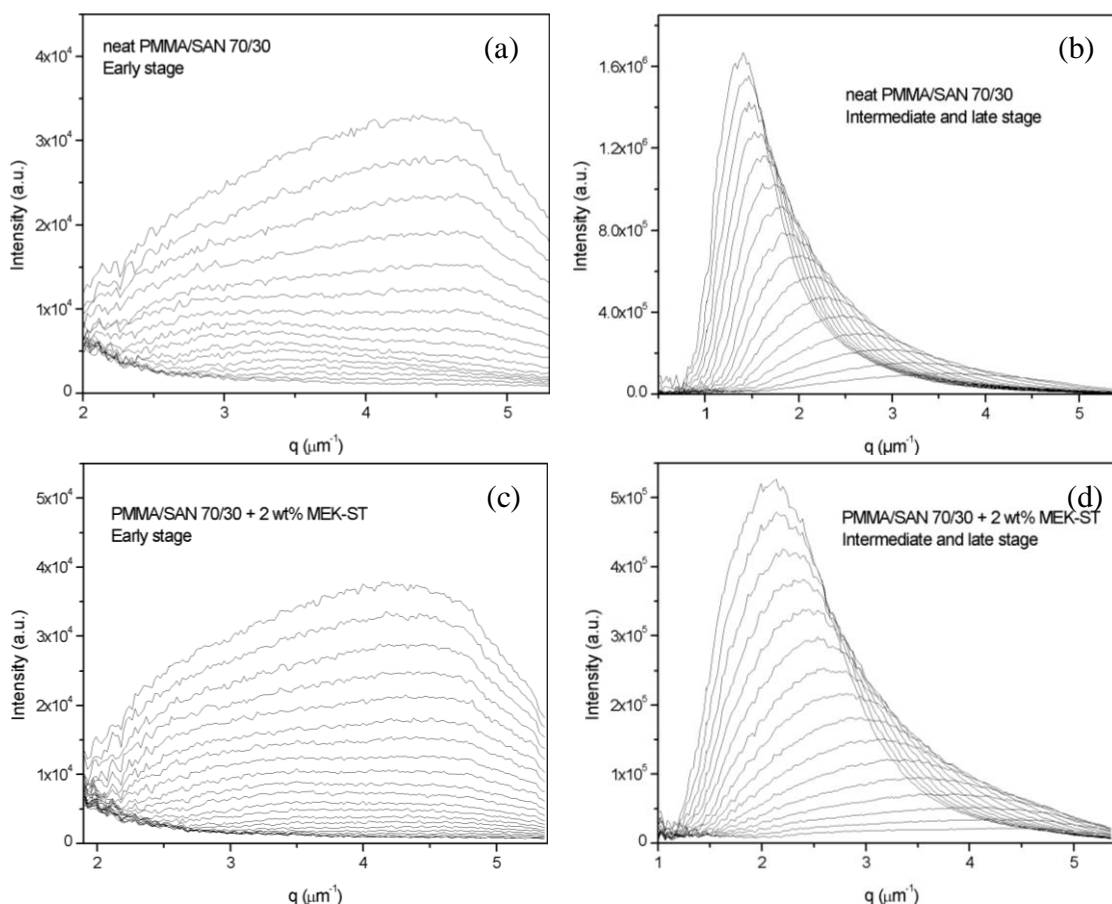


Figure 2.9: 1-D scattering curves as a function of q in the early and late stage of the phase separation for (a,b) the neat and (c,d) the 2 wt% MEK-ST silica-filled 70/30 mixture of PMMA/SAN at 240 °C.

In Figure 2.9a, the neat PMMA/SAN sample, the initial peak develops at $q = 4.6 \mu\text{m}^{-1}$ corresponding to an average structure size of $d (= 2\pi/q) = 1.3 \mu\text{m}$. Then, the structure coarsens to a size of $4.5 \mu\text{m}$ in approximately 50 min as shown in Figure 2.9b. Comparing the 2 wt% MEK-ST silica-filled PMMA/SAN with the neat one (Figures 2.9a and c), the initial peak of the filled PMMA/SAN blend appears at a similar q -value as for the neat blend. However, the average diameter of the final structure of the filled PMMA/SAN blend is around $3 \mu\text{m}$ as shown in Figure 2.9d. The analysis of the initial stage of the phase separation is done separately from the intermediate and late stages phase separation. The diffusion coefficient D_{app} obtained in early stage and the scaling coefficient of the nonlinear phase-growth obtained in the intermediate and late stages show the different effect of the silica particles on different stages of phase separation,

which will be discussed in the next section.

2.3.3.1 Analysis of early stage of phase separation

To obtain the diffusion coefficient D_{app} and the gradient energy parameter κ , the results of early stage of the phase separation were analyzed with the linearized Cahn-Hilliard-Cook (CHC)-model.³⁰ The CHC-model equation reads as:

$$I(q,t) = I(q,0) \exp(2R(q)t) \quad (2.1)$$

where $I(q,0)$ is the scattered intensity as a function of q at time $t = 0$ min and $R(q)$ is the relaxation rate. The values of the apparent diffusivity and gradient energy parameter can be obtained from the relaxation rate with the following relation:

$$R(q) = -q^2 (D_{app} + 2M\kappa q^2) \quad (2.2)$$

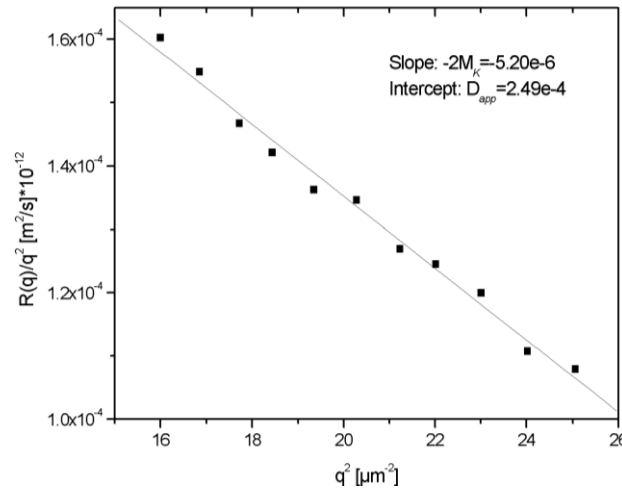


Figure 2.10: The results from the Cahn-Hilliard-Cook-analysis ($R(q)/q^2$) for the early stage of the phase separation of the neat PMMA/SAN 70/30 blend at 240 °C.

The relaxation rate is plotted versus q^2 in Figure 2.10. From the intercept and slope of the curve, the apparent diffusivity D_{app} and $2M\kappa$ values are obtained for 240 °C. The plots of $R(q)/q^2$ vs. q^2 follow a linear relationship at large q -values, close to the q_{max} , which indicates that this stage of spinodal decomposition can be well described by the linearized Cahn-Hilliard-Cook theory. The values for different temperatures with different silica concentrations are summarized in Table 2.1. The apparent diffusivity values are in the order of $10^{-4} \mu\text{m}^2/\text{s}$. Similar values were found by Prusty *et al.*²⁷

With addition of MEK-ST silica, especially higher content (2 wt%) silica nanoparticles, the obvious decrease of the apparent diffusivity D_{app} and $2M\kappa$ values shows that the slow-down

effect already occurs in the early stage of the phase separation. Furthermore, the decrease of D_{app} shows that the diffusion of the two polymers is getting slower because of the addition of MEK-ST silica.

Table 2.1: The results from the Cahn-Hilliard-Cook-fit (slope and intercept) at different temperatures of neat and MEK-ST silica-filled PMMA/SAN blends.

Temperature (°C)	PMMA/SAN 70/30	D_{app} ($\mu\text{m}^2/\text{s}$)	$2M\kappa$ ($\mu\text{m}^4/\text{s}$)
235	Neat blend	1.51×10^{-4}	3.71×10^{-6}
	1 wt% MEK-ST	1.06×10^{-4}	2.55×10^{-6}
	2 wt% MEK-ST	1.06×10^{-4}	2.68×10^{-6}
240	Neat blend	2.49×10^{-4}	5.96×10^{-6}
	1 wt% MEK-ST	2.11×10^{-4}	5.20×10^{-6}
	2 wt% MEK-ST	1.69×10^{-4}	4.26×10^{-6}
245	Neat blend	4.37×10^{-4}	8.20×10^{-6}
	1 wt% MEK-ST	3.47×10^{-4}	8.20×10^{-6}
	2 wt% MEK-ST	3.00×10^{-4}	6.97×10^{-6}

2.3.3.2 Analysis of intermediate and late stages of phase separation

In the intermediate and late stages of spinodal demixing, q_{\max} starts to decrease with time. Namely, the concentration fluctuations with the dominant correlation length increase with time, when the kinetics starts to deviate from the linearized Cahn-Hilliard-Cook theory and be affected by the coarsening effect. The non-linear phase growth in the intermediate and late stages can be analyzed with a power-law scaling equation. The scaling coefficients were obtained to study the influence of the silica nanoparticles on the phase separation kinetics. The position of the scattering ring, $q_{\max}(t)$, and the corresponding intensity at that q -value, $I_{\max}(t)$, as a function of time can be linked by the following equations:

$$q_{\max}(t) \propto t^{-\alpha} \quad (2.3)$$

$$I_{\max}(t) \propto t^{\beta} \quad (2.4)$$

where α is a scaling coefficient and β is again a power-law scaling coefficient presenting the refractive index contrast between the two separated phases. Siggia showed that in the intermediate and late stages for most phase-separating polymer blends a hyper-scaling relation exists: $\beta=3\alpha$.³¹ For binary polymer blends, quenched at the critical concentration, α varies from

0.33, with coarsening controlled by diffusion (viscous force effect), to 1.0, with coarsening controlled by hydrodynamic forces.^{32,33}

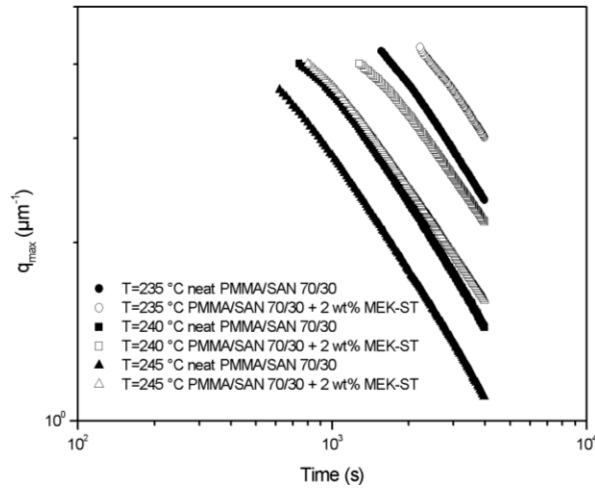


Figure 2.11: The maximum q -values as a function of time of neat and filled 70/30 PMMA/SAN collected at different temperatures.

Figure 2.11 shows the corresponding $q_{\max}(t)$ as a function of time collected at different temperatures. From the intermediate stage to the late stage, the slope of the curve $q_{\max}(t)$ (scaling coefficient α) increases. This shows that the coarsening in the intermediate stage is more dominated by diffusion, whereas at the late stage the system is more dominated by hydrodynamics. The q_{\max} follows the power law and the value of scaling coefficient α for the late stage is given in Table 2.2. α varies from 0.60 to 0.70, which shows that all studied systems are between diffusion-controlled and hydrodynamics-controlled. At different temperatures for the neat PMMA/SAN, some variation in the slope of the curves is found, but no relation exists in the sense that with increasing temperature the extent of hydrodynamic interactions increases. However, the temperature dependence of the structure development is very important. In order to obtain a similar average structure size around $2.7 \mu\text{m}$, another 45 min is needed at $235 \text{ }^\circ\text{C}$ compared to $245 \text{ }^\circ\text{C}$ for the neat blend.

Except the influence of the temperature, the silica-filled blends always show a smaller slope compared to the neat blends. The difference is shown in Table 2.2. The value of α decreases when the mixture is filled with MEK-ST particles of a certain concentration at all investigated temperatures, implying that the nanoparticles force the system towards the diffusion-controlled regime. The higher content silica particles show more obvious slow-down effect on the phase separation. This is consistent with the decrease of the apparent diffusivity D_{app} calculated by the linearized Cahn-Hilliard-Cook theory for the early stage phase separation. As a result, the phase separation can be slowed down by the addition of silica nanoparticles during both early stage and

late stage.

More information can be found by calculating the other coefficient β , which is found to increase upon the addition of 2.0 wt% MEK-ST. This is related to the refractive index difference between the two phases becomes larger than for the neat blend, since the value of β represents the contrast between the two separate phases. Further, the hyper-scaling relation is changed to $\beta > 3\alpha$ when the silica particles are added. For our system, the relationship of these two coefficients is almost 3 for the neat PMMA/SAN. This can be explained by the selective localization of silica particles to the PMMA phase, thereby changing the refractive index.

Table 2.2: The results from the power-law scaling coefficient at different temperatures of neat and MEK-ST silica-filled PMMA/SAN blends.

Temperature (°C)	PMMA/SAN 70/30	α	β
235	Neat blend	0.66	2.33
	1 wt%	0.65	2.39
	2 wt%	0.61	2.53
240	Neat blend	0.70	2.08
	1 wt%	0.70	2.15
	2 wt%	0.61	2.26
245	Neat blend	0.66	1.76
	1 wt%	0.64	1.87
	2 wt%	0.60	1.94

To compare the results between the neat blends and the blends with the two different silica particles, all the blends are prepared from melt-mixing, followed by compressing molding to thin films. The thickness of the films is controlled approx. 100 μm . Table 2.3 shows that the apparent diffusivity values, D_{app} , are in the order of $10^{-5} \mu\text{m}^2/\text{s}$, which is one order smaller than for the solvent-cast films.

The diffusion coefficient D_{app} and the mobility parameter $M\kappa$ were analyzed for the early stage of the phase separation. The decrease of D_{app} and the $2M\kappa$ values shows that upon adding silica nanoparticles, the slow-down effect already takes place in the early stage of the phase separation, although the influence of the hydrophobic silica is less. Especially, the reduction of the D_{app} and $M\kappa$ isn't observed in the 1.5 wt% SiR7200 silica-filled blend at 235 °C, what might be related to the migration of the hydrophobic silica particle to the PMMA/SAN interface, which

induces a higher mobility of the polymer chains in the early stage of the phase separation. This is consistent with the results of TEM images in Figures 2.7 c and e. The samples annealed at 230 °C for 30 min (in between the early stage and intermediate stage) show that the average characteristic length of the morphology of the hydrophobic Si-R7200 silica-filled blend is similar to that of the neat blend.

Further, the power-law scaling coefficient α of the filled systems is lower in comparison to the neat blends, demonstrating that in the intermediate and late stages of the phase separation both types of nanoparticles slow down the phase separation and force the coarsening mechanism towards the diffusion-controlled regime, although the reduction of α for the hydrophobic silica-filled blend is less prominent than for the hydrophilic silica-filled blend.

Table 2.3 The results of apparent diffusivity D_{app} , mobility parameter $M\kappa$ and the power-law scaling coefficient (α , β) at different temperatures of neat and silica-filled PMMA/SAN blends prepared by melt-mixing.

Temperature (°C)	PMMA/SAN 70/30	D_{app} ($\mu\text{m}^2/\text{s}$)	$2M\kappa$ ($\mu\text{m}^4/\text{s}$)	α	β
230	Neat blend	3.06×10^{-5}	4.80×10^{-7}	0.69	1.92
	2.0 wt% MEK-ST	2.28×10^{-5}	4.27×10^{-7}	0.56	2.26
	1.5 wt% SiR7200	2.61×10^{-5}	3.56×10^{-7}	0.65	1.98
235	Neat blend	4.03×10^{-5}	4.99×10^{-7}	0.64	1.49
	2.0 wt% MEK-ST	2.36×10^{-5}	3.47×10^{-7}	0.48	1.76
	1.5 wt% SiR7200	4.00×10^{-5}	5.97×10^{-7}	0.52	1.51

As mentioned before, for the hydrophilic silica particles, the significant reduction effect on the D_{app} and α might arise from the local increase of the viscosity and the concomitant reduction of the mobility of PMMA induced by the selective migration of the silica particles in the PMMA phase (see Figure 2.12a), therefore leading the coarsening mechanism towards the diffusion-controlled regime. However, no obvious enhancement of the viscosity of the PMMA was observed after adding different concentrations of silica.³⁴ Thus, the other explanation of the redistribution of the PMMA chains between the filler surface and the bulk based the molar mass is also possible and will be further discussed in a later section. For the hydrophobic silica particles, the formation of a solid interface by the silica particles prevents the coarsening, as seen in Figure 2.12b, of which the reduction of α might be related to the change of the surface tension

or the immobilization of the droplets.

The scaling coefficient β provides information about the refractive index difference between two phases. In comparison to the neat blend, β is found to increase with the addition of 2 wt% MEK-ST, while a similar value is found for the system with the addition of 1.5 wt% Si-R7200, see Table 2.3. This is related to the fact that the hydrophobic silica particles migrate to the interface of the two polymer phases and the change of the refractive index difference is less than for the MEK-ST particles, which influence the bulk behavior of the PMMA phase.

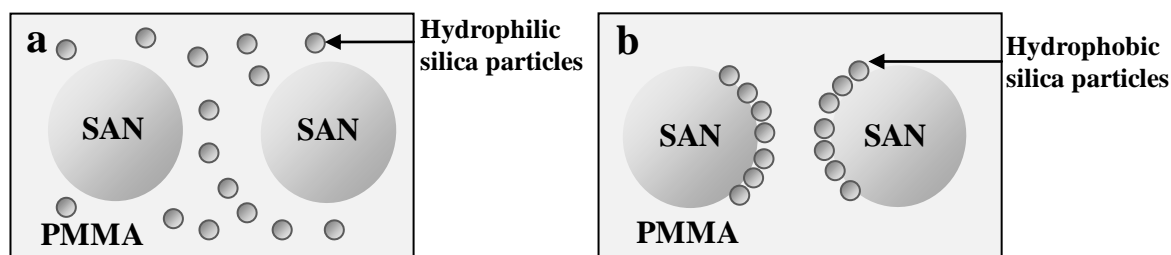


Figure 2.12: Schematic representation of (a) the hydrophilic and (b) hydrophobic silica particles in the PMMA/SAN blend.

In conclusion, the spinodal decomposition kinetics of the PMMA/SAN is slowed down by both the hydrophilic or hydrophobic silica nanoparticles. The slow-down effect of the hydrophilic silica particles is prominent in all stages of the phase separation, while the hydrophobic silica particles are mainly effective in the intermediate and late stages. A distinction has to be made between the effect of the hydrophilic particles, which selectively migrate to the PMMA phase and thereby force the coarsening mechanism more towards the diffusion-controlled regime, and the hydrophobic particles, which move towards the interface and are, therefore, only active during the intermediate and late stages of the phase separation.

2.3.4 Phase behavior of silica-filled PMMA/SAN blends evaluated by rheology

Rheometry has proven to be a viable method for studying the phase behavior of polymer blends, block copolymers and filled polymers.³⁵⁻³⁸ In this section, the phase separation temperatures of neat and silica-filled PMMA/SAN blends are determined by dynamic shear rheology. The phase stability of binary polymer blends is influenced by the addition of the silica nanoparticles, depending on the interaction between the silica surface and the polymer component.

All the samples used for the rheological tests were prepared by melt mixing. A typical curve of the loss modulus, G'' , versus temperature is shown in Figure 2.13a for the neat and MEK-ST silica-filled PMMA/SAN blends. In both experiments, a fixed heating rate was applied:

0.5 °C/min. In both systems, at low temperatures the loss modulus decreases upon increasing the temperature. This can be attributed to the greater mobility of the polymer chains as the system moves away from its glass transition temperature. As the temperature increases further to the vicinity of the binodal and spinodal decomposition curves, the slope of the loss modulus decreases as a function of temperature, indicating that the elasticity is enhanced. This observation stems from a competition between mobility and thermodynamics. The temperature corresponding to the point that the slope of G' - T curve starts to decrease is referred to as the phase separation temperature (or cloud point) of the matrix of PMMA/SAN blend. For the neat blend, the phase separation temperature is approx. 208 °C, while for the PMMA/SAN/5 wt% MEK-ST blend the phase separation point shifts only 1 °C upwards. The PMMA/SAN/2 wt% MEK-ST blend, which is not shown here, displays a similar curve as the 5 wt% blend. For the hydrophobic Si-R7200 silica, the same trend is obtained (Figure 2.13b). Given the uncertainty in the temperature control and the fact that the nanoparticles slow down the phase separation kinetics, the effect of the silica particle on the phase boundary as assessed by applying a temperature sweep is only marginal if not absent.

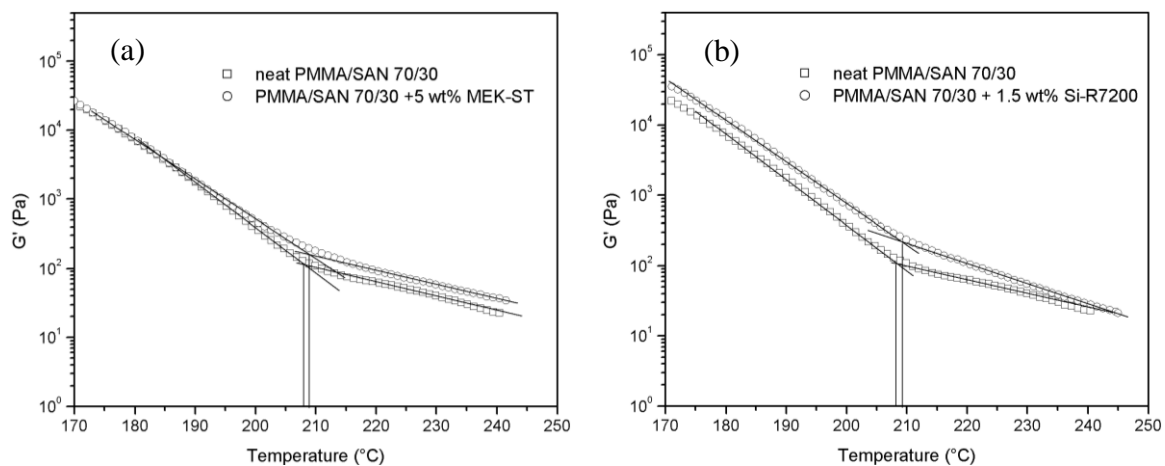


Figure 2.13: Dynamic temperature sweep performed at 1% strain with a heating rate of 0.5 °C/min of (a) the neat and the 5 wt% MEK-ST silica-filled blend and (b) the neat and the 1.5 wt% Aerosil Si-R7200 silica-filled blend.

To further assess the possibility that the addition of nanoparticles might change the position of the binodal and spinodal decomposition curves, dynamic frequency sweeps were performed at a fixed temperature and strain within the linear region. It has been shown in earlier work that when the experimental data are presented in so-called Cole-Cole plots the appearance of two clear peaks or under certain conditions a main peak with a drift tail can be used as a signature for the onset of phase separation.^{10,39} Figure 2.14a shows the Cole-Cole plot for neat PMMA/SAN 70/30 blend at temperatures of between 190 and 210 °C in steps of 5 °C. It can be observed that

at 200 °C a small tail appears on the right-hand side of the arc, which originates from chains with a different relaxation mechanism.⁴⁰ The tail becomes more prominent upon further increasing the temperature. This implies that the onset of phase separation occurs between 195 and 200 °C, which is approx. 10 °C lower than observed by the temperature sweep experiment. For both the 2 and 5 wt% hydrophilic MEK-ST silica-filled PMMA/SAN blends, the tail already appears at 195 °C, see Figure 2.14b, demonstrating that 2 wt% silica is already enough to change the phase boundary of the PMMA/SAN blends, while a higher concentration does not have more effect. It has to be noted that the Cole-Cole plot for the PMMA/2 wt% silica system (data not shown here) displays only one arc over the whole experimental temperature range, which supports the experimental observation that the phase separation temperature is approx. 190-195 °C of these filled blends. The Cole-Cole plots for the neat blend and the blends filled with different concentration of MEK-ST silica at 195 and 200 °C are depicted in Figure 2.15. The results show that the onset of phase separation of MEK-ST silica-filled blends occurs at least 5 °C lower than for the neat blend. The addition of the hydrophilic silica nanoparticles shifts the phase boundary down to lower temperatures. In addition, since the phase separation temperature is reduced by the silica particles thereby extending the quench depth of the blend, the slow-down effect on the phase separation kinetics analyzed via SALS measurement is quite significant.

Also for the Si-R7200 silica-filled PMMA/SAN blend, the tail on the right-hand side, characteristic for the phase separation, can be observed at 200 °C, which means that phase separation occurs between 195 and 200 °C seen in Figure 2.16. This cloud point is similar to the neat blends, implying that there is no apparent shift of the phase boundary with addition of the hydrophobic silica.

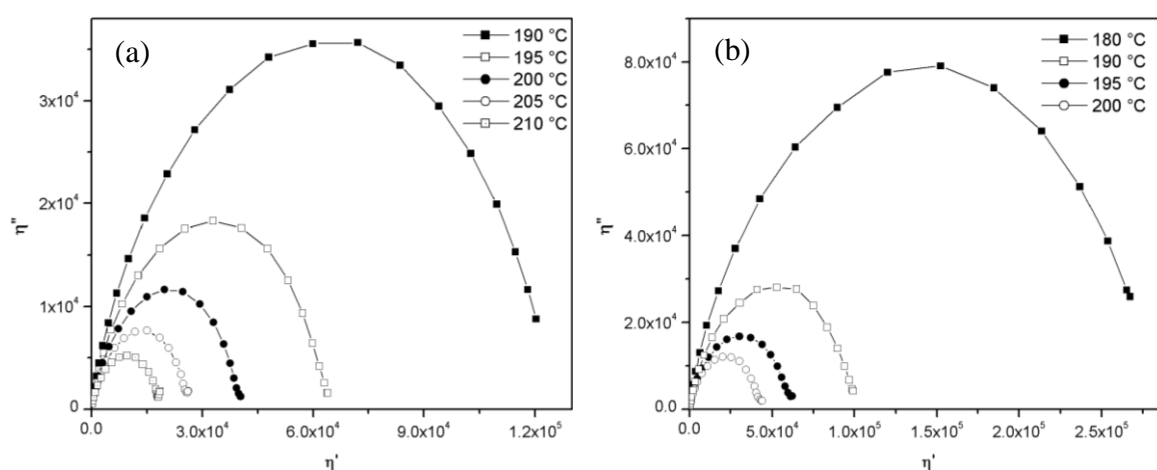


Figure 2.14: Cole-Cole plots for the (a) neat PMMA/SAN 70/30 blend at 190, 195, 200, 205 and 210 °C and (b) 2 wt% MEK-ST silica-filled PMMA/SAN 70/30 blends at 180, 190, 195 and 200 °C.

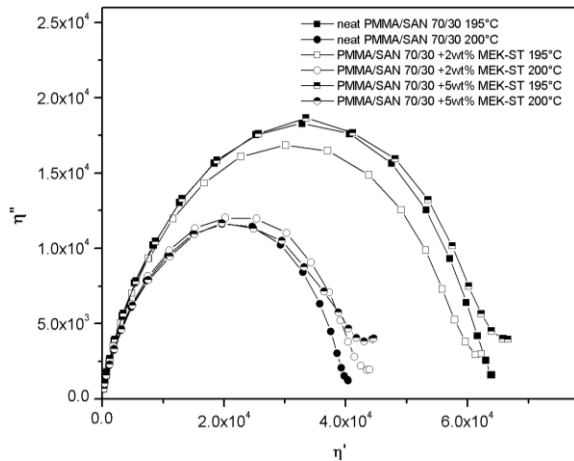


Figure 2.15: The comparison of Cole-Cole plot between neat and MEK-ST silica-filled blends at 195 and 200 °C.

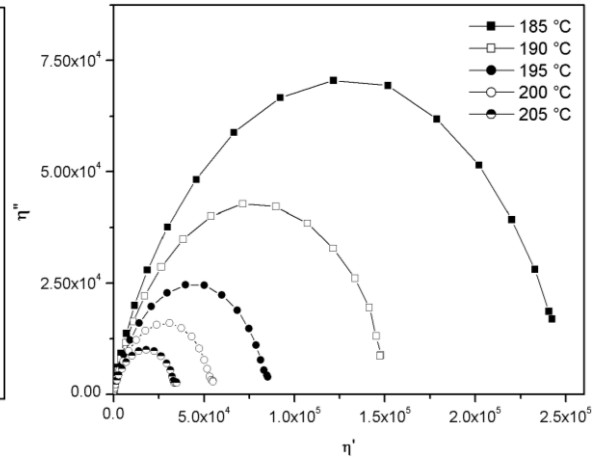


Figure 2.16: Cole-Cole plots for 1.5 wt% Si-R7200 silica-filled PMMA/SAN 70/30 blends at 185, 190, 195, 200 and 205 °C.

The introduction of nanoparticles in partially miscible polymer blends can either increase or decrease the temperature of phase separation, which was already reported by several groups.^{10,12-15} The common explanation for the enhancement of the miscibility region (increase of the phase separation temperature for LCST behavior) is the change of the thermodynamic interaction parameter of the binary system, which is correspondingly decreased because of the filler. In our case, the phase separation boundary shifts down by the introduction of the hydrophilic silica nanoparticles. This may also be attributed to a redistribution of the PMMA chains between the filler surface and the bulk based the molar mass. It has to be remarked that the PMMA used in this study has a relatively broad molar mass distribution (PDI ~ 2.1). Based on the hypothesis put forward by Lipatov *et al.*,¹⁴ selective adsorption of polymers can take place which is governed by the molar mass distribution and the polymer-filler interaction. First, the situation is considered for systems with weak polymer-filler interactions. For dilute solutions, adsorption of the high molar mass component occurs at the surface of the particles using entropy-based arguments,^{41,42} but for semi-dilute solutions or melts, the opposite situation may occur and the lower molar masses are preferentially adsorbed. For systems with strong polymer-filler interactions, the lower molar masses are preferentially adsorbed due to the strong enthalpic interactions, which strongly govern the thermodynamics in this case. For the PMMA/SAN systems with the hydrophilic silica nanoparticles of the present study, preferential adsorption of the lower molar mass part on the filler surface is the most dominating mechanism due to the strong polymer-filler interaction, which leads to an enrichment of the bulk with the higher molar mass part, thereby inducing a decrease of the LCST phase separation temperature. This is also

consistent with the reduction of diffusivity parameter analyzed via SALS measurement. Since the hydrophobic silica nanoparticles have no preferred (strong) interaction with any component of this blend, the silica-filled system does not show an obvious shift of the phase boundary.

2.4 Conclusions

Thin film libraries of a binary blend of two polymers, i.e. PMMA and SAN, was prepared successfully using the HTE setup with ϕ -gradients covering the whole composition range and a temperature gradient between 200-290 °C. The evolution of the morphology was studied by OM and AFM after a fixed time on the temperature gradient heating stage at different compositions. The effect of silica nanoparticles was studied and it was shown that the nanoparticles have a large effect on the morphology development. With the nanoparticle-controlled phase behavior of PMMA/SAN we have demonstrated that the HTE setup is a promising tool to study the phase behavior of complex polymer blend systems.

The effect of the silica nanoparticles on the spinodal decomposition kinetics of the PMMA/SAN was studied via SALS and it was shown that a slow-down effect on the coarsening can be observed for both hydrophilic and hydrophobic silica nanoparticles. For the hydrophilic silica, a preferential segregation of nanoparticles in the PMMA phase is observed as a result of the strong hydrogen bonding interaction between the hydroxyl groups at the surface of the silica and the carbonyl groups of PMMA. For the hydrophobic silica, the nanoparticles are localized at the PMMA/SAN interface. Both silica particles force the coarsening mechanism more towards the diffusion-controlled regime. It has to be remarked that the slow-down effect of the hydrophilic silica particles is prominent in all stages of the phase separation, while the hydrophobic silica particles are mainly effective in the intermediate and late stages. The distinction might be related to the movement of the hydrophobic particles towards the interface, which occurs in the early stage of the phase separation, therefore, only active during the intermediate and late stages of the phase separation.

The influence of silica nanoparticles is not only limited to the kinetics of phase separation, but also on the position of the phase boundary. Depending on the interaction between the silica and the polymer chains, an obvious reduction of the phase separation temperature is found for the hydrophilic silica-filled system.

Three explanations were considered for the slow down on the coarsening rate by hydrophilic silica particles: i) local increase of the viscosity and the concomitant reduction of the mobility of PMMA because of an increase of the silica concentration; ii) selective adsorption of low molar

mass PMMA chains on the surface of the silica nanoparticles, thereby increasing the average molar mass of the bulk, which is consistent with the shift of the phase diagram; iii) reduction of the interfacial tension. The slow-down effect of hydrophobic silica particles could be related to the changing of the interface tension or a dense layer of solid particles which influences the interfacial mobility, followed by preventing coarsening in the PMMA/SAN blend.

2.5 References

- ¹ Utracki, L. A., *Commercial Polymer Blends*, Chapman & Hall, London, **1998**.
- ² Hashimoto, T., Takenaka, M., and Jinnai, H., *J. Appl. Crystal.*, **1991**, 24, 457-466.
- ³ Balazs, A.C., Emrick, T., Russell, T. P., *Science*, **2006**, 314, 1107-1110.
- ⁴ Fenouillot, F., Cassagnau, P., Majeste, J. C., *Polymer*, **2009**, 50, 1333-1350.
- ⁵ Chung, H-J., Taubert, A., Deshmukh, R. D., Composto, R. J., *Europhys. Lett.*, **2004**, 68, 219-225.
- ⁶ Yurekli, K., Karim, A., Amis, E. J., Krishnamoorti, R., *Macromolecules*, **2003**, 36, 7256-7267.
- ⁷ Walther, A., Matussek, K., Muller, A. H. E., *ACS NANO*, **2008**, 2, 1167-1178.
- ⁸ Lipatov, Y. S., *J. Macromol. Sci. Part B: Phys.*, **2006**, 45, 871-888.
- ⁹ Bose, S., Ozdilek, C., Leys, J., Seo, J. W., Wübbenhorst, M., Vermant, J., Moldenaers, P., *ACS Applied Materials & Interfaces*, **2010**, 2, 800-807.
- ¹⁰ Huang, Y., Jiang, S., Li, G., Chen, D., *Acta Mater.*, **2005**, 53, 5117-5124.
- ¹¹ Chung, H-J., Ohno, K., Fukuda, T., Composto, R. J., *Macromolecules*, **2007**, 40, 384-388.
- ¹² Lipatov, Y. S., *Prog. Polym. Sci.*, **2002**, 27, 1721-1801.
- ¹³ Lipatov, Y. S., *J. Macromol. Sci. Part B: Phys.*, **2006**, 45, 871-888.
- ¹⁴ Lipatov, Y. S., Nesterov, A. E., Ignatova, T. D., Nesterov, D. A., *Polymer*, **2002**, 43, 875-880.
- ¹⁵ Nesterov, A. E., Lipatov, Y. S., *Polymer*, **1999**, 40, 1347-1349.
- ¹⁶ Ginzburg, V. V., *Macromolecules*, **2005**, 38, 2362-2367.
- ¹⁷ He, G., Ginzburg, V. V., Balazs, A. C., *J. Polym. Sci. Part B: Polym. Phys.*, **2006**, 44, 2389-2403.
- ¹⁸ Utracki, L. A., *Polymer Blends Handbook*, Kluwer Academic Publishers, Dordrecht, **2002**.
- ¹⁹ Meredith, J. C., Karim, A., Amis, E. J., *Macromolecules*, **2000**, 33, 5760-5762.
- ²⁰ Cabral, J. T., Karim, A., *Meas. Sci. Technol.*, **2005**, 16, 191-198.
- ²¹ Meredith, J.C., Karim, A., Amis, E. J., *MRS Bull.*, **2002**, 27, 330-335.
- ²² Smith, A. P., Douglas, J. F., Meredith, J. C., Amis, E. J., Karim, A., *J. Polym. Sci. Part B: Polym. Phys.*, **2001**, 39, 2141-2158.
- ²³ L'Abbe, R., Li, W., Goossens, H., Van Duin, M., *Macromol. Symp.*, **2008**, 265, 281-289.
- ²⁴ Dickinson, T. A., Walt, D. R., White, J., Kauer, J. S., *Anal. Chem.*, **1997**, 69, 3413-3418.
- ²⁵ Picchioni, F., Goossens, J. G. P., Van Duin, M., Magusin, P., *J. Appl. Polym. Sci.*, **2003**, 89, 3279-3291.
- ²⁶ Yoshitake, K., Yokoyama, T., *Process of producing hydrophobic organosilica sol.*, Nissan Chemical Inc., US Patent 60025455A, **2000**.
- ²⁷ Prusty, M., Keestra, B. J., Goossens, J. G. P., Anderson, P. D., *Chem. Eng. Sci.*, **2007**, 62, 1825-1837.
- ²⁸ Elias, L., Fenouillot, F., Majeste, J. C., Cassagnau, Ph., *Polymer*, **2007**, 48, 6029-6040.
- ²⁹ Sumita, M., Sakata, K., Asai, S., Miyasaka, K., Nakagawa, H., *Polym. Bull.*, **1991**, 25, 265-271.
- ³⁰ Cook, H. E., *Acta Metall.*, **1970**, 18, 297-306.
- ³¹ Siggia, E. D., *Phys. Rev. A*, **1979**, 20, 595-605.
- ³² Wang, H., Composto, R. J., *Phys. Rev. E*, **2000**, 61, 1659-1663.
- ³³ Chen, H., Chakrabarti, A., *J. Chem. Phys.*, **1998**, 108, 6006-6013.
- ³⁴ Ertem, E. *Influence of copolymer content on the rheology of PMMA/EA copolymer nanocomposites*, B.Sc. Thesis, TU/e, Eindhoven, the Netherlands, **2011**.
- ³⁵ Carreau, P. J., De Kee, D., Chhabra, R., *Rheology of polymeric systems principles and applications*, Carl Hanser, Munich, Germany, **1997**.
- ³⁶ Van Hemelrijck, E., Van Puyvelde, P., Velankar, S., Macosko, C. W., Moldenaers, P., *J. Rheol.*, **2004**, 48, 143-159.
- ³⁷ Elias, L., Fenouillot, F., Majeste, J. C., Cassagnau, Ph., *Polymer*, **2007**, 48, 6029-6040.

- ³⁸ Vinckier, I., Laun, H. M., *Rheol. Acta*, **1999**, 274-286.
- ³⁹ Dumoulin, M. M., Utracki, L. A., Carreau, P. J., *Two-phase polymer systems*, New York, NY Hanser, **1991**.
- ⁴⁰ Carreau, P. J., Bousmina, M., Aji, A., *Rheological properties of blends: facts and challenges*, Ghiggino KP, *Progress in Pacific polymer science 3*, Springer, Berlin, Heidelberg, New York, 25-40, **1994**.
- ⁴¹ Kalfus, J., Jancar, J., *Polym. Compos.*, **2007**, 28, 365-371.
- ⁴² Zheng, X., Sauer, B. B., van Alsten, J. G., Schwarz, S. A., Rafailovich, M. H., Sokolov, J., Rubinstein, M., *Phys. Rev. Lett.* **1995**, 74, 407-410

Chapter 3

Morphology and rheology of silica-filled PC/PMMA blends

The effect of silica nanoparticles on the morphology and the rheological properties of the partially miscible polymer blend poly(carbonate)/poly(methyl methacrylate) (PC/PMMA) was investigated for solvent casting and melt mixing. It was shown that the solvent-cast method can be used to prepare a partially miscible PC/PMMA blend with a LCST behavior, while the melt-mixing method only leads to a phase-separated blend, since the mixing temperature is always higher than the cloud point. Two types of silica particles, i.e. hydrophilic and hydrophobic, were used to study the effect on the morphology of PC/PMMA blends and it was shown that the distribution of the nanoparticles depends on the balance of interactions between the surface of the particles and the polymer components. For the hydrophilic silica, migration of the nanoparticles to the PMMA phase can be observed independent on the compounding sequence, while for the hydrophobic silica, localization at the PC/PMMA interface is the preferred state. The silica nanoparticles have a large effect on the morphology development. A reduction of the size of PMMA droplet phase in the PC/PMMA 80/20 blend with 3 wt% hydrophilic MEK-ST silica can be observed. The stabilization of coarsening can be attributed to the local increase of the viscosity and a concomitant reduction of the mobility of the PMMA phase. The hydrophobic silica particles have the same stabilization effect on the coarsening of the PC/PMMA blend by inhibiting the coalescence through the presence of a immobilized layer of nanoparticles around the polymer droplets. Compared to the hydrophilic silica, a better compatibilization can be obtained by introducing the hydrophobic silica particles at the PC/PMMA interface as the solid barrier.

3.1 Introduction

Bisphenol A poly(carbonate) (PC) and poly(methyl methacrylate) (PMMA) derivatives are customarily used in all kinds of optical applications like optical disk, write-once or erasable memory disk, video disk, optical fiber, and waveguide applications. The criteria for such optical materials include low birefringence, low moisture absorption, dimensional and thermal stability, high glass transition temperature (T_g) and good processability. It is very difficult for a homopolymer to meet all these requirements because of such stringent criteria. For instance, PC is a tough material with good thermal and dimensional stability, high T_g , and good processability. However, large intrinsic birefringence, thermal stress cracking, and poor scratch resistance are drawbacks of PC. On the other hand, PMMA shows outstanding transparency, low intrinsic birefringence, and good scratch resistance, but it is relatively brittle and has a low dimensional (due to water absorption) and thermal stability. Therefore, blends of PC with PMMA have received considerable attention, both in industry and academia, because of the potential application as gas separation membranes, substrates of the optical data storage discs, and for the stabilization effect of PC towards PMMA photodegradation, for the enhancement of toughness, for the reduced price due to the PMMA, in a PC melt mixed with PMMA.¹⁻³

The miscibility of PC/PMMA blends was extensively investigated by a number of groups and it was shown that the interaction parameter χ between PC and PMMA is very small (~ 0.04).⁴ According to Kambour *et al.*, when χ is slightly positive, a miscible blend can be achieved under particular blending conditions.⁵ It was first reported that PC/PMMA blends obtained via melt-blending are immiscible.⁶ In other cases, they were characterized as partially miscible.⁶⁻¹¹ Gardlung proposed a specific interaction between the ester group of the PMMA and the phenyl ring of the PC.⁶ Immiscible or miscible films can also be obtained depending on the solvent and the casting technique, i.e. air casting or non-solvent precipitation. Kyu and Saldanha published numerous studies on PC/PMMA.⁷⁻⁹ It appears from their work that cast films from methylene chloride (MC), cyclohexanone and tetrahydrofuran (THF) at room temperature are immiscible, but cast films from THF at 47 °C yields partially miscible systems with a lower critical solution temperature (LCST) behavior. Later on, an upper critical solution temperature (UCST) behavior at approx. 240 °C was reported.^{10,11} Moreover, heptane-precipitated films from THF solutions showed miscibility and exhibited a LCST behavior ($T_{crit} = 180$ °C), whereas cast films from THF or MC are immiscible according to Paul and coworkers.¹² Nishimoto *et al.* stated that for high molar

masses the miscibility window is over-estimated due to the non-equilibrium state of the solvent-cast blends, which are kinetically trapped in a homogeneous state by quenching below T_g , and that the behavior above T_g cannot be assigned to a LCST behavior and that the measured cloud point curve is due to a slow phase separation process.¹³

Even though the solvent blending method generally gives a better mixing, it is difficult to remove the solvent afterwards. As a result, this mixing method is rarely used in industry, where mechanical mixing (melt mixing) is the common technique. In the melt state, compatibilizers are widely used to reduce the droplet size of the dispersed phase. In this context, the use of premade block copolymers that migrate to the interface has been proven to be a successful strategy in suppressing especially the coalescence process.¹⁴⁻¹⁷ However, block copolymers are expensive and may induce micellization which may form microphase-separated domains, thereby reducing the efficiency of the compatibilization. Recently, a new concept of compatibilization by using inorganic nanoparticles, like carbon black, organoclay and silica particles, to stabilize the phase morphology of polymer blends has been reported.¹⁸

Clarke *et al.* showed that carbon black has a compatibilizing effect when the particles are present at the interface between natural rubber and nitrile butadiene rubber.¹⁹ Elias *et al.* concluded that the stabilization effect of silica (hydrophilic/hydrophobic) on the PP/PS blend is the reason of the reduction in the interfacial tension or acting as a rigid layer preventing the coalescence of PS droplets.²⁰ Regarding PC/PMMA blends, Ray and Bousmina reported in a series of papers that at a concentration of organoclay of approx. 5 wt% the normally immiscible PC/PMMA blends display characteristics of a “miscible” blend with only one alpha relaxation peak.²¹⁻²² However, it is risky to use clay as a compatibilizer because transesterification reaction between PC and PMMA chains can be catalyzed as this aluminosilicate can produce Lewis or Brønsted sites at high temperatures.

From an experimental point of view, the study of linear viscoelastic behavior of a blend can be a very important tool to evaluate the interfacial tension or understand the morphology of polymer blends or its evolution.^{23,24} In addition, for nanocomposites, the linear rheology is also a sensitive way to assess the particle size, structure, shape and the state of dispersion of the filler.²⁵ Consequently, the use of linear rheology has found its way in studying the behavior of nanocomposites in the melt state. Regarding nanoparticle-filled immiscible polymer blends, Vermant *et al.* reported on the effect of nanometer-sized silica particles on the coalescence in a model blend consisting of poly(dimethyl siloxane) (PDMS)/poly(isobutylene) (PIB).²⁶ Well-defined flow histories followed by dynamic frequency sweeps were used to interpret the influence of silica on the blend morphology. The authors

clearly demonstrated that the change in the properties of the interface by silica adsorption is responsible for the suppression or delay of coalescence. Emulsion models as developed by Paliarne²⁷ and Bousmina²⁸ have been used to study the relationship of between the viscoelastic properties of nanoparticle-filled immiscible polymer blends and their interfacial tension between the polymer components.^{20,26,29,30}

A blend consisting of PMMA and PC was studied as a model system for the category of immiscible polymer blends in this chapter, as a comparison to the study on partially miscible polymer blends presented in Chapter 2. The effect of silica nanoparticles on the morphology and the rheological properties was investigated in the PC/PMMA blends prepared via melt mixing. Two types of silica particles, i.e. hydrophilic and hydrophobic, were added to study the effect of the sequence of mixing in the different components on the distribution of the nanoparticles.

3.2 Experimental

3.2.1 Materials

A bisphenol-A based PC with a weight-average molar mass (M_w) of 30 kg/mol and a polydispersity index (PDI) of 2.6 was supplied by SABIC Innovative Plastics (SIP), the Netherlands. PMMA was provided by Arkema (France), with a M_w of 88 kg/mol and PDI of 2.1. Small amounts of ethyl acrylate (EA) are usually incorporated into PMMA to prevent unzipping of the polymer at elevated temperatures during processing. The PMMA used in this study contains 0.5 wt% EA.

Pre-made colloidal MEK-ST silica nanoparticles used as hydrophilic particles with a diameter of 10-15 nm, dispersed in methyl ethyl ketone (MEK) with approx. 30 wt% silica, were purchased from Nissan Chemical (USA) and will be referred to as MEK-ST. Hydrophobic nanosilica, Aerosil R972, with a diameter of 12 nm, was supplied by Evonik (Germany) and has a surface treated with dimethyldichlorosilane. This hydrophobic silica nanoparticle will be referred to as Si-R972. Tetrahydrofuran (THF) was obtained from Biosolve (The Netherlands). All materials were used as received.

3.2.2 Blend preparation

Solvent casting

Solvent-cast samples were prepared by casting a 8 wt% polymer (PC/PMMA) solution on glass slides or in petri dishes at 20 or 47 °C. The solvent THF was evaporated slowly over 3

days at room temperature. Afterwards, the films were dried in a vacuum oven by stepwise increasing the temperature from 60, 80, 100 and 150 °C under reduced pressure with a low nitrogen flow for 5 more days to ensure complete solvent removal.

Melt mixing

A series of PC/PMMA/silica nanocomposites with silica content ranging from 1-5 wt% were blended by using a twin-screw mini-extruder. The temperature was set at 250-270 °C depending on the blend composition. The extruder was filled with 6 g of material. The screw speed was set at 75 rpm and the total mixing time was fixed at 10 min. The extruder was filled with 6 g of material. All the experiments were performed under a nitrogen atmosphere in order to prevent oxidative degradation. Approx. 0.1 wt% processing stabilizer tris(2,4-ditert-butylphenyl) phosphate was added to the polymer powder before further processing. PC and PMMA were dried under reduced pressure with a low nitrogen flow for 12 hrs at 150 °C and 120 °C, respectively, before compounding. The silica nanoparticles were used without any further surface modification.

- (1) Silica nanoparticles were pre-compounded with PC and PMMA separately by wetting the PC powder or PMMA powder by the MEK-ST silica suspension just before extrusion. Subsequently, the obtained PC/silica and PMMA/silica nanocomposites were blended during a second extrusion step.
- (2) The MEK-ST silica suspension or Si-R972 powder was pre-compounded with PC at 270 °C. Then, the obtained material (PC/silica) was blended with PMMA during a second extrusion step.
- (3) All components (PC, PMMA, silica particles) were charged to the mixing chamber simultaneously and compounded at 250-270 °C, depending on the blend composition, for 10 min.

Compression molding

PC/PMMA/silica nanocomposite sheets with a thickness of 0.5 mm were prepared by using compression molding at 230-250 °C, depending on the blend composition, for 5 min under a pressure of 100 bars. Samples for rheological characterization (8 mm in diameter, 0.5 mm in thickness) were cut from the compression-molded sheets.

3.2.3 Characterization techniques

Transmission electron microscopy (TEM)

Morphological investigations were performed by using a Tecnai 20 transmission electron microscopy (TEM), operated at 200 kV. Ultrathin sections (50-70 nm) were obtained at room temperature by using a Leica Ultracut E microtome. Chemical staining of the sections was not required, since the difference of electron density between two polymers was large enough and the electron density of the silica is much higher than that of both polymers.

Thermogravimetric analysis (TGA)

A Q500 TGA (TA Instruments) was used for the quantitative determination of the silica content in the nanocomposites. Samples were heated under a pressed air atmosphere at 10 °C/min from 30 to 800 °C and held at 800 °C for 15 min. The residue was assumed to be only composed of silica.

Differential scanning calorimetry (DSC)

The glass transition temperature was determined by a Q1000 DSC (TA Instruments). Each sample with sample mass of 3-5 mg was heated from 30-200 °C, cooled down to 30 °C, and heated again to 200 °C, all at 10 °C/min in standard DSC Tzero pans. For the melt-mixed sample, the inflection point of the second heating cycle as a function of temperature was taken as the glass transition temperature (T_g). For modulated temperature DSC (MDSC) measurement, the samples with sample mass between 9-11 mg were heated from 30-270 °C at 3 °C/min, with a modulation period of 60 s and an amplitude of ± 0.47 °C. The combination of underlying heating rate and period was always chosen such that there were at least four modulation cycles during the glass transition.

Rheology

Dynamic shear measurements were performed on a stress-controlled AR-G2 rheometer (TA Instruments) by using an 8 mm parallel plate-plate geometry and disk-shaped specimens (8 mm in diameter; 0.5 mm in thickness). Frequency sweeps were performed in one sequence decreasing the frequency from 500 to 0.001 rad/s at 220 °C under a N₂ atmosphere, with a constant strain of 10%, which was within the linear viscoelastic range.

Atomic force microscopy (AFM)

The AFM investigations were performed by using a Smena P47H microscope (NT-MDT Ltd, Moscow, Russia). The AFM was operated in semi-contact mode under an air atmosphere using a silicon cantilever (NSG 11 NT-MDT), which was coated with a gold layer for a higher laser beam reflectivity. The resonance frequencies applied were 115-190 kHz.

3.3 Results

Before studying the influence of the nanoparticles on the morphology of the blends, the miscibility of pure PC/PMMA blends needs to be understood, since it was shown that the miscibility window strongly depends on the mixing condition.⁸⁻¹² A stable and reproducible blending procedure should be identified for the PC/PMMA system. First, the conditions for solvent casting will be optimized followed by a discussion on the effect of the compounding sequence order on the morphology. Subsequently, the effect of the silica on the rheology will be investigated. Finally, the obtained results will be discussed in view of the interaction between the polymer and silica filler.

3.3.1 The influence of the solvent-casting conditions on the miscibility of PC and PMMA

All compositions of PC/PMMA blend films cast from THF solutions at room temperature were translucent. Optical microscopy studies of these films showed phase separation and in some cases birefringent entities could be observed, suggesting that crystallization of PC may have occurred. The extent of phase separation and the occurrence of crystallization is normally checked by normal DSC, but since the glass transitions may become very weak and not well-separated modulated DSC (MDSC) is more suitable for this system. The MDSC results of the PC/PMMA 40/60 blend are shown in Figure 3.1. The total heat flow curve is identical to that from standard non-modulated DSC. Two glass transition temperatures at 120 °C, which can be assigned to the PMMA-rich phase and 139 °C, which can be assigned to the PC-rich phase, and one melting endotherm at 237 °C can be observed in the first heating curve of total heat flow, which reveals that indeed partial phase separation and crystallization of PC occurred. Due to the pronounced crystallization in combination with the concomitant rigid amorphous fraction, the Δc_p of the glass transition of PC, which only is related to the mobile amorphous fraction,^{31,32} is much smaller as for fully amorphous PC. After cooling from the molten state from 270 °C down to room temperature, no melting peak is observed in the second heating cycle; however, the two T_g 's become more distinct and move to the T_g 's of the pure polymers. The DSC results demonstrate that phase separation took place during solvent evaporation, but that this is also accompanied by crystallization of the PC phase. The melting enthalpy of the non-reversing heat flow is much larger than that of reversing heat flow, implying that the crystallization of PC in PC/PMMA blends is only induced by the solvent.

A transparent PC/PMMA 40/60 blend film can be obtained by casting from THF at elevated temperatures (50 °C), even though the transparency of the film depends on the film thickness or solvent evaporation rate. In Figure 3.2, the DSC curve shows a pronounced single T_g in the first heating cycle of the transparent part of the cast film with an enthalpy overshoot related to aging. In the subsequent heating, after quenching from 260 °C, the blend shows two glass transitions that are very close to the pure polymers. Thus, thermally-induced phase separation must have occurred during heating in the first run, which is confirmed in the following AFM studies. The transparent PC/PMMA 40/60 film as subjected to a temperature gradient with temperatures ranging from 150 to 250 °C for 30 min under a nitrogen flow and subsequently quenched to room temperature to freeze in the structure. Afterwards, the part of film with the temperature gradient from 190-250 °C was cloudy, while the part of film with the temperature gradient from 150-180 °C was still transparent. Figure 3.3 shows the AFM phase images of the PC/PMMA (40/60) film annealed 30 min at 180 °C (a) and 190 °C (b). A homogeneous single phase is observed in Figure 3.3a. The phase separation took place on annealing at 190 °C or higher. The same observation was also obtained for the blends with compositions of 50/50 and 30/70. Thus, the PC/PMMA blends solvent cast from THF at 50 °C can be identified as a partially miscible blend with a LCST behavior.

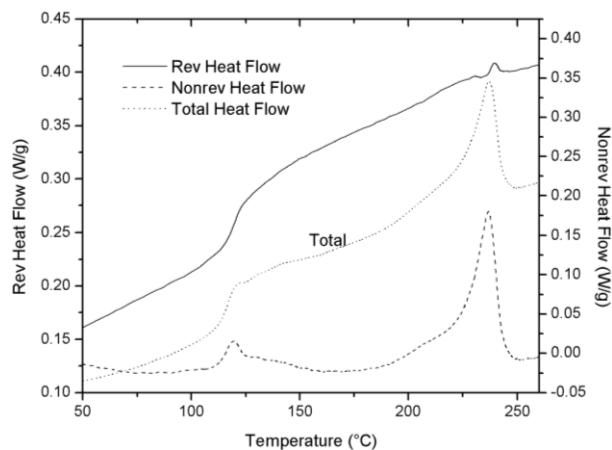


Figure 3.1: Modulated temperature DSC curves of the PC/PMMA 40/60 blend cast from THF at 20 °C.

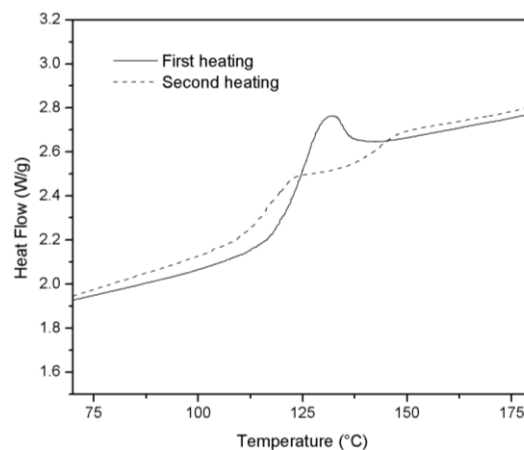


Figure 3.2: DSC curves of the PC/PMMA 40/60 blend cast from THF at 50 °C.

However, the final miscibility of the pure PC/PMMA is also sensitive to other factors. For example, the evaporation rate in the fume hood (due to an unstable air flow) will affect the final miscibility. As a result, a few small cloudy areas can be found in a sample which is mostly transparent. The unreliable preparation will complicate the results of the system with

fillers. Therefore, the melt-mixing method was applied for this system for the remainder of the chapter. The PC/PMMA blends prepared with melt mixing always show phase separation, since the compounding temperature is higher than the cloud point measured for the solvent-cast systems.

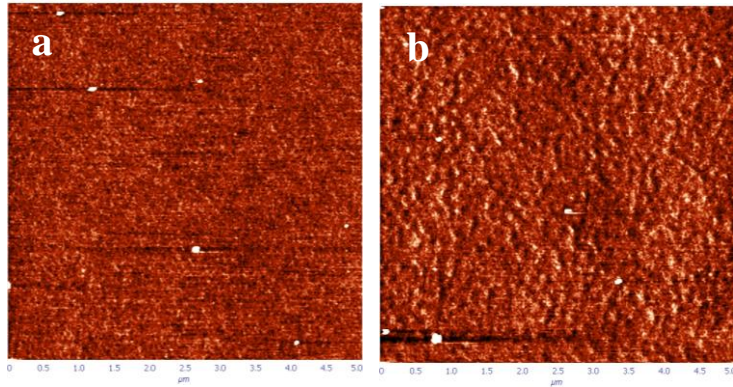


Figure 3.3: AFM phase images of PC/PMMA 40/60 film (cast from THF) annealed for 30 min at: (a) 180 °C and (b) 190 °C.

3.3.2 The influence of the compounding sequence on the morphology of hydrophilic silica-filled PC/PMMA systems

In this section, we investigate how the mixing sequence of the hydrophilic silica nanoparticles with PC and PMMA affects the morphology. In earlier studies it was shown that the order of addition of the components can have a strong effect on the final distribution of the nanoparticles, as reported by e.g. Cassagnau *et al.*¹⁸

To achieve an optimal dispersion, the silica particles were pre-compounded with both homopolymers, targeting at the equal silica concentrations, in procedure 1. This was followed by mixing both silica-filled polymers in the molten state by extrusion. The MEK-ST silica was used as the hydrophilic silica, which is partly covered hydroxyl groups on the surface, while the remainder are methyl groups.

The final morphologies of the neat polymer blend and the silica-filled polymer blends are shown in Figure 3.4. A kind of co-continuous morphology is observed for the neat 40/60 PC/PMMA blend. The silica-filled polymer blends show a non-homogeneous distribution of the silica particles after extrusion. Figures 3.4b-d show that the silica particles are mainly localized in the continuous PMMA phase. Despite the fact that silica particles were evenly added to PC and PMMA separately in advance, they migrate to the PMMA domains even during short mixing times (10 min). However, the final morphology of the 40/60 PC/PMMA blend is not affected by the silica particles and is still co-continuous with a similar length

scale. The only difference is that the presence of the silica particles swells the PMMA phase because of the migration. Further, clustering of the silica particles starts to occur in the PMMA phase on increasing the silica concentration.

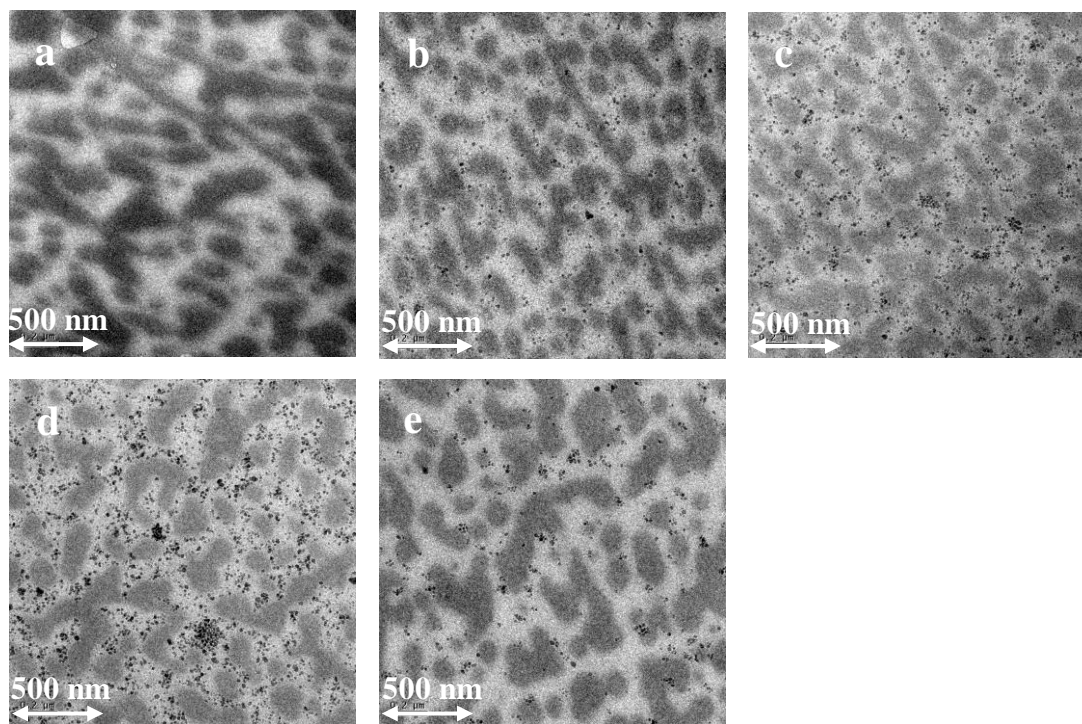


Figure 3.4: TEM images of PC/PMMA 40/60 blends prepared via different compounding procedures. Via procedure 1: (a) neat blend, (b) filled with 1 wt%, (c) 3 wt% and (d) 5 wt% MEK-ST silica; Via procedure 2: (e) 1 wt% MEK-ST silica is predispersed in PC.

To study the migration behavior of the silica particles, different compounding procedures were used. In procedure 2, small amounts of silica particles (approx. 1 wt%) were mixed with PC (high viscosity) in advance, followed by blending with the pure PMMA (low viscosity). Figures 3.4e shows that the compounding sequence does not have a significant influence on the final distribution of the silica particles. The same migration of silica can be observed, although a few silica nanoparticles still remain in the PC phase, but can be controlled by the compounding time. The observed migration can be linked to the balance of the interactions between the surface of the particles and the polymer components. For this system, the strong hydrogen bonding interaction between the hydroxyl groups on the surface of colloidal MEK-ST silica with the carbonyl groups of the PMMA is the major driving force for the migration. To unify the preparation method, a compounding procedure was used in which all components are mixed simultaneously for all the silica-filled samples discussed in the remainder of the chapter.

The previous results showed that the co-continuous structure of the binary blend is not influenced by the addition of the silica nanoparticles. However, for the droplet-matrix structure (PC/PMMA 80/20), the silica nanoparticles significantly decrease the size of the PMMA droplets and results in a finer dispersion of PMMA in the PC matrix, as shown in Figures 3.5a-c. On the other hand, Figures 3.5d-e show that there is no effect of the silica on the morphology of PC/PMMA 20/80 blends, same as in the PC/PMMA 40/60 blend. For all investigated blend ratios, the MEK-ST silica particles selectively distribute in the PMMA phase.

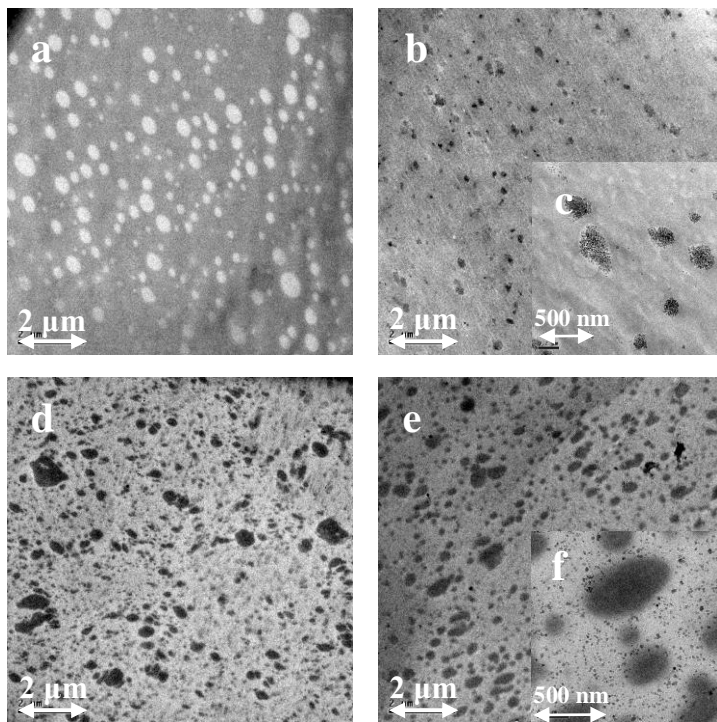


Figure 3.5: TEM images of PC/PMMA blends prepared via simultaneous addition of all components: (a) neat 80/20 blend, (b-c) 3 wt% MEK-ST silica-filled 80/20 blend, (d) neat 20/80 blend and (e-f) 3 wt% MEK-ST silica-filled 20/80 blend.

In conclusion, the hydrophilic silica nanoparticles are found to be selectively distributed in the PMMA phase, independent on the compounding sequence, as a result of the strong interaction between the hydroxyl groups on the surface of MEK-ST silica and PMMA. For co-continuous morphologies, the addition of the silica nanoparticles has no influence on the length scale of the morphology except that some swelling of the PMMA domains occurs. If the silica particles are confined in the dispersed PMMA phase, the extent of coalescence is strongly reduced by the local increase of the viscosity and a concomitant reduction of the mobility of the PMMA phase.

3.3.3 Rheology of hydrophilic silica-filled PC/PMMA blends

The influence of the silica nanoparticles on the melt state of polymer blends is an essential factor on the final morphology. Furthermore, the linear viscoelastic behavior of the polymer blend can be used to study the morphology of blends and its evolution, i.e. the co-continuous or droplet-matrix morphologies can be determined and the occurrence of phase separation can be investigated by the change of the storage modulus in the low frequency region. Hence, it is important to investigate the linear viscoelastic behavior of the filled polymer blends. It has to be remarked that the addition and migration of the silica particles may change the viscosity ratio, which may induce a phase inversion.

Figure 3.6 shows the effect of the MEK-ST silica particles on the storage modulus and the complex viscosity of 40/60 blends which were obtained from a frequency sweep test at 220 °C and at a constant strain of 10%. When submitted to small amplitude oscillatory shear, immiscible binary blends show a higher elasticity in the low frequency range which can result in the presence of a secondary plateau in the curve of the storage modulus vs. frequency for low frequencies. Additionally, at low frequencies, G' is very sensitive to the addition of the fillers. In Figure 3.6a, the second plateau appears at low frequencies and the modulus increases with the silica content, which is an indication of a “solid-like” response by the filler above a critical concentration. It is due to the formation of a gel-like structure by solid particles. This behavior can also be observed in the complex viscosity (η^*) in the low frequency region.

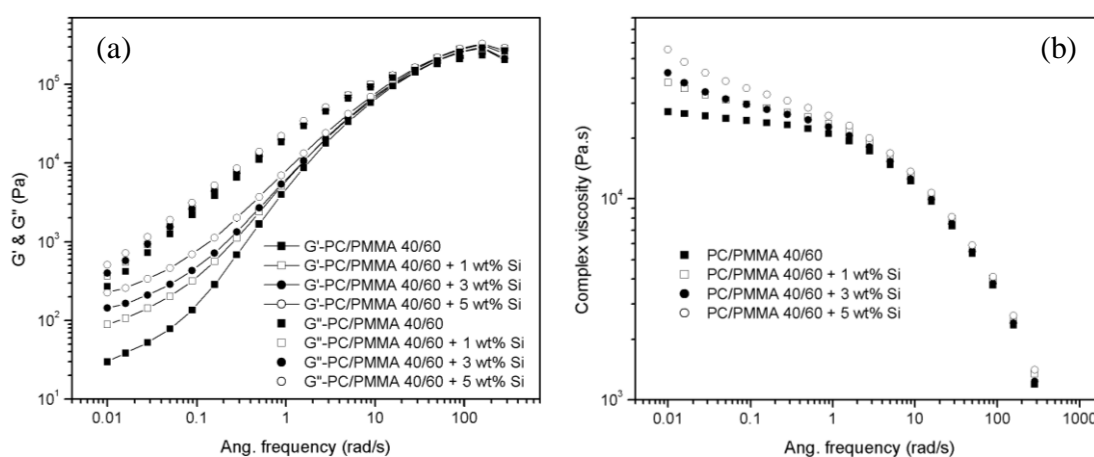


Figure 3.6: Viscoelastic behaviors of neat or MEK-ST silica filled PC/PMMA 40/60 blends ($T=220$ °C): (a) Frequency dependence of the storage and loss modulus and (b) frequency dependence of complex viscosity.

More information about the relaxation behavior and its evolution can be obtained in a Cole-Cole plot, in which the imaginary viscosity (η'') versus real viscosity (η') are plotted. It is a well-known curve for the investigation of the rheology of two-phase systems like polymer blends and filled polymer. Cole-Cole plots can distinguish between different relaxation mechanisms, e.g. what is the dominant relaxation, in polymer blends.^{33,34} For a homogeneous system, there is only one circular arc in the curve. If a tail or a second circular arc appears on the right-hand side of the arc, which is indicative for a second relaxation mechanism, phase separation has occurred with symmetric or off-symmetric conditions, respectively. In other words, this means a co-continuous or droplet-matrix morphologies. Figure 3.7 shows a circular arc with a tail for the neat 40/60 blend, which indicates a co-continuous morphology with two relaxation mechanisms. With increasing the silica content, the tail becomes longer, which means that the relaxation time of the filled blends is longer than the pure blends. The concentration and the distribution of the silica nanoparticles obviously alter the viscoelastic properties of the blend.

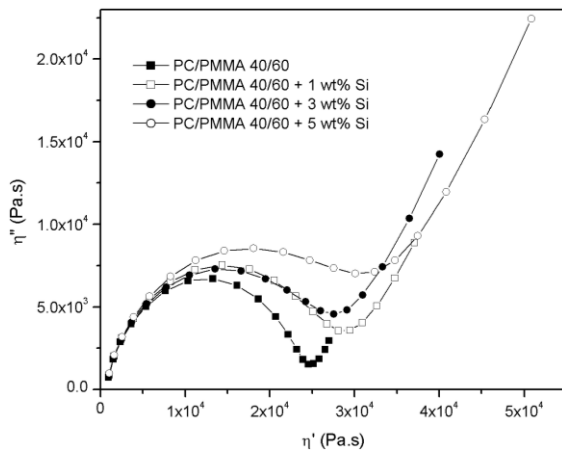


Figure 3.7: Cole-Cole plot for the neat and MEK-ST silica-filled PC/PMMA 40/60 blends at 220 °C.

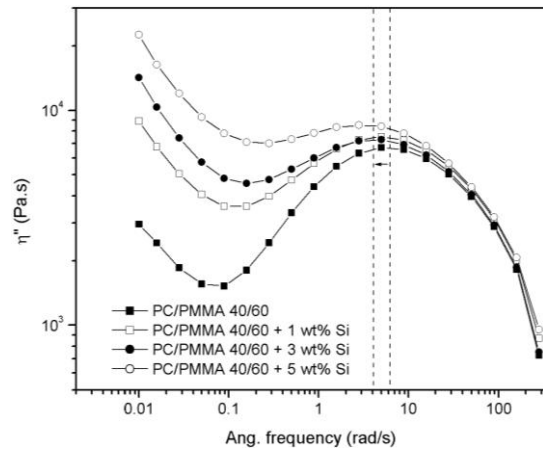


Figure 3.8: Frequency dependence of $\eta''(\omega)$ for the neat and MEK-ST silica-filled PC/PMMA 40/60 blends.

Figure 3.8 shows the effect of the spatial distribution of silica particles on the relaxation behavior of the blend. According to the component relaxation, the corresponding relaxation time is generally determined by calculating the continuous relaxation spectrum based on the dynamic modulus.^{30,35} However, in a straightforward and simple manner, the variation of $\eta''(\omega)$ describes qualitatively the relaxation spectra of the blend.²⁰ As shown in Figure 3.8, a relaxation peak reflecting the matrix relaxation of PMMA is clearly seen in the domain of high frequencies. When 1-5 wt% of MEK-ST silica is added to the blend, the relaxation of the PMMA matrix is shifted to lower frequencies compared to the neat PC/PMMA blend. In

other words, the matrix relaxation becomes slower due to the redistribution of the silica particles towards the PMMA phase.

For the PC/PMMA 20/80 blends with a matrix-droplet morphology, the same observations were found (see in Figure 3.9), i.e., the second plateau appears at low frequencies and the modulus and the complex viscosity increases with the silica content. Since the silica particles are distributed in the PMMA matrix, the relaxation time of the filled blends is longer than for the pure blends, see Figures 3.10 and 3.11. It has to be remarked that the relaxation of the dispersed PC droplets cannot be observed in both the Cole-Cole plot and the relaxation spectra within the used frequency range.

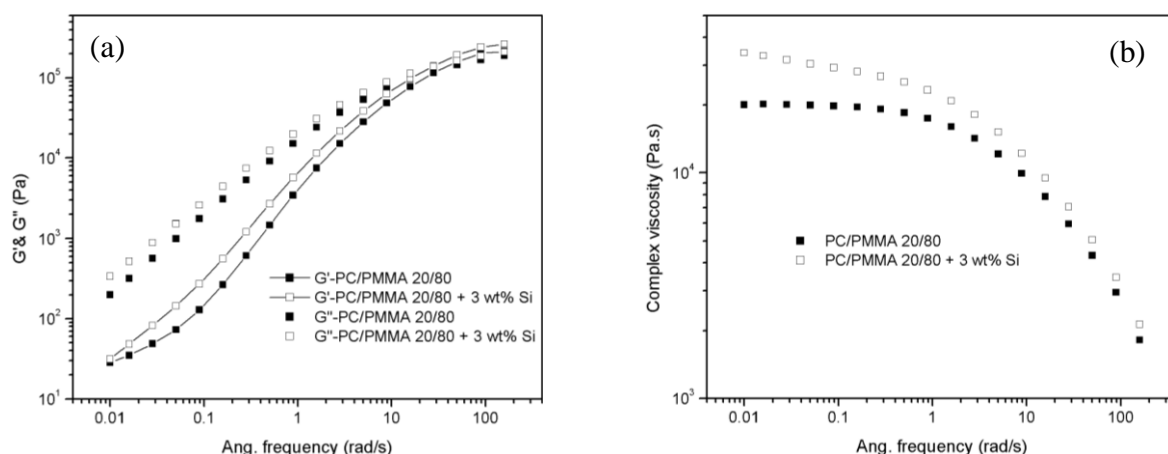


Figure 3.9: Viscoelastic behavior of neat or MEK-ST silica-filled PC/PMMA 20/80 blends ($T=220$ °C): (a) Frequency dependence of the storage and loss modulus and (b) frequency dependence of the complex viscosity.

Compared to the PC/PMMA 20/80, more information can be found in the PC/PMMA 80/20 blends because the contribution of deformed droplets is well visible in the G' curve for this composition. It is known that for blends with a spherical morphology there is an interface contribution to the storage modulus in the range of low frequencies.³⁶ In other words, an increase in size as well as in the volume fraction of the droplet phase leads to an increase of G' at low frequencies.³⁷ As shown in Figure 3.12a, the existence of the dispersed droplet phase is characterized by an increase in the elasticity, which manifests itself as a shoulder at low frequencies. However, the silica-filled 80/20 sample shows a less pronounced plateau which moves to lower frequencies. A lower complex viscosity is observed in the filled 80/20 blend, shown in Figure 3.12b. This can be explained by the fact that the dispersed PMMA droplets are crowded with silica nanoparticles, which leads to smaller and undeformable droplets, as already shown in Figure 3.5c. The silica-filled PMMA droplets behave like hard spherical particles dispersed in the PC matrix. Compared to the neat blend, the silica-filled

system is more like particle suspension system, which leads to an unobvious shoulder at low frequencies in storage modulus curve.

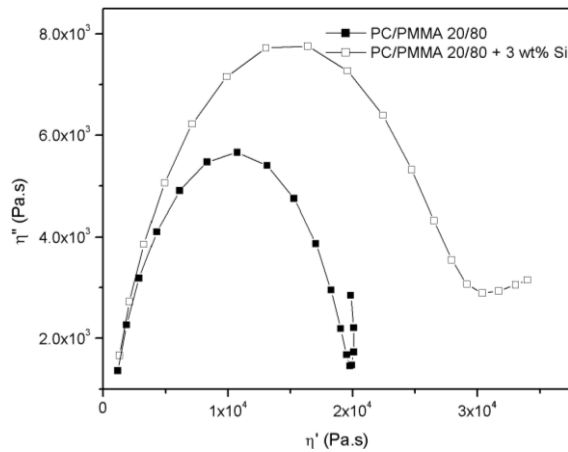


Figure 3.10: Cole-Cole plot for the neat and MEK-ST silica-filled PC/PMMA 20/80 blends at 220 °C.

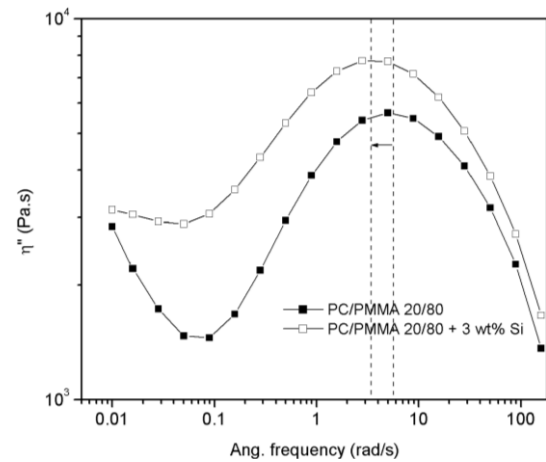


Figure 3.11: Frequency dependence of $\eta''(\omega)$ for the neat and MEK-ST silica-filled PC/PMMA 20/80 blends.

Figure 3.13 shows the Cole-Cole plot for the neat and silica-filled 80/20 blends. The second circular arc appears on the right-hand side of the arc, which corresponds to the second relaxation mechanism (droplets relaxation). However, with addition of the silica, the whole curve becomes shorter, displaying that the entire relaxation process of the MEK-ST silica-filled blend occurs at shorter time than the pure blend. The reason is the same with the presence of an unobvious secondary plateau of storage modulus at low frequencies, which is due to the existence of the hard silica-filled PMMA particles (Figure 3.5a-c). Furthermore, the spatial distribution of silica particles can be observed in Figure 3.14. In the droplet-matrix structure system, at high frequencies the relaxation is essentially due to matrix relaxation mechanisms, whereas at low frequencies the relaxation mainly stems from the deformability of the suspended droplets.³⁸ When 3 wt% silica particles were added in the 80/20 blend, the relaxation peak of PMMA droplets is shifted to lower frequencies compared to the neat blend, i.e., that droplet relaxation occurred at longer times with addition of the silica particles.

For this droplet-matrix blend, the influence of silica particles on the coalescence can be studied with rheological methods. Moldenaers *et al.* reported the suppression effect of silica particles on the coalescence in a model blend composed of poly(dimethyl siloxane) (PDMS)/poly(isobutylene) (PIB) by studying the dynamic frequency sweeps after well-defined flow histories and using the Palierne model for the interpretation.^{26,39} The authors demonstrated that nanoparticles do not behave as classical compatibilizers, but as interfacial mobility

modifiers. But in our case, the Palierne model cannot be used to fit the data because of the silica aggregation in the PMMA phase. Instead, the silica effect on the stability of the morphology was studied by TEM.

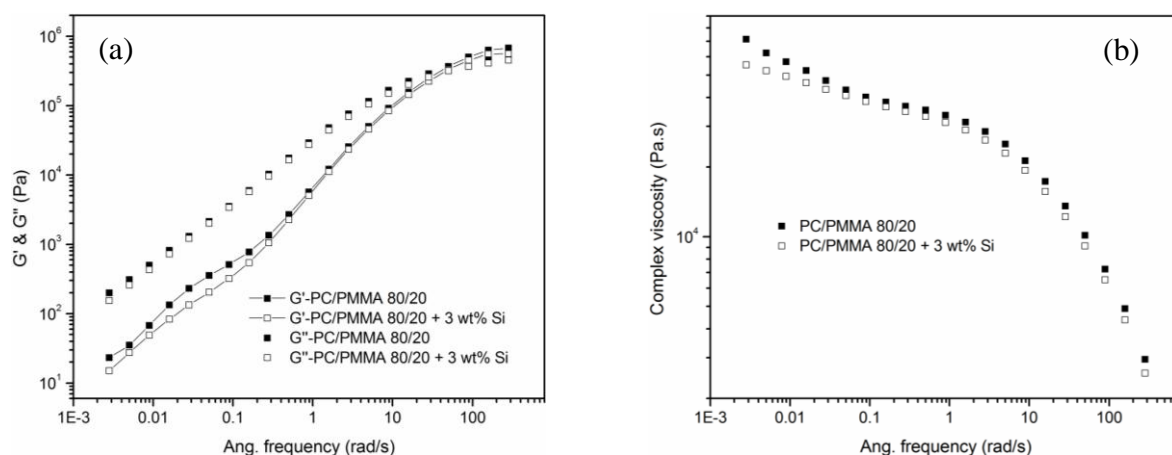


Figure 3.12: Viscoelastic behavior of neat or MEK-ST silica-filled PC/PMMA 80/20 blends ($T=220$ °C): (a) Frequency dependence of the storage and loss modulus and (b) frequency dependence of the complex viscosity.

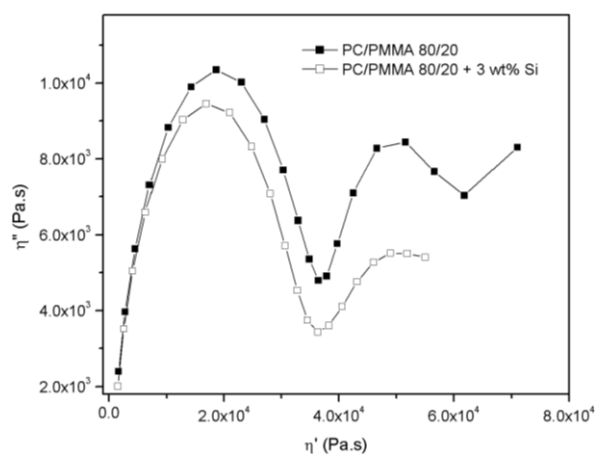


Figure 3.13: Cole-Cole plot for the neat and MEK-ST silica-filled PC/PMMA 80/20 blends at 220 °C.

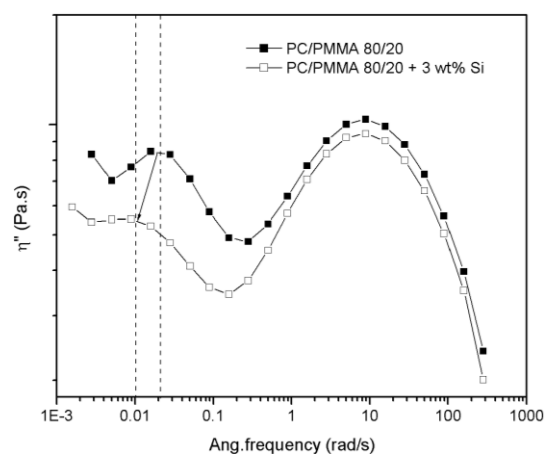


Figure 3.14: Frequency dependence of $\eta''(\omega)$ for the neat and MEK-ST silica-filled PC/PMMA 80/20 blends.

From the experimental results, the linear viscoelastic properties of the nanocomposites proved to be extremely sensitive to the morphology and the state of distribution of the silica nanoparticles in the melt state. The addition of the MEK-ST hydrophilic silica particles lead to a finer morphology in blends with PMMA as the dispersed phase, which is consistent with the TEM results. The shape relaxation of the dispersed phase, which is evidenced from the variation of $\eta''(\omega)$, can provide information on the redistribution of the silica particles.

3.3.4 Stability of the morphology in relation to polymer-silica interaction

The stability of the morphology is another important aspect in polymer blends, which is required to ensure constant properties that will not be altered after a second extrusion or injection molding step. Besides, in the nanoparticle-filled system, the final morphology with the localization of nanoparticles may differ from the thermodynamic equilibrium if the medium viscosity is high or the processing time is short. Thus, in this section, the stability of the morphology and the silica particles will be studied in the PC/PMMA blends. The most common experiment was used, annealing the samples and observing the morphology after several hours at high temperature.

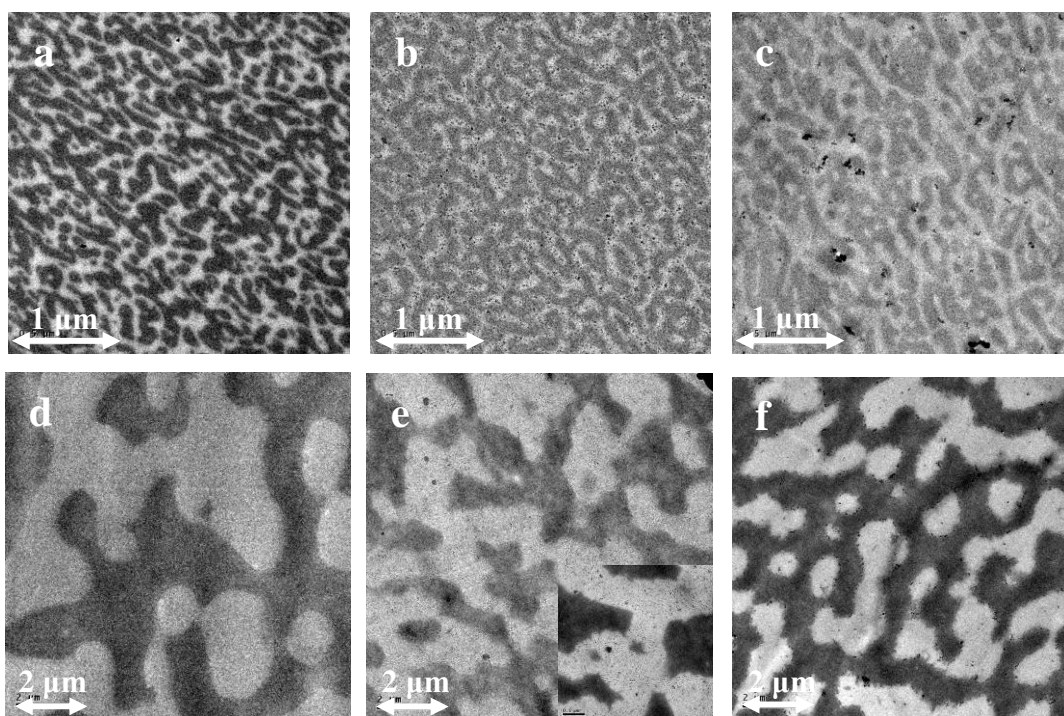


Figure 3.15: TEM images of non-annealed (a-c) and annealed (d-f) PC/PMMA 50/50 blends: (a,d) neat PC/PMMA, (b,e) 3 wt% MEK-ST silica-filled PC/PMMA and (c,f) 1.5 wt% Si-R972 silica-filled PC/PMMA.

To study the effect of the silica particles on the stability of the morphology in relation to the interaction between the surface of nanoparticles and the polymers, a hydrophobic nanosilica Si-R972 was used, of which surface is treated with dimethyldichlorosilane. The hydrophobic silica-filled blend was prepared via pre-compounding the Si-R972 particles with PC followed by blending with PMMA, the Si-R972 particles are found to preferentially localize themselves at the PC/PMMA interface (Figure 3.15c).

As shown in Figure 3.15a-c, both the neat and silica-filled PC/PMMA 50/50 blends show a co-continuous morphology after extrusion (before annealing). The MEK-ST silica distributes in the PMMA phase in Figure 3.15b and the Si-R972 silica localizes at the interface of PC/PMMA in Figure 3.15c. Before annealing, the scale of the phase separation of the PC/PMMA blend is not obviously affected by addition of two types of the silica. After annealing at 190 °C for 15 hrs, it is evident that the scale of the phase separation is suppressed significantly by silica nanoparticles, seen in Figure 3.15d-f. On comparing Figure 3.15e and f, the 1.5 wt% Si-R972 silica particles show slightly more efficient on suppressing the coarsening than the 3 wt% MEK-ST silica particles.

Additionally, it is obvious that the co-continuous morphology is consistent after annealing in the neat and MEK-ST silica-filled blends. However, a droplet-matrix morphology can be obtained in the Si-R972 silica-filled 50/50 blend in Figure 3.15f. The change of the morphology after annealing can further make clear what the mechanism of the suppression effect of the silica is. As hypothesized in previous section, the stabilization of MEK-ST silica corresponds to the local increase of the viscosity and the reduction of the mobility of the PMMA phase. Thus, the annealing (increasing the mobility of the polymer chains) will not influence the morphology of the blend, of which the co-continuous morphology should be the same. In the other case, the hydrophobic Si-R972 particles, which selectively localize on the interface of the PC/PMMA, change a co-continuous structure of the 50/50 blend to a droplet-matrix structure (like immobilization of the dispersed drops). This is consistent with the mechanism of the inhibition of coalescence by the presence of a solid barrier. Moreover, the compatibilization induced by the silica solid barrier is more efficient than the viscosity enhancement of one of the phases by the silica.

3.4 Discussion

In the majority of binary polymer blends, the nanoparticles distribute unequally between the polymer phases. This behavior was earlier reported in studies on poly(ethylene) (PE)/poly(propylene) (PP), PE/PMMA and PP/PMMA blends filled with carbon black by Sumita *et al.*⁴⁰ They concluded that two situations can be distinguished depending on the balance of interactions between the surface of the particles and the polymer components: (i) the particles are distributed mainly and homogeneously in one of the two phases and (ii) the particles are confined at the interface between the two polymers.

Given the results presented in Section 3.3, the relation between the polymer-particle interaction, as varied by using two different silica particles, i.e. hydrophilic MEK-ST and hydrophobic Si-R972 silica particles, and the observed selective localization of the nanoparticles needs to be addressed. For the hydrophilic particle systems, the nanoparticles are found to be selectively distributed in the PMMA phase, independent on the compounding sequence, as a result of the strong interaction between the hydroxyl groups on the surface of MEK-ST silica and PMMA. However, for the hydrophobic particle systems, the localization of the silica particles depends on the compounding sequence. When the sample was prepared via pre-compounding the Si-R972 particles with PC followed by blending with PMMA (procedure 2), the Si-R972 particles are preferentially localized at the PC/PMMA interface, as shown in Figure 3.16c-d. Further annealing at 190 °C for 15 hrs confirms that the distribution of the silica particles at the interface of the two polymers is the thermodynamically stable state, as observed in Figure 3.16e. When the three components were mixed simultaneously with a mixing time of 10 min (procedure 3), the Si-R972 particles were dispersed in both the PC and PMMA phases, Figures 3.16a-b, but it was shown the exact localization is dependent on the mixing and annealing time and temperature and, ultimately, the thermodynamically stable localization of the particles is at the interface.

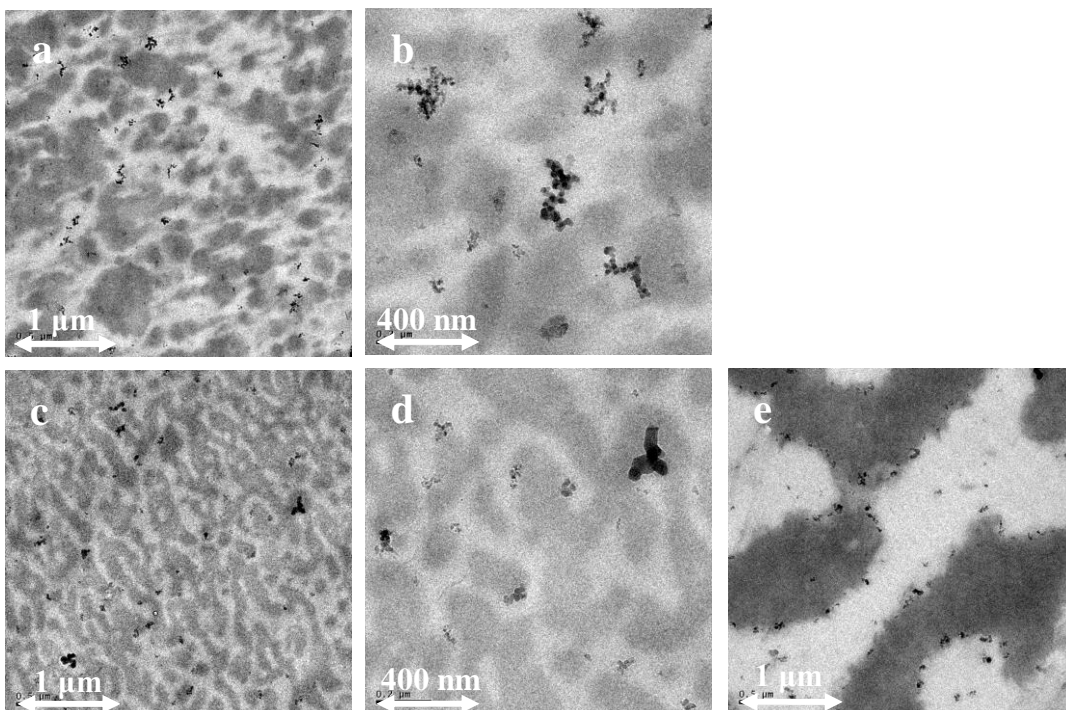


Figure 3.16: TEM images of 1.5 wt% Si-R972 silica-filled PC/PMMA 50/50 blends: (a-b) prepared via compounding procedure 3 (three components were mixed simultaneously) and (c-e) prepared via compounding procedure 2 (Si-R972 silica was pre-compounded with PC, subsequent blending with PMMA), of which (e) is the annealed Si-R972-filled PC/PMMA.

The results demonstrate that the mixing procedure is very important for the PC/PMMA systems and has a strong effect on the dispersion of the nanoparticles. As mentioned previously, the final distribution of nanoparticles is related to the balance of interactions between the surface of the particles and polymer components, which can be predicted qualitatively by comparing the surface tension of the three components. The distribution of the particles in the thermodynamic equilibrium state can be predicted by calculating the wetting parameter, ω_{12} , defined in Eq. 3.1.

$$\omega_{12} = \frac{\gamma_{S-2} - \gamma_{S-1}}{\gamma_{12}} \quad (3.1)$$

Where γ_{S-i} is the interfacial tension between the nanoparticles and polymer i , γ_{12} is the interfacial tension between the two polymers. If $\omega_{12} > 1$, the particles are only present in polymer 1. If $\omega_{12} < -1$, they are only found in polymer 2. If $-1 < \omega_{12} < 1$ or stated differently, the particles are concentrated at the interface between the two polymers, which is most likely the case for polymer blends with a high degree of incompatibility or when the differences in the filler/polymer interactions are small.

While some experimental data can be found for polymer/polymer surface tensions, it is almost impossible to find these data for polymer/filler surface tensions. Therefore, they are estimated with the help of theoretical models such as the well-known Owens-Wendt equation:

$$\overline{\gamma}_{12} = \gamma_1 + \gamma_2 - 2\sqrt{\gamma_1^d \gamma_2^d} - 2\sqrt{\gamma_1^p \gamma_2^p} \quad (3.2)$$

Only the surface tension of component i , γ_i , needs to be known, in which the exponents d and p stand for the dispersive and the polar contribution to the surface tension, respectively.

Table 3.1 Surface tension data of the components of the blends

	γ	γ^d	γ^p
PC ^a	24.6	18	6.6
PMMA ^b	28.1	20.2	7.9
Hydrophilic MEK-ST silica ^b	80	29.4	50.6
Hydrophobic Si-R972 silica ^b	32	30	2

γ^d, γ^p : dispersive and polar components; *a* values from Refs.[41], *b* values from Ref.[18]

For the PC/PMMA system, we found $\omega_{PC-PMMA} = -13.5$ for the hydrophilic silica particles and $\omega_{PC-PMMA} = 0.75$ for the hydrophobic ones. At thermodynamic equilibrium, the hydrophilic MEK-ST silica particles should be preferentially located in the PMMA phase, while the hydrophobic Si-R972 silica should be found at the interface.

Based on the calculated ω and the results of the different compounding procedures of PC/PMMA blends, in the molten polymers, it is found that the thermodynamic equilibrium may be difficult to attain and the kinetic effects may dominate if the viscosity is high and/or the processing times are short. In other words, the morphology observed after a given mixing time may differ from that at the equilibrium, since the particles migrate slowly towards their preferred phase. Thus, depending on the sequence of addition of the components, the filler may migrate from one phase to the other to reach its equilibrium state. The easiest way to promote the occurrence of particle movement is to incorporate solid particles in the polymer having the lower affinity and then to add the higher affinity polymer.

3.5 Conclusions

The miscibility of PC/PMMA blends was studied via different preparation methods. It was shown that the solvent-cast method can be used to prepare a partially miscible PC/PMMA blend with a LCST behavior, while the melt-mixing method only leads to a phase-separated blend, since the mixing temperature is always higher than the cloud point.

Two types of silica particles, i.e. hydrophilic and hydrophobic, were used to study the effect on the morphology of PC/PMMA blends and it was shown that the distribution of the nanoparticles depends on the balance of interactions between the surface of the particles and the polymer components. For the hydrophilic silica, migration of the nanoparticles to the PMMA phase can be observed independent on the compounding sequence, while for the hydrophobic silica, localization at the PC/PMMA interface is the preferred state. The order of mixing the components has a strong effect on the dispersion of the nanoparticles and shows that the kinetics are very important for the hydrophilic silica-filled PC/PMMA systems, especially when the viscosity ratio of two components is high and/or the processing time is short.

Furthermore, it was shown that the silica nanoparticles have a large effect on the morphology development. A reduction of the size of PMMA droplet phase in the PC/PMMA 80/20 blend with 3 wt% hydrophilic MEK-ST silica can be observed. The stabilization of coarsening can be attributed to the local increase of the viscosity and a concomitant reduction

of the mobility of the PMMA phase. In the study of the stability effect of silica on the morphology, the hydrophobic silica particles show the same stabilization effect on the coarsening of the PC/PMMA blend by inhibiting the coalescence through the presence of a immobilized layer of nanoparticles around the polymer droplets. Compared to the hydrophilic silica, a better compatibilization can be obtained by introducing the hydrophobic silica particles at the PC/PMMA interface as the solid barrier.

3.6 References

- ¹ Rincon, A., McNeill, I. C., *Polym. Degrad. Stab.*, **1987**, 18, 99-110.
- ² Koo, K. K., Inoue, T., Miyasaka, K., *Polym. Eng. Sci.*, **1985**, 27, 741-746.
- ³ Ray, S. S., Bousmina, M., *Macromol. Rapid Commun.*, **2005**, 26, 450-455.
- ⁴ Kim, W. N., Burns, C. M., *Macromolecules*, **1987**, 20, 1876.
- ⁵ Kambour, R. P., Gundlach, P. E., Wang, I-C. W., White, D. M., Yeager, D. W., *Polym. Prep. (Am. Chem. Soc., Div. Polym. Sci.)*, **1987**, 28, 140.
- ⁶ Gardlund, Z. G., *Polymer blends and composites in multiphase systems*, American Chemical Society, Washington, DC, *Advances in Chemistry*, **1984**, 206, Chapter 9.
- ⁷ Saldanha, J. M., Kyu, T., *Macromolecules*, **1987**, 20, 2840-2847.
- ⁸ Kyu, T., Saldanha, J. M., *J. Polym. Sci., Part C: Polym. Lett.*, **1988**, 26, 33-40.
- ⁹ Kyu, T., Saldanha, J. M., *Macromolecules*, **1988**, 21, 1021-1026.
- ¹⁰ Lim, D. S., Kyu, T., *J. Chem. Phys.*, **1990**, 92, 3944-3950.
- ¹¹ Kyu, T., Lim, D. S., *J. Chem. Phys.*, **1990**, 92, 3951-3956.
- ¹² Chiou, J. S., Barlow, J. W., Paul, D. R., *J. Polym. Sci., Part B: Polym. Phys.*, **1987**, 25, 1459-1471.
- ¹³ Nishimoto, M., Keskkula, H., Paul, D. R., *Polymer*, **1991**, 32, 272-278.
- ¹⁴ Paul, D. R., Newman, S., *Polymer blends I and II*, Academic Press, New York, **1997**.
- ¹⁵ Sundararaj, U., Macosko, C. W., *Macromolecules*, **1995**, 28, 2647-2657.
- ¹⁶ Macosko, C. W., Guegan, P., Khandpur, A. K., Nakayama, A., Marechal, P., Inoue, T., *Macromolecules*, **1996**, 29, 5590-5598.
- ¹⁷ Tan, N. C., Tai, S. K., Briber, R. M., *Polymer*, **1996**, 37, 3509-3519.
- ¹⁸ Fenouillot, F., Cassagnau, P., Majeste, J. C., *Polymer*, **2009**, 50, 1333-1350.
- ¹⁹ Clarke, J., Clarke, B., Freakley, P. K., Sutherland, I., *Plast. Rubber Compos.*, **2001**, 30, 39-44.
- ²⁰ Elias, L., Fenouillot, F., Majeste, J. C., Cassagnau, P., *Polymer*, **2007**, 48, 6029-6040.
- ²¹ Ray, S. S., Bousmina, M., *Polym. Eng. Sci.*, **2006**, 46, 1121-1129.
- ²² Ray, S. S., Bousmina, M., *Macromol. Rapid Commun.*, **2005**, 26, 1639-1646.
- ²³ Van Hemelrijck, E., Van Puyvelde, P., Velankar, S., Macosko, C. W., Moldenaers, P., *J. Rheol.*, **2004**, 48, 143-159.
- ²⁴ Van Hemelrijck, E., Van Puyvelde, P., Velankar, S., Macosko, C. W., Moldenaers, P., *J. Rheol.*, **2005**, 49, 783-798.
- ²⁵ Cassagnau, P., *Polymer*, **2008**, 49, 2183-2196.
- ²⁶ Vermant, J., Cioccolo, G., Golapan Nair, K., Moldenaers, P., *Rheol. Acta*, **2004**, 43, 529-538.
- ²⁷ Paliarne, J. F., *Rheol. Acta*, **1990**, 29, 204-214.
- ²⁸ Bousmina, M., *Rheol. Acta*, **1999**, 38, 73-83.
- ²⁹ Yee, M., Calvao, P. S., Demarquette, N. R., *Rheol. Acta*, **2007**, 46, 653-664.
- ³⁰ Huo, Y., Groeninckx, G., Moldenaers, P., *Rheol. Acta*, **2007**, 46, 507-520.
- ³¹ Cheng, S. Z. D., Cao, M.-Y., Wunderlich, B., *Macromolecules*, **1986**, 19, 1868-1876.
- ³² Schick, C., Wurm, A., Merzlyakov, M., Minakov, A., Marand, H., *J. Therm. Anal. Calorim.*, **2001**, 64, 549-555.
- ³³ Manchado, M. A. L., Biagiotti, J., Kenny, J. M., *J. Appl. Polym. Sci.*, **2001**, 81, 1-10.
- ³⁴ Li, R., Yu, W., Zhou, Ch., *Polymer Bull*, **2006**, 56, 455-466.
- ³⁵ Riemann, R. E., Cantow, H. J., Friedrich, C., *Macromolecules*, **1997**, 30, 5476-5484.
- ³⁶ Friedrich, C., Gleinser, W., Korat, E., Maier, D., Weese, J., *J. Rheol.*, **1995**, 39, 1411-1425.
- ³⁷ Vinckier, I., Laun, H. M., *Rheol. Acta*, **1999**, 38, 274-286.
- ³⁸ Carreau, P. J., Bousmina, M., Ajjji, A., *Rheological properties of blends: facts and challenges*, Ghigino KP,

- Progress in Pacific Polymer Science 3*, Springer, Berlin Heidelberg New York, 25-40, **1994**.
- ³⁹ Vandebril, S., Vermant, J., Moldenaers, P., *Soft Matter*, **2010**, 6, 3353-3362.
- ⁴⁰ Sumita, M., Sakata, K., Asai, S., Miyasaka, K., Nakagawa, H., *Polym. Bull.*, **1991**, 25, 265-271.
- ⁴¹ Hobbs, S. Y., Dekkers, M. E. J., Watkins, V. H., *Polymer*, **1988**, 29, 1598-1602.

Chapter 4

Morphology control of PS-PB-PMMA/PMMA blends by silica nanoparticles

The effect of the silica nanoparticles on the morphology of a blend consisting of poly(methyl methacrylate) (PMMA) and the poly(styrene)-b-poly(butadiene)-b-poly(methyl methacrylate) (SBM) triblock copolymer was studied. Upon blending PMMA with SBM, macrophase separation between the block copolymer and homopolymer occurred, in which the higher molar mass chains of homopolymer separate into homopolymer-rich domains due to the 'dry-brush' regime, whereas the lower molar mass chains of homopolymer tend to be selectively solubilized in the block copolymer-rich domains due to the 'wet-brush' regime. Upon adding the hydrophilic (MEK-ST) silica nanoparticles to the PMMA/SBM blend, a significant suppression effect on the extent of macrophase separation between the homopolymer and block copolymer can be observed. It was shown that the silica particles are preferentially localized in the PMMA phase due to the strong hydrogen bonding interaction between the hydroxyl groups on the surface of silica nanoparticles with the carbonyl groups of the PMMA. The suppression effect of the silica particles may be related to the selective adsorption of the high molar mass PMMA on the surface of the silica particles, which may force the system into the 'wet-brush' regime, but this was only observed for the systems with a low silica content. For the systems with a high silica content, both the homopolymer PMMA and the PMMA block of the SBM block copolymer interact with the silica surface, which becomes the connecting part between both polymers, thereby suppressing the extent of macrophase separation. The suppression effect of silica particles was found to occur for all three preparation methods, i.e. solvent casting, melt mixing and in-situ polymerization of MMA in presence of the silica particles and triblock copolymer.

4.1 Introduction

The preparation of a tough, heterogeneous system based on brittle amorphous polymers such as poly(methyl methacrylate) (PMMA) and poly(styrene) (PS) has been the subject of numerous studies.^{1,2} As discussed in Chapter 1, the toughness of a brittle polymer can be improved by the introduction of a second (rubber) phase as impact modifier.³⁻⁹ The need for heterogeneities is universal and its role is to prevent the first cavity of the first craze to start to grow.²

A possible route to prepare these systems could be through the use of self-organizing block copolymers, which are able to form a morphology of nanosized core-shell particles in the amorphous matrix. In contrast to conventional rubber impact modifiers that phase separate during mixing, amphiphilic block copolymers containing a block that is miscible with the matrix and a block that is immiscible with the matrix microphase separate into ordered or disordered microstructures. The morphology of the system can be controlled by optimizing the block copolymer constituents, architecture, and composition.

For ABC triblock copolymers, unique morphologies have been observed and reported over the past decades, which can offer an increased potential to create systems with tailored chemical, physical and mechanical properties.¹⁰⁻¹⁴ Compared to mixing a diblock copolymer BC with a homopolymer A, microphase separation of triblock copolymers ABC has been found to generate much finer and richer morphologies. For homopolymer/block copolymer systems, three regimes of phase separation can be distinguished: microphase separation, macrophase separation, and macro/microphase separation. In the microphase separation regime, phase separation of the blocks of the triblock copolymer occurs together with swelling of one block with the homopolymer. For small amounts of block copolymer, the blend is characterized by individual micelles. In the macrophase separation regime, the homopolymer is separated from the block copolymer, which is in the disordered state. The macro/microphase separation regime can be described by the coexistence of the microphase-separated block copolymer and the macrophase-separated homopolymer.

To toughen a brittle matrix, the block copolymer is required to self-assemble into a core-shell structure. The size of the dispersed rubber-phase should be decreased to nanometer scale in order to combine the ductile mechanical behavior with a minimum loss in modulus and strength. Therefore, ABC triblock copolymers could be an ideal candidate to obtain a combination of a nanosized rubber shell with an easily-cavitating core, as was already demonstrated in earlier work.⁸⁻¹⁶

The three observed phase separation regimes of homopolymer/block copolymer systems are governed by the length of the homopolymer chains compared to that of the miscible block in the block copolymer, as discussed in Chapter 1.¹⁷⁻²⁰ The microphase separation occurs if $N_{Ah} < N_{Ac}$, where N_{Ah} and N_{Ac} represent the degree of polymerization of the homopolymer and the miscible block of the block copolymer, respectively. The homopolymer A selectively swells the A domains of the microphase-separated copolymer. This state is referred to as the ‘wet-brush’ regime. If $N_{Ah} > N_{Ac}$, the regime is called ‘dry-brush’ and macrophase separation occurs between the homopolymer and block copolymer.

For many practical systems, the molar mass distribution has to be taken into account. In general, two effects are observed, i.e. coexistence of different morphologies and disruption of the long-range order of the thermodynamically stable morphology with a high curvature, since a broad molar mass distribution can lead to a redistribution of the chains over the different phases and at the interface.

Generally, two blending techniques can be considered for introducing the block copolymer in the matrix: physical and chemical blending. The most common technique is physical blending via solvent casting or melt mixing. The final morphology is determined by the processing conditions, compatibility, solvent and viscosity ratio of the polymers involved. However, it is very difficult to prepare nanosized morphologies via physical blending. Therefore, chemical blending, in which at least one of the components is synthesized in the presence of the other one, is used. Starting from an initially homogeneous solution, the final morphology is the result of a chemically-induced phase separation during the polymerization. The final morphology can be controlled by adjusting the polymerization conditions and starting concentration. Van Casteren⁸ and Kierkels⁹ introduced the self-assembly of tri- or diblock copolymers, e.g. poly(acrylate)-*b*-polyolefin, in brittle matrices (PS/PMMA) by in-situ polymerization of monomer/copolymer solutions, but unfortunately both monomers are not selective enough to induce micellization at the normally applied polymerization temperatures. But even lowering the polymerization temperature below the Order-Disorder Temperature (ODT) did not prevent the occurrence of macrophase separation between the homopolymer and di- and triblock copolymer due to the ‘dry-brush’ condition: $N_{Ah} > N_{Ac}$. In the work of Van Casteren, macrophase separation was prevented by chemically modifying the PS by in-situ copolymerization with 0.5-5 mol% of *p*-(hexafluoro-2-hydroxy isopropyl) styrene (HFS) to introduce hydrogen bonding between the block copolymer and the homopolymer PS, which improved the stability of the micelles, and led to a transition of the

local deformation mechanism from crazing to cavitation-induced shear yielding within a certain HFS-concentration range.⁶

Recently, researchers found that nanoparticles can be used as a compatibilizer to reduce domain coarsening during macrophase separation of polymer blends, similar to the observations reported in Chapters 2 and 3 for partially miscible and immiscible homopolymer blends, respectively.²¹ Depending on the physical interaction between the surface of the nanoparticles and the polymer components, the nanoparticles can migrate to the interface and thereby affect the coalescence process or can be selectively incorporated in one of the polymer phases. Other studies showed that the incorporation of nanoparticles into self-assembled block copolymers can lead to alteration of the morphology by selective distribution of nanoparticles in one of the phases or at the interface.²²⁻²⁵ The cooperative self-organization of nanoparticles and block copolymers could yield a wide variety of structures with well-controlled particle arrangements. Experiments imply that the spatial distribution of nanoparticles in the microphase-separated morphologies can be controlled by tailoring the nanoparticle surface and the size of the nanoparticles relative to the radius of gyration of the polymer.²⁶⁻²⁸ Therefore, the introduction of nanoparticles in block copolymer/homopolymer systems may influence the thermodynamics and kinetics of micro/macrophase separation.

In this chapter, the effect of silica nanoparticles on the thermodynamics and kinetics of micro/macrophase separation is studied with PMMA as matrix material with poly(styrene)-*b*-poly(butadiene)-*b*-poly(methyl methacrylate) (PS-PB-PMMA) as the triblock copolymer. Three different mixing methods will be used: solvent casting, in-situ polymerization, and melt mixing.

4.2 Experimental

4.2.1 Materials

PMMA was provided by Arkema (France), with a number-averaged molar mass (M_n) of 42 kg/mol and a polydispersity index (PDI) of 2.1. Small amounts of ethyl acrylate (EA) are usually incorporated into PMMA to prevent unzipping of the polymer at elevated temperatures during processing. The PMMA used in this study contained 0.5 wt% EA. The poly(styrene)-*b*-poly(butadiene)-*b*-poly(methyl methacrylate) (SBM) ($M_n=55$ kg/mol) was supplied by Arkema (France), coded as $S_{20}B_{25}M_{55}$, where the subscripts represent the weight fractions of the respective blocks. The as-received triblock copolymer contained 29 wt% SB diblock and was used without any further purification, while the S and B blocks had the same

molar mass in the triblock and the diblock copolymer. Two monodisperse PMMAs were provided by Polymer Source (Canada), one with a M_n of 15 kg/mol and a PDI of 1.06, another with a M_n of 75 kg/mol and a PDI of 1.05. These two monodisperse PMMAs will be referred to as PMMA15k and PMMA75k, respectively. MMA and methyl ethyl ketone (MEK) were obtained from Sigma Aldrich and were used as received. Pre-made colloidal silica nanoparticles with a diameter of 10-15 nm, dispersed in MEK with approx. 30 wt% silica, were purchased from Nissan Chemical (USA) and the surface was covered with methyl and hydroxyl groups. This silica nanoparticle will be referred to as MEK-ST. The silica nanoparticles were used without any further surface modification.

4.2.2 Sample preparation

Solvent casting

The MEK-ST nanoparticles dispersions were diluted with MEK and the two polymers were dissolved separately to obtain two separate silica-filled solutions. Next, the two obtained solutions were mixed followed by solvent casting on a glass substrate. A doctor blade was used to control the thickness of the film. The polymer concentration in the solution was 8 wt%. The solvent-cast samples were dried in a fume-hood at room temperature for 2 days followed by a final drying step at 100 °C under reduced pressure with a low nitrogen flow for 1 more day to ensure complete solvent removal. The final thickness of the samples was approximately 2 μm . The dried films were annealed at 135 °C for 7 days under a nitrogen atmosphere. The samples were subsequently cooled to room temperature.

Solvent casting using high throughput experimentation setup (HTE)

Two solutions were prepared from the as-received MEK-ST nanoparticle dispersions, which were diluted with MEK to the required concentration. Subsequently, the two polymers were separately dissolved in the silica-filled solutions. Next, the two obtained solutions were mixed and solvent cast on a glass substrate with a size of 70 x 70 mm by using the HTE setup. For a detailed description of the film gradient preparation and the HTE settings, see Chapter 2. The whole film preparation takes less than 20 s and the thickness of the coating varied from 1.0 to 1.8 μm in the direction orthogonal to the ϕ -gradient.

The drying procedure of the thin film with the ϕ -gradient is the same as for the samples prepared via ‘solvent casting’.

Melt mixing

Silica nanoparticles were pre-dispersed in PMMA by melt mixing in a twin-screw mini-extruder, followed by blending the obtained PMMA/silica mixture with S₂₀B₂₅M₅₅ in a second step. The temperature was set at 220 °C for the PMMA/S₂₀B₂₅M₅₅ 60/40 blends. The extruder was fed with 6 g of material with the screw speed set at 50 rpm and the total mixing time was fixed at 10 min. All the experiments were performed under a nitrogen atmosphere in order to prevent oxidative degradation.

In-situ polymerization

The free radical polymerization of MMA/triblock copolymer solutions was performed over a broad range of temperatures to minimize void formation due to polymerization shrinkage and to get more control over the morphology. 0.2 wt% 2,2-azobis(isobutyronitrile)(AIBN) was used as initiator. Homogeneous solutions of MMA, triblock copolymer, initiator and silica particles were prepared at room temperature. The solutions were poured into glass bottles which were hermetically sealed after being purged with nitrogen for several min. The solutions were left overnight at room temperature during which the free radical polymerization was initiated by the initiator. Subsequently, the bottles were placed in a heating cell with a programmed temperature profile: 20 hrs at 30 °C and subsequently at 50, 70, 90 °C, followed by two post polymerization steps at 110 and 120 °C for 2 hrs each. For the in-situ SAXS measurements, the polymerizations were performed at 100 °C and initiated by 0.2 wt% AIBN.

4.2.3 Characterization techniques

Atomic force microscopy (AFM)

The AFM investigations were performed by using a Smena P47H microscope (NT-MDT Ltd, Moscow, Russia). The AFM was operated in semi-contact mode under an air atmosphere using a silicon cantilever (NSG 11 NT-MDT), which was coated with a gold layer for a higher laser beam reflectivity. The resonance frequencies applied were 115-190 kHz.

Transmission electron microscopy (TEM)

Morphological investigations were performed by using a Tecnai 20 transmission electron microscopy (TEM), operated at 200 kV. Samples were trimmed at -120 °C and subsequently bulk-stained for 2 weeks with an Osmium tetroxide (OsO₄) solution prepared according to Montezinos *et al.*²⁹, which predominantly reacts with the PB phase. Ultrathin sections (\pm 70

nm) were obtained at room temperature using a Reichert UltracutS/FCS ultramicrotome equipped with a diamond knife.

Thermogravimetric analysis (TGA)

A Q500 TGA (TA Instruments) was used for the quantitative determination of the silica content in the nanocomposites. Samples were heated under a pressed air atmosphere at 10 °C/min from 30 to 800 °C and held at 800 °C for 15 min. The residue was assumed to be only composed of silica.

Small-angle X-ray scattering (SAXS)

To study the morphology development upon in-situ polymerization of the monomer, time-resolved small-angle X-ray scattering experiments (SAXS) were performed on the DUBBLE beamline (BM26B) at the European Synchrotron Radiation Facility (ESRF) in Grenoble (France). The SAXS data were collected on a multiwire two-dimensional (2D) detector positioned at 8 m from the sample. MMA/block copolymer solutions were transferred into Lindemann capillaries, which were subsequently sealed. The capillaries were placed in a capillary holder fixed on a Linkam THMS 600 hot-stage mounted on the optical bench. The silver heating block of the hot-stage contained a 4 mm² conical hole allowing the X-rays to pass through unhindered. For calibration of the SAXS detector, the scattering pattern from an oriented specimen of wet collage (rat-tail tendon) was used. The experimental data were corrected for background scattering, i.e. subtraction of the scattering from the camera, hot-stage and capillary. The two-dimensional SAXS data were transformed into one-dimensional plots by performing integration along the azimuthal angle using the FIT2D program of Dr. Hammersley of ESRF. Two different exposure times were used for the time-resolved measurements: 24 and 30 s.

4.3 Results and discussion

Three mixing methods were applied to study the influence of the silica nanoparticles on the morphology, i.e. solvent casting, in-situ polymerization, and melt mixing. First, the effect on the morphology of the SBM triblock copolymer prepared via solvent casting and melt mixing will be discussed as a reference. This is followed by the effect of the silica particles on the morphology of the blends using solvent casting including the effect of the molar mass distribution. Then, the influence of silica nanoparticles on the morphology (development) is discussed for the in-situ polymerization method. Finally, the melt-mixing method is evaluated.

4.3.1 The effect of silica nanoparticles on the morphology of the SBM triblock copolymer

Block copolymers self assemble into ordered structures via microphase separation and the morphology can be influenced by the preparation method. The solvent used for the solvent casting was MEK which has a preferential affinity for the majority block PMMA. The morphologies of the triblock copolymer $S_{20}B_{25}M_{55}$, prepared by compression molding and solvent casting, are depicted in the TEM-images displayed in Figures 4.1a and b, respectively. Since the as-received SBM triblock copolymer is composed of SBM triblock and SB diblock copolymer, micro/macrophase separation might occur. In Figure 4.1a, three domains are clearly present with different grey scale levels. The bright phase corresponds to the PMMA domains, and the grey phase corresponds to PS domains, while the dark phase corresponds to the PB domains. The compression-molded $S_{20}B_{25}M_{55}$ triblock (from the melt below ODT) shows a worm-like lamellar structure with almost no long-range order with a high curvature due to the presence of SB diblock impurity. The average domain spacing is approx. 100 nm. Compared to the compression-molded sample, the solvent-cast sample shows a higher long-range ordering. This could be due to the solvent selectivity to the PMMA block or to the higher mobility during the solvent-casting process, which enables a better ordered structure during microphase separation. It has to be remarked that the block copolymer concentration during solvent casting is so high (8 wt%) that at the casting temperature (ambient) the system is below the ODT. Both cylindrical and lamellar structures coexist in Figure 4.1b. For the pure triblock copolymer the lamellar structure is the thermodynamically stable state. The cylindrical structures are related to the phase separation between the SB diblock copolymer and the SBM triblock copolymer during annealing of the solvent-cast films resulting in a lot of defects in the lamellar morphology.³⁰ The lamellar structure has a higher long-range order with a lower curvature and its domain spacing appears to be smaller, i.e. approx. 60 nm.

With the addition of MEK-ST silica nanoparticles, the silica particles are found to have a preference to be dispersed in PMMA phase (bright). Figure 4.1c shows the result of mixing the nanoparticles with the triblock copolymer $S_{20}B_{25}M_{55}$. Compared to the neat $S_{20}B_{25}M_{55}$ in Figure 4.1b, the morphology is changed. The PMMA domains are swollen by the selective localization of the silica particles and there are more cylindrical domains (defects from SB diblocks). This is also shown in a higher magnification image (Figure 4.1d). The selective localization is due to the strong hydrogen bonding interaction between the hydroxyl groups on the surface of the silica nanoparticles and the carbonyl groups of the PMMA. A disruption

of lamellar structure of $S_{20}B_{25}M_{55}$ can be observed, which implies that the silica particles induce a (macrophase) separation between the SB diblock and SBM triblock copolymers. This was also observed in the homopolymer/block copolymer blends as will be discussed later in more detail.

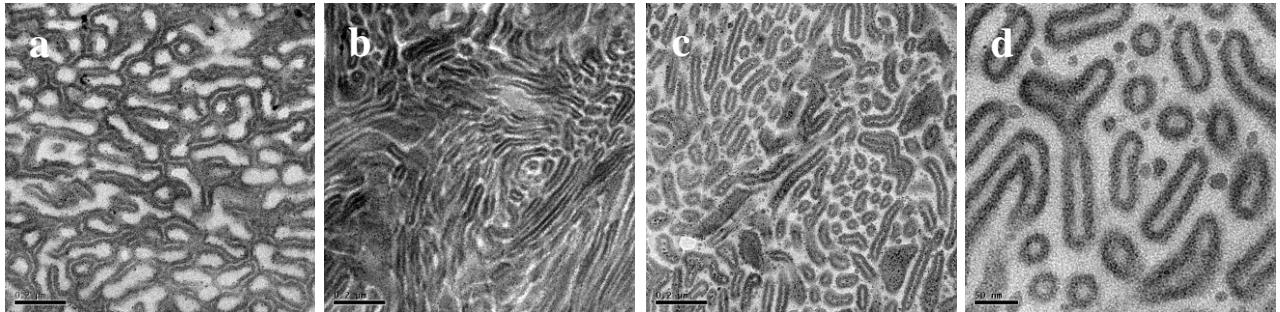


Figure 4.1: TEM images of (a) compression-molded $S_{20}B_{25}M_{55}$, (b) solvent-cast $S_{20}B_{25}M_{55}$ and (c-d) solvent-cast $S_{20}B_{25}M_{55}$ with 3 wt% MEK-ST at various magnifications.

4.3.2 The effect of silica nanoparticles on the morphology of solvent-cast PMMA/ $S_{20}B_{25}M_{55}$ blends

The improvement of properties of the amorphous polymers modified with di- or triblock copolymers depends strongly on the morphology of the blend. In order to obtain good mechanical properties, a high molar mass amorphous polymer as the matrix is needed. Therefore, as outlined in the introduction, the main problem with dispersing block copolymers in homopolymers is the occurrence of macrophase separation in the ‘dry-brush’ condition: $N_{Ah} > N_{Ac}$. In this section, the effect of nanoparticles on the morphologies of the block copolymer/homopolymer blend is studied via solvent casting. In addition, the effect of the molar mass of the homopolymer and the PDI on the extent of phase separation is discussed to understand the behavior of the silica nanoparticles.

4.3.2.1 The morphology of PMMA/ $S_{20}B_{25}M_{55}$ blends and the effect of the molar mass distribution of the PMMA

First, the morphology of the neat block copolymer/homopolymer blend PMMA/ $S_{20}B_{25}M_{55}$ is investigated. The HTE setup is helpful to get insight in this complex phase behavior due to its fast screening. Commercial polymers like PMMA usually have a relatively high polydispersity index. The PMMA used in this blend has a M_n of 42 kg/mol and a PDI of 2.1. PMMA/ $S_{20}B_{25}M_{55}$ films with a ϕ -gradient were prepared from MEK by using the HTE setup.

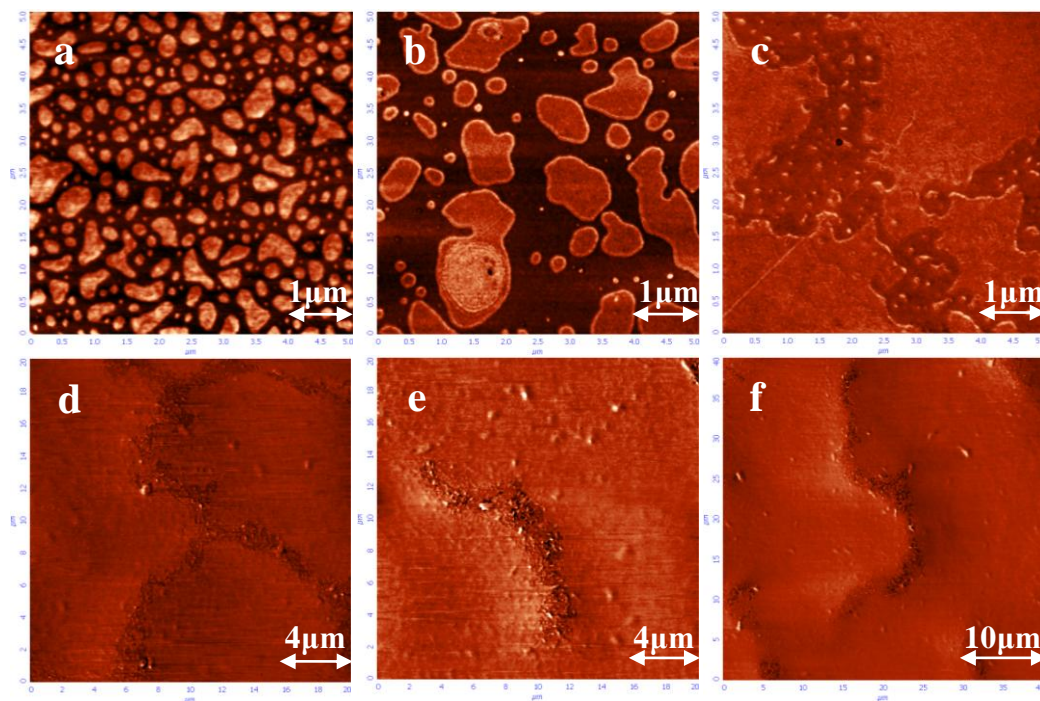


Figure 4.2(a-f): AFM phase angle images of neat PMMA(broad PDI=2.1)/ $S_{20}B_{25}M_{55}$ blend prepared with the HTE setup at six positions separated by a distance of 10 mm from one side of the sample to the other. In the neat polymer blend, the dark regions in the phase angle images correspond to lower phase angles or higher stiffness (PMMA domain). Light regions correspond to the $S_{20}B_{25}M_{55}$ -rich domains.

The morphology was investigated with AFM and the measurements were performed from one side of the film on the glass substrate to the other, at six different positions separated by a distance of 10 mm. The chosen positions are in the center of the glass slide. The obtained contrast is based on the relatively low stiffness of the butadiene block of SBM relative to PMMA. Figure 4.2a shows the morphology with $S_{20}B_{25}M_{55}$ domains dispersed in the PMMA matrix. It is evident that with increasing $S_{20}B_{25}M_{55}$ concentration, the domain size of $S_{20}B_{25}M_{55}$ increases (Figure 4.2b). Furthermore, a co-continuous morphology is observed in Figure 4.2c. Moving to position d, phase inversion occurs and $S_{20}B_{25}M_{55}$ becomes the matrix with PMMA as the dispersed phase and the extent of macrophase separation grows to larger length scales at positions e and f.

As mentioned in the introduction, the molar mass of the homopolymer is of importance to determine the phase behavior of the homopolymer/block copolymer blend. Besides, the polydispersity of the matrix is also a key factor on the length scale of the macrophase separation. Before studying the effect of the silica nanoparticles, the phase separation behavior based on the polydispersity of the PMMA homopolymer is explored first. The

homopolymer PMMA of the previous blend has a M_n of 42 kg/mol and a PDI of 2.1 and the majority of polymer chains have a molar mass which is higher than that of the PMMA block of the $S_{20}B_{25}M_{55}$ (the M_n of PMMA block is around 30 kg/mol). The higher molar mass chains separate into homopolymer-rich domains, whereas the lower molar mass chains tend to be selectively solubilized in the block copolymer-rich domains. To study the influence of the molar mass (distribution), two monodisperse PMMAs with different molar masses and their mixture were chosen. One has a M_n of 15 kg/mol ('wet-brush' regime), while the other has a M_n of 75 kg/mol ('dry-brush' regime).

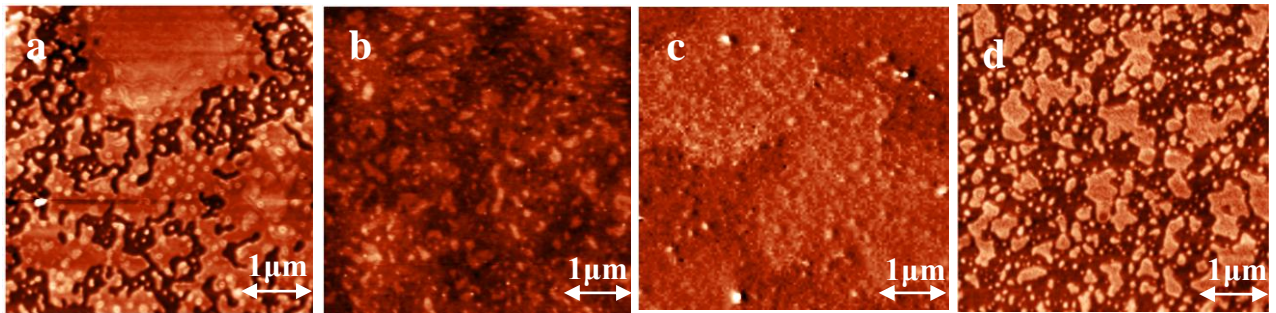


Figure 4.3: AFM images of the PMMA/ $S_{20}B_{25}M_{55}$ 50/50 blend, of which the homopolymer PMMA is with different polydispersity (a) broad PMMA PDI=2.1, (b) monodisperse PMMA15k, (c) monodisperse PMMA75k and (d) bimodal PMMA15k:PMMA75k 50:50.

The PMMA/ $S_{20}B_{25}M_{55}$ blend with a fixed composition of 50/50 is used in the polydispersity study and the same annealing condition was applied as before. Standard solvent casting was used, since only one composition is explored. In Figure 4.3, the different length scales of phase separation are observed when blending the $S_{20}B_{25}M_{55}$ with different PMMAs. Macrophase separation with similar length scales is revealed in the blends of PMMA(broad)/ $S_{20}B_{25}M_{55}$ and PMMA(monodisperse75k)/ $S_{20}B_{25}M_{55}$, in which the molar mass of homopolymer PMMA exceeds the molar mass of the PMMA block of the block copolymer ($N_{Ah} > N_{Ac}$). On the other hand, in Figure 4.3b, wetting of the PMMA phase of the block copolymer occurs if the molar mass of the PMMA homopolymer is smaller than the molar mass of the PMMA block ($N_{Ah} < N_{Ac}$) in the blend of PMMA(monodisperse15k)/ $S_{20}B_{25}M_{55}$. The small light domains arise from the SB diblock copolymer, which phase separated from the SBM triblock. The reason is related to the change of the curvature of the lamellar structure of SBM when the PMMA15k is soluble in the PMMA block of $S_{20}B_{25}M_{55}$, which induces swelling of the PMMA domain. As a result, the SB diblock is easily expelled from the matrix. Furthermore, a bimodal homopolymer PMMA, which contains a mixture of 50/50 PMMA15k/PMMA75k, was used to blend with the $S_{20}B_{25}M_{55}$. In Figure 4.3d, the scale

of macrophase separation of the PMMA(bimodal) / $S_{20}B_{25}M_{55}$ blend is in between of the PMMA(broad PDI)/ $S_{20}B_{25}M_{55}$ and PMMA15k / $S_{20}B_{25}M_{55}$. The four blends will be studied in the next section to understand how the silica particles affect the phase behavior of the homopolymer/block copolymer blends.

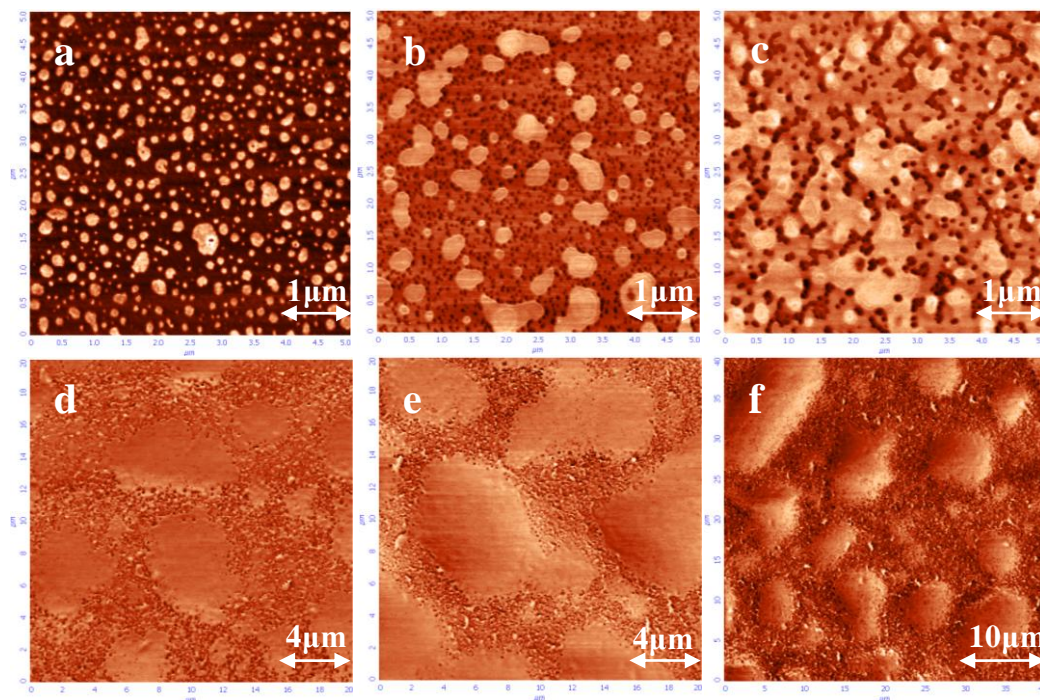


Figure 4.4(a-f): AFM phase angle images of PMMA(broad PDI=2.1)/ $S_{20}B_{25}M_{55}$ blends with 2 wt% MEK-ST silica prepared with the HTE setup at six positions separated by a distance of 10 mm from one side of the sample to the other. The dark spheres correspond to silica particles.

4.3.2.2 The suppression effect of silica nanoparticles

In Figure 4.2, the PMMA(broad)/ $S_{20}B_{25}M_{55}$ homopolymer/triblock copolymer systems showed a combination of macro- and microphase separation for the whole composition range studied. The occurrence of macrophase separation can be explained by a number of effects. The most important one is that the used SBM material contains a substantial amount of SB diblock copolymer. In addition, the system is in the ‘dry-brush’ regime. On addition of the PMMA homopolymer with a broad molar mass distribution, either swelling of the PMMA phase of the block copolymer can occur if the molar mass of the PMMA homopolymer is smaller than the molar mass of the PMMA block (‘wet-brush’ regime) or macrophase separation takes place if the molar mass of the PMMA homopolymer is larger than the molar mass of the PMMA block (‘dry-brush’ regime). In this case, the distinction between the ‘dry-brush’ and ‘wet-brush’ regimes becomes less clear. The presence of SB diblock copolymer in

such a system complicates the phase behavior, since the SB diblock copolymer has to be accommodated at the interfacial regions of the SB part of the triblock copolymer. Due to the complex phase behavior of PMMA(broad)/S₂₀B₂₅M₅₅, the effect of nanoparticles is studied for this system first.

For the solvent casting the silica-filled blends by using the HTE setup, both starting solutions were mixed with MEK-ST silica to a final weight percentage of 2 wt%. Using the same settings as for the blends without silica, films with the required composition gradient were prepared on the glass substrates. The blends were subsequently annealed under the same condition as the neat samples. The morphologies of the silica-filled blend were investigated at the same positions a-f as that of the neat polymer blend, of which the results are shown in Figure 4.4. The hydrogen bonding interaction facilitates the dispersion of the silica nanoparticles in the PMMA-rich phase, as can clearly be distinguished in Figures 4.4a-b. On comparing Figure 4.2 with 4.4, it is evident that the addition of silica particles has a significant impact on the coarsening of the morphology during annealing. After adding 2 wt% silica nanoparticles, the macrophase separation is strongly suppressed. One possible reason is that the strong hydrogen bonding interaction between the silica surface and PMMA makes the homopolymer PMMA binding on the silica surface together with the PMMA block of S₂₀B₂₅M₅₅, which disrupts the extent of macrophase separation. Another explanation is similar with the one used by Huang *et al.*,³¹ i.e. selective adsorption of the high molar mass PMMA on the surface of the silica particles, by which the addition of the silica nanoparticles may force the system into the ‘wet-brush’ regime. This also leads to a suppression of the extent of macrophase separation. The comparison between Figures 4.2a,b and 4.4a,b reveals that the domain size of the S₂₀B₂₅M₅₅-rich phase is reduced by adding 2 wt% silica. In addition, phase inversion has not occurred at positions d, e and f of the silica-filled blends, which implies that the PMMA-rich phase is still the matrix as shown in Figure 4.4d-f.

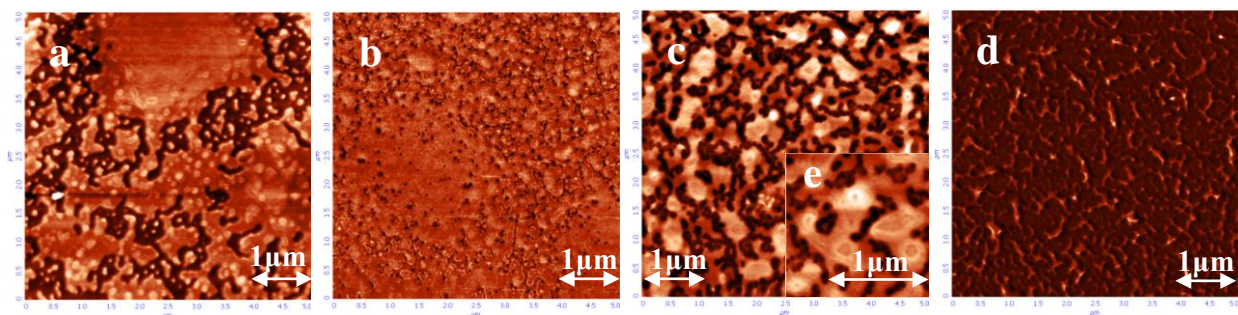


Figure 4.5: AFM phase angle images of neat PMMA(broad PDI=2.1)/S₂₀B₂₅M₅₅ 50/50 blend: (a) neat blend, (b-d) 1, 3, 5 wt% MEK-ST silica-filled blend and (e) high magnification of 3 wt% MEK-ST silica-filled blend.

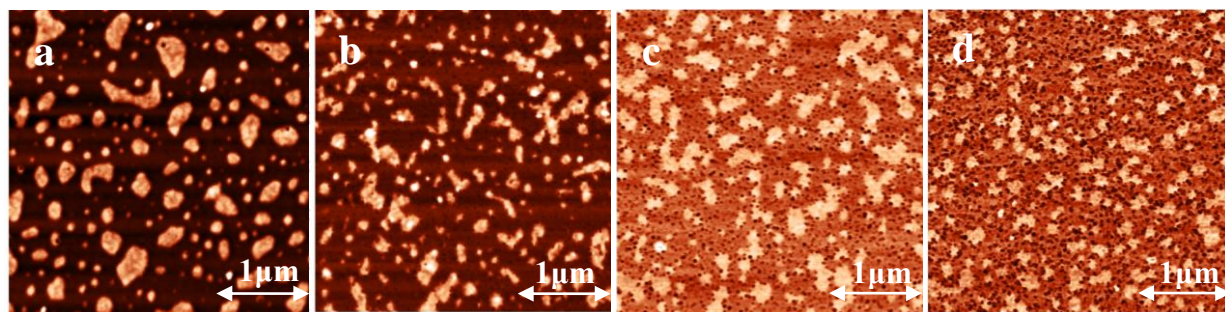


Figure 4.6: AFM phase angle images of PMMA/S₂₀B₂₅M₅₅ 80/20 blend: (a) neat blend and (b-d) 2, 5, 7 wt% MEK-ST silica-filled blends.

The influence of the silica concentration is further studied by two fixed compositions (50/50 and 80/20) of the PMMA(broad)/SBM blends, of which the morphologies correspond to co-continuous and droplet-matrix structures, respectively. Normal solvent casting was used, since only two compositions were studied. Figures 4.5a and 4.6a show the AFM phase images of the surface morphologies for the films of the neat PMMA/S₂₀B₂₅M₅₅ 50/50 and 80/20 blends, respectively. The morphologies are similar with those of the positions c and a in the HTE sample (Figure 4.2a, c). In addition, the worm-like lamellar and cylindrical structures can be found to coexist in the microphase-separated S₂₀B₂₅M₅₅-rich domains in Figure 4.5a. The S₂₀B₂₅M₅₅ domains seem to be more than 50 wt% in Figure 4.5a, which may be related to the fact that the fraction with a relatively low molar mass (below the M_n of the PMMA block) swells the PMMA phase of the triblock copolymer domain due to the ‘wet-brush’ condition. The same observation can be seen in the 80/20 blend (Figure 4.6a). In Figure 4.5b, with addition of 1 wt% silica, no apparent influence on the large length scale macrophase separation can be observed, although the silica particles were well dispersed in the matrix. At higher silica concentrations, a transition occurs from macrophase separation with large length scale to microphase separation with a co-continuous morphology after adding 3 and 5 wt% silica (Figures 4.5c-d). In the high magnification image (Figure 4.5e), the worm-like lamellar structure of S₂₀B₂₅M₅₅ can be found to be isolated in the PMMA matrix and surrounded by silica particles. The microphase-separated morphology does not change after adding more than 5 wt% silica (image is similar to Figure 4.5d, not shown here). However, the bright phase that represents the SB diblock copolymer is still present.

In the silica-filled 80/20 blends, the morphology does not change as obvious as for the 50/50 blends. Although increasing the silica content up to 7 wt%, the size of the dispersed SBM domains only slightly decreased.

Based on these results of 50/50 or 80/20 blends, the suppression effect of the silica particles is limited to low silica concentrations. Although the existence of the strong interaction between the silica surface and PMMA is the key factor, there are no indications that selective adsorption of the high molar mass PMMA on the surface of the silica particles is the reason of the effect of the silica on the extent of macrophase separation. In order to explore the possibility of this mechanism, the molar mass distribution of the homopolymer PMMA is considered as a way to help understanding the effect of the silica particles on the morphology.

4.3.2.3 The effect of the molar mass distribution of the homopolymer PMMA

This section describes the influence of the silica particles on the morphology the homopolymer/copolymer blends with different molar mass distributions for the PMMA homopolymer. In this study, the PMMA/S₂₀B₂₅M₅₅ blend with a fixed composition of 50/50 is used, since the silica particles shows the most profound effect on the macrophase separation.

Figure 4.7 shows the AFM images of the (monodisperse)PMMA15k/S₂₀B₂₅M₅₅ 50/50 blend and the blends with silica nanoparticles. The AFM height images are used here to investigate the coarsening effect, since that there is no clear phase contrast in these system, which may be related to the fact that PMMA has a stronger interaction with air and therefore prefers to migrate to the surface. Therefore, the microphase-separated structure of block copolymer cannot be observed in these images.

The ‘wet-brush’ condition is expected for mixing the monodisperse PMMA15k with S₂₀B₂₅M₅₅ in Figure 4.7a. The dispersed light domains mainly arise from the separation of the SB diblock impurity from the matrix, as explained in the last section. This can be further proved after adding the silica nanoparticles. The AFM height images only show a slight decrease of the dispersed domain size with addition of the silica nanoparticles in Figures 4.7b-c. The bright domains are still dispersed in the matrix. The silica nanoparticles do not show a strong effect on the phase separation of the (monodisperse)PMMA15k/S₂₀B₂₅M₅₅ 50/50 blend. The main reason is that the neat PMMA15k/S₂₀B₂₅M₅₅ is already in a ‘wet-brush’ ($N_{Ah} < N_{Ac}$) condition and the migration of silica particles in the hPMMA/cPMMA(of S₂₀B₂₅M₅₅) domain will not influence the microphase separation, as schematically depicted in Figure 4.10a-b.

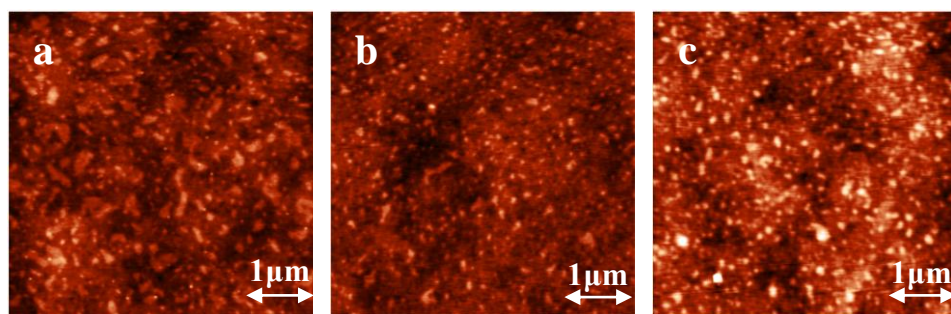


Figure 4.7: AFM height images of PMMA(monodisperse PMMA15k)/S₂₀B₂₅M₅₅ 50/50 blend: (a) neat blend and (b-c) 1 and 3 wt% MEK-ST silica-filled blends.

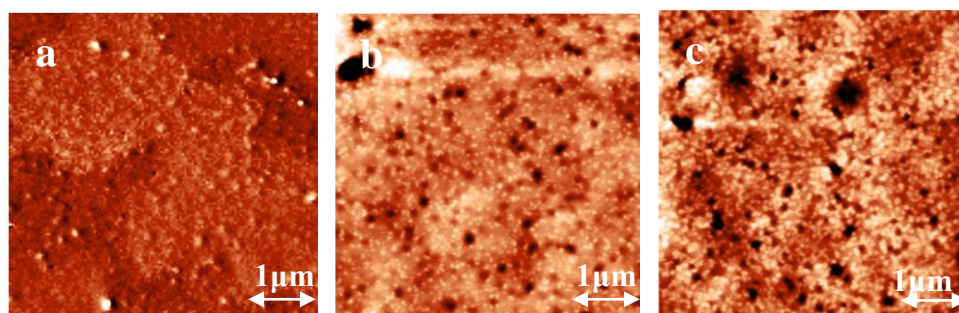


Figure 4.8: AFM height images of PMMA(monodisperse PMMA75k)/S₂₀B₂₅M₅₅ 50/50 blend: (a) neat and (b-c) 1 and 3 wt% MEK-ST silica-filled blends.

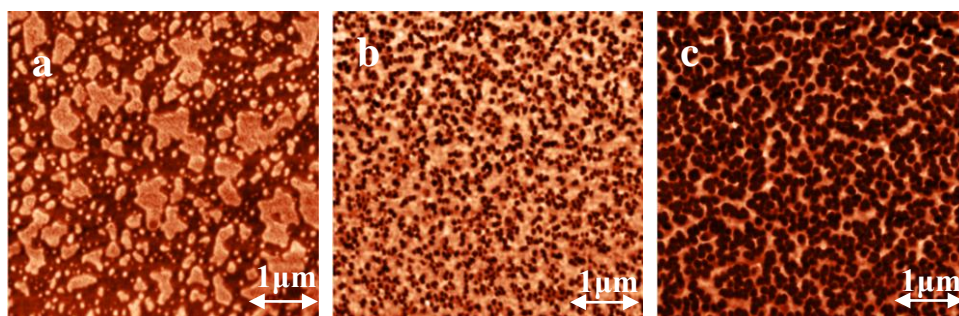


Figure 4.9: AFM phase angle images of PMMA(bimodal PMMA15k:PMMA75k 50:50)/S₂₀B₂₅M₅₅ 50/50 blend: (a) neat and (b-c) 1 and 3 wt% MEK-ST silica-filled blends.

The ‘dry-brush’ regime is applicable to the case of PMMA75k blended with S₂₀B₂₅M₅₅, of which the results are shown in Figure 4.8. The effect of the silica particles on the coarsening of the blend is obvious from the observation that the large length scale macrophase separation is substantially suppressed. On comparing the 1 wt% silica-filled PMMA75k/S₂₀B₂₅M₅₅ blend (Figure 4.8b) with the 1 wt% silica-filled PMMA(broad PDI)/S₂₀B₂₅M₅₅ blend (Figure 4.5b), the effect of the silica is more pronounced for the monodisperse PMMA75k system. Based on this result, the selective adsorption of the high molar mass PMMA on the surface of the silica particles is probably the reason of the disruption effect of the silica on the extent of macrophase separation. In order to further test

this hypothesis, a bimodal homopolymer PMMA containing a mixture of 50/50 PMMA15k/PMMA75k was used.

The scale of macrophase separation of the neat PMMA(bimodal)/S₂₀B₂₅M₅₅ 50/50 blend is smaller than that of the PMMA(broad)/S₂₀B₂₅M₅₅ system and PMMA75k/S₂₀B₂₅M₅₅, since half of the homopolymer PMMA is 15 kg/mol, see Figure 4.9a. For the PMMA(bimodal)/S₂₀B₂₅M₅₅ blend, the reduction of the length scale of the macrophase separation by 1 wt% silica is not as large as that of the PMMA75k/S₂₀B₂₅M₅₅ blend, which can be explained by the tendency of the selective adsorption of the high molar mass PMMA on the surface of the silica particles, which provide a possibility to force the low molar mass PMMA to solubilize in the S₂₀B₂₅M₅₅ ('wet-brush': $N_{Ah} < N_{Ac}$). However, after adding more silica, the selective adsorption of high molar mass PMMA is not significant. The hydroxyl groups on the surface of silica nanoparticles can interact with most of the carbonyl groups either of the homopolymer PMMA or the PMMA block of the triblock copolymer, which lead to microphase separation in all systems, as depicted in the scheme of Figure 4.10c-d. Therefore, the selective adsorption of the high molar mass PMMA on the silica particles exists in this system, although it is only significant for low silica contents.

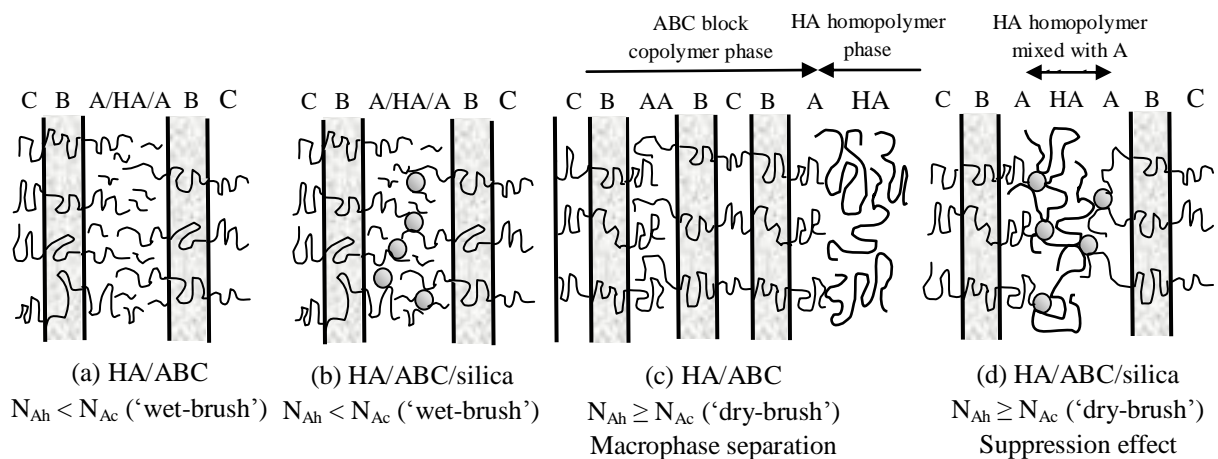


Figure 4.10: The effect of silica on the phase behavior of homopolymer/block copolymer blends in 'dry-brush' or 'wet-brush' conditions. N_{Ah} and N_{Ac} represent the degree of polymerization of the homopolymer and the similar block of the block copolymer, respectively.

In conclusion, a reducing effect of silica nanoparticles on the macrophase separation is observed for the PMMA/S₂₀B₂₅M₅₅ blends in the 'dry-brush' regime, which can be attributed to the strong hydrogen bonding interaction between the silica surface and the homopolymer PMMA or the PMMA block of S₂₀B₂₅M₅₅. In the system with the homopolymer PMMA with

the broad molar mass distribution, the selective adsorption of the high molar mass PMMA on the surface of the silica particles, which may force the system into the ‘wet-brush’ regime, can be observed with low silica content, especially in the PMMA(broad PDI)/S₂₀B₂₅M₅₅. For the system with high silica content, this selective adsorption phenomenon of high molar mass PMMA is not significant. Instead, both the homopolymer PMMA and the PMMA block of S₂₀B₂₅M₅₅ interact with the silica surface, which becomes the connecting part between both polymers and thereby suppresses the extent of macrophase separation.

4.3.3 Morphology development of triblock copolymer/monomer with addition of silica nanoparticles upon in-situ polymerization

The most common route to prepare homopolymer/block copolymer blends is physical blending via solvent casting or melt blending. However, it is very difficult to prepare nanosized morphologies via this route. Therefore, in-situ polymerization of monomer/copolymer solutions, in which one block is chemically identical to the monomer, is studied. Earlier work showed that this leads to macrophase separation for di- and triblock copolymers due to the fact that the system is in the ‘dry-brush’ regime. One possibility to overcome this problem is the use of chain transfer agents to lower the molar mass of the matrix, but this is detrimental for the mechanical properties. Therefore, we explore the use of nanoparticles to either induce micellization or to help suppressing the macrophase separation.

The morphology after polymerization as observed by TEM is shown in Figure 4.11. A combination of a lamellar and core-shell morphology can be found in the pure PMMA/S₂₀B₂₅M₅₅ system. Since OsO₄ is used for selective staining (PB is dark, PS is grey, and PMMA is light), it can be concluded that the lamellar structures are the phase-separated SB diblock copolymers, while the triblock copolymers are preserved in the core-shell structures. Although macrophase separation seems to have occurred, the size of the dispersed domain is still small (~ 100 nm).

The morphology obtained for the system with silica nanoparticles is comparable in size with the core-shell structure with the pure system, but the phase separation of the SB diblock copolymer seems to be suppressed, although it has to be remarked that the contrast between the different blocks after the OsO₄ staining is not so pronounced. The silica particles are reasonably well dispersed with soft clusters composed of 5-20 particles separated by small polymer layers, which is as good as in the system prepared via solvent-casting, for which mainly individual particles were observed.

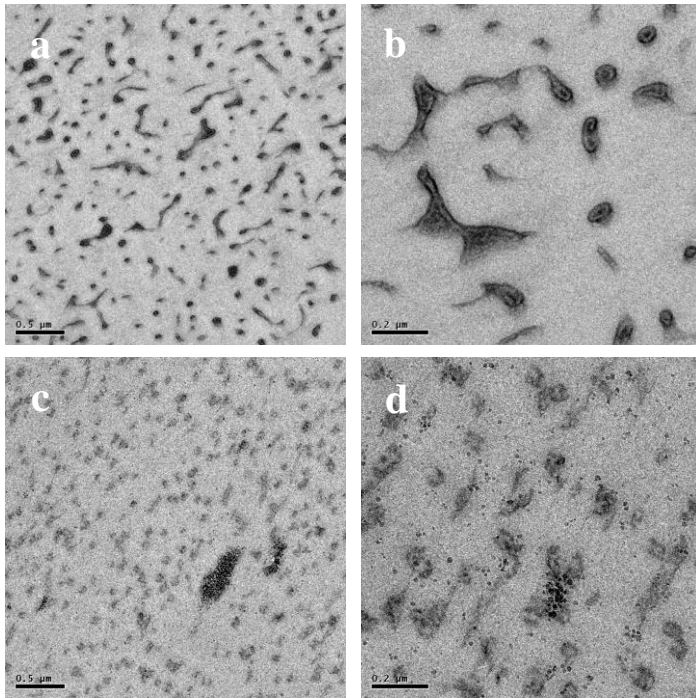


Figure 4.11: TEM images of in-situ polymerization samples: (a-b) PMMA with 10 wt% $S_{20}B_{25}M_{55}$ and (c-d) PMMA with 10 wt% $S_{20}B_{25}M_{55}$ and 2 wt% silica at various magnifications. The polymerizations were started at ambient temperature.

The obtained SAXS data of the system with 10 wt% of $S_{20}B_{25}M_{55}$ in MMA during polymerization are shown in Figure 4.12 as a three-dimensional plot of intensity, $\log I(q)$, versus scattering vector q , which is defined as $q = (4\pi/\lambda \sin(\theta))$, where 2θ is the scattering angle and λ is the x-ray wavelength, versus polymerization time. The time-resolved SAXS patterns include also the heating stage from -50 to 100 °C at 5 °C/min to obtain information about the formation, size and disassociation of the micelles, followed by the isothermal polymerization at 100 °C after 30 min.

For the pure MMA/ $S_{20}B_{25}M_{55}$ solution, a primary scattering peak at $q^* = 0.0060 \text{ \AA}^{-1}$ is present during heating from -50 to 100 °C, which can be assigned to the structure factor. It is expected that the PS-PB blocks form a core-shell structure, while the PMMA block dissolves in the MMA matrix, but the higher q -range peaks needed for identifying the form factor are not distinguishable, probably due to the low electron density contrast. The structure factor is constant up to 100 °C, before the polymerization starts, which implies that the core-shell structure does not change. The stabilization arises from the good compatibility between the PMMA block of the triblock copolymer with the monomer MMA in combination with the relatively high ODT for the SB part. Kierkels⁹ reported for the poly(ethylene-*co*-butylene)-*b*-poly(butyl acrylate)-*b*-poly(methyl methacrylate) (PEB-PBA-PMMA)/MMA system that the

micellar structure was thermally stable up to a rather low temperature, which could be controlled by the length of the PEB-block. However, during the in-situ UV-initiated polymerization at temperatures below the ODT macrophase separation was still observed.

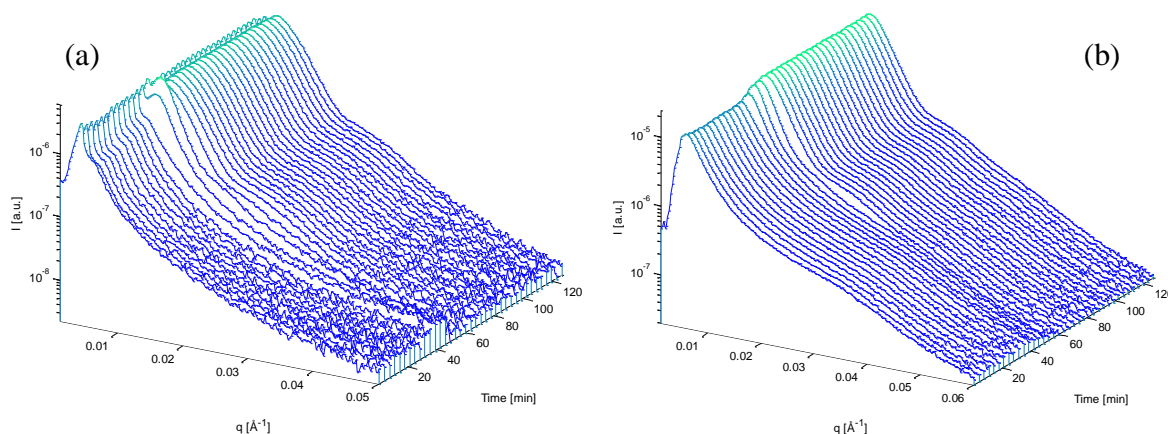


Figure 4.12: SAXS profiles collected during a heating ramp from -50 to 100 °C at 5 °C/min and isothermal polymerization of MMA at $T = 100$ °C for (a) MMA with 10 wt% $S_{20}B_{25}M_{55}$ and (b) MMA with 10 wt% $S_{20}B_{25}M_{55}$ and 2 wt% silica. The isothermal polymerization temperature is reached after 30 min.

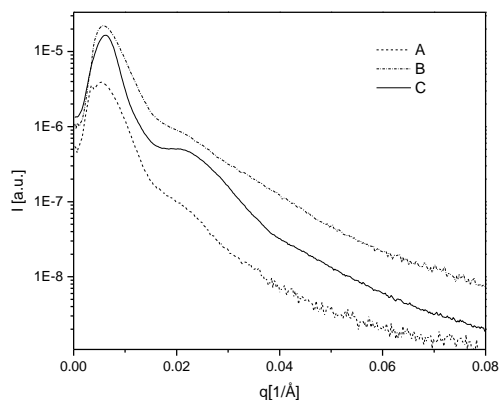


Figure 4.13: SAXS patterns of PMMA blends with 10 wt% of $S_{20}B_{25}M_{55}$. A: after in-situ polymerization of neat MMA with $S_{20}B_{25}M_{55}$ B: after in-situ polymerization of silica-filled MMA with $S_{20}B_{25}M_{55}$ and C: compression-molded pure $S_{20}B_{25}M_{55}$.

Upon heating, the intensity of the structure factor peak increases together with a slight movement of the peak position to lower q -values up to 40 °C, which is caused by swelling of the shell (PMMA block) by the MMA monomer, which increases the distance between the cores. After the temperature reaches 100 °C and polymerization is initiated, a sharp increase of the scattering intensity close to the beam stop ($q \rightarrow 0$ Å $^{-1}$) can be observed after an isothermal polymerization time of 7.5 min at $T=100$ °C, due to macrophase separation. At the

same time, a sharp diffraction peak at $q^* = 0.0063 \text{ \AA}^{-1}$ develops, followed by a second higher order reflection at $q = 0.0235 \text{ \AA}^{-1}$. The presence of the higher order reflections indicates that more ordered microphases of the triblock copolymer are formed, reflecting the microphase separation process of the block copolymer. The scattering pattern is close to the pattern of the pure triblock copolymer, see Figure 4.13, suggesting that upon polymerization the triblock copolymer macrophase separates from the PMMA phase and forms separate domains with its original bulk morphology, i.e. lamellar structure.

In comparison to the pure MMA/S₂₀B₂₅M₅₅ system, the silica-filled MMA/S₂₀B₂₅M₅₅ shows during heating from -50 to 100 °C a broad peak with a relatively high intensity at $q = 0.035 \text{ \AA}^{-1}$, which can be attributed to the form factor of the silica nanoparticles, while the sharp structure factor peak, which was observed for the system without silica particles, is not present. This implies that the silica particles are well dispersed in the solution without any specific ordering.

Upon polymerization, the structural order of the triblock copolymer appears at $q^* = 0.0065 \text{ \AA}^{-1}$ and $q = 0.023 \text{ \AA}^{-1}$ (same as the final lamellar structure of the pure system) after isothermal 15 min at T = 100 °C. This means that upon addition of the silica nanoparticles the macrophase separation of the triblock copolymer from the PMMA phase occurred later than in the pure system, suggesting the effect of the particles on the stabilization between the monomer MMA, homopolymer PMMA and PMMA block of the triblock copolymer. The strong interactions between hydroxyl groups of the particles with the carbonyl groups induces an adsorption of the PMMA and monomer MMA together on the surface of the silica particles, which might postpone the macrophase separation during the polymerization. However, the final lamellar morphology is the same as the pure system since the diffraction peaks are present at same positions, as shown in Figure 4.13.

The development of the scattering invariant during the polymerization, as shown in Figure 4.14, can provide additional information about the morphology development, since it reflects electron density differences in the sample and thus the presence and development of different phase. To calculate the absolute value of the invariant absolute intensity measurements are required and corrections have to be made for thermal fluctuations and q has to be extrapolated to $q \rightarrow 0$ and $q \rightarrow \infty$. Due to experimental constraints, the experimental invariant is calculated by integrating from the first to the last reliable data point. For two-phase systems, the invariant is defined as:

$$Q = \frac{1}{2\pi^2} \int_{q=0}^{q=\infty} I(q)q^2 dq = \phi_1\phi_2(\rho_1 - \rho_2)^2 \quad (4.1)$$

where Q is the invariant, ϕ_x the volume fraction of phase x , and ρ_x the electron density of phase x .

In Figure 4.14, the experimental invariant shows a low plateau value at the start of the polymerization, since the copolymer is dissolved in MMA and no separate phases are present. The invariant starts to increase when the conversion of MMA to PMMA is sufficient to induce macrophase separation into a copolymer-rich phase and a PMMA-rich phase, both swollen by the monomer. The sudden jump at $t = 20$ min, in Figure 4.14a, is a result of readjusting the X-ray beam intensity to protect the detector from permanent damage, which does not influence the structure development in this system. In Figure 4.14, the macrophase separation of the neat system starts almost immediately after the polymerization temperature of $100\text{ }^\circ\text{C}$ is reached, while that of the silica-filled system starts 10 min later. This corresponds to the moment of the appearance of the structural order of the triblock copolymer in the SAXS profiles.

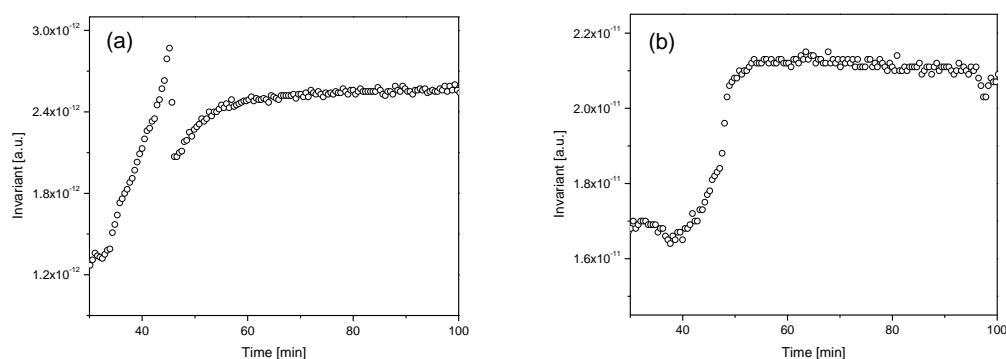


Figure 4.14: Experimental scattering invariant for the polymerization of MMA with 10 wt% S₂₀B₂₅M₅₅ at $T = 100\text{ }^\circ\text{C}$: (a) neat system, (b) 2 wt% silica-filled system.

In the in-situ polymerization method, the monomer is polymerized in the presence of the block copolymer yielding a homopolymer/block copolymer blend. The final morphology after the polymerization of MMA/S₂₀B₂₅M₅₅ solutions shows a small length scale macrophase separation in both the neat and the silica-filled blends. During polymerizing the silica-filled solution, the chemically-induced phase separation via the growth of PMMA chains is slowed down by the silica particles. The effect arises from the strong interactions between the silica particles with the growing PMMA and the monomer MMA together. The reduction of the lamellar morphology arises from the association of the PMMA matrix and PMMA block of the S₂₀B₂₅M₅₅ induced by the silica, which enhances the compatibility of the triblock copolymer and matrix then the stability of the core-shell structure.

4.3.4 Morphologies of PMMA/S₂₀B₂₅M₅₅ nanocomposites: Melt-mixing

Since the sample preparation method has a large effect on the final morphology, the general industrial route (melt-mixing) is used to investigate the effect of the silica particles on the phase separation in this section. During solvent casting and in-situ polymerization more time for phase separation during processing is available together with a higher mobility in the solution, leading to more ordered morphologies, whereas during melt mixing a much lower mobility (high viscosity) is encountered. Therefore, the effect of silica nanoparticles on the phase separation of polymer blends in the high viscosity state needs to be studied.

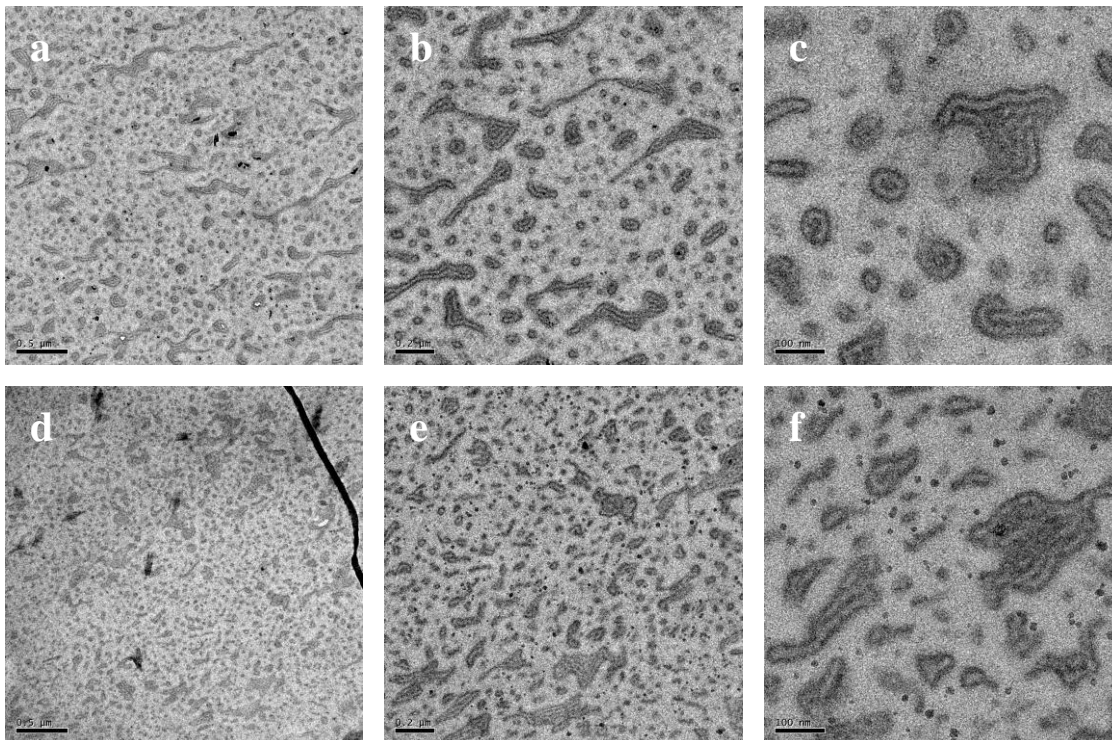


Figure 4.15: TEM images of melt-mixed samples: (a-c) neat PMMA/S₂₀B₂₅M₅₅ 60/40 blends and (d-f) PMMA/S₂₀B₂₅M₅₅ 60/40 blends with 2 wt% MEK-ST silica at various magnifications.

The TEM images are shown in Figure 4.15 for the morphologies of the neat PMMA/S₂₀B₂₅M₅₅ 60/40 blend and the 2 wt% silica-filled blend at various magnifications. The homopolymer PMMA used has a broad molar mass distribution. PMMA forms the matrix and the triblock copolymer forms the dispersed phase, which shows well-ordered micellar and lamellar structures in the matrix. The core-shell structure comes from the SBM triblock copolymer, while the lamellar structure exists mostly because the presence of the SB diblock copolymer impurities. Compared to the annealed solvent-cast 50/50 blend, the melt-mixed samples show macro/microphase separation at a much smaller length scale due to the high viscosity of polymers and high shear forces during melt mixing. Although the triblock

copolymer is still macrophase separated from the PMMA matrix, the dispersed domain size is only 50-200 nm. The PMMA matrix material with a high polydispersity index provides sufficient compatibility between the PMMA matrix and the longer PMMA-block of triblock copolymer.

After adding the silica particles, no apparent silica cluster can be found in the matrix. The silica nanoparticles are well dispersed in the PMMA matrix as single particles or multiple twin particles (Figures 4.15d-f). Although there is no obvious difference of the scale of phase separation between the neat blend and the silica-filled blend at the highest magnification images, shown in Figures 4.15c and f, the suppression effect on the macrophase separation can be undoubtedly seen in the low-magnification images (Figure 4.15a and 4.15d). This is consistent with the results of the other preparation methods. The size of the microdomains of the dispersed triblock copolymer decreases by the addition of the silica. In Figures 4.15d-e, the size of the lamellar and core-shell structures is much smaller than that of the neat blend.

The melt-mixing samples have, compared to the solvent-cast samples with higher mobility and longer annealing times, a much smaller length scale macrophase separation due to its high melt viscosity and high shear stresses. Therefore, the suppression effect of silica particles on the phase separation of the melt-mixing samples is not as apparent as on that of the solvent-cast samples.

4.4 Conclusions

In this chapter, the effect of silica nanoparticles on the morphology of the homopolymer/block copolymer PMMA/SBM blend was studied. It was shown that the hydrophilic MEK-ST silica particles can suppress the extent of macrophase separation between the block copolymer and homopolymer. This is related to the selective localization of the silica particles in the PMMA phase during phase separation due to the strong hydrogen bonding interaction between the hydroxyl groups on the surface of silica nanoparticles and the carbonyl groups of the PMMA. The observations can be explained by selective adsorption of the high molar mass PMMA on the surface of the silica particles, which may force the system into the ‘wet-brush’ regime, similar to the experimental results as presented by Huang *et al.*³¹ This hypothesis was tested by using PMMA homopolymers with different molar mass distributions. In the system with PMMA with the broad molar mass distribution, the selective adsorption of the high molar mass PMMA on the surface of the silica particles can be observed with low silica content. However, for the systems with a high silica content, where

enough specific surface is available for PMMA to interact with, the selective adsorption of the high molar mass PMMA is not significant. Instead, both the homopolymer PMMA and the PMMA block of $S_{20}B_{25}M_{55}$ can interact with the silica surface, which becomes the connecting part between both polymers and thereby suppressing the macrophase separation to a large extent.

The suppression effect of the silica nanoparticles was observed in PMMA/SBM blend for all three preparation methods, i.e. solvent casting, melt mixing and in-situ polymerization of MMA in presence of the silica particles and triblock copolymer. During solvent casting, more time for phase separation during annealing is available together with a higher mobility in the solution, which leads to more ordered morphologies and larger length scale macrophase separation. Thus, the suppression effect of the silica nanoparticles on the phase separation is more obvious for the sample prepared via solvent casting.

In the in-situ polymerization method, the chemically-induced phase separation is slowed down by the silica particles. And a reduction of the lamellar morphology can be observed, which arises from the association of the PMMA matrix and PMMA block of the $S_{20}B_{25}M_{55}$ induced by the silica, which enhances the compatibility of the triblock copolymer and matrix then the stability of the core-shell structure.

The high viscosity and high shear stress during melt-mixing strongly restrict the morphology development. Thus, the morphology obtained from the melt-mixing only shows small length scale macrophase separation and the effect of the silica is less apparent. This might also be related to the possibility that the adsorption of high molar mass chain is lower in the melt state.

These results demonstrate that the silica nanoparticles have a significant suppression effect on the extent of macrophase separation in the PMMA/SBM based on the PMMA selective adsorption on the silica surface. The silica nanoparticles provide a larger processing window to obtain an immiscible homopolymer/copolymer blend with a nanosized core-shell morphology. In Chapter 5, the selective distribution of silica particles will be further studied in PS/SBM triblock copolymer/homopolymer systems.

4.5 References

- ¹ Bucknall, C. B., *Toughened plastics*, Appl. Sci. Publishers Ltd., London, **1977**.
- ² Meijer, H. E. H., Govaert, L. E., *Progress Pol. Sci.*, **2005**, 30, 915-938.
- ³ Jansen, B. J. P., Rastogi, S., Meijer, H. E. H., Lemstra, P. J., *Macromolecules*, **1999**, 32, 6283-6289.
- ⁴ Jansen, B. J. P., Rastogi, S., Meijer, H. E. H., Lemstra, P. J., *Macromolecules*, **2001**, 34, 3998-4006.

- ⁵ Jansen, B. J. P., Rastogi, S., Meijer, H. E. H., Lemstra, P. J., *Macromolecules*, **2001**, 34, 4007-4018.
- ⁶ Van Casteren I. A., Van Trier, R. A. M., Goossens, J. G. P., Meijer, H. E. H., Lemstra, P. J., *J. Polym Sci, Part B: Pol. Phys.* **2004**, 42, 2137-60.
- ⁷ Van Asselen, O. L. J., Van Casteren, I. A., Goossens, J. G. P., Meijer, H. E. H., *Macromol. Symp.*, **2004**, 205, 85-94.
- ⁸ Van Casteren, I. A., *Control of microstructures to induce ductility in brittle amorphous polymers*, Ph.D. Thesis, TU/e, Eindhoven, the Netherlands, **2003**.
- ⁹ Kierkels, J. T. A., *Tailoring the mechanical properties of amorphous polymers*, Ph.D. Thesis, TU/e, Eindhoven, the Netherlands, **2006**.
- ¹⁰ Thomas, E. L., *Science*, **1999**, 286, 1307.
- ¹¹ Hardy, D. M., Bates, F. S., Kim, M. H., Wignall, G. D., *Macromolecules*, **2002**, 35, 3189-3197.
- ¹² Ritzenthaler, S., Court, F., David, L., Girard-Reydet, E., Leibler, L., Pascault, J. P., *Macromolecules*, **2002**, 35, 6245-6254.
- ¹³ Brinkmann, S., Stadler, R., Thomas, E. L., *Macromolecules*, **1998**, 31, 6566-6572.
- ¹⁴ Krappe, U., Stadler, R., Voigt-Martin, I., *Macromolecules*, **1995**, 28, 4558-4561.
- ¹⁵ Hydro, R. M., Pearson, R. A., *J. Polym. Sci. Part B: Polym. Phys.*, **2007**, 45, 1470-1481.
- ¹⁶ Fine, T., Pascault, J-P., *Macromol. Symp.*, **2007**, 245, 375-385.
- ¹⁷ Hamley, I. W., *The physics of block copolymers*, **1998**, Oxford University Press, Oxford New York.
- ¹⁸ Hashimoto, T., Yamasaki, K., Koizumi, S., Hasegawa, H., *Macromolecules*, **1993**, 26, 2895-2904.
- ¹⁹ Winey, K. I., Thomas, E. L., and Fetters, L. J., *Macromolecules*, **1991**, 24, 6182-6188.
- ²⁰ Kinning, D. J., Thomas, E., Fetters, L. J., *J. Chem. Phys.*, **1989**, 90, 5806-5825.
- ²¹ Fenouillot, F., Cassagnau, P., Majeste, J. C., *Polymer*, **2009**, 50, 1333-1350.
- ²² Kim, B. J., Chiu, J. J., Yi, G. R., Pine, D. J., Kramer, E. J., *Adv. Mater.*, **2005**, 17, 2618-2622.
- ²³ Kim, B. J., Fredrickson, G. H., Hawker, C. J., Kramer, E. J., *Langmuir*, **2007**, 23, 7804-7809.
- ²⁴ Kim, B. J., Fredrickson, G. H., Bang, J., Hawker, C. J., Kramer, E. J., *Macromolecules*, **2009**, 42, 6193-6201.
- ²⁵ Balazs, A. C., Emrick, T., Russell, T. P., *Science*, **2006**, 314, 1107-1110.
- ²⁶ Thompson, R., Ginzburg, V., Matsen, M., Balazs, A. C., *Science*, **2001**, 292, 2469-2472.
- ²⁷ Lee, J. Y., Thompson, R., Jasnow, D., Balazs, A. C., *Phys. Rev. Lett.*, **2002**, 89, 155503.
- ²⁸ Kim, J. U., O'Shaughnessy, B., *Macromolecules*, **2006**, 39, 413-425.
- ²⁹ Montezinos, D., Wells, B. G., Burns, J. L., *J. Polym. Sci., Polym. Lett. Ed.*, **1985**, 23, 421-425.
- ³⁰ Corte, L., Yamauchi, K., Court, F., Cloitre, M., Hashimoto, T., Leibler, L., *Macromolecules*, **2003**, 36, 7695-7706.
- ³¹ Huang, Y., Jiang, S., Li, G., Chen, D., *Acta Mater.*, **2005**, 53, 5117-5124.

Chapter 5

Selective distribution of silica nanoparticles and the morphology control of PS-PB-PMMA/PS blends

The selective distribution behavior of silica nanoparticles was studied in blends consisting of poly(styrene) (PS) and a poly(styrene)-b-poly(butadiene)-b-poly(methyl methacrylate) (SBM) triblock copolymer. In the blend, macro/microphase separation between the block copolymer and the homopolymer occurred both in the 'dry-brush' and 'wet-brush' regime due to the broad molar mass distribution of the homopolymer PS. A combination of core-shell and cylindrical structures of the SBM triblock copolymer was observed, since the triblock copolymer also contains SB diblock impurities. On adding silica nanoparticles, the silica particles are distributed in different phases and the location depends on the interaction between the silica surface and the polymer, which can also be influenced by the compounding procedure. Upon adding hydrophilic silica to the PS/SBM blend, the silica nanoparticles are found preferentially in the core (PMMA phase) of the core-shell structures without macrophase separation due to the strong hydrogen bonding interaction between the silica surface and PMMA. On the other hand, hydrophobic silica nanoparticles suppress the extent of macrophase separation between the homopolymer and block copolymer blend based on a selective distribution within the PS phase. However, this effect was limited to two preparation methods, i.e. solvent casting and in-situ polymerization of styrene in presence of the silica particles and triblock copolymer. The selective distribution of the silica particles in the PMMA core might lead to extra internal stresses in the core-shell phase during cooling, thereby possibly inducing pre-cavitation.

5.1 Introduction

As discussed in Chapter 1, the toughness of a brittle polymer can be improved by the introduction of a second (rubber) phase as impact modifier.¹⁻⁸ A possible route to prepare these systems can be through the use of self-organizing block copolymers that are able to form a morphology of nanosized core-shell particles in the amorphous matrix.

It is well known that the use of ABC triblock copolymers opens a wide field of possibilities due to the various obtainable microphase-separated morphologies,⁹⁻¹³ which induce particular mechanical properties.¹⁴⁻¹⁵ In comparison to mixing homopolymer A with BC diblock copolymers, the addition of a third miscible block A to the block copolymer enhances the compatibility with homopolymer A. However, macrophase separation between homopolymer and triblock copolymer can still occur if the system is in the 'dry-brush' regime, i.e. $N_{Ah} > N_{Ac}$ (the length of the homopolymer chains is longer than that of the miscible block in the block copolymer), which prevents the formation of nanosized core-shell morphologies. In Chapter 4, silica nanoparticles were observed to have a suppression effect on the extent of macrophase separation of a homopolymer/block copolymer blend composed of poly(methyl methacrylate) (PMMA)/poly(styrene)-*b*-poly(butadiene)-*b*-poly(methyl methacrylate) (SBM), yielding a possible route to prepare heterogeneous blends with a nanosized dispersed elastomeric phase. This was related to the selective distribution of the silica nanoparticles in the PMMA phase, which was considered as the key point for the suppression effect.

A number of researchers reported that nanoparticles might be unequally distributed between the different phases in polymer blends. This was not only observed in homopolymer blends, but also in the blends with block copolymers and proved to be dependent on the interactions between the nanoparticles and the polymers, the compounding procedure, and the viscosity ratio of the polymers.¹⁶ Additionally, for systems with block copolymers, the spatial distribution of nanoparticles can lead to specific and stable morphologies.¹⁷⁻²⁰

Since it was shown that the strong interaction between the hydrophilic silica and the PMMA is the key parameter for the suppression effect of the macrophase separation in PMMA/SBM with PMMA as the major component in Chapter 4, it is interesting to investigate the effect of the hydrophilic silica on the morphology of PS/SBM with PMMA as the minor component. In this chapter, the selective distribution and the different effects of the hydrophilic and hydrophobic silica particles on the morphology of PS/SBM blends are studied. Three preparation methods were used to control the final distribution of the silica

nanoparticles and the morphology development: solvent casting, in-situ polymerization and melt mixing.

5.2 Experimental

5.2.1 Materials

PS was provided by Shell (the Netherlands) with a number-averaged molar mass (M_n) of 79.3 kg/mol and a polydispersity index (PDI) of 3.51. SBM ($M_n=55$ kg/mol) was supplied by Arkema (France), coded as S₂₀B₂₅M₅₅ and S₅₂B₃₀M₁₈, where the subscripts represent the weight fraction of the respective blocks. The as-received triblock copolymers contain approx. 29-30 wt% SB diblock and were used without any further purification. The S and B blocks have the same molar mass in the triblock and the diblock copolymer. Methyl ethyl ketone (MEK), toluene and styrene were obtained from Sigma Aldrich and were used as received. Two kinds of pre-made colloidal silica nanoparticles with a diameter of 10-15 nm, dispersed in MEK and toluene with approx. 30 and 40 wt% silica, respectively, were purchased from Nissan Chemical (USA) and the surface is covered with methyl and hydroxyl groups. These silica nanoparticles will be referred to as MEK-ST and TOL-ST, respectively. The silica nanoparticles were used without any further surface modification.

5.2.2 Sample preparation

Solvent casting

The MEK-ST or TOL-ST nanoparticles were first dispersed in MEK or toluene, followed by dissolving the homopolymer or the block copolymer, respectively. Then, the silica-filled homopolymer and silica-filled block copolymer solutions were mixed and solvent cast on a glass substrate (thin film) or a petri dish (thick film). A doctor blade was used to control the thickness of the film on the glass substrate. The polymer concentration in the solution was 8 wt%. The solvent-cast samples were dried in a fume-hood at room temperature for 2 days followed by a drying step at 60, 80 and 100 °C under reduced pressure with a low nitrogen flow for 5 days to ensure complete solvent removal. The final thickness of the samples was approximately 2 μm (thin film) and 0.2 mm (thick film). The dried films were annealed at 135 °C for 7 days under a nitrogen atmosphere. The samples were subsequently cooled to room temperature.

Precipitation

The TOL-ST nanoparticles were first dispersed in toluene, followed by dissolving the homopolymer or the block copolymer, respectively. Then, the silica-filled homopolymer and silica-filled block copolymer solutions were mixed. The obtained nanocomposite solution was added drop-wise into a large volume of methanol (the solution is continuously stirred using a magnetic stirring bar) to enable co-precipitation of polymers and the nanoparticles (~10 mL of methanol is used for every 1 mL of solution). The solids were filtered from methanol and dried by the same drying steps as the solvent-casting method.

Melt mixing

Silica nanoparticles were pre-dispersed in SBM by solvent casting. The obtained SBM/silica was melt blended with PS in a second step in a twin-screw mini-extruder. The temperature was set at 200 °C for the PS/SBM 80/20 blends. The extruder was fed with 6 g of material and the screw speed was set at 50 rpm and the total mixing time was fixed at 10 min. All the experiments were performed under nitrogen atmosphere in order to prevent oxidative degradation.

In-situ polymerization

The free radical polymerization of styrene/triblock copolymer solutions was performed over a broad range of temperatures to minimize void formation because of polymerization shrinkage and to get more control over the morphology. 0.2 wt% 2,2-azobis(isobutyronitrile) (AIBN) was used as initiator. Homogeneous solutions of styrene, triblock copolymer, initiator and silica particles were prepared at room temperature. The solutions were poured into glass bottles that were hermetically sealed after being purged with nitrogen gas for several min. The solutions were left at room temperature for overnight during which the free radical polymerization was initiated. Subsequently, the bottles were placed in a heating cell with a programmed temperature profile: 20 hrs at 30 °C and subsequently at 50, 70, and 90 °C, followed by two post-polymerization steps at 110 and 120 °C for 2 hrs each. The polymerizations for the in-situ SAXS experiments were performed at 100 °C and initiated by 0.2 wt% AIBN.

5.2.3 Characterization techniques

Atomic Force Microscopy (AFM)

The AFM investigations were performed by using a Smena P47H microscope (NT-MDT Ltd, Moscow, Russia). The AFM was operated in semi-contact mode under an air atmosphere

using a silicon cantilever (NSG 11 NT-MDT), which was coated with a gold layer for a higher laser beam reflectivity. The resonance frequencies applied were 115-190 kHz.

Transmission Electron Microscopy (TEM)

Morphological investigations were performed by using a Tecnai 20 transmission electron microscope (TEM), operated at 200 kV. Samples were trimmed at -120°C and subsequently bulk-stained for 2 weeks with an Osmium tetroxide (OsO₄) solution prepared according to Montezinos *et al.*,²¹ which predominantly reacts with PB. Ultrathin sections (± 70 nm) were obtained at room temperature using a Reichert UltracutS/FCS ultramicrotome equipped with a diamond knife.

Thermogravimetric Analysis (TGA)

A Q500 TGA (TA Instruments) was used for the quantitative determination of the silica content in the nanocomposites. Samples were heated under a pressed air atmosphere at 10 °C/min from 30 to 800 °C and held at 800 °C for 15 min. The residue was assumed to be only composed of silica.

Small-Angle X-ray Scattering (SAXS)

To study the morphology development upon in-situ polymerization of the monomer, time-resolved small-angle X-ray scattering experiments (SAXS) were performed on the DUBBLE beam line (BM 26B) at the European Synchrotron Radiation Facility (ESRF) in Grenoble (France). The SAXS data were collected on a multiwire two-dimensional (2D) detector positioned at 8 m from the sample. MMA/block copolymer solutions were transferred into Lindemann capillaries, which were subsequently sealed. The capillaries were placed in a capillary holder fixed on a Linkam THMS 600 hot-stage mounted on the optical bench. The silver heating block of the hot-stage contained a 4 mm² conical hole allowing the X-rays to pass through unhindered. For calibration of the SAXS detector, the scattering pattern from an oriented specimen of wet collage (rat-tail tendon) was used. The experimental data were corrected for background scattering, i.e. subtraction of the scattering from the camera, hot-stage and capillary. The two-dimensional SAXS data were transformed into one-dimensional plots by performing integration along the azimuthal angle using the FIT2D program of Dr. Hammersley of ESRF. The exposure time for the time-resolved measurements was as 24 and 45 s.

5.3 Results and discussion

The phase behavior of the self-assembly block copolymer can be influenced by both the mixing method as well as the choice of solvent. Thus, three mixing methods were applied to study the influence of the silica nanoparticles on the morphology of the PS/SBM blend, i.e. solvent casting, in-situ polymerization, and melt mixing. The selective localization of the silica particles and the morphology development of the systems were first studied by adding two types of silica via solvent casting. Next, the influence of the silica nanoparticles on the morphology (development) of the PS/SBM prepared via the in-situ polymerization route is discussed. Finally, the melt-mixing route is discussed to obtain a core-shell morphology with localized silica particles. To obtain the heterogeneous system with PS as the matrix the $S_{52}B_{30}M_{18}$ block copolymer with PS as the major component was used.

5.3.1 The effect of silica nanoparticles on the morphology of the SBM triblock copolymer

The morphologies of the triblock copolymer $S_{52}B_{30}M_{18}$ prepared either by compression molding or by solvent casting from MEK and toluene were investigated by TEM (see Figure 5.1). Since the as-received SBM triblock copolymer is composed of SBM triblock and SB diblock copolymer, micro/macrophase separation might occur. The compression-molded $S_{52}B_{30}M_{18}$ shows a worm-like lamellar structure without any long-range order and with a high curvature due to the presence of SB diblock copolymer, as can be observed in Figure 5.1a. The grey domains, which correspond to PS as a major component, form the matrix and the white domains, corresponding to PMMA, are surrounded by the dark domains (PB).

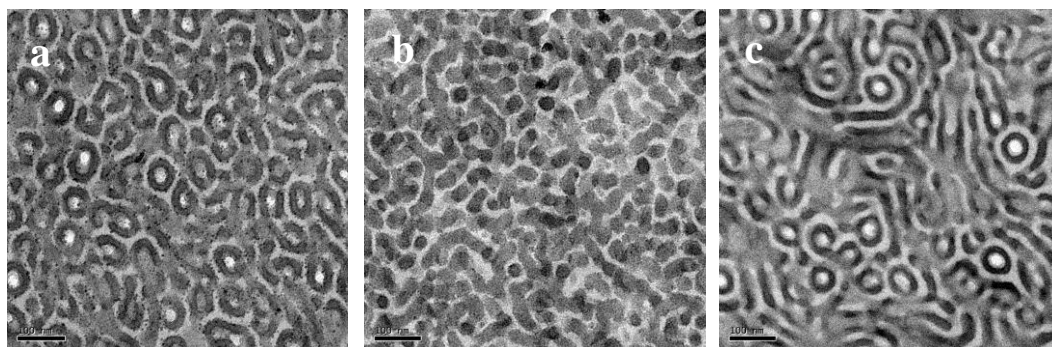


Figure 5.1: TEM images of (a) compression-molded $S_{52}B_{30}M_{18}$, (b) solvent-cast $S_{52}B_{30}M_{18}$ (solvent: MEK) and (c) solvent-cast $S_{52}B_{30}M_{18}$ (solvent: toluene). The solvent-cast samples were annealed at 135 °C for 4 days. The bright phase corresponds to the PMMA domains, and the grey phase corresponds to PS domains, while the dark phase corresponds to the PB domains.

Since the two colloidal silica particles used in this study are suspended in MEK and toluene, the morphologies of the neat $S_{52}B_{30}M_{18}$ cast from MEK and toluene need to be identified. In Figure 5.1b, the TEM image of the MEK-cast film shows a worm-like lamellar morphology, although the contrast between the PMMA and PS phase cannot be recognized, which can be related to the preferential affinity of MEK to the minority block PMMA. Further, the films cast from toluene, which is a non-selective solvent, shows the same morphology as the compression-molded sample.

The morphologies of the silica-filled $S_{52}B_{30}M_{18}$ samples prepared via solvent casting were investigated by AFM and are shown in Figures 5.2a and b. In comparison to the compression-molded sample visualized by using TEM (Figure 5.1), the AFM images of the solvent-cast samples show a similar morphology, although the contrast of the phase angle is altered by the addition of the silica particles. In Figure 5.2a, with addition of MEK-ST silica, the phase angle image shows only three phases, which means that the silica nanoparticles make one phase invisible on the surface of the films. As mentioned in Chapter 4, the MEK-ST silica is preferentially localized in the PMMA phase of the $S_{20}B_{25}M_{55}$ triblock copolymer due to the strong hydrogen bonding interaction between the surface of silica nanoparticles with the PMMA. Thus, the MEK-ST silica nanoparticles are assumed to be localized in the PMMA phase of $S_{52}B_{30}M_{18}$ as well, which means the spherical structure (dark domain) is filled with the silica particles. As a result, the silica particles which are dispersed in the PMMA phase show up as dark domains (highest stiffness) in the AFM phase contrast image. This will be confirmed in later AFM results of the PS/SBM blends. However, since the TOL-ST silica-filled $S_{52}B_{30}M_{18}$ film also does not show the silica particles in Figure 5.2b, the sample was investigated by TEM to find the localization of the silica particles. In Figure 5.2c, the TOL-ST silica can be observed to be crowded in the PS matrix without a homogeneous dispersion. The preferential localization of the TOL-ST silica is reasonable, since the TOL-ST silica particles are stable in the hydrophobic solvent (toluene), which can be assumed as a hydrophobic nanoparticle and prefer to be dispersed in the hydrophobic polymer (PS phase). However, the hydroxyl group on the surface of the TOL-ST silica will still disturb the stabilization of the nanoparticles during evaporating the solvent; therefore, silica clusters may be observed in the PS phase. It has to be remarked that the silica clusters shown in the thick film which is prepared for TEM cannot be observed in the thin film used for the AFM measurements, see Figure 5.2b. This could be related to the sample preparation procedure. Since long evaporating times are needed for complete removal of the toluene from the thick film, the stabilization of the TOL-ST silica particles in toluene will be lost during the

procedure. However, the thin films for the AFM measurement need much less time to dry than the thick films used for TEM; therefore, it is relatively easy to fix the silica particles in a stable state unless there is high loading of the silica particles, which will be discussed in Section 5.3.2.2. Furthermore, the apparent disappearance of the TOL-ST silica particles in the AFM images could also be related to unfavorable interactions with air.

As we know from the results of Chapter 4, selective localization of the silica particles is the key factor on the phase behavior of homopolymer/block copolymer blend. Thus, the effect of these two kinds of silica particles, which show a different preferential localization in the SBM triblock copolymer, on the morphology of the PS/SBM system will be discussed in the next section.

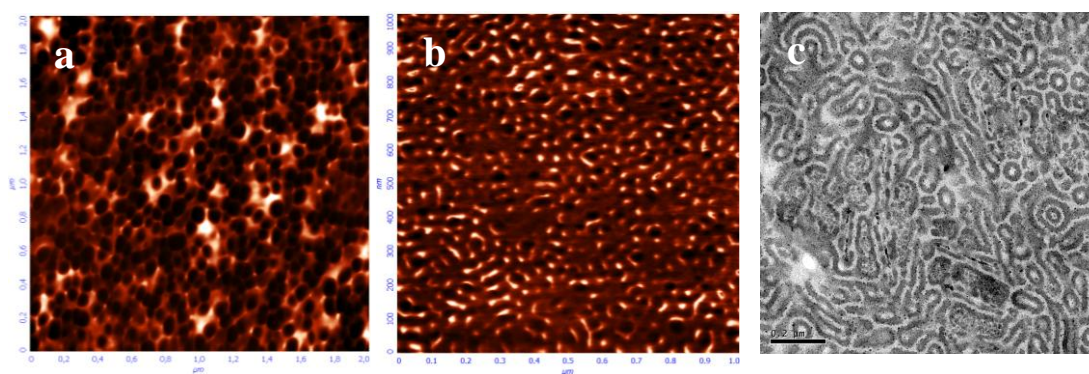


Figure 5.2: AFM phase angle images of (a) MEK-cast $S_{52}B_{30}M_{18}$ filled with 1 wt% MEK-ST silica and (b) toluene-cast $S_{52}B_{30}M_{18}$ filled with 0.5 wt% TOL-ST silica; TEM images of (c) toluene-cast $S_{52}B_{30}M_{18}$ filled with 0.5 wt% TOL-ST silica. For AFM, the dark regions in the phase angle images correspond to lower phase angles or higher stiffness. Light regions correspond to the PB domains.

5.3.2 The effect of silica nanoparticles on the morphology of solvent-cast PS/SBM blends

The polymer chains in the solvent-cast samples have a higher mobility during the solution processing and a much longer time to phase separate during the annealing process. Therefore, the solvent-cast samples can form better-ordered morphologies with macrophase separation in the block copolymer/homopolymer blend with larger length scales, thereby providing a more obvious effect of the silica particles on the morphology development. In this section, the effect of nanoparticles on the morphologies of the block copolymer/homopolymer blend is studied via solvent casting. Additionally, for the solvent-cast films, the easiest detectable method is AFM that can give an overview on a much larger scale than TEM, although AFM can only perform the measurement on the surface of the samples. Since the surface morphology of the neat SBM show a good agreement with the morphology of the bulk

sample (see Figures 5.1 and 5.2), AFM is used to discern the effect of two different silica suspensions (MEK-ST and TOL-ST) on the phase behavior of the blends.

5.3.2.1 The selective distribution of MEK-ST silica nanoparticles in PS/S₂₀B₂₅M₅₅

Since the MEK-ST silica-filled PS/S₅₂B₃₀M₁₈ blend prepared via solvent casting always show silica clusters after evaporation of the solvent, even with low silica content (1 wt%), the triblock copolymer S₂₀B₂₅M₅₅ with PMMA as the major component is used to study the MEK-ST silica-filled PS/SBM system. In addition, MEK is used to dissolve and mix the polymers in combination with the MEK-ST silica particles.

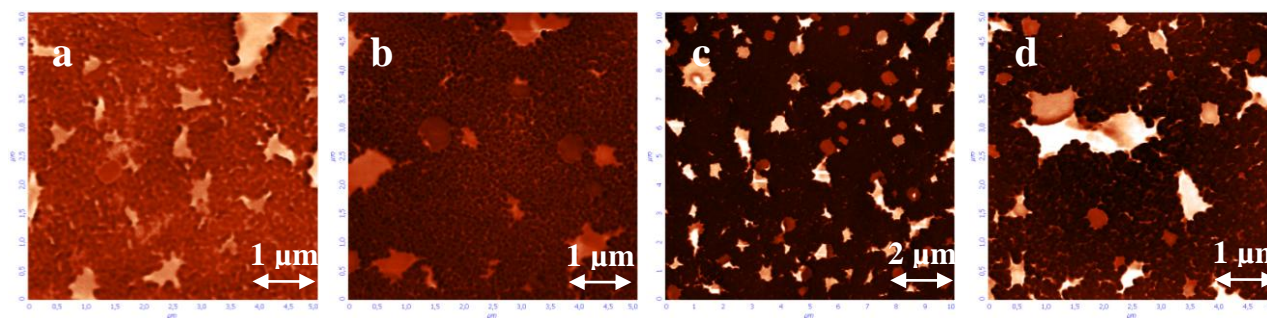


Figure 5.3: AFM phase angle images of (a) neat PS/S₂₀B₂₅M₅₅ 50/50 blend, (b-c) 1 and 2 wt% MEK-ST silica-filled PS/S₂₀B₂₅M₅₅ 50/50 blends (d) high magnification of the 2 wt% MEK-ST silica-filled blend. In comparison to the neat polymer, the contrast of the phase angle changed after adding silica. The darkest domains correspond to silica particles.

As discussed in Chapter 4, the occurrence of macrophase separation between the block copolymer S₂₀B₂₅M₅₅ and homopolymer PMMA can be suppressed by the addition of the MEK-ST silica, due to the selective adsorption of the high molar mass PMMA on the surface of the silica particles, which may force the system into the ‘wet-brush’ regime. In this chapter, the homopolymer PMMA is replaced by PS as matrix, followed by mixing with the MEK-ST silica and S₂₀B₂₅M₅₅ in MEK. The morphologies of the neat PS/S₂₀B₂₅M₅₅ 50/50 and silica-filled PS/S₂₀B₂₅M₅₅ 50/50 as investigated by AFM are shown in Figure 5.3. The obtained contrast is based on the different phase angles between PS and PMMA. The PMMA-rich (S₂₀B₂₅M₅₅-rich) phase is observed as relatively dark domains. Figure 5.3a shows the morphology with macrophase separation between the S₂₀B₂₅M₅₅ block copolymer and the homopolymer PS, for which the molar mass of the homopolymer PS ($M_n = 79.3$ kg/mol, PDI = 3.51) exceeds the molar mass of the PS block ($M_n \sim 11$ kg/mol) of the block copolymer, i.e. the system is in the ‘dry-brush’ regime. A disordered lamellar structure can be

observed in the microphase-separated $S_{20}B_{25}M_{55}$ domains. It has to be remarked that the area of the $S_{20}B_{25}M_{55}$ domains comprises more than 50 wt% in Figure 5.3a, which could be related to the preferential interaction between PMMA and the air.

With addition of 1 wt% MEK-ST silica particles, the length scale of the macrophase separation does not change as can be observed in Figure 5.3b. It is evident that the silica particles are well dispersed in the PMMA-rich domains, which is further confirmed in the higher magnification image of the 2 wt% MEK-ST silica-filled blend (Figure 5.3d). However, a suppression effect on the extent of macrophase separation is not observed for this system, even after adding 2 wt% MEK-ST silica. On the contrary, the length scale of the macrophase separation is much larger than for the 1 wt% MEK-ST silica-filled blend. The swelling of the PMMA-rich domains induced by the insert of silica particles is evident from Figure 5.3c, which is an enlargement of the $S_{20}B_{25}M_{55}$ domain. This effect is more apparent with higher silica loadings (3-5 wt%), not shown here. The swelling effect of the silica particles on the length scale of macrophase separation is also obvious for the PS/ $S_{20}B_{25}M_{55}$ 80/20 blend.

Figure 5.4a shows that the $S_{20}B_{25}M_{55}$ block copolymer is well dispersed in the PS matrix in the blends of PS/ $S_{20}B_{25}M_{55}$ 80/20. The PMMA phase can be observed as dark spherical/worm-like domains, surrounded by the light PB-domains. After a loading of 1 wt% MEK-ST silica particles, the silica particles are found to be well confined in the center of the worm-like $S_{20}B_{25}M_{55}$ domains (PMMA phase) are visible as small black dots. Further, Figure 5.4b shows that the silica particles have no effect on the length scale of the phase separation. However, after adding 2 wt% MEK-ST silica or more, the $S_{20}B_{25}M_{55}$ domains expand to larger length scales because of the swelling of the PMMA phase. Together with a further growth of the length scale of macrophase separation, a co-continuous morphology is obtained with addition of 5 wt% MEK-ST silica (see Figure 5.4d).

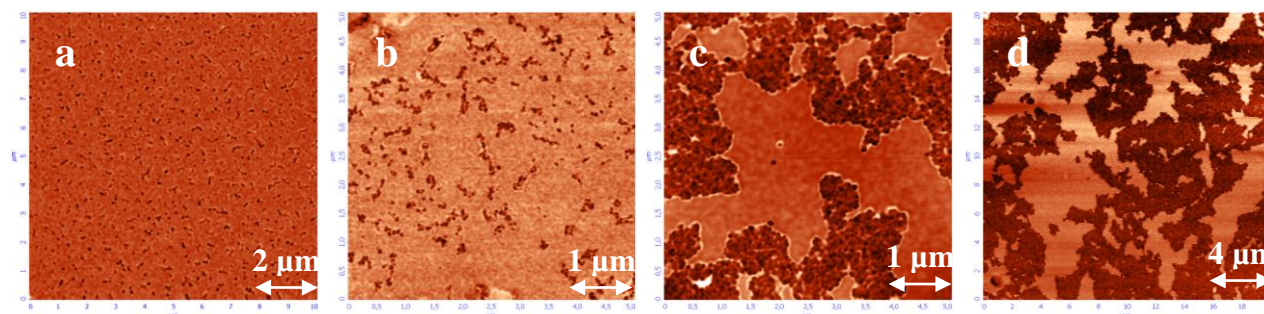


Figure 5.4: AFM phase angle images of (a) neat PS/ $S_{20}B_{25}M_{55}$ 80/20 blend and (b-d) PS/ $S_{20}B_{25}M_{55}$ 80/20 blend with 1, 2, 5 wt% MEK-ST silica.

In comparison to the MEK-ST silica-filled PMMA/S₂₀B₂₅M₅₅ discussed in Chapter 4, the opposite effect of same silica particles on the phase separation of the PS/S₂₀B₂₅M₅₅ blend is observed due to the strong interaction with PMMA phase. The preferential localization of the MEK-ST silica particles being a hydrophilic silica induces either a suppression effect (PMMA/S₂₀B₂₅M₅₅) or an acceleration effect (PS/S₂₀B₂₅M₅₅) on the macrophase separation. The spatial distribution of the nanoparticles is crucial to achieve the required properties, which will be discussed in Section 5.3.4.

5.3.2.2 The suppression effect of the TOL-ST silica nanoparticles in PS/S₅₂B₃₀M₁₈

TOL-ST silica is a colloidal silica suspension in toluene, which is a hydrophobic solvent. In other words, the TOL-ST silica can be classified as hydrophobic nanoparticles stable in hydrophobic solvent. To investigate the effect of the hydrophobic TOL-ST silica nanoparticles on the phase behavior of the homopolymer/block copolymer blends, PS and S₅₂B₃₀M₁₈ were dissolved in toluene together with the TOL-ST silica, followed by solvent casting on the substrate.

Figure 5.5 shows the AFM phase images of the surface morphologies of the neat and TOL-ST silica-filled PS/S₅₂B₃₀M₁₈ 50/50 films. In the neat 50/50 blend, macrophase separation occurs between S₂₀B₂₅M₅₅ and homopolymer PS. The PMMA-rich (S₅₂B₃₀M₁₈) phase is observed as dark region. In addition, small isolated S₅₂B₃₀M₁₈ domains can also be found well dispersed in the PS matrix. The area of the S₅₂B₃₀M₁₈ domains is more than 50 vol% of the surface of the film as investigated by AFM (Figure 5.5a) due to the preferential interaction between PMMA with air. This is more obvious for the PS/S₅₂B₃₀M₁₈ 80/20 blend in Figure 5.6a.

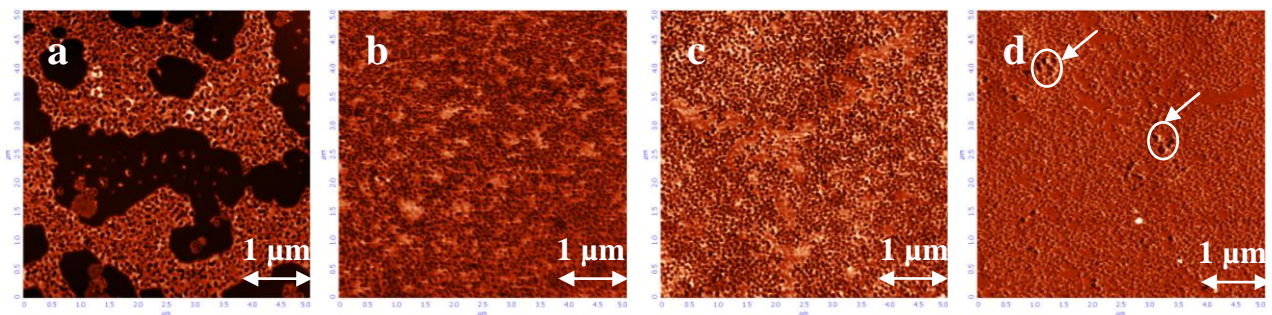


Figure 5.5: AFM phase angle images of (a) neat PS/S₅₂B₃₀M₁₈ 50/50 blend and (b-d) 1, 2 and 5 wt% TOL-ST silica-filled PS/S₅₂B₃₀M₁₈ 50/50 blend. In the neat polymer blend, the dark regions correspond to PMMA domain. PS domain can be observed as the light domain.

After a silica loading of 1 wt% TOL-ST silica in the PS/S₅₂B₃₀M₁₈ 50/50 blend, the extent of the macrophase separation is suppressed, as shown in Figure 5.5b. Instead, more isolated microphase-separated block copolymer S₅₂B₃₀M₁₈ domains can be observed homogeneously dispersing in the homopolymer matrix, although the TOL-ST silica particles cannot be observed on the surface of these films, only when the silica aggregates appear. The silica aggregates are observed when the silica loading is high (Figure 5.5d), of which the phase angle is lowest and corresponds to the darker dots compared with the PMMA-rich phases. The suppression effect of TOL-ST silica on the phase separation is also investigated after adding 2-5 wt% silica (see Figure 5.5c-d).

In this section, the solvent-casting method was used to prepare the mixture of PS/SBM with different colloidal silica particles. Depending on the solvent of the silica suspension used in this blend, the selective distribution of nanoparticles can be found in the homopolymer/block copolymer blend. The hydrophilic silica MEK-ST selectively distributes in the PMMA phase, while the hydrophobic silica TOL-ST can be found in the PS phase. The specific affinity of the silica arises from the interactions between particle surface with the polymer. This particular behavior of silica particles induces different effects on the morphology of the PS/SBM blend, which is either suppressing or accelerating the extent of the macrophase separation.

5.3.3 Morphology development of triblock copolymer/monomer with addition of silica nanoparticles upon in-situ polymerization

The solvent-casting method demonstrated the possibility to control the localization of silica particles in specific domains of the self-organized block copolymer. Compared to solvent casting, in-situ polymerization of monomer/block copolymer solutions lead to a better dispersion in the block copolymer/homopolymer blends. For the PMMA/S₂₀B₂₅M₅₅ system studied in Chapter 4, the chemically-induced phase separation is slowed down by the silica particles during in-situ polymerization, with a reduction of the size of the domains of the lamellar morphology. Therefore, the effect of the silica particles on the morphology of the PS/SBM during in-situ polymerization needs to be addressed. Only the hydrophobic TOL-ST silica is used, since the hydrophilic MEK-ST silica is not stable in the styrene monomer solution.

The TEM images of the morphology of the blends after polymerization are shown in Figure 5.6. The TOL-ST silica-filled systems show silica clusters with a size of 200-500 nm

in the PS matrix (Figures 5.6b-c), which means that the silica particles are instable in the PS matrix after polymerization. However, the mixture of the styrene/TOL-ST/block copolymer is transparent before heating to the required polymerization temperature, thus possible clustering of the silica particles must occur during the polymerization, because the stabilization of the TOL-ST silica particles is lost at some point. Additionally, some ring-like silica structures can be observed in some polymerizations, independent of the concentration of the triblock copolymer, as shown in Figure 5.6b. But these structures cannot be observed in the polymerization of styrene/silica systems without block copolymer. The ring-like structures have very similar features as Pickering emulsions, which are studied a lot in the nanocomposite synthesis of silica/polymer in the emulsion polymerization. The interaction as hydrogen bonding between the silica surface and the polymer is known to be important.²²⁻²⁴ Although it is still unknown that how the ring-like silica structures are formed during the in-situ polymerization process, the interaction (like hydrogen bonding) between the block copolymer and the silica surface could be the reason of the formation. Besides, the final morphology after the polymerization shows microphase separation in both the neat and the silica-filled styrene/S₅₂B₃₀M₁₈ blends, containing a combination of core-shell and cylindrical structures, which come from the SBM triblock copolymer and the SB diblock copolymer, respectively. Although the silica nanoparticles are not well dispersed in the PS/S₅₂B₃₀M₁₈ blend, the in-situ SAXS measurements still show the effect of the silica particles on the development of the phase separation.

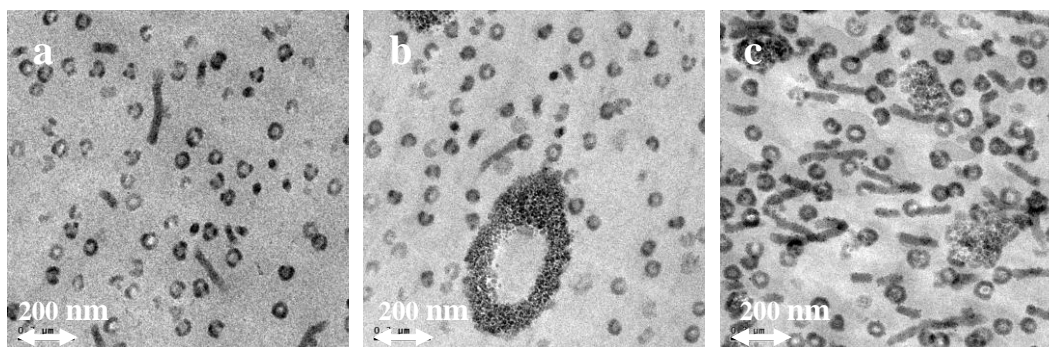


Figure 5.6: TEM images of the in-situ polymerization samples: (a) PS with 10 wt% S₅₂B₃₀M₁₈, (b) PS with 10 wt% S₅₂B₃₀M₁₈ and 2 wt% silica and (c) PS with 20 wt% S₅₂B₃₀M₁₈ and 2 wt% silica. The polymerizations were started at ambient temperature.

The obtained SAXS patterns of the system with 10 wt% of S₅₂B₃₀M₁₈ in styrene during polymerization are shown in Figure 5.7. The time-resolved SAXS data include also the heating stage from -50 to 100 °C at 5 °C/min to obtain information about the formation, size

and possible disassociation of the micelles, followed by the isothermal polymerization at 100 °C after 30 min.

The SAXS patterns of the neat styrene/S₅₂B₃₀M₁₈ system are shown in Figure 5.7a. A primary scattering peak at $q^* = 0.0063 \text{ \AA}^{-1}$ which can be assigned to the structure factor and a second peak at higher angles at $q = 0.018 \text{ \AA}^{-1}$ from the form factor are present at -50 °C, which means that the ordered microstructures already exist in the frozen solution. It is expected that the PB-PMMA blocks form a core-shell structure, while the PS block is swollen by the styrene matrix. Upon heating, the higher q-range peak at $q = 0.018 \text{ \AA}^{-1}$ moves to slightly lower q-values and cannot be distinguished at -20 °C, which means that the size of the dispersed core-shell structure is expanding due to the thermodynamic unstable of the core-shell structure in the mixture. The disappearance of the higher order peak may be related to the change of the electron density profile. However, the peak related to the structure factor is constant even after the beginning of the polymerization at $T = 100 \text{ °C}$, which means that the core-shell structure does not break up. The compatibility of the PS block in S₅₂B₃₀M₁₈ with styrene enhances the stability of the core-shell structure. After reaching the isothermal polymerization temperature of $T = 100 \text{ °C}$ for 20 min, the original ordered structures is regained. The first order diffraction peak at $q^* = 0.0065 \text{ \AA}^{-1}$ develops, followed by a higher order scattering at $q = 0.0126 \text{ \AA}^{-1}$, reflecting the microphase separation process of the block copolymer. After another 35 min, the third-order reflection at $q = 0.0207 \text{ \AA}^{-1}$ appears, which indicates that more ordered microphases of the triblock copolymer are formed.

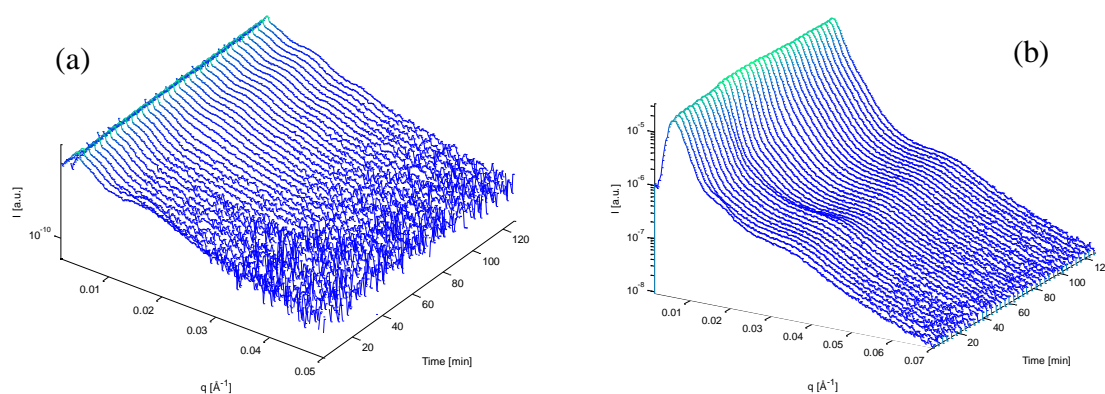


Figure 5.7: SAXS profiles collected during a heating ramp from -50 to 100 °C at 5 °C/min and isothermal polymerization of styrene at $T = 100 \text{ °C}$ for (a) styrene with 10 wt% S₅₂B₃₀M₁₈ and (b) styrene with 10 wt% S₅₂B₃₀M₁₈ and 2 wt% silica. The isothermal polymerization temperature is reached after 30 min.

Compared to the neat styrene/S₅₂B₃₀M₁₈ system, the 2 wt% TOL-ST silica-filled styrene/S₅₂B₃₀M₁₈ system shows a similar structure development during polymerization.

Although the sharp structure factor peak is absent during heating from -50 to -20 °C, due to overlap with the scattering of the direct beam close to the beam-stop, the form factor peak is shown at $q = 0.0178 \text{ \AA}^{-1}$, which originate from the core-shell structures. Different with the neat system, during heating from -50 to 100 °C, a broad peak with a relatively high intensity at $q = 0.035 \text{ \AA}^{-1}$ can be constantly observed in the silica-filled system. This implies that the silica particles are well dispersed in the solution without any specific ordering. The form factor peak at $q = 0.0178 \text{ \AA}^{-1}$ disappears after heating up to -20 °C, which is the same as for the neat system. Upon polymerization, the structure factor peak of the core-shell structure appears at $q = 0.0173 \text{ \AA}^{-1}$ and $q = 0.0345 \text{ \AA}^{-1}$.

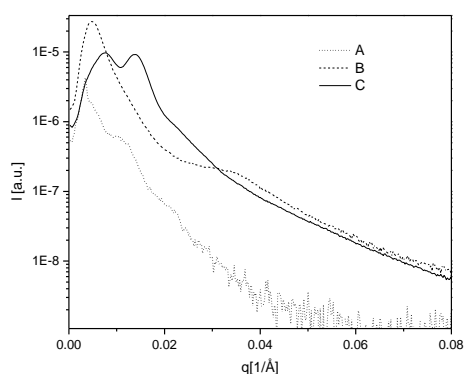


Figure 5.8: SAXS patterns of PS blends with 10 wt% of $S_{52}B_{30}M_{18}$. A: after in-situ polymerization of neat styrene with $S_{52}B_{30}M_{18}$, B: after in-situ polymerization of silica-filled styrene with $S_{52}B_{30}M_{18}$ and C: compression-molded pure $S_{52}B_{30}M_{18}$.

In Figure 5.8, the final peak position of the diffraction pattern of the neat styrene/ $S_{52}B_{30}M_{18}$ blend is slightly different in comparison to the silica-filled styrene/ $S_{52}B_{30}M_{18}$ blend after polymerization, but both the scattering patterns can be considered as core-shell structures, which were also observed by TEM (see Figure 5.6). However, the SAXS pattern of the compression-molded pure $S_{52}B_{30}M_{18}$ is quite different from the sample prepared via in-situ polymerization. This agrees well with the different morphologies of the pure $S_{52}B_{30}M_{18}$ in comparison to the PS/ $S_{52}B_{30}M_{18}$ blend, as shown in Figure 5.1a and 5.6a. The pure $S_{52}B_{30}M_{18}$ has a disordered worm-like lamellar morphology, because of the combination of SBM triblock copolymer and SB block copolymer, which leads to a system with a high curvature. However, after mixing with styrene or PS, the SBM and SB are separated to core-shell and cylindrical structures, which are well dispersed in the matrix, although the cylindrical structure might not be distinguished in the SAXS pattern due to its low concentration.

During the polymerization, the presence and development of different phases can be reflected in the scattering invariant, which can provide the information of the morphology development. In Figure 5.9, both systems show a low plateau value of the experimental invariant at the start of the polymerization. The invariant of the neat system starts to increase immediately at the polymerization temperature of 100 °C, while that of the silica-filled system starts 30 min later. According to the TEM images after polymerization in Figure 5.6, there is only microphase separation in the PS/S₅₂B₃₀M₁₈ blends. A combination of a core-shell and cylindrical morphology can be found in both neat and silica-filled PS/S₅₂B₃₀M₁₈ system. The minority cylindrical structures arise from the SB diblock copolymer. The size of the well-dispersed core-shell phase is approx. 50 nm, implying that there is no apparent macrophase separation between PS and S₅₂B₃₀M₁₈. Thus, the increasing of the invariant value comes from the microphase separation of the triblock copolymer. The delay of the microphase separation of the S₅₂B₃₀M₁₈ from the PS matrix might be related to the interaction of the silica with the triblock copolymer.

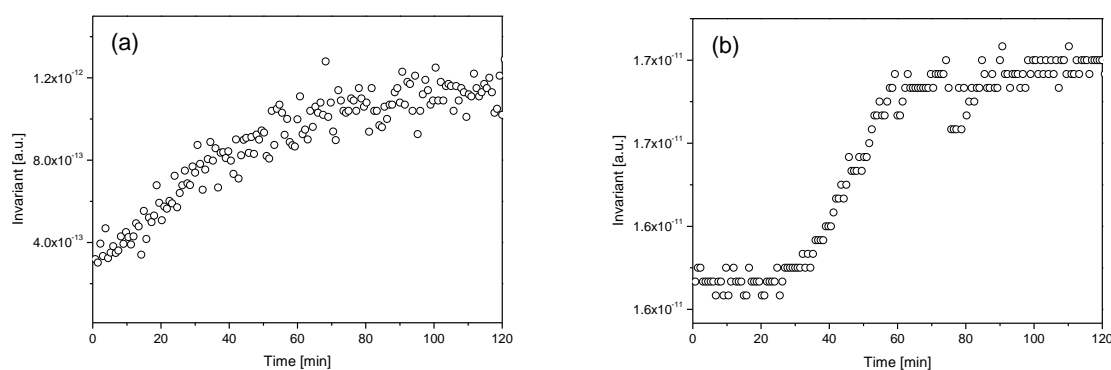


Figure 5.9: Experimental scattering invariant for the polymerization of styrene with 10 wt% S₅₂B₃₀M₁₈ at T=100 °C: (a) neat system and (b) 2 wt% silica-filled system.

Although the silica clusters can be observed in the PS/S₅₂B₃₀M₁₈ blend after the in-situ polymerization, the slow-down effect of the silica particles on the development of the phase separation can be still observed from the invariant results. In addition, the final morphology after the polymerization shows microphase separation in the styrene/S₅₂B₃₀M₁₈ blends, which provides a possibility to obtain a nanosized heterogeneous blend prepared by an industrial route (melt-mixing).

5.3.4 Morphologies of PS/SBM nanocomposites: Melt mixing

Based on the previous results, the solvent-cast films show macrophase separation with large length scales, induced by the higher mobility of the polymer chain during solution processing combined with longer annealing times. However, the triblock copolymer $S_{52}B_{30}M_{18}$ shows a good (nanosized) dispersion in the PS matrix after the in-situ polymerization. In this section, two different types of silica particles are used to investigate the effect of the silica particles with different interactions with the polymers on the morphology of the PS/ $S_{52}B_{30}M_{18}$ blends via melt mixing. Different compounding procedures were used to control the distribution of the silica particles.

5.3.4.1 Controlling the localization of silica nanoparticles by compounding

In order to confine the silica particles in the core-shell rubbery phase in the PS/SBM blend, MEK-ST silica was pre-dispersed in $S_{52}B_{30}M_{18}$ by solvent casting, followed by drying steps. The obtained SBM/silica was melt blended with PS in a second step in a twin-screw mini-extruder.

Figures 5.10a-c show the morphologies of the neat PS/ $S_{52}B_{30}M_{18}$ 80/20 blend at various magnifications. The homopolymer PS used here is the one with a broad molar mass distribution ($M_n = 79.3$ kg/mol, PDI = 3.5), which forms the matrix (grey domain), leading to sufficient compatibility between the PS matrix and the longer PS-block of triblock copolymer $S_{52}B_{30}M_{18}$ (PS-block: $M_n = 29$ kg/mol). The core-shell structures of the $S_{52}B_{30}M_{18}$ can be observed as a good dispersion with a size of 50-100 nm in Figure 5.10a, in which the PMMA-block (light domain) forms the core well surrounded by the PB-block (dark domain). The small length scale microphase separation is related to the high viscosity of polymers and high shear forces during melt mixing.

The morphology of the MEK-ST silica-filled PS/ $S_{52}B_{30}M_{18}$ 80/20 blend at various magnifications is displayed in Figures 5.10d-f. There are no apparent silica clusters visible at lower magnifications in the silica-filled blend. Since the addition of the silica particles change the electron density differences between the different blocks, different OsO_4 staining processes were used to enhance the contrast. The silica-filled PS/ $S_{52}B_{30}M_{18}$ shows a similar morphology as the neat blend, although the morphology of the silica-filled system seems slightly different due to the vapour staining process (Figures 5.10d-e), comparing to the bulk staining (Figures 5.10b-c) neat system. It is evident that there is no obvious difference of the dispersed phase scale between the neat and silica-filled blends. The observed silica particles

are confined in the PMMA-block of the core-shell structure. This is very clear in the non-stained sample, which shows the MEK-ST silica well dispersed as single or multiple twin particles in the light domains (PMMA-blocks), although the PB block is invisible without staining. Due to the strong interaction between the hydroxyl groups on the surface of silica nanoparticles with the carbonyl groups of the PMMA, the MEK-ST silica has no tendency to migrate to the matrix, which is consistent with the results of the solvent-cast sample in Figure 5.4b.

This nanosized core-shell structure of the PS/S₅₂B₃₀M₁₈ 80/20 blend prepared via melt mixing, with the confined localization of the silica in the PMMA-core surrounded by PB rubber shell, is well consistent with the idea of a tough heterogeneous system based on an easily-cavitating rubber modifier, as described in Chapter 1. The silica embedded in the PMMA block core might induce precavitation during cooling due to the different thermal expansion coefficient of silica and PMMA. This will be further discussed.

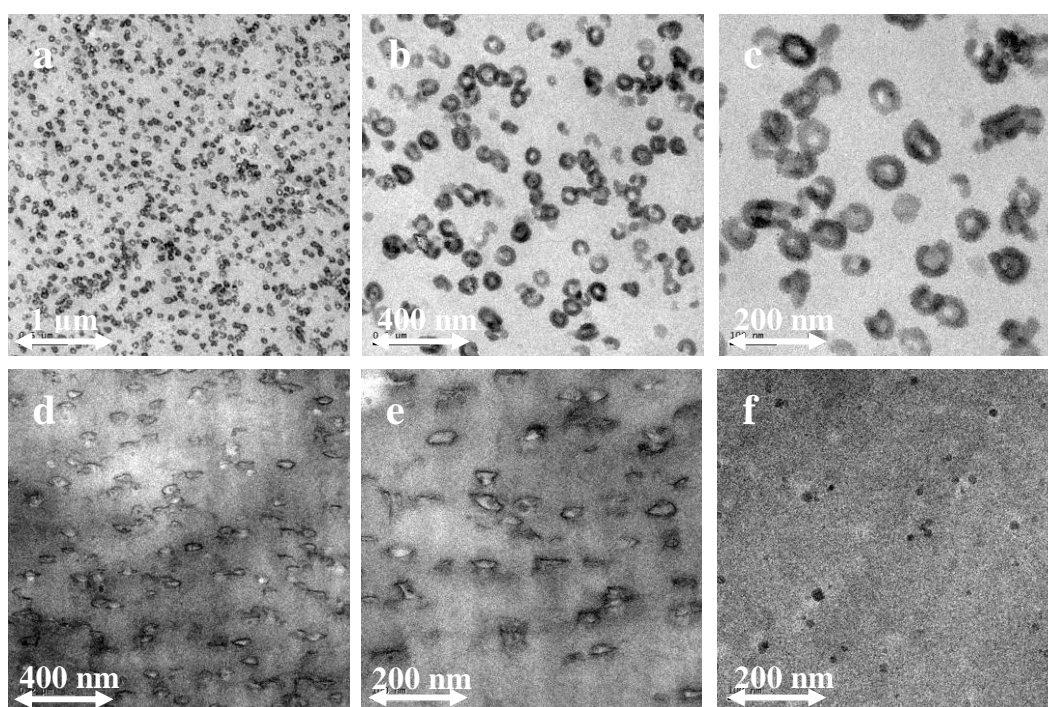


Figure 5.10: TEM images of melt-mixing samples: (a-c) neat PS/S₅₂B₃₀M₁₈ 80/20 blend and (d-f) MEK-ST silica-filled PS/S₅₂B₃₀M₁₈ 80/20 blend (1 wt% MEK-ST silica were first compounded with S₅₂B₃₀M₁₈ by solvent casting) at various magnifications. For image (f), the non-stained sample was prepared to obtain the enhanced contrast between silica and polymers.

5.3.4.2 Suppression effect of the silica nanoparticles

In the study of the suppression effect of the silica particles on the PS/S₅₂B₃₀M₁₈ system, which is observed in the solvent-cast samples of Section 5.3.2.2, the dispersion of the silica

particles is found to be an important factor. The MEK-ST silica nanoparticles aggregated easily in the blend of PS with $S_{52}B_{30}M_{18}$, of which the PS block is the major component. This is related to the hydrophilic surface of the MEK-ST silica (hydroxyl groups), which cannot be stabilized in the hydrophobic (PS) medium. However, the TOL-ST colloidal silica particles suspended in toluene can be considered as hydrophobic particles and are found to yield a suppression effect on the macrophase separation of the PS/ $S_{52}B_{30}M_{18}$. Thus, it is necessary to study whether the TOL-ST silica has the same effect on the phase separation of PS/ $S_{52}B_{30}M_{18}$ blends via melt mixing. Since the effect is limited by the dispersion of the silica particles, the precipitation method is used, followed by melt mixing in the mini-extruder.

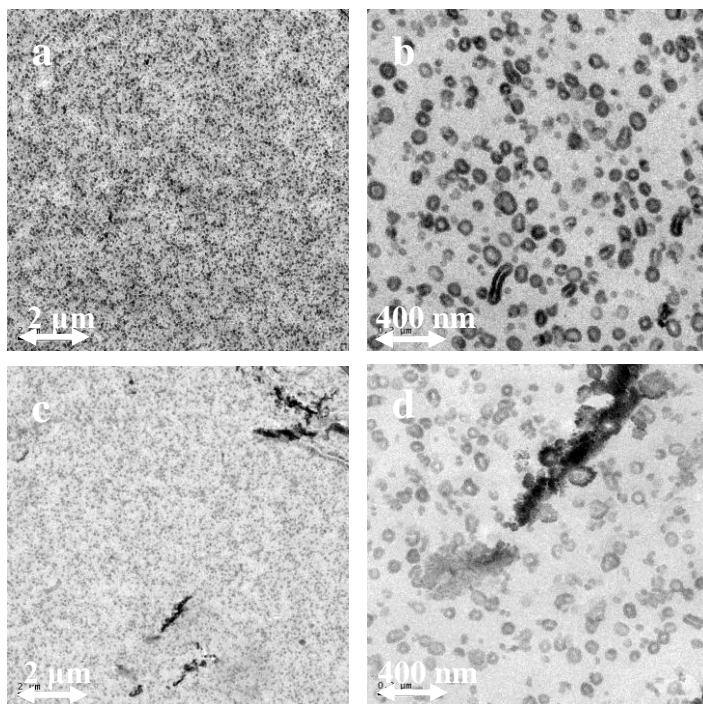


Figure 5.11: TEM images of melt-mixing samples: (a-b) neat PS/ $S_{52}B_{30}M_{18}$ 80/20 blend and (c-d) 2 wt% TOL-ST silica-filled PS/ $S_{20}B_{25}M_{55}$ 80/20 blends at various magnifications. Both are prepared from precipitation, followed by extrusion.

Figure 5.11 show the morphologies of the neat and 2 wt% TOL-ST silica-filled PS/ $S_{52}B_{30}M_{18}$ 80/20 blends at various magnifications. Both of them display a well-ordered core-shell structure formed by $S_{52}B_{30}M_{18}$ in the PS matrix and the size of the SBM domains is around 50-100 nm. However, the TOL-ST silica particles can be observed as aggregates in the matrix, seen in Figures 5.11c-d. The appearance of the silica clusters demonstrates that the TOL-ST silica cannot be stabilized in the hydrophobic PS system without toluene.

In brief, for the melt-mixed sample, due to its high melt viscosity and high shear stresses, the neat and silica-filled blend only show microphase separation, unlike the large length scale

macrophase separation induced by the solvent casting. Since the instability of the silica particles in the PS/S₅₂B₃₀M₁₈ system, the suppression effect cannot be observed in the TOL-ST silica-filled PS/S₅₂B₃₀M₁₈ 80/20 blend via melt mixing.

5.3.5 Deformation mechanism

As mentioned before in the introduction on the modeling results, a way to toughen the brittle amorphous polymers like PS is to let a rubber shell locally support the straining filaments, not changing the PS properties, but changing the local structure properties to make it easier to delocalize the strain by the cavitation in the rubber phase. Further, an optimal rubber modifier is a nanosized pre-cavitating rubber core which can induce a change from crazing to cavitation-induced shear yielding. Thus, in order to investigate the capability of pre-cavitation of the PMMA-PB core-shell structure after addition of the silica nanoparticles, the sample which showed the selective localization of the silica particles in the PMMA core was prepared via the compounding procedure mentioned in Section 5.3.4.1. The difference of the thermal expansion coefficient between the silica nanoparticles and the PMMA might induce pre-cavitation in PMMA domains during cooling.

The morphologies of the neat and silica-filled PS/SBM blends after impact loading were explored by TEM, by using films which were microtomed from the stress whitened part after deformation. The results are shown in Figure 5.12. In the neat system, the localized crazes in the plane perpendicular to the loading direction are visible in Figures 5.12a-c. The nanosized core-shell structures are deformed by the growth of the crazes. No cavitation can be found in this system, since the cavitation capability of rubbery domains is dependent on the particle size. This means the voids can be hardly formed in the nanosized particles, which are approx. 30-50 nm. Unfortunately, the silica-filled PS/SBM blend also does not show cavitation in the PMMA-PB core-shell particles, in which only the localized crazes are observed, although the silica particles are homogeneously dispersed in the PMMA core as single particle or multiple twin particles (Figure 5.12f). This means that the silica particles do not lead to pre-cavitation inside the rubber phase during cooling. As discussed before, the affinity of the MEK-ST silica to the PMMA due to the hydrogen bonding is really strong, which induces an excellent dispersion of the silica particles in the PMMA. In other words, the strong interaction makes a good interfacial adhesion between the particles and the polymer, which might be the reason that internal stresses developed during cooling are still not enough to induce pre-cavitation in the nanosized PMMA core similar to the neat system. The tensile test also did not show much

difference of the modulus, yield stress and strain at break between the neat and silica-filled systems, which means the toughness is not enhanced by the addition of the silica.

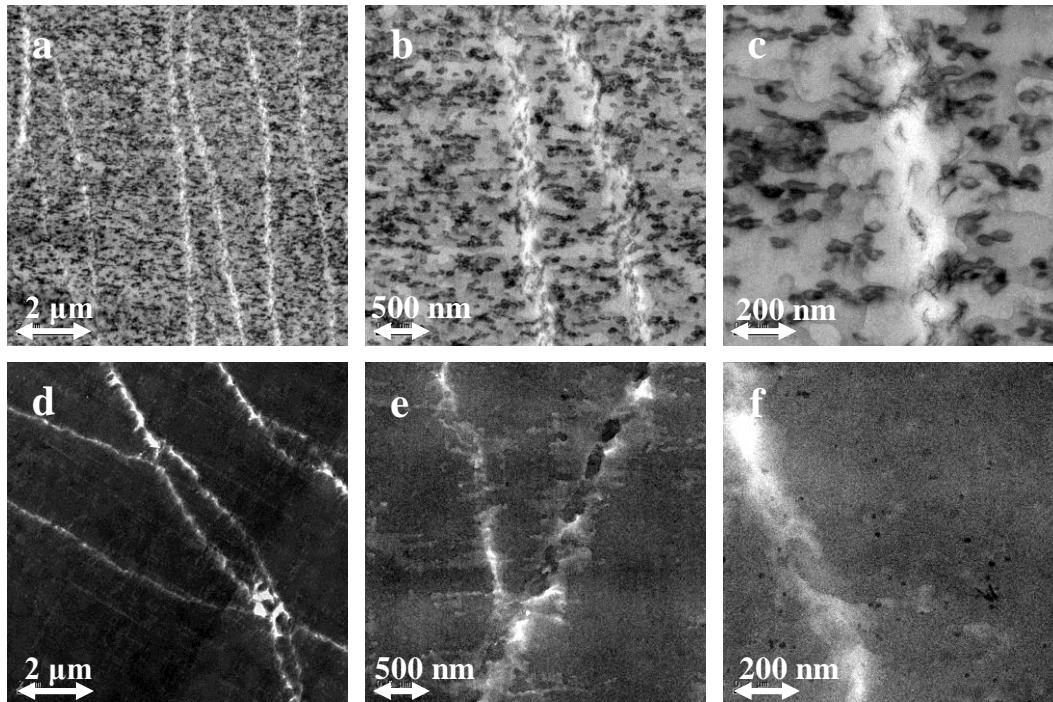


Figure 5.12: TEM images of the samples after deformation: (a-c) neat PS/S₅₂B₃₀M₁₈ 80/20 blend and (d-f) MEK-ST silica-filled PS/S₅₂B₃₀M₁₈ 80/20 blend (1 wt% MEK-ST silica were first compounded with S₅₂B₃₀M₁₈ by solvent casting) at various magnifications. For image (d-f), the non-stained sample was prepared to obtain the enhanced contrast between silica and polymers.

5.4 Conclusions

The effect of silica nanoparticles on the morphology of the homopolymer/block copolymer PS/SBM blend was studied. It was found that the morphology strongly depends on the distribution of the silica nanoparticles. Based on the interactions between the surface of the particles and the polymer components, the distribution of the silica particles over the different phases of the blend can be controlled by the surface characteristics of the silica particles.

The preferential localization of silica particles can induce either the suppression effect or the acceleration effect on the extent of macrophase separation between the block copolymer and homopolymer in PS/SBM blend. The hydrophilic MEK-ST silica particles are found preferentially localized in the dispersed PMMA phase due to the strong hydrogen bonding interaction between the silica and PMMA. Beyond a certain silica content, the selective localization behavior induces an swelling effect on the PMMA phase, accelerating the macrophase separation. However, if with a proper content of silica particles, this selective

distribution in the PMMA core may introduce extra internal stress in the core-shell rubbery phase via silica particles, which can be an optimal impact modifier in the amorphous brittle PS, although the silica-filled PS/SBM is not a successful example of the pre-cavitation.

It was also shown that a suppression effect on the extent of macrophase separation can be obtained by adding the TOL-ST silica particles in the PS/SBM blend, which occurred only if the silica particles were distributed in the PS phase and with a good dispersion. Since only large TOL-ST silica clusters can be obtained in the sample via melt mixing, the suppression effect was observed only for the other two preparation methods, i.e. solvent casting and in-situ polymerization of styrene in presence of the silica particles and triblock copolymer.

The larger length scale macrophase separation can be obtained in the blend prepared via solvent casting, since there is more time for phase separation during annealing. Further, the suppression effect of the TOL-ST silica nanoparticles is more obvious for the sample prepared via solvent casting. For the in-situ polymerization method, the phase separation is slowed down by the TOL-ST silica particles, although small silica clusters can be observed during the late stage of the polymerization. The silica with ring-like structures can be observed in the samples prepared in the polymerization, which are very similar as the Pickering features in the emulsion polymerization of silica/polymer nanocomposite in the literature. The interaction (like hydrogen bonding) between the block copolymer and the silica surface could be the reason of the formation.

In this chapter, the study of selective distribution of silica particles shows that there is a chance to enhance the capability of the pre-cavitation of the rubbery phase, which is dispersed in the core-shell rubbery phase in the brittle amorphous PS matrix, by introducing extra internal stress from the solid silica particles. Although the MEK-ST silica-filled PS/SBM blend does not show the enhancement of the pre-cavitation capability in the PMMA-PB core-shell, the system of which only show the localized crazes, the idea of this will be further studied in the PS/SBS blend shown in the appendix.

5.5 References

- ¹ Jansen, B. J. P., Rastogi, S., Meijer, H. E. H., Lemstra, P. J., *Macromolecules*, **1999**, 32, 6283-6289.
- ² Jansen, B. J. P., Rastogi, S., Meijer, H. E. H., Lemstra, P. J., *Macromolecules*, **2001**, 34, 3998-4006.
- ³ Jansen, B. J. P., Rastogi, S., Meijer, H. E. H., Lemstra, P. J., *Macromolecules*, **2001**, 34, 4007-4018.
- ⁴ Van Casteren I. A., Van Trier, R. A. M., Goossens, J. G. P., Meijer, H. E. H., Lemstra, P. J., *J. Polym. Sci., Part B: Pol. Phys.* **2004**, 42, 2137-2160.
- ⁵ Van Asselen, O. L. J., Van Casteren, I. A., Goossens, J. G. P., Meijer, H. E. H., *Macromol. Symp.*, **2004**, 205, 85-94.

- ⁶ Van Casteren, I. A., *Control of microstructures to induce ductility in brittle amorphous polymers*, Ph.D. Thesis, TU/e, Eindhoven, the Netherlands, **2003**.
- ⁷ Kierkels, J. T. A., *Tailoring the mechanical properties of amorphous polymers*, Ph.D. Thesis, TU/e, Eindhoven, the Netherlands, **2006**.
- ⁸ Meijer, H. E. H, Govaert, L. E., *Progress Pol. Sci.*, **2005**, 30, 915-938.
- ⁹ Thomas, E. L., *Science*, **1999**, 286, 1307.
- ¹⁰ Hardy, D. M., Bates, F. S., Kim, M. H., Wignall, G. D., *Macromolecules*, **2002**, 35, 3189-3197.
- ¹¹ Ritzenthaler, S., Court, F., David, L., Girard-Reydet, E., Leibler, L., Pascault, J. P., *Macromolecules*, **2002**, 35, 6245-6254.
- ¹² Brinkmann, S., Stadler, R., Thomas, E. L., *Macromolecules*, **1998**, 31, 6566-6572.
- ¹³ Krappe, U., Stadler, R., Voigt-Martin, I., *Macromolecules*, **1995**, 28, 4558-4561.
- ¹⁴ Hydro, R. M., Pearson, R. A., *J. Polym. Sci. Part B: Polym. Phys.*, **2007**, 45, 1470-1481.
- ¹⁵ Fine, T., Pascault, J-P., *Macromol. Symp.*, **2007**, 245, 375-385.
- ¹⁶ Fenouillot, F., Cassagnau, P., Majeste, J. C., *Polymer*, **2009**, 50, 1333-1350.
- ¹⁷ Kim, B. J., Chiu, J. J., Yi, G. R., Pine, D. J., Kramer, E. J., *Adv. Mater.*, **2005**, 17, 2618-2622.
- ¹⁸ Kim, B. J., Fredrickson, G. H., Hawker, C. J., Kramer, E. J., *Langmuir*, **2007**, 23, 7804-7809.
- ¹⁹ Kim, B. J., Fredrickson, G. H., Bang, J., Hawker, C. J., Kramer, E. J., *Macromolecules*, **2009**, 42, 6193-6201.
- ²⁰ Balazs, A. C., Emrick, T., Russell, T. P., *Science*, **2006**, 314, 1107-1110.
- ²¹ Montezinos, D., Wells, B. G., Burns, J. L., *J. Polym. Sci., Polym. Lett. Ed.*, **1985**, 23, 421-425.
- ²² Schmid, A., Tonnar, J., Armes, S. P., *Adv. Mater.*, **2008**, 20, 3331-3336.
- ²³ Percy, M. J., Amalvy, J. I., Randall, D. P., Armes, S. P., *Langmuir*, **2004**, 20, 2184-2190.
- ²⁴ Luna-Xavier, J. L., Bourgeat-Lami, E., Guyot, A., *Colloid Polym. Sci.*, **2001**, 279, 947-958.

Chapter 6

Effect of silica nanoparticles on the morphology of PMMA-PBA-PCL triblock copolymer blends with a crystallizable block

The triblock copolymer consisting of poly(methyl methacrylate) (PMMA), poly(butyl acrylate) (PBA), and a crystallizable block poly(ϵ -caprolactone) (PCL) and its blends with PMMA as the matrix are investigated by atomic force microscopy (AFM), transmission electron microscopy (TEM) for the morphology, and differential scanning calorimetry (DSC) for the thermal behavior. Due to the small volume fraction of PCL and the volume ratios of PBA and PCL, a well-dispersed core-shell spherical structure can be found as a major morphology in the triblock copolymer or its blend. The silica nanoparticles selectively localized in the PCL phase, which is consistent with the reason that the interaction between the hydroxyl groups of silica nanoparticles with the carbonyl groups of the PCL is stronger than the one between silica and the carbonyl groups of the PMMA. It is found that the silica nanoparticles have a large effect on the morphology of the blend of homopolymer/block copolymer, which will induce a transition of spherical to spherical/cylindrical morphology. The thermal behavior of the blends is strongly influenced by both the interactions between the silica surface with the polymer chain and the different morphologies.

6.1 Introduction

The toughness of brittle amorphous, glassy polymers can be improved by the addition of ABA or ABC block copolymers containing at least one rubbery block, which form micellar or cylindrical structures within the matrix.¹⁻⁵ The capability of rubbery particles to cavitate depends on their cross-link density and particles size; the smaller the particles, the more difficult they cavitate.⁶ As reported by Van Casteren³ and Kierkels⁴, a nanosized rubber particle with a core-shell morphology that can be precavitated may overcome the size-dependence of the cavitation process. In Chapters 4 and 5, block copolymers which comprise the core-shell structure, containing a high elastic modulus block as a core with a low glass transition temperature (T_g) rubbery block as a shell, were used as the cavitating material. Replacing the core-forming (high elastic modulus block) by a semi-crystalline block may even further improve the toughness of the matrix, since additional internal stresses can build up during crystallization due to volumetric shrinkage, which may facilitate precavitation.⁷ The occurrence of this confined crystallization is related to the geometry of the crystallizable domain.

Many studies were performed on the confinement of a crystallizable block within AB or ABC microphase-separated block copolymers.⁸⁻¹² Register and co-workers studied the structure formation of the crystallizable diblock copolymer poly(ethylene-*b*-(ethylene-*alt*-propylene)) (E/EP) and showed that the driving force for microphase separation of the block copolymers with a crystallizable block is not only the block incompatibility but also the confined crystallization, of which the mechanism and kinetics of the ordering process differs from amorphous block copolymers which have been studied thus far.^{10,11} The crystallization process could either lead to morphology or induce a transition between two different morphologies, which depends on the segregation strength between the blocks and whether the matrix is crystallized from a microphase-separated melt or crystallizes from a homogeneous melt or solution.¹³

The type of nucleation in confined crystallization is strongly governed by the size and the geometry of these crystallizable domains.^{14 - 15} Similar to homopolymers, so-called heterogeneous nucleation can occur in large domains of the crystallizable block, such as

present in cylindrical or lamellar morphologies, where the probability to find heterogeneities that can act as nucleation site is high. On the other hand, homogeneous nucleation will occur if the crystallizable domains are relatively small, such as present in spherical morphologies, where heterogeneous nucleation is strongly suppressed because of the small number of active heterogeneities. These two nucleation events, resulting in so-called fractionated crystallization, can either occur separately or as a combination of both, and was studied by many researchers.^{5,8,9,12-15}

Mueller *et al.*⁸ investigated the fractionated crystallization in AB and ABC block copolymers with a crystallizable poly(ethylene oxide) (PEO) block. The confinement of the crystallizable block could be tailored by the adequate choice of composition and molar mass. Guo *et al.*⁹ observed a confinement effect of the crystallizable block in a self-organizing block copolymer/thermoset blend with nanoscale spherical particles.

Balsamo *et al.*^{5,14-15} reported that the confined crystallization is affected by the presence of both amorphous blocks, using various high molar mass poly(styrene)-*b*-poly(butadiene)-*b*-poly(ϵ -caprolactone) (PS-PB-PCL) triblock copolymers, with a crystallizable PCL-block. A general decrease in crystallinity as well as the occurrence of fractionated crystallization was observed in block copolymers, especially for those with low crystallizable content. Due to small volume fraction of PCL, the crystallization took place in two steps through a combination of heterogeneous and homogeneous nucleation. They showed that the mechanical response of the material with the crystallizable PCL-block strongly depends on the thermal history and the morphology.

In their studies, the excellent properties can be obtained in the system with both homogeneous and heterogeneous nucleation, which can be achieved only in cylindrical structure. It was observed that an increase of the crystallinity occurs, due to the two nucleation steps, i.e., heterogeneous and homogeneous nucleation, after an additional quenching step in liquid nitrogen after rapid cooling from the melt to room temperature, which can enhance the modulus and strain at break from 450 to approx. 900% in the study of Balsamo *et al.*¹⁴⁻¹⁵ They considered that the high ductility of these blends must be attributed to the crystallinity of the core in the irregular core-shell cylinders. However, cylindrical

systems may not be efficient to prevent the formation and growth of microcrazes, since the long-range ordering of the cylindrical structures is very sensitive to the processing.⁵ As reported by Van Casteren,³ after treating the solvent-cast and compression-molded PS-PB-PCL block copolymers in equal thermal treatment (two quenching steps in water and liquid nitrogen), a similar resistance against cavitation occurs in both samples. However, the solvent-cast sample shows a more brittle behavior than the compression-molded sample, due to the long range ordering of the cylindrical structure after solvent casting, in which the crazes can propagate in the PS domains along the oriented cylindrical axis.

One way to circumvent the processing dependency of the cylindrical structures, or stated otherwise the long-range order, is using a block copolymer where the matrix-compatible block has a high molar mass distribution, as reported by Kierkels.⁴ To accommodate the different molar mass blocks, the interfacial curvature of the cylindrical morphology will be maximized and many defects will be introduced,¹⁶ which avoid catastrophic growth of the microcracks developed in the matrix, while preserving the possibility of fractionated crystallization to precavitate the rubber particles. In addition, the broad molar mass distribution of the matrix block facilitates mixing with the PMMA homopolymer. However, these cylindrical structures are not preferable, since a large amount of block copolymer is required with a concomitant drop in the Young's modulus. Thus, if both homogeneous and heterogeneous nucleation could occur in a spherical morphology, it might be the excellent system, which can either induce the precavitation or stop the microcraze growth in all loading directions.

In a number of studies it was demonstrated that incorporating nanoparticles into a polymer matrix can influence the bulk behavior in a number of ways, a.o. reducing the viscosity and thermal degradation, increasing modulus or stiffness, and improved electrical performance.¹⁷⁻²³ These properties generally depend on the interaction between the surface of particles and the polymer, the dispersion and localization of the particles in the polymer domains (especially in polymer blends and block copolymers). As a result, the ability to control the positioning of the particles is important.

Compared to the poly(styrene)-*b*-poly(butadiene)-*b*-poly(methyl methacrylate) triblock copolymer used in Chapters 4 and 5, the poly(methyl methacrylate)-*b*-poly(butyl acrylate)-*b*-poly(ϵ -caprolactone) (MBC) triblock copolymer with the crystallizable PCL block is studied in blends with PMMA in this chapter. Since the silica nanoparticles selectively distribute in the PCL crystallizable block, it is interesting to study their effect on the thermal behavior and the final morphology of the blends. The copolymer with the end block PMMA as the major component, which has favorable interactions with the homopolymer matrix, is selected to prevent macrophase separation upon blending. Since the glass transition temperature of the matrix is higher than the crystallization temperature of the crystallizable PCL block, the matrix is already vitrified when the crystallization occurs inside the confined domains. The overall block copolymer morphology is, therefore, unaffected by this crystallization process.

6.2 Experimental

6.2.1 Materials

PMMA was provided by Arkema (France), with a number-averaged molar mass (M_n) of 42 kg/mol and a polydispersity index (PDI) of 2.1. Small amounts of ethyl acrylate (EA) are usually incorporated into PMMA to prevent unzipping of the polymer at elevated temperatures during processing. The PMMA used in this study contained 0.5 wt% EA. The PMMA-*b*-PBA-*b*-PCL triblock copolymer ($M_n = 87$ kg/mol) was prepared by Bertin and co-workers,^{24,25} i.e. $M_{54}B_{23}C_{10}$, where the subscripts represent the weight fraction of the respective blocks. This triblock copolymer contains 31 wt% BC diblock and was used without further purification. The B and C blocks have the same molar mass in the MBC triblock copolymer and BC diblock copolymer. Methyl ethyl ketone (MEK) was obtained from Sigma Aldrich and was used as received. Pre-made colloidal silica nanoparticles with a diameter of 10-15 nm, dispersed in MEK with approx. 30 wt% silica particles, was purchased from Nissan Chemical (USA) and a surface covered with methyl and hydroxyl groups. These silica nanoparticles will be referred to as MEK-ST. The silica nanoparticles were used without further surface modification.

6.2.2 Sample preparation

The polymers and MEK-ST nanoparticles were dissolved separately in MEK and the two solutions were mixed and solvent cast in a petri dish. The polymer concentration in the solution was 10 wt%. The solvent-cast films were put into fume-hood at room temperature for 2-3 days followed by a drying step at 60 and 80 °C under reduced pressure with a low nitrogen flow for 3 more days to ensure complete solvent removal. The final thickness of the samples was approx. 0.1 mm. For further equilibration, the dried films were annealed at 140 °C for 2 hrs under a nitrogen atmosphere. The samples were subsequently cooled to room temperature.

6.2.3 Characterization techniques

Atomic force microscopy (AFM)

The AFM investigations were performed by using a Smena P47H microscope (NT-MDT Ltd, Moscow, Russia). The AFM was operated in semi-contact mode under an air atmosphere using a silicon cantilever (NSG 11 NT-MDT), which was coated with a gold layer for a higher laser beam reflectivity. The applied resonance frequencies were 115-190 kHz.

Transmission electron microscopy (TEM)

Morphological investigations were performed by using a Tecnai 20 transmission electron microscopy (TEM), operated at 200 kV. Ultrathin sections (± 70 nm) were obtained at low temperature (-80°C) using a Reichert UltracutS/FCS ultramicrotome equipped with a diamond knife. The sections were subsequently vapor-stained for 10 min with a Ruthenium tetroxide (RuO₄) solution prepared according to Montezinos *et al.*,²⁶ which predominantly reacts with PCL. Different to the other chapters, the bright phase corresponds to the PMMA phase, and the dark phase corresponds to PCL domains.

Thermogravimetric analysis (TGA)

A Q500 TGA (TA Instruments) was used for the quantitative determination of the silica content in the nanocomposites. Samples were heated under a pressed air atmosphere at 10 °C/min from 30 to 800 °C and held at 800 °C for 15 min. The residue was assumed to be only composed of silica.

Differential scanning calorimetry (DSC)

DSC was performed by a Q1000 DSC (TA Instruments). The DSC cell was purged with a nitrogen flow of 50 mL/min. The temperature was calibrated using the onset of the melting peak of indium. Each sample with sample mass of 9-11 mg was analyzed in standard DSC Tzero aluminum pans. For modulated temperature DSC (MDSC) measurement, the samples were heated from -90-180 °C at 3 °C/min, with a modulation period of 60 s and an amplitude of 0.47 °C. The combination of the heating rate and period was always chosen, so that there were at least four modulation cycles during the transition of interest.

6.3 Results and discussion

6.3.1 Morphology of the pure triblock copolymer $M_{54}B_{23}C_{10}$ and blends with PMMA

Since the solvent-cast samples have a higher mobility and more time to phase separate during solvent evaporation, they can form a better ordered morphology than obtained from compression-molded samples.⁴ Hence, the samples of triblock copolymers and the blends with PMMA in this chapter were prepared by solvent casting.

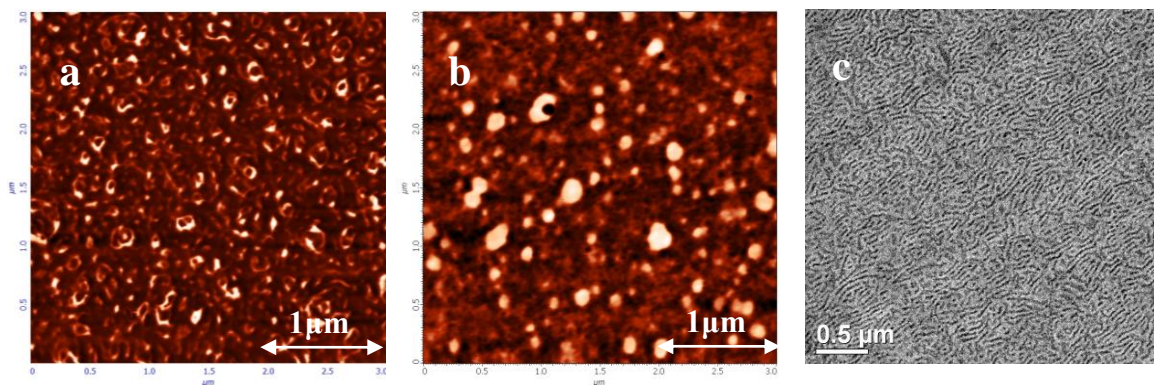


Figure 6.1: AFM phase angle images of (a) $M_{54}B_{23}C_{10}$ and (b) $PMMA/M_{54}B_{23}C_{10}$ 50/50 blend, annealed at 140 °C for 2 hrs. The dark regions correspond to lower phase angles or higher stiffness (PMMA or PCL domains). Light regions correspond to the PBA domains. (c) TEM image of the $M_{64}B_{23}C_{10}$ block copolymer investigated by Kierkels.⁴

For an asymmetric ABC triblock copolymer, if one of the end blocks is the major component (for example A), block A forms the matrix and the sum of the volume ratios of component B and C will define whether a lamellar, cylindrical or spherical morphology is

formed.²⁷ In the study of Kierkels,⁴ the synthesised triblock copolymers MBC had different morphologies, depending on the ratio of the three components. In the present study, the AFM images of the solvent-cast triblock copolymer $M_{54}B_{23}C_{10}$ and the 50/50 blend with PMMA are shown in Figure 6.1a-b. Figure 6.1c show the lamellar structure of the solvent-cast $M_{64}B_{23}C_{10}$ triblock copolymer, as prepared by Kierkels. Compared to the $M_{64}B_{23}C_{10}$, the $M_{54}B_{23}C_{10}$ triblock copolymer shows a combined structure with spherical and cylindrical domains, with PMMA as the matrix. Taking a closer look, small core-shell structures of approx. 100 nm can be distinguished dispersed in the matrix. Blending $M_{54}B_{23}C_{10}$ with PMMA results in spherical morphology of the triblock copolymer dispersed in the PMMA matrix, which is same as the blend of $M_{64}B_{23}C_{10}$ and PMMA, with a size of approx. 150 nm.⁴ The well-organized structure is related to the ‘wet-brush’ condition with a high compatibility between the PMMA matrix, which has a lower molar mass of 42 kg/mol and relatively broad molar mass distribution (PDI = 2.1), and the high molar mass PMMA block ($M_n = 54$ kg/mol).

6.3.2 The effect of silica nanoparticles on the morphology

After adding the silica particles, the silica nanoparticles are found to be preferentially dispersed in the middle of light spherical region shown in a higher magnification image (Figure 6.2c), which corresponds to the soft domains consisting of the PBA-PCL part. Since the PCL and PBA blocks show a core-shell structure in Figure 6.1a, the silica particles are considered to be dispersed in the PCL cores is in the middle of the PBA shell. A cylindrical structure can be observed as well together with the spherical structure. Compared to the pure PMMA/MBC 50/50 blend, the silica-filled systems show higher content of cylindrical structures due to the particle-induced separation of the BC diblock copolymer, similar to observations in Chapter 4 on the SBM/PMMA systems. Upon increasing the silica content to 2 wt%, the MBC-rich phases are less observed on the surface of the solvent-cast sample. The details will be discussed in the bulk sample of next section.

Further, the selective localization of silica particles is consistent with the stronger interaction between the hydroxyl groups of silica nanoparticles with the carbonyl groups of the PCL in comparison to the carbonyl groups of the PMMA.

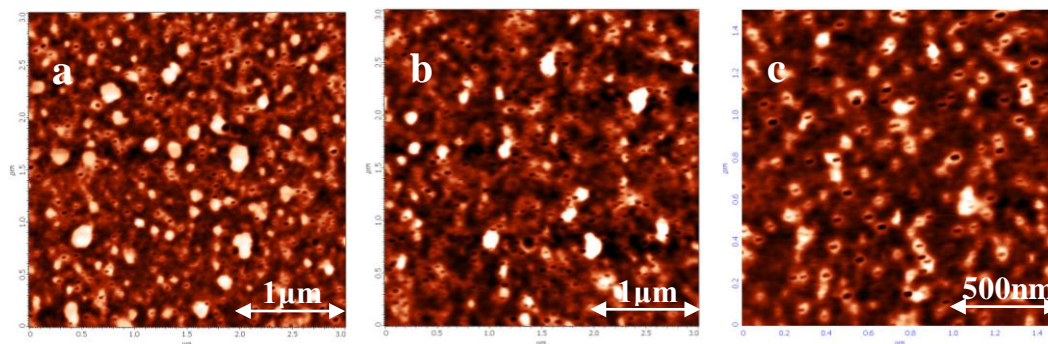


Figure 6.2: AFM phase angle images of PMMA/M₅₄B₂₃C₁₀ 50/50 blends with (a) 1 wt% and (b-c) 2 wt% MEK-ST silica at various magnifications.

6.3.3 Thermal behavior of the triblock copolymers and its blends with PMMA

The incorporation of the nanoparticles into the polymers has generated a lot of attention, especially in relation to the mobility of polymer chains.^{28,29} Several effects have been reported in relation to the glass-transition temperature and the crystallization behavior, which can be changed depending on the interaction between the surface of particles and polymer. The effect of silica nanoparticles on the glass transition and the crystallization behavior of self-organized triblock copolymers will be discussed in this section with emphasis on the semi-crystalline PCL-block.

6.3.3.1 Effect of silica nanoparticles on the glass transition temperatures of the different blocks

The samples for thermal analysis by MDSC of the pure and silica-filled triblock copolymer or the PMMA/M₅₄B₂₃C₁₀ blends were all prepared by solvent casting. The samples were first heated to 180 °C to ensure complete melting and to erase possible melt memory effects which may influence the nucleation process. Figures 6.3 and 6.4 show the heating and cooling curves of the MDSC run and the results are summarized in Tables 6.1-6.2. The benefits of the MDSC is its ability to separate reversible (glass transition) and non-reversible (crystallization) processes by measuring the reverse heat flow and non-reverse heat flow in

the total heat flow during a transition.³⁰⁻³¹ This ability is helpful to the samples which has similar glass transition temperature and crystallization temperature like the MBC block copolymer.

For triblock copolymer $M_{54}B_{23}C_{10}$, the reversing heat flow of the heating run is shown in Figure 6.3a. Since the glass transition temperatures (T_g) of PCL and PBA is close to each other, the derivative heat flow curve (Figure 6.3a'), dW/dT , is used which is very sensitive to the change of glass transition temperatures. The T_g 's of them can be observed at approx. -66 °C and -52 °C, respectively. The glass transition temperature of the PMMA block is 118 °C.

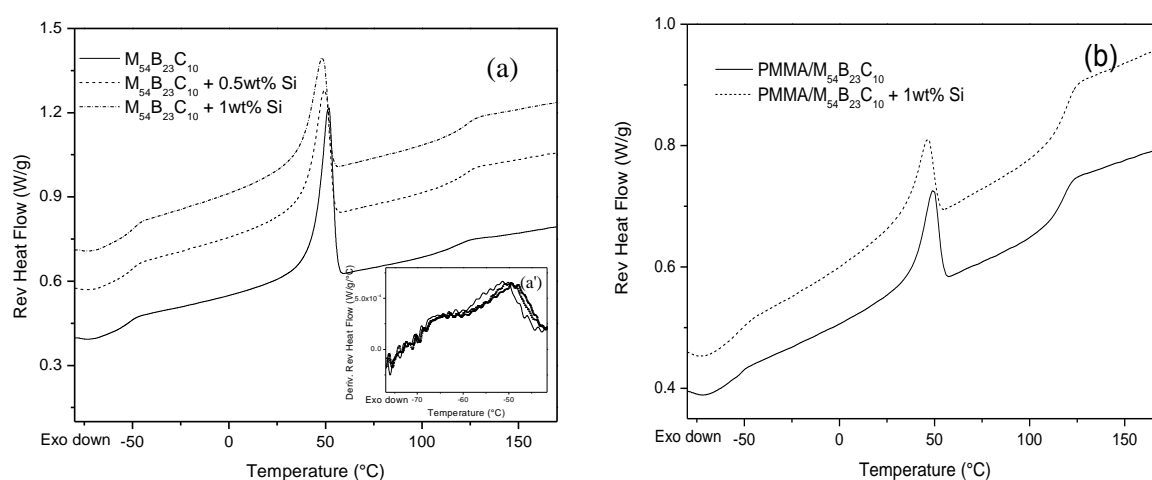


Figure 6.3: Reversing heat flow of MDSC heating run of (a) triblock copolymers $M_{54}B_{23}C_{10}$ and (b) PMMA/ $M_{54}B_{23}C_{10}$ 50/50 blends.

In Table 6.1, the results show that there are enhancements of T_g 's of all the three blocks PCL, PBA and PMMA after the addition of the silica nanoparticles. The range of the enhancement is between 2-5 °C. Based on the selective localization of silica particles in PCL core shown in the AFM images, the enhanced T_g of the PCL block is related to the existence of the strong hydrogen bonding between the PCL and silica surface which reduces the cooperative segmental mobility of the polymer chain. The enhancement of the T_g 's of the PBA and PMMA is related to a better microphase separation between the PCL and the PBA/PMMA. Although the T_g of PCL can not be detected in the PMMA/ $M_{54}B_{23}C_{10}$ 50/50 blend due to the low amorphous content of PCL in the blend, the same influence of the silica on the other two T_g 's can be found in the silica-filled PMMA/ $M_{54}B_{23}C_{10}$ 50/50 blend.

Table 6.1: Overview of the thermal properties of the $M_{54}B_{23}C_{10}$ triblock copolymer and the blend with PMMA.

Block copolymer and its blend	T _g of PCL (°C)	T _g of PBA (°C)	T _g of PMMA (°C)
$M_{54}B_{23}C_{10}$	-66	-52	118
$M_{54}B_{23}C_{10}$ +Si 0.5 wt%	-64	-50	123
$M_{54}B_{23}C_{10}$ +Si 1 wt%	-64	-49	123
PMMA/ $M_{54}B_{23}C_{10}$ 50/50	-	-55	118
PMMA/ $M_{54}B_{23}C_{10}$ 50/50 + Si 1 wt%	-	-52	120

6.3.3.2 Effect of silica nanoparticles on the fractionated crystallization of the PCL block and the morphology of the triblock copolymer

As mentioned before, for amorphous triblock copolymers ABC, the end block A (the major component) forms the matrix, while the sum of the B and C component will define whether a cylindrical or spherical morphology. However, if one or more of the blocks are able to crystallize, a much more complex phase behavior can be expected because of the interplay of crystallization and microphase separation.⁵ In the present system, since the glass transition temperature of the glassy matrix PMMA is higher than the crystallization temperature of the crystalline PCL block, the matrix of the block copolymer MBC is already vitrified when the crystallization occurs inside the confined domains. Since the segregation strength is strong in the MBC triblock copolymer, no break-out will occur during crystallization and the overall block copolymer morphology is unaffected by the crystallization. Further, for this kind of self-organizing block copolymers which contain a semi-crystalline block, the confined crystallization occurring in the microphase-separated structure strongly depends on the shape and size of the semi-crystalline domain. This so-called fractionated crystallization was observed in triblock copolymer PMMA-PBA-PCL by Kierkels⁴ and PS-PB-PCL by Balsamo *et al.*⁵. As reported by Kierkels, the spherical, cylindrical and lamellar morphology can be obtained in the MBC triblock copolymer, by

varying the ratio of the three components. After mixing the triblock copolymer with the homopolymer PMMA, either spherical or the cylindrical structure can be obtained as the dispersed phase. As reported by Balsamo and Van Casteren, the best properties are expected in the system with the combined heterogeneous and homogeneous nucleation, which can be only obtained in cylindrical dispersed phase. However, the cylindrical structure is not the most preferred impact modifier, since the amount of the soft phase lowers the Young's modulus substantially, while long range ordering in the cylindrical structure due to processing can lead to growth of crazes causing a brittle fracture. The embrittlement occurred also in the PS-PB-PCL triblock copolymer reported by Balsamo⁵ and Van Casteren³.

In this section, the nanoparticles will be introduced in the nanosized spherical structure to improve the properties in all loading directions, by introducing heterogeneous nucleation sites in the spherical PCL-phase, which normally crystallizes via homogeneous nucleation.

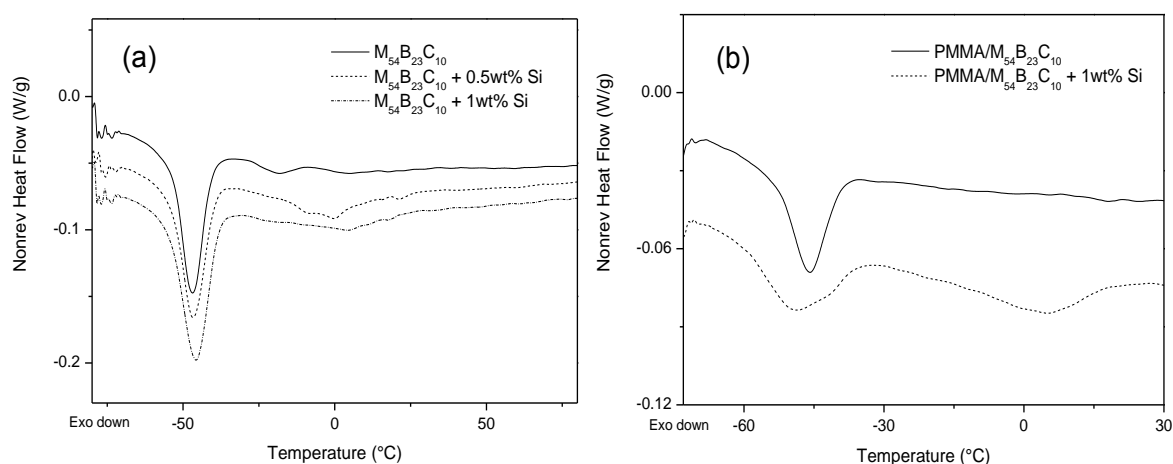


Figure 6.4: Non-reversing heat flow of MDSC cooling run of (a) triblock copolymers $M_{54}B_{23}C_{10}$ and (b) $\text{PMMA}/M_{54}B_{23}C_{10}$ 50/50 blends.

In Figure 6.4a, $M_{54}B_{23}C_{10}$ shows two crystallization exotherms, around -47 °C and -18 °C (temperature at the maximum of the crystallization exotherm). The 0.5 wt% and 1 wt% silica-filled $M_{54}B_{23}C_{10}$ also exhibits two crystallization exotherms, -47 , 0 °C and -46 , 5 °C, respectively. These crystallization temperatures, the lower related to homogeneous and the higher temperature to heterogeneous nucleation, vary strongly with the domain size of the crystallizable block. In bulk crystallizable polymers, relatively many impurities or nucleation sites are present for heterogeneous nucleation and, consequently, crystallization will be

initiated at higher temperatures. Moreover, if the crystallizable block in the copolymer is the minority component and forms the dispersed phase whose average size is so small that the number of particles is much greater than the number of active heterogeneities, crystallization takes place via homogeneous nucleation and is detected as a low-temperature exothermic event. The existence of homogeneous and heterogeneous nucleation is termed “fractionated crystallization”.⁵

In brief, the type of nucleation in the fractionated crystallization of MBC is strongly influenced by the domain size of the semi-crystalline phase PCL and is related to the morphology, which is schematically visualized in Figure 6.5. When the domain size is relatively large, e.g. for block copolymers that are organized in a lamellar (L) morphology, heterogeneous nucleation occurs and only the high-temperature exotherm can be observed. On the other hand, when small spherical (S) semi-crystalline microdomains are present, then the homogeneous nucleation is the only type of crystallization possible. A cylindrical (C) microstructure can, dependent on the exact morphology, show either one type of nucleation, or a combination of both.

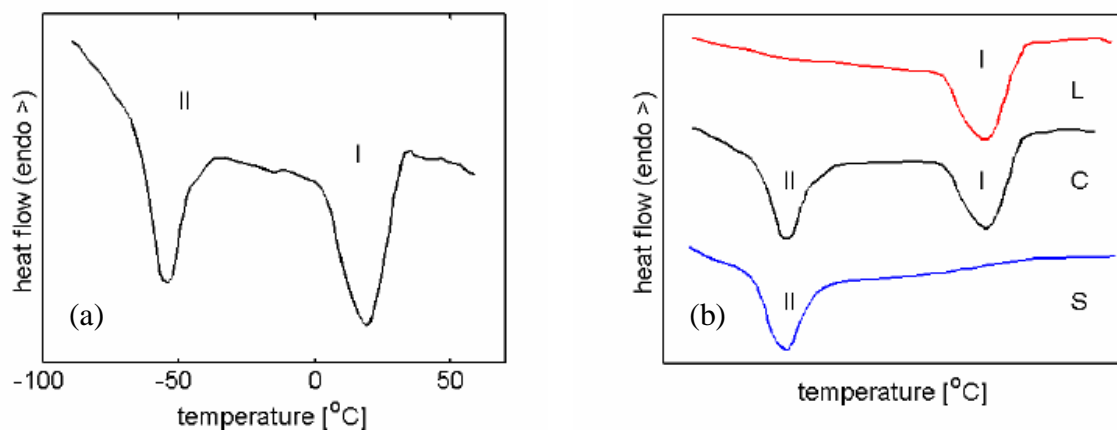


Figure 6.5: (a) DSC cooling scan of PS-PB-PCL showing both heterogeneous (I) and homogeneous (II) nucleation. Reproduced from Balsamo et al.⁵ (b) Schematic cooling scan representing the types of fractionated crystallization that can occur. Heterogeneous nucleation is represented by (I), whereas homogeneous nucleation is represented by (II) for lamellar (L), cylindrical (C), and spherical (S) morphologies.

In the pure triblock copolymer $M_{54}B_{23}C_{10}$, the homogeneous nucleation can be observed at approx. -46 °C and is the dominating type of nucleation. This means the spherical structure

as the major type of the microstructure exists together with the cylindrical structure, which correlated well to the AFM results presented in Figure 6.1. After adding silica nanoparticles, the occurrence of homogeneous nucleation seems not to change, while the heterogeneous nucleation of PCL occurs at higher temperatures. This is due to the fact that the surface of the nanoparticles act as nucleating sites inducing the heterogeneous nucleation to occur easier which appears as a crystallization exotherm at a temperature closer to the crystallization temperature of the bulk homopolymer at 25 °C, but this nucleation effect only happens in the large semi-crystalline domains, i.e. the heterogeneous nucleation is affected. The homogeneous nucleation from the nanoscale confinement is not affected by the silica particles. Furthermore, the melting temperature (T_m) of the PCL block in the nanoparticles-filled system is reduced by approx. 4 °C. The presence of the silica nanoparticles in the semi-crystalline PCL block induces more defects of the PCL crystal, which arise from the reduction of the segmental mobility of the polymer chain due to the strong interaction between the polymer and the silica surface, thereby reducing the melting temperature.

Table 6.2: Crystallization data of the $M_{54}B_{23}C_{10}$ triblock copolymer and the blend with PMMA.

PCL block	$M_{54}B_{23}C_{10}$	$M_{54}B_{23}C_{10}$ +Si 0.5 wt%	$M_{54}B_{23}C_{10}$ +Si 1 wt%	PMMA/ $M_{54}B_{23}C_{10}$ 50/50	PMMA/ $M_{54}B_{23}C_{10}$ 50/50 + Si 1 wt%
T_c (°C)	-47/-18	-47/0	-46/5	-46	-49/5
ΔH_c (J/g)	2.67/0.68	2.01/1.31	2.66/0.89	1.28	0.88/0.79
T_m (°C)	52	49.5	48	49	46

In Figure 6.4b, the MDSC results of the PMMA/ $M_{54}B_{23}C_{10}$ 50/50 blends show a change of the nucleation type after adding the silica particles. The pure PMMA/ $M_{54}B_{23}C_{10}$ 50/50 blend only shows a single exotherm related to homogeneous nucleation at -46 °C. However, the 1 wt% silica-filled 50/50 blend has two crystallization exotherms at around -49 °C and 5 °C (temperature at the maximum of the crystallization exotherm). The transition of the

nucleation type in the PMMA/M₅₄B₂₃C₁₀ blend could imply that the microstructure has changed by the addition of silica particles. Homogeneous nucleation is the only type of crystallization in the pure PMMA/M₅₄B₂₃C₁₀ 50/50 blend, which assumes that the spherical structure formed by the triblock copolymer is the only one dispersed in the PMMA matrix. However, the combination of heterogeneous and homogeneous nucleation in the silica-filled PMMA/M₅₄B₂₃C₁₀ 50/50 blend, which is usually a signature of a cylindrical morphology, could imply that the cylindrical structures is present together with the spherical structures in the PMMA matrix. Further, it might also be related to that the localization of silica particles in the PCL domains which will induce the occurrence of the heterogeneous nucleation together with the homogeneous nucleation as well in spherical domains. The morphology is confirmed by the TEM images shown in Figure 6.6.

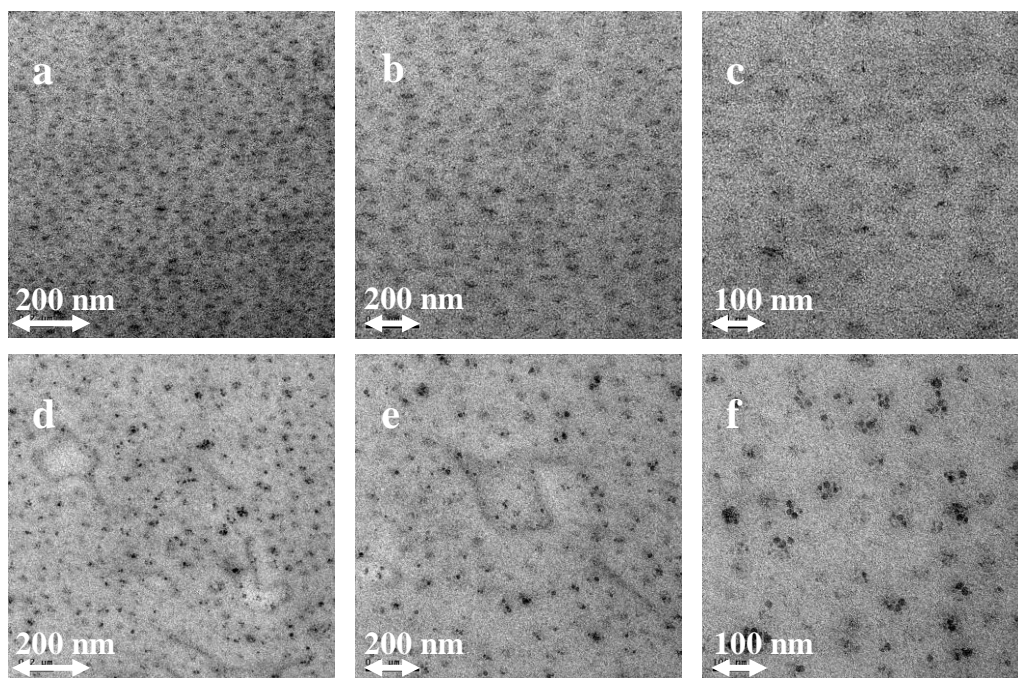


Figure 6.6: TEM images of (a-c) solvent-cast pure PMMA/M₅₄B₂₃C₁₀ 50/50 at various magnifications, (d-f) solvent-cast PMMA/M₅₄B₂₃C₁₀ 50/50 with 1 wt% MEK-ST at various magnifications. The bright phase corresponds to the PMMA matrix, and the dark phase corresponds to PCL domains, since Ruthenium tetroxide preferentially reacts with PCL. In figures d-f, the electron density of silica is much higher than that of polymer.

Figures 6.6a-c show the morphology of the pure PMMA/M₅₄B₂₃C₁₀ 50/50 blend with a pronounced spherical ordering, although the electron density of the PBA block is similar as

that of the PMMA and can not be distinguished here. At high magnifications, the size of diameter proves to be approx. 30 nm, caused by the high compatibility of the PMMA matrix with the high molar mass PMMA block. Adding silica nanoparticles to the blend results in a combination of spherical and cylindrical microstructures, as shown in Figures 6.6d-f. The silica nanoparticles show a good dispersion in the PCL core. The cylindrical structures arise from the presence of diblock copolymer BC impurities. The addition of silica nanoparticles induces separation of the diblock copolymer from the triblock copolymer, which results in the formation of the independent cylindrical microstructures, similar to observations in AFM results (Figure 6.2). The spherical morphology as the dominant morphology combined with some cylindrical structures might be able to dramatically improve the stress-strain behavior compared to the single spherical or single cylindrical morphology and make the system less sensitive to processing-induced long-range ordering and thus more efficient to stop craze growth.⁵

Since the morphology of the block copolymer determines the microscopic mode of deformation and hence the overall mechanical performance, the morphology transition induced by the silica nanoparticles can be used to optimize the toughness improvement of the amorphous glassy polymer/block copolymer blend.

6.4 Conclusions

Triblock copolymer PMMA-PBA-PCL and blends with homopolymer PMMA were mixed with silica nanoparticles by solvent casting. The effect of silica particles on the thermal behavior and final morphologies was discussed. Due to the high compatibility between the long PMMA block of the block copolymer and the homopolymer PMMA matrix, the blend is in the wet-brush regime, where the PMMA block of the MBC is ‘solubilized’ by the PMMA matrix. The blend shows a well-ordered core-shell spherical morphology dispersed in the PMMA matrix. The silica nanoparticles have a preference to be dispersed in the PCL domains, which arises from the strong hydrogen bonding between the hydroxyl groups of silica nanoparticles with the carbonyl groups of the PCL.

The effect of silica particles on the glass transition temperature or melting temperature of the PCL/PBA/PMMA blocks was discussed. The reduction of the segmental mobility of the PCL chain comes from the strong interaction between the hydroxyl groups of silica nanoparticles with the carbonyl groups of the PCL, which induces an enhancement of the T_g .

The pure block copolymer $M_{54}B_{23}C_{10}$ shows both homogeneous and heterogeneous nucleation, whereas the PMMA/ $M_{54}B_{23}C_{10}$ 50/50 blend only shows the homogeneous nucleation. In the wet-brush blend PMMA/ $M_{54}B_{23}C_{10}$ 50/50, the copolymer containing a very short PCL block shows only homogeneous nucleation, possibly due to the fact that the PCL domains are even smaller than those in the pure $M_{54}B_{23}C_{10}$ and, as a consequence, the number of nucleation sites is much smaller than the number of PCL domains, which only allows for homogeneous nucleation. After adding the silica nanoparticles, the morphology of the PMMA/ $M_{54}B_{23}C_{10}$ 50/50 blend shows a transition from spherical to spherical/cylindrical structure, which arises from the separation of the triblock copolymer MBC and the block copolymer BC, together with the localization of the silica particles in the spherical PCL domains. These behaviors induce the existence of both homogeneous and heterogeneous nucleation.

The morphology of the triblock copolymer, influenced by the silica nanoparticles, can develop different nucleation behaviors of the crystalline block, which influence the internal stresses introduced during crystallization upon cooling from the melt.

6.5 References

- ¹ Matsuo, M., Ueno, T., Horino, H., Chujo, S., Asai, H., *Polymer*, **1968**, 9, 425-436.
- ² Brinkmann, S., Stadler, R., Thomas, E. L., *Macromolecules*, **1998**, 31, 6566-6572.
- ³ Van Casteren, I. A., *Control of microstructures to induce ductility in brittle amorphous polymers*, Ph.D Thesis, TU/e, Eindhoven, the Netherlands, **2003**.
- ⁴ Kierkels, J. T. A., *Tailoring the mechanical properties of amorphous polymers*, Ph.D. Thesis, TU/e, Eindhoven, the Netherlands, **2006**.
- ⁵ Balsamo, V., Von Gydenfeldt, F., Stadler, R., *Macromolecules*, **1999**, 32, 1226-1232.
- ⁶ Bucknall, C. B., Karpodinis, A., Zhang, X. C., *J. Mater. Sci.*, **1994**, 29, 3377-3383.
- ⁷ Bucknall, C. B., Ayre, D. S., Dijkstra, D. J., *Polymer*, **2000**, 41, 5937-5947.
- ⁸ Mueller, A. J., Balsamo, V., Arnal, M. L., Jakob, T., Schmalz, H., Abetz, V., *Macromolecules*, **2002**, 35, 3048-3058.
- ⁹ Guo, Q., Thomann, R., Gronski, W., Staneva, R., Ivanova, R., Stuehn, B., *Macromolecules*, **2003**, 17, 3635-3645.
- ¹⁰ Rangarajan, P., Register, R. A., Adamson, D. H., Fetters, L. J., Bras, W., Naylor, S., Ryan, A. J., *Macromolecules*, **1995**, 28, 1422-1428.

- ¹¹ Rangarajan, P., Register, R. A., Fetters, L. J., *Macromolecules*, **1993**, 26, 4640–4645.
- ¹² Bailey, T. S., Pham, H. D., Bates, F. S., *Macromolecules*, **2001**, 34, 6994–7008.
- ¹³ Hamley, I. W., *Adv. Polym. Sci.*, **1999**, 148, 113–137.
- ¹⁴ Balsamo, V., Von Gyldenfeldt, F., Stadler, R., *Macromol. Chem. Phys.*, **1996**, 197, 3317–3341.
- ¹⁵ Balsamo, V., Urdaneta, N., Perez, L., Carrizales, P., Abetz, V., Muller, A. J., *Eur. Pol. J.*, **2004**, 40, 1033–1049.
- ¹⁶ Corte, L., Yamauchi, K., Court, F., Cloître, M., Hashimoto, T., Leibler, L., *Macromolecules*, **2003**, 36, 7695–7706.
- ¹⁷ Jain, S., Goossens, J. G. P., Peters, G. W. M., Van Duin, M., Lemstra, P. J., *Soft Matter*, **2008**, 4, 1848–1854.
- ¹⁸ Rittigstein, P., Torkelson, J. M., *J. Pol. Sci. Part B: Pol. Phys.*, **2006**, 44, 2935–2943.
- ¹⁹ Liu, J., Tanaka, T., Sivula, K., Alivisatos, A. P., Frechet, J. M. J., *J. Am. Chem. Soc.*, **2004**, 126, 6550–6551.
- ²⁰ Paul, D. R., Robeson, L. M., *Polymer*, **2008**, 49, 3187–3204.
- ²¹ Ajayan, P. M., Schadler, L. S., Braun, P. V., *Nanocomposite science and technology*, Wiley-VCH, **2003**.
- ²² Fornes, T. D., Paul, D. R., *Polymer*, **2003**, 44, 4993–5013.
- ²³ Fornes, T. D., Yoon, P. J., Keskkula, H., Paul, D. R., *Polymer*, **2001**, 42, 9929–9940.
- ²⁴ Vinas, J., Chagneux, N., Gimes, D., Trimaille, T., Favier, A., Bertin, D., *Polymer*, **2008**, 49, 3639–3647.
- ²⁵ Gimes, D., Vinas, J., Chagneux, N., Lefay, C., Phan, T. N. T., Trimaille, T., Dufils, P.-E., Guillaneuf, Y., Carrot, G., Boue, F., Bertin, D., *ACS Symp. Ser.*, **2009**, 1024, 245–262.
- ²⁶ Montezinos, D., Wells, B. G., Burns, J. L., *J. Polym. Sci., Polym. Lett. Ed.*, **1985**, 23, 421–425.
- ²⁷ Breiner, U., Abetz, V., Krappe, U., Stadler, R., *Macromol. Chem. Phys.*, **1997**, 198, 1051–1083.
- ²⁸ Bansal, A., Yang, H., Li, C., Cho, K., Benicewicz, B. C., Kumar, S. K., Schadler, L. S., *Nat. Mater.*, **2005**, 4, 693–698.
- ²⁹ Balazs, A. C., Emrick, T., Russell, T. P., *Science*, **2006**, 314, 1107–1110.
- ³⁰ Gill, P. S., Sauerbrunn, S. R., Reading, M., *J. Therm. Anal.*, **1993**, 40, 931–939.
- ³¹ Verdonck, E., Schaap, K., Thomas, L. C., *Int. J. Pharm. Sci.*, **1999**, 192, 3–20.

Appendix one

The effect of silica nanoparticles on the deformation behavior of PS/SBS blends

The linear poly(styrene)-b-poly(butadiene)-b-poly(styrene) (SBS) triblock copolymers, typically based on styrene concentrations varying from 10-60%, represent a typical thermoplastic elastomer (TPE), which comprise approximately 50% of the TPE industry. The commercial rubbery/glassy block copolymers SBS, of which the dispersed rigid poly(styrene) (PS) domains act as physical crosslinks for the poly(butadiene) (PB), can be conventionally processed including extrusion, injection molding and blow molding. In most cases of the styrene-based copolymer systems, the microphase-separated morphologies in the nanometer scale are too small to initiate crazing or cavitation in the rubbery phase.¹⁻² In Chapter 5, the selective distribution of silica particles in the core-shell rubbery phase shows that there is a chance to enhance the capability of the pre-cavitation of the rubbery phase, by introducing extra internal stress from the solid silica particles. In this appendix, this idea is further studied in the PS/SBS blend. The silica nanoparticles were selectively distributed in the PB rubbery phase and the effect of the nanoparticles on the microscopic deformation mechanisms were studied.

A.1 The effect of silica nanoparticles on the morphology of PS/SBS blends

Since the morphology of block copolymer is influenced by the preparation methods, the original microstructure of the homopolymer/block copolymer blend is necessary to be investigated before the further deformation study. Two mixing methods were applied to study the influence on the morphology, i.e. solvent casting and melt mixing.

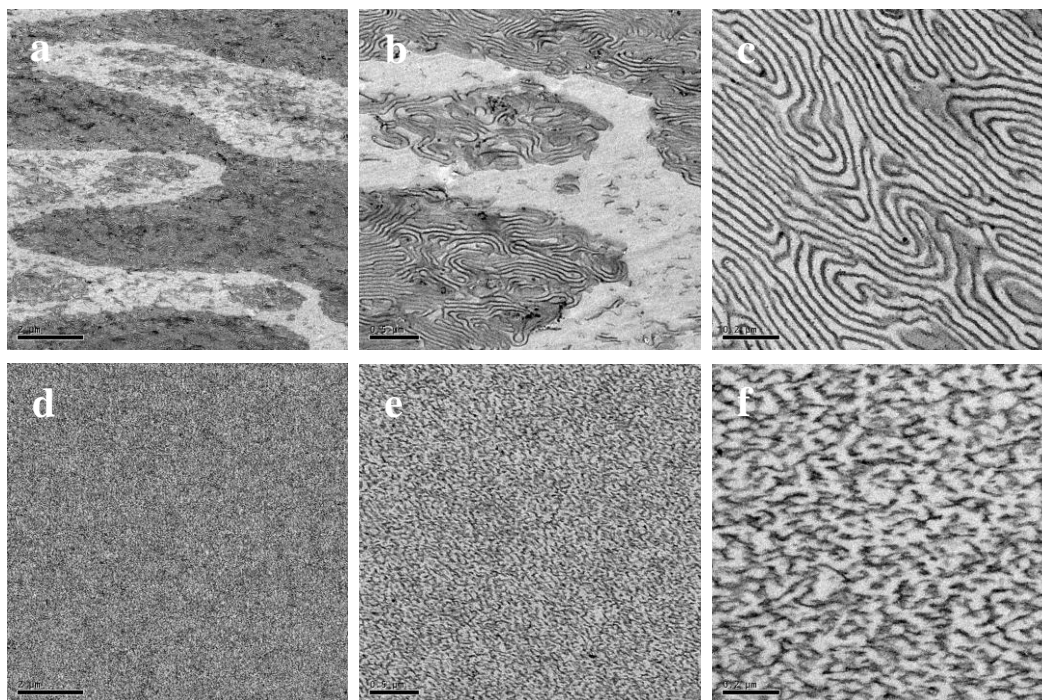


Figure A.1: TEM images of neat PS/SBS 50/50 blends: (a-c) solvent-cast sample and (d-f) melt-mixed sample at various magnifications.

For the blend of homopolymer (A)/block copolymer (ABA), the macrophase separation occurs in the ‘dry-brush’ condition when the homopolymer molar mass exceeds the molar mass of the soluble block of the block copolymer, which is expected in the PS/SBS 50/50 blend. For the solvent-cast method, Figures A.1a-b show macrophase separation in the solvent-cast PS/SBS blend, in which the grey phase corresponds to PS domains and the dark phase corresponds to the PB domains. In this study, the SBS triblock copolymer has a composition of 75 wt% styrene and 25 wt% poly(butadiene) (PB) and a total molar mass of 91 kg/mol (PDI=1.72). The homopolymer PS has a M_n of 79.3 kg/mol and a broad molar mass distribution of 3.51, therefore, part of the homopolymer PS have a molar mass which is higher than that of the PS block of the SBS. During the solvent casting process the PS is encapsulated but upon additional annealing, the PS with higher molar mass separated from the SBS and that of the lower molar mass dissolved in the PS block of the SBS triblock copolymer, which will result in an increase in d-spacing as reported by Van Casteren.³ Figure

A.1c shows a lamellar structure with long range order in the SBS-rich domain, which is in the thermodynamically equilibrium state.

For the melt-mixing method, a homogeneous dispersion of the SBS triblock copolymer in the PS matrix without large scale macrophase separation can be observed in Figure A.1d, which is related to the high melt viscosity and high shear stresses during melt mixing. The long range order of the SBS-rich domain via solvent-cast method is replaced by the randomly non-equilibrium multigrain lamellar morphology dispersed in the PS matrix. A complete random orientation of the lamellae is observed.

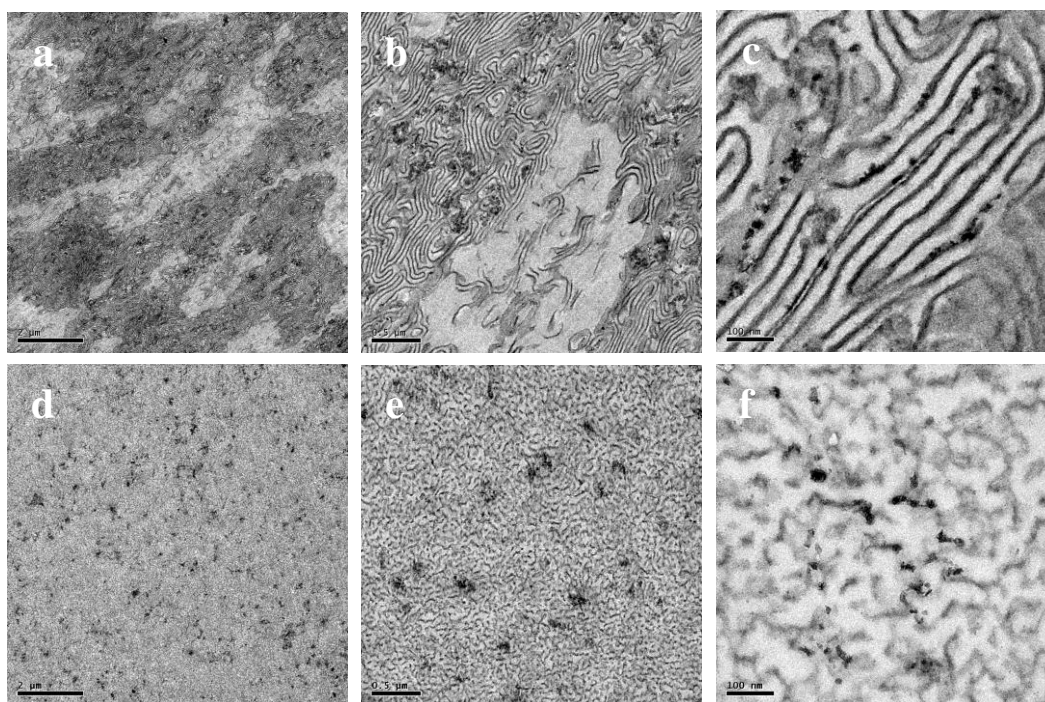


Figure A.2: TEM images of 1 wt% Si-R805 silica-filled PS/SBS 50/50 blends: (a-c) solvent-cast sample and (d-f) melt-mixed sample at various magnifications.

A hydrophobic nanosilica, Aerosil R805, with a diameter of 12 nm and surface treated with octylsilane, was used in this study and will be referred to as Si-R805. Upon adding the Si-R805 in the PS/SBS blends, the silica particles are found to have a preference to be dispersed in PB phase (dark), independent on the preparation methods, seen in Figures A.2c and f. Although single and multiple silica particles can be found well dispersed in the PB phase, the dispersion is not homogeneous and silica aggregates can be observed with size of approx. 100-200 nm in Figures A.2 b and e. The size of the aggregates is much smaller in the sample prepared via melt mixing, because of the precipitation of polymer/silica from solution before the extrusion and high shear force during extrusion. Further, the scale of the

macrophase separation is not influenced by the silica particles, which is shown Figures A.2a and d.

A.2 The effect of silica nanoparticles on the deformation behavior of PS/SBS blends

Since the macroscopic and microscopic deformation of the block copolymer is strongly influenced by the nanosized morphology and the degree of orientation, a homogeneous microstructure without orientation, like the sample prepared via melt-mixing, is chosen to study the effect of the silica particles on the deformation behavior of the PS/SBS system.

Table A.1 Yield stress and E-modulus of PS/SBS blends

	Yield stress (MPa)	E-modulus (MPa)
Neat PS/SBS 50/50	38.5	864
1 wt% Si-R805 silica-filled PS/SBS 50/50	36.0	1009

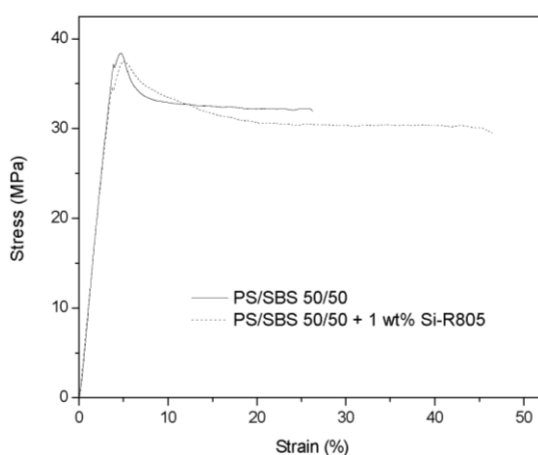


Figure A.3: Stress-strain behavior of neat and 1 wt% Si-R805 silica-filled PS/SBS 50/50 blends.

The stress-strain behavior of the neat and silica-filled PS/SBS 50/50 blends is depicted in Figure A.3. The yield stress and E-modulus is given in Table A.1. Upon deformation, stress whitening was observed for the both systems most probably due to the formation of voids or crazes. Both samples show a considerable amount of strain softening without strain hardening. Compared to the neat system, the elastic modulus and the maximum strain at break is higher in the silica-filled system. Usually, the tensile modulus can be reinforced with the organic nanoparticles, whereas the tensile elongation could be decreased.⁴⁻⁵ Thus, the enhanced

elongation behavior of the silica-filled system might be related to the different deformation mechanism. To obtain information about the microscopic mode of deformation of these systems, a TEM investigation was performed.

As shown by TEM, the long-range order is drastically reduced and changed to non-oriented multigrain lamellar structure when the triblock copolymer SBS is melt-mixed with PS instead of solvent casting from chloroform. Upon deformation, crack-like structures can be observed in the neat PS/SBS system, seen in Figures A.4a-c. In Figure A.4c, compared to the non-tensile sample, the PB domain (dark) is obviously stretched with a little orientation parallel to the tensile direction, showing a disordered multigrain lamellar and rod structure. It is evident that the crazes cannot propagate over a long distance along the grain boundaries of the dispersed rubber phase. This is related to the deformation study of the neat SBS by Van Casteren,³ which shows that the propagating of the cracks (perpendicular to the tensile direction) is successfully terminated by the SBS rich phase with stacked lamellar morphology in the compression-molded sample. Furthermore, the PS/SBS blend will mainly show craze formation due to the reduction of the rubber content in blend by adding the homopolymer.

However, no obvious formation of the crazes and cavitations can be found in the silica-filled PS/SBS system, seen in Figure A.4d. Only small voids can be observed along with the tensile direction in the matrix, which is in the PB domain and only occurred around the silica aggregates. It can be shown much more clear in the non-stained sample (Figure A.4f).

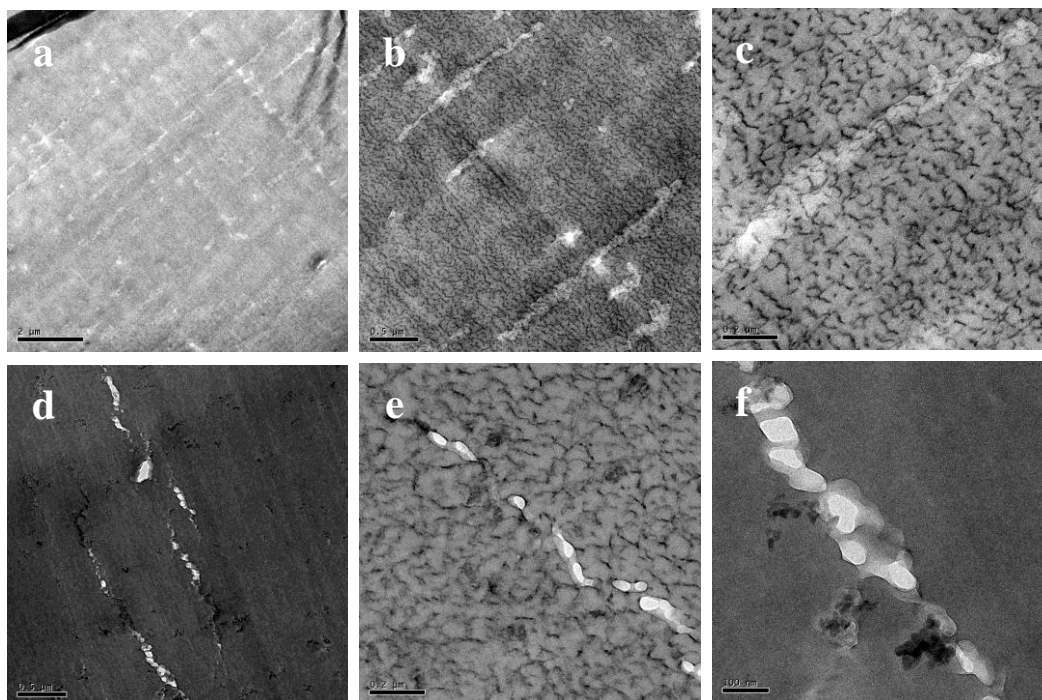


Figure A.4: TEM images of the deformed PS/SBS 50/50 blends via melt-mixing: (a-c) neat blend and (d-f) 1 wt% Si-R805 silica-filled blend at various magnifications.

Compared to the PS/SBM system, it is evident that the size of the rubbery phase in PS/SBS is much smaller with a thickness of approx. 10 nm, of which the capability of cavitation is much less. Further, the silica particles, especially the aggregates of the silica, seem to be able to induce debonding between the particles and the rubber phase, which does not occur in the PS/SBM system. It might be related to the interfacial adhesion between the silica particles and polymer. In the MEK-ST silica-filled PS/SBM, the silica particles are homogeneously dispersed as single particle in the PMMA core with a rubber shell, showing that there is good adhesion between the silica and PMMA. But the hydrophobic silica Si-R805 is shown partly as aggregates in the rubbery phase, which means the adhesion occurring at the interface of the silica-PB is poor. The larger silica aggregates means the weaker adhesion between the silica and the rubbery phase, which might induce voids more easily during cooling compared to the system with strong interaction. Meanwhile, there is still no obvious cavitation induced by silica particles, which is related to the limited size of the rubber phase. Although the pre-cavitation doesn't occur in the silica-filled system, the debonding voids induced by the silica particles might still influence the deformation behavior, which did not show craze-like structures in the matrix (Figures A.4d-f).

For the PS/SBS system, although the voids are induced by the silica aggregates, the capability of cavitation of the rubbery phase still cannot be enhanced by the silica because of the small size of the dispersed rubber domain.

A.3 References

- ¹ Argon, A. S., Cohen, R. E., Gebizlioglu, O. S., Brown, H. R., Kramer, E. J., *Macromolecules*, **1990**, 23, 3975-3982.
- ² Schwier, C. E., Argon, A. S., Cohen, R. E., *Phil. Mag. A.*, 1985, 52, 581-603.
- ³ Van Casteren, I. A., *Control of microstructures to induce ductility in brittle amorphous polymers*, Ph.D. Thesis, TU/e, Eindhoven, the Netherlands, **2003**.
- ⁴ Paul, D. R., Robeson, L. M., *Polymer*, 2008, 49, 3187-3204.
- ⁵ Zou, H., Wu, S., Shen, J., *Chem. Rev.*, 2008, 108, 3893-3957.

Technology assessment

The development of new synthetic polymers has become seemingly unpopular over the last few decades with the main reason that no novel polymers can satisfy the current market requests. As a result, the trend in the industry is to optimize existing polymer materials with a focus on additives, referred to as 'salt and pepper technology'.

Currently, nano-technology is considered as the manufacturing future, also in the polymer additives area, with the expectation that it is a very efficient way to enhance the properties at very low loadings. Prime examples are polymers with (exfoliated) nano-clays, carbon nanotubes (CNTs) and silica nanoparticles.^{1,2}

It is well known that blending different polymers and additives has been explored as the most versatile and economic way to satisfy the complex demands for performance, such as optical, mechanical, electrical, thermal, and barrier properties. However, one of the outstanding problems of polymer blends (a combination of different polymers) is the control of the morphology.³ Recent studies show that the addition of nanoparticles in polymer blends could lead to a significant effect on their morphology development with well-controlled particle arrangements.⁴ In this thesis, a suppression effect of silica nanoparticles on the phase separation kinetics of polymer blends was reported, which was found in all studied polymer blends. It was demonstrated as an efficient way to suppress coarsening of the morphology with only 1-3 wt% silica.

In addition, it was observed that nanoparticles could be selectively distributed in a specific domain of polymer blends or block copolymers without special particle surface modification. This behavior opens new perspectives for functional materials. For example, a conductive network in a co-continuous morphology of polymer blends at very low filler content could be built up, since the location of nanoparticles can be controlled in one of the phases or at the interface after phase separation. This migration behavior could also be used to enhance the properties of multi-layered materials, of which an example is shown for a PC/PMMA multi-layered system. Figure T-1(a) shows a hydrophilic silica-filled PC/PMMA multi-layer system, in which the particles were pre-dispersed in PC, followed by co-extrusion with PMMA. The localization of silica particles can be controlled by the residence time in the melt. As shown in Figure T-1(b), for the used annealing time, the particles remain at the interface after cooling to room temperature. Since the migration of the nanoparticles can be

easily controlled in between the layers, it could be an approach in preparing films with conduction in one direction utilizing very low concentrations of fillers.

Furthermore, such precise control of the nanoparticle within a specific domain of the block copolymer could provide ideal applications for the organic-inorganic thin films prepared by the block copolymers for chemical sensing, separation, and electronic devices.

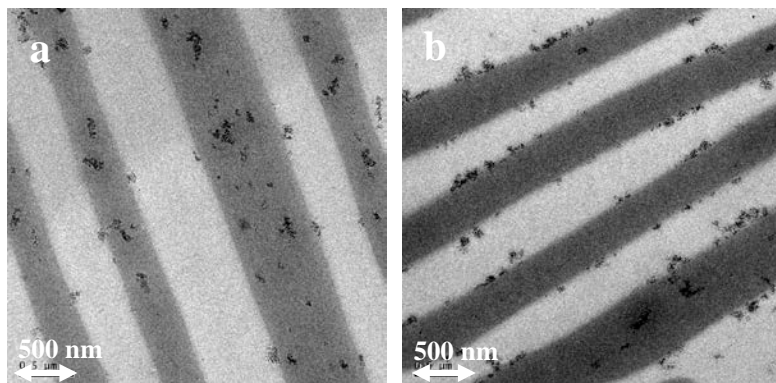


Figure T-1: TEM images of PC/PMMA multi-layered film (3 wt% MEK-ST silica is pre-dispersed in PC): (a) non-annealed and (b) annealed at 170 °C for 24 hrs.

In conclusion, this thesis shows that a small amount nanoparticles can be considered as an efficient way to influence the type and fineness of the morphology of polymer blends, which is the key for the final properties. And the use of nanoparticles could provide a variety of applications based on their distribution in specific domains of polymer blends and block copolymers.

References

- ¹ Paul, D. R., Robeson, L. M., *Polymer*, **2008**, 49, 3187-3204.
- ² Ajayan, P. M., Schadler, L. S., Braun, P. V., *Nanocomposite science and technology*, Wiley-VCH, **2003**.
- ³ Harrats, C., Thomas, S., Groeninckx, G., *Micro- and nanostructured multiphase polymer blend systems: Phase morphology and interfaces*, CRC Press, Taylor & Francis Group, **2006**.
- ⁴ Balazs, A. C., Emrick, T., Russell, T. P., *Science*, **2006**, 314, 1107-1110.

Samenvatting

Polymere materialen zijn vaak een combinatie van verschillende polymeren en weekmakers, stabilisatoren en (an)organische additieven om de eigenschappen te optimaliseren. Het type en de grootte van de morfologie is de belangrijkste factor voor de uiteindelijke eigenschappen van polymere blends. Zeer recent is het gebruik van anorganische nanodeeltjes, zoals roet, klei, koolstof nanobuisjes, en silica, geïntroduceerd om de morfologie van polymeermengsels te controleren.

Het doel van het beschreven in dit proefschrift onderzoek is om het effect van de silica nanodeeltjes op de morfologie van het polymere blends te bestuderen. Aangezien blends van polymeren worden ingedeeld in verschillende categorieën op basis van hun mengbaarheid, is het effect van silica nanodeeltjes onderzocht voor de verschillende blend categorieën. De eerste categorie wordt een volledig mengbaar blend genoemd, waarbij de polymeren mengbaar zijn bij alle samenstellingen en over een breed temperatuurgebied vanwege specifieke interacties. De tweede categorie wordt een gedeeltelijk mengbaar blend genoemd, waarvoor mengbaarheid alleen is waargenomen in een specifieke temperatuur en/of concentratie gebied. De derde categorie wordt een niet-mengbaar blend genoemd, waarbij de polymeren niet mengbaar zijn bij elke temperatuur of concentratie. Omdat volledige mengbaarheid uitzonderlijk is, is deze studie gericht op de gedeeltelijk mengbaar en niet-mengbaar blends.

Voor de categorie van gedeeltelijk mengbare blends, was een mengsel bestaande uit poly(methyl methacrylaat) (PMMA) en poly(styreen-*co*-acrylonitril) (SAN) met een Lower Critical Solution Temperature (LCST) gebruikt als modelsysteem. De interactie tussen het oppervlakte van de deeltjes en de polymeer componenten bleek de belangrijkste factor voor de verdeling van de silica nanodeeltjes, d.w.z. in een van de polymeer fasen of op de PMMA/SAN-interface na fasescheiding. Hydrofiele silica nanodeeltjes migreren bij voorkeur naar de PMMA-fase als gevolg van de sterke interactie tussen de hydroxylgroepen op het oppervlakte van silica en de carbonyl groepen van de PMMA. Migratie van de deeltjes leidt tot een vertraging van de vergroevingsnelheid van de morfologie en een lagere temperatuur van fasescheiding. Drie verklaringen werden besproken voor dit effect: i) lokale toename van de viscositeit als gevolg van een toename van de silica concentratie, ii) selectieve adsorptie van lage molmassa PMMA ketens op het oppervlakte van de silica nanodeeltjes, waardoor de

gemiddelde molmassa van de bulk afneemt. Dit leidt tot een verschuiving van het fase-diagram en iii) verlaging van de grensvlakspanning. De hydrofobe silica nanodeeltjes lokaliseren zich aan de PMMA/SAN-interface, waardoor ze de grensvlak mobiliteit kunnen beïnvloeden.

Voor de categorie van de niet-mengbare blends, werd een blend bestaande uit PMMA en poly(carbonaat) (PC) gebruikt als het model systeem met twee soorten van silica deeltjes (hydrofiele en hydrofobe). Voor de hydrofiele silica werd een selectieve verdeling van de nanodeeltjes naar de PMMA-fase waargenomen, die onafhankelijk was van de volgorde van blenden. De stabilisatie van de morfologie kan worden toegeschreven aan de lokale toename van de viscositeit en een gelijktijdige vermindering van de mobiliteit van de ketens in de PMMA-fase. Voor de hydrofobe silica, lokalisatie van de nanodeeltjes aan de PC/PMMA-interface is de thermodynamisch stabiele situatie, maar de kinetiek van vergroving van de structuur kan worden beïnvloed door de volgorde van blenden. Het waargenomen stabilisatie effect van de hydrofobe silica deeltjes kan worden gerelateerd aan de aanwezigheid van een geïmmobiliseerd laag van nanodeeltjes rondom de polymeer druppels. Dit mechanisme is zeer efficiënt voor de controle van de morfologie.

Voor niet-mengbare blends van polymeren met een blokcopolymeer treedt macrofase scheiding op tussen het homopolymeer en di- of triblokcopolymeren wanneer de polymerisatiegraad van polymeer A in het homopolymeer groter is dan de polymerisatiegraad van polymeer A in het copolymeer. De silica nanodeeltjes onderdrukken de mate van macrofasescheiding tussen PMMA homopolymeren en poly(styreen)-b-poly(butadieen)-b-poly(methyl methacrylaat) (SBM) triblokcopolymeren, hetgeen gerelateerd kan worden aan de sterke waterstofbrugvorming tussen de hydroxylgroepen op het oppervlakte van de silica nanodeeltjes en de carbonyl groepen van de PMMA. Door gebruik te maken van verschillende molmassa verdelingen voor het PMMA homopolymeer kon het onderdrukkend effect van nanodeeltjes worden toegeschreven aan selectieve adsorptie van de hoge molmassa van de PMMA op het oppervlakte van de silica deeltjes, waardoor het systeem kan geforceerd tot het zogenaamde 'wet-brush' regime. Voor blends van SBM met poly(styreen) (PS) werden silica nanodeeltjes met verschillende oppervlakte-eigenschappen gebruikt. De locatie van de silica deeltjes hangt af van de interactie tussen het oppervlakte van de silica en het polymeer, hetgeen ook kan worden beïnvloed door de volgorde van blenden. Wanneer hydrofiele silica nanodeeltjes worden toegevoegd aan PS/SBM blends, gaan de silica nanodeeltjes bij voorkeur naar de kern (PMMA fase) van de core-shell structuren zonder macrofasescheiding vanwege de sterke interactie in de vorm van waterstofbruggen tussen het

silica oppervlakte en de PMMA. Dit in tegenstelling tot hydrofoob silica nanodeeltjes die de mate van macrofase scheiding tussen de homopolymeer en het blokcopolymeer onderdrukken vanwege de selectieve verdeling in de PS-fase. Het onderdrukkingseffect op de fasescheiding en de daarmee gepaard gaande kinetiek kan worden gecontroleerd door de bereidingswijze, d.w.z. verwerking via oplosmiddel en smelt of in-situ polymerisatie.

De taaiheid van brosse amorfe, glasachtige polymeren kan worden verbeterd door de toevoeging van ABA- of ABC-blokcopolymeren met een rubberachtig blok en een semi-kristallijn blok, die micellaire of cilindrische structuren vormen in de matrix. Bij afkoeling kunnen zich extra interne spanningen opbouwen tijdens gefractioneerde kristallisatie, d.w.z. homogene en heterogene nucleatie, hetgeen kan leiden tot pre-cavitatie, zoals getoond in een eerdere studie met systemen met een cilindrische morfologie. Het toevoegen van de silica nanodeeltjes leidt tot een overgang van een sferische morfologie tot een combinatie van sferische en cilindrische morfologie voor een PMMA/poly(methyl methacrylaat)-*b*-poly(butylacrylaat)-*b*-poly(ϵ -caprolacton) (MBC) blend. Dit wordt veroorzaakt door de scheiding tussen het MBC triblokcopolymeer en het aanwezige BC diblokcopolymeer, tesamen met lokalisatie van de silica deeltjes in de bolvormige PCL-domeinen, hetgeen leidt van een gefractioneerde kristallisatie van de PCL.

In dit proefschrift is aangetoond dat silica nanopartikels een significant effect op de morfologie van blends van gedeeltelijk-mengbare, mengbare polymeer blends en blends met blokcopolymeren hebben. De verdeling van de nanodeeltjes is afhankelijk van de interactie tussen de polymeren en de silica oppervlakte aan de interface tussen de polymeren of in één van de fasen. De kinetiek van verdeling van de silica nanodeeltjes kan worden beïnvloed door de blend preparatie, d.w.z. verwerking via oplossing of smelt en/of in-situ polymerisatie in aanwezigheid van de nanodeeltjes.

Acknowledgements

I believe that the completion of this thesis was only possible through lots of help by many people within and outside of the SKT group. It is my pleasure to use the last words of my thesis to express my gratitude to a great number of people who have contributed to this thesis and to my wonderful four years in Eindhoven.

In the first place I would like to thank Prof. Piet Lemstra and Dr. Han Goossens for giving me this opportunity to pursue my PhD in SKT group. I am grateful to Prof. Piet Lemstra for his impressive teaching and innovative thinking. His support and kindness gave me confidence during my study in TU/e. Dear Piet, the Asia-Link program brought me from China to the Netherlands, which has changed my life. Because of this program, I got the opportunity to start my PhD and successfully finished this thesis. Piet, Thank you so much!

Special thanks owe to Han Goossens, my daily supervisor. His expertise, understanding and patience considerably helped the research present here. He shared with me his profound knowledge and gave me continuous support and professional guidance. Dear Han, you taught me so much and gave me complete freedom to work on this project. Your never-ending encouragement and confidence in me has been always driving me go further. Thank you very much for all the impressive ideas and discussions for this project. This thesis wouldn't have been finished without you. I am grateful to you for intensively structuring and correcting my thesis.

This project would not be possible without funding from the STW and helpful discussions with the members of the program committee and contact persons representing the various companies involved in this project. Theo Hoeks (SABIC Innovative Plastics), Pierre Gerard (Arkema), Paul Steeman (DSM), Ellen van Hemelrijck (DSM), Sachin Jain (BASF Aktiengesellschaft), Jan Stamhuis (Dutch Polymer Institute), Tung Pham (Borealis), Mark van Heeringen (Dow) and Monique Wiegel (STW), thank all of you for the questions and supports.

I would like to extend my heartiest thanks to Prof. Piet J. Lemstra, Prof. Ton Peijs, Dr. Han Goossens, Prof. Han Meijer, Prof. Paula Moldenaers for accepting to be the core-committee members and reading the manuscript of my thesis. I was impressed by their valuable comments. Also thanks to Prof. Rene Janssen for his kindness and time to be member of my defense committee.

Collaborations with many people and groups inside and outside of SKT were crucial in the completion of my PhD project. First of all, I would like to thank Anne Spoelstra. Dear Anne, I cannot finish this thesis without your help, thank you very much for all the TEM measurements. I enjoyed a lot of beautiful, professional images done by you in this project. In addition, I want to express my thanks to Pauline Schmit. You are the first one who guided me to the SKT lab and the safety. And you also helped me for the SEM measurements. Pauline, thank you. I would like to thank Joost Valetton for his patient and carefulness to teach me how to work with the DSC machine. I would like to express my thanks to Marco, Sasha and Günter (SMG) for their kindness and supports to my AFM measurements. I enjoyed to work with you in the AFM lab. Working within SKT is a great pleasure and nice experience to me. I would like to thank all the previous and present SKT colleagues. Special thanks to Elly, Bob, Ineke for your kindness and help all the times. Special thanks to Roy l’Abee for your great help to my experiments. Special thanks to my roommates Rafiq, Gosia and Karl. Special thanks to Giuseppe for the SAXS measurements in Grenoble and ALS. Special thanks to Maria for your efficient TGA support. Special thanks to Tamara, Yogesh, Yoseli for taking DSC work, your work will be appreciated by everyone. Further, I would like to thank Denka, Gizella, Elena, Martijn, Cees, Bjorn, Marloes, Luigi, Irina, Jules, Benny, Thierry, Paul, Maurizio, Arthur, Pim, Matthijs and the rest of my colleagues from SKT, SFD group and PTG for their help throughout this four years.

I would like to thank my dearest Chunxia Sun. Dear 孙 mm, 如果没有你, 不能想象这四年博士会是什么样。你每天的热情和唠叨是我读博士的动力。每次实验上碰到问题和你讨论, 你总是那么的仔细认真。还有你作为八卦女王也给了我很多很多的快乐, 谢谢你。祝你和 Peter 天天幸福! Shufen, mian, 跟你们在一起就会很开心, 一起逛街一起”欺负”xx, 感觉日子过得特别快, 现在特别想念可以和你们随时去逛街的日子。淑芬, 祝你和 duy 幸福快乐! 戴冕, 时间很快的, 你马上可以毕业了, 不要再做工作狂了。小马(Piming), 晓霞(Xiaoxia), 认识你们是很幸运的, 你们那么善良稳重和热心, 给了我这么多的帮助, 真的谢谢你们。殷杰(Yinjie), 还是叫考拉亲切, 认识你十几年了, 自从你成了我的室友开始, 你的乐观开朗, 大大咧咧的性格一直给我和周围的人带来很多快乐, 谢谢你! 祝你天天那么开心! 薛丽晶师姐(Lijing), 田明文师兄(Mingwen), 记得刚到荷兰 2004 年的时候就受到你们很多无私的关怀和帮助, 不论生活上还是工作上。谢谢你们一直以来对我们的关心! 祝你们和雷雷全家幸福! 吕康博(Kangbo), 宋立国(Liguo), 谢谢你们夫妇这四年真诚的建议和帮助, 愿你们一家四口

和和美美！楼长， Marshall， 肖艳， 汤栋霖， 东为富， 王莉莉， 黄汝彬， 张奕， 王琦， 关庆玲， 张学庆， 关业军， 还有很多中国朋友们， 谢谢你们对我各方面的关心和支持！

Last but not least, my appreciation to my parents: Mr. Li Shanjun and Mrs. Zhou Yi; my husband: Mr. Hu Xin, for their endless love and great support throughout my work and life.

这本论文要特别献给我的爸爸妈妈和老公， 你们的理解和支持是这本论文得以完成的源泉和动力， 而你们的关爱和包容是我永远的避风港。亲爱的胡欣， 跟你在荷兰相知相爱， 现在还有了 MAX， 是我最幸福的事， 谢谢你一直在我身边爱我， 包容我， 帮我处理各种问题。亲爱的， 谢谢你给我的一切！最后的感谢要给我最爱的爸爸妈妈， 感谢你们对我这么多年悉心养育和无私关爱， 包容我所有的优缺点。是你们的爱鼓励着我， 成就了这篇论文， 爸爸妈妈， 辛苦了！

In the end, I would like to extend my thanks to all my family, colleagues and friends who have helped me directly or indirectly.

李唯真

2011年10月

Curriculum vitae

The author of this thesis was born on Feb 21th 1981 in Shanghai, China. After finishing her bachelor study in 2003 at the Department of Macromolecular Science, Fudan University, Shanghai, China, she started her master study and participated in the Asia-Link program between the Department of Macromolecular Science in Fudan University, China, and the Department of Chemical Engineering and Chemistry of the Eindhoven University of Technology, Eindhoven, the Netherlands. In 2006, she obtained her Master degree in Material Science within the Department of Macromolecular Science of the Fudan University, on ‘Two-dimensional correlation spectroscopic study on the properties of polymers’.

In March 2007, she started a PhD project at the Eindhoven University of Technology, Eindhoven, the Netherlands, of which the results are presented in this dissertation. During her PhD study, the author completed three modules of the course ‘Registered Polymer Scientist’ (RPK) organized by the ‘National Dutch Graduate School of Polymer Science and Technology’ (PTN), which include Polymer Chemistry, Polymer Physics, Polymer Rheology and Processing.

